

University of Bath



PHD

Computer-aided design and simulation of fibre optic systems for power system protection

Li, Haiyu

Award date:
1994

Awarding institution:
University of Bath

[Link to publication](#)

General rights

Copyright and moral rights for the publications made accessible in the public portal are retained by the authors and/or other copyright owners and it is a condition of accessing publications that users recognise and abide by the legal requirements associated with these rights.

- Users may download and print one copy of any publication from the public portal for the purpose of private study or research.
- You may not further distribute the material or use it for any profit-making activity or commercial gain
- You may freely distribute the URL identifying the publication in the public portal ?

Take down policy

If you believe that this document breaches copyright please contact us providing details, and we will remove access to the work immediately and investigate your claim.

**COMPUTER-AIDED DESIGN AND SIMULATION OF
FIBRE OPTIC SYSTEMS
FOR POWER SYSTEM PROTECTION**

A thesis submitted for the degree of
Doctor of Philosophy

by

Haiyu Li

A handwritten signature in black ink that reads "Haiyu Li". The signature is written in a cursive style with a large initial 'H' and a distinct 'Li' at the end.

School of Electronic and Electrical Engineering
University of Bath
United Kingdom

January 1994

UMI Number: U059625

All rights reserved

INFORMATION TO ALL USERS

The quality of this reproduction is dependent upon the quality of the copy submitted.

In the unlikely event that the author did not send a complete manuscript and there are missing pages, these will be noted. Also, if material had to be removed, a note will indicate the deletion.



UMI U059625

Published by ProQuest LLC 2013. Copyright in the Dissertation held by the Author.
Microform Edition © ProQuest LLC.

All rights reserved. This work is protected against
unauthorized copying under Title 17, United States Code.



ProQuest LLC
789 East Eisenhower Parkway
P.O. Box 1346
Ann Arbor, MI 48106-1346

UNIVERSITY OF BATH
LIBRARY

33	15 AUG 1994
----	-------------

PHD

S082904

ABSTRACT

Extra High Voltage (EHV) electrical power transmission line protection systems essentially require reliable and high-performance communication channels for data transfer and control. Accurate and economical voltage and current measuring devices are also desirable in order to obtain better monitoring and protection results. Theoretically, the inherent advantages of optical fibre and the characteristics of electrical power line protection relaying system have determined the unique and ideal position of the application of the former in the latter, while in reality, little work has been published on this application field; hence a systematic study and a general investigation are of potential theoretical and practical importance.

This thesis focuses on two major aspects of optical fibre applications, fibre optic link as a communication medium and fibre optic current sensor as electrical current measurement devices. CAD simulation techniques are used as a general tool for carrying out the modelling, analysis and system performance evaluation of a fibre optic link and a fibre optic current sensor. The applications of the fibre optic link and the fibre optic current sensor are mainly discussed in the domain of electrical power transmission line systems, but the generality of the study methods employed makes them equally applicable to a large variety of systems.

This thesis describes comprehensive CAD study models of both fibre optic links and fibre optic current sensors applications in power system protection, in particular in line protection relaying. The fibre optic link simulation model employs a laser equivalent electrical circuit model, a single-mode fibre transfer function and a photo-receiver model with either p-type intrinsic n-type photodiode or avalanche photodiode. The fibre optic current sensors simulation model is composed of a spun single-mode fibre model and a mirror Faraday rotator model. The reasoning process of these models is described, where appropriate, with the modelling techniques explained in detail

accordingly. The simulation results are obtained by using simulated power system fault waveforms generated from a CAD fault simulation package. Available experimental results as obtained by other researchers are used to compare with the simulation results. It can be generally concluded that both of these simulation models can provide tools for analysis and design of a practical application. What is more important is that the insight into system performance is provided both by the modelling process itself and by the experience gained from the simulation experiments.

A test and control board for conducting a complete laboratory fibre optic link testing system is also developed. The hardware configuration is partially implemented and some monitoring software experiments are carried out. It is expected that this test & control board will provide an interface between a physical relay and a solid fibre optic link in real laboratory experiments.

ACKNOWLEDGEMENTS

First and most of all, I would like to thank my supervisor, Dr. Raj K Aggarwal, for his excellent supervision. I am very grateful for all his comments, advice, criticisms, encouragements, guidance, and for his friendly attitude throughout the research course and the preparation of this thesis, also for his general support beyond this research.

I would like to thank my parents for their continuing support in my life.

My special thanks goes to my wife, Fenglan, because of her patience, constant support and encouragements, and for being an excellent caring companion, also for her help in typing and reading part of the draft of this thesis.

I would like to thank Prof. A T Johns for his general guidance.

I would like to thank my examiners, Prof. K.T.V. Grattan and Dr. P.J. Moore, for their constructive suggestions during the oral examination

I would also like to thank everyone at the School of Electrical & Electronic Engineering, especially members of the Power System Research Group at the University of Bath, for their general help, friendship and encouragements.

This research has been made possible by the Overseas Research Scholars Award, and has been partially supported by the Gunter Charitable Trust, the Great Britain-China Educational Trust and myself.

COPYRIGHT

Attention is drawn to the fact that copyright of this thesis rests with its author. This copy of the thesis has been supplied on condition that anyone who consults it is understood to recognise that its copyright rests with its author and that no quotation from the thesis and no information derived from it may be published without prior written consent of the author

This thesis may be available for consultation within the University Library and may be photocopied or lent to other libraries for the purpose of consultation, subject to normal conditions of acknowledgement.

CONTENTS

ABSTRACTi
ACKNOWLEDGEMENTSiii
COPYRIGHT DECLARATIONiv
CONTENTSv
LIST OF SYMBOLSx
CHAPTER 1 INTRODUCTION1
1.1 Fibre Optic System in Power System	1
1.2 Objectives	4
1.3 The Structure of This Thesis	6
CHAPTER 2 BACKGROUND & RELATED WORK8
2.1 Power System Protection	8
2.1.1 General Descriptions	8
2.1.2 Differential Line Protection Schemes	11
2.1.2.1 Algorithms Based on Phasor Relaying	12
2.1.2.2 Algorithms Based on Time Variation	13
2.1.2.3 Algorithms Based on Superimposed Components	14
2.1.3 Communication Links	16
2.2 Fibre Optic System	18
2.2.1 Historical Developments of Optical Fibres	18
2.2.2 Optical Fibres	20
2.2.2.1 Classifications	20
2.2.2.2 Basic Operations	22
2.2.3 Single-Mode Fibre Properties	23
2.2.3.1 Optical Dispersion	23
2.2.3.2 State of Polarization	24

2.2.3.3	Birefringence	24
2.2.3.4	Polarization-Maintaining Single-Mode Fibre	27
2.2.3.5	Faraday Effect	28
2.2.4	Fibre Optic Links	29
2.2.5	Measurements	30
2.3	Related Works	33
2.3.1	Fibre Optic Links for Power System Protection	34
2.3.2	Computer Simulation of Fibre Optic Links	36
2.3.3	Fibre Optic Current Sensors	37
2.4	Fault Waveform Simulations	43
2.5	Summary	44
 CHAPTER 3 FIBRE OPTICAL LINKS SIMULATION		48
3.1	Introduction	48
3.2	Fibre Optic Link Designing Considerations	49
3.2.1	Pulse Code Modulation	49
3.2.2	Link Configuration	51
3.3	Modelling of a Fibre Optic Link	53
3.3.1	Optical Source Models	53
3.3.2	Single-Mode Fibre Transfer Function	56
3.3.2.1	Fibre Loss	56
3.3.2.2	Dispersion	57
3.3.2.3	Fibre Transfer Function	58
3.3.3	Receiver and Noise Models	61
3.3.3.1	Photodiodes	62
3.3.3.2	Shot Noise	62
3.3.3.3	Circuit Noise	63
3.3.3.4	Mode Partition Noise	63

3.4	Design Considerations	64
3.4.1	Bit Error Rate Estimation	64
3.4.2	Dispersion Penalty	67
3.4.3	Link Power Budget	67
3.5	Fibre Optic Link Simulations	68
3.5.1	Laser Source Spectrum Simulation	68
3.5.2	Laser Transient Waveform Simulation	69
3.5.3	Fibre Loss Estimations	70
3.5.4	Fibre Transfer Function Simulation	71
3.5.5	Dispersion Penalty Evaluation	72
3.5.6	Link Power Budget Calculation	74
3.5.7	Noise Analysis	75
3.5.8	Bit Error Rate Curve Simulation	76
3.5.9	Decision Circuit Simulation	77
3.6	Summary	78
CHAPTER 4 FIBRE OPTIC LINKS APPLICATIONS.		89
4.1	Introduction	89
4.2	Fibre Optic Links Simulation Test	89
4.2.1	The Simulation Process	90
4.2.2	Available Laboratory Experimental Results	91
4.2.3	Simulation Results and Discussions	91
4.3	Fibre Optic Links Model for Line Protection Schemes	93
4.3.1	Channel/Modem Time Delay	94
4.3.2	Fibre Optic Links Model Testing	95
4.4	Test and Control Board	97
4.4.1	General Considerations	98
4.4.2	Hardware Design	100
4.4.3	Software Considerations	101
4.4.4	Results	102

4.5	Summary	103
CHAPTER 5	FIBRE OPTIC CURRENT SENSORS SIMULATION.	112
5.1	Introduction	112
5.2	The State of the Art of Fibre Optic Sensors	112
5.3	Fibre Optic Current Sensors Theory and Design	117
5.3.1	Spun Fibre Model	117
5.3.2	Faraday Rotator Model	120
5.3.3	Phase Conjugate Mirror	121
5.3.4	Design and Configuration	122
5.4	Simulation Results Analysis	124
5.4.1	Available Laboratory Experimental Results	124
5.4.2	Simulation Results Evaluation and Comparative Study	125
5.5	Fibre Optic Current Sensor Simulations Performance Evaluation	130
5.5.1	Measurement Range	130
5.5.2	Operation Bandwidth	132
5.5.3	Noise Limitations	133
5.5.4	Sensitivity	137
5.5.5	Testing with Typical Fault Waveforms	138
5.6	Summary	140
CHAPTER 6	CONCLUSIONS AND FURTHER WORK.	153
6.1	Summary of Work	153
6.1.1	Fibre Optic Links	153
6.1.2	Practical Applications of Fibre Optic Links	155
6.1.3	Fibre Optic Current Sensors	156
6.2	Conclusions	157
6.3	Suggestion for Further Work	160
6.3.1	A Complete Prototype of Fibre Optic Links Test	160
6.3.2	Applications of Fibre Optic Current Sensors	161

6.3.3 Testbed Generation	161
--------------------------	-----

REFERENCES	162
-------------------------	------------

APPENDIX A Fault Waveforms Simulation	168
---	------------

APPENDIX B Detailed Inferences of Laser and Fibre Models	180
--	------------

APPENDIX C Detailed Inference of Spun Fibre Model	190
---	------------

PUBLISHED WORK	197
-----------------------------	------------

LIST OF SYMBOLS

A	optical gain parameter
APD	avalanche photodetector
B	bit rate
B_l	linear birefringence
B_{circ}	circular birefringence
B_e	elliptical birefringence
B_w	waveguide shape birefringence
B_s	stress birefringence
BER	bit error rate
B_N	bandwidth of low-pass noise filter at receiver
BS	beam splitter
C	diffusion capacitance in laser equivalent circuit
c	light speed.
CAD	computer aided design
CT	current transducer
DP	dispersion penalty
e	electron charge
EMI	electromagnetic interferences
EMTP	electromagnetic transient program
EHV	extra high voltage
FET	field effect transistor
FOCS	fibre optic current sensor
FOL	fibre optical link
FFT	fast fourier transform
FWHM	full width half maximum of laser source spectrum
f	unit Faraday rotation
G_0	average photo gain
g	photo gain

$\langle G \rangle$	average photodiode gain,
I	electrical current.
$I_1(\omega)$	spectrum of laser injected current
$I_{n,j}$	total rms noise current
$I_{nc,j}$	rms circuit noise current
$I_{ns,j}$	rms shot noise current
$I_{s,j}$	photo-current
I_{th}	decision threshold level current
$I_{mp,j}$	mode partition noise current
ISI	intersymbol interference
k_B	Boltzmann's constant.
L	inductance in laser equivalent circuit
L_p	fibre beat length
L_s	fibre spin pitch
LD	laser diode
LED	light emitter diode
M	phase conjugate mirror
[M]*	Phase conjugate mirror matrix
MFR	mirror Faraday rotator
MMF	multi-mode fibre
MFRC	mirror Faraday rotator configuration
MPN	mode partition noise
N	fibre coil turns
n	refractive index
n_e	electron density,
NA	numerical aperture
NRZ	non return zero
P	sensor response signal
P_e	error probability
P_{e_j}	error probability of a binary signal $j = "1" \text{ or } "0"$

P_j	average received power of a optical power signal $j = "1" \text{ or } "0"$
P_r	receiver power
P_n	receiver sensitivity power
P_t	light source transmission power
PIN	p-type intrinsic n-type photodiode
PCM	pulse code modulation
R	resistance in laser equivalent circuit
RZ	return zero
R_{RE}	resistor in series with L
RBC	reflect-back configuration
s_p	photon density
s_1	photon signal density
SNR	signal to noise ratio
$S(\lambda)$	Spectrum of light source
$S_1(\omega)$	spectrum of the photon density s_1
$S_{zz}(\lambda)$	Spectrum of complex envelop of light source in wavelength domain
$S_{zz}(\omega)$	Spectrum of complex envelope of light source in frequency domain
SHB	spun highly birefringent
SOP	state of polarization
SMF	single mode fibre
SIC	Sagnac interferometer configuration
TDS	transputer development system
TCB	test and control board
T_h	voltage threshold level
v_n	voltage noise source
V_H	Verdet constant
WP	Wollaston prism
z	fibre length
α	average fibre loss

β_x	propagation constant in the direction x axis
β_y	propagation constant in the direction y axis
Δ	the relative difference between a fibre core refractive index n_1 and the fibre cladding refractive index n_2 .
$\Delta\beta$	difference in propagation constants
Θ	reciprocal signal rotation(rad)
θ	orientation angle
$\theta(0)$	initial orientation angle
$\theta(z)$	orientation angle at fibre length z
θ_c	critical angle
λ	light wavelength
λ_0	light operating wavelength
ξ	fibre spinning rate or twisted rate
τ_p	photon lifetime
τ_s	spontaneous emission lifetime
σ_0	light source rms spectrum width
ρ	fraction of spontaneous emission to photon in laser rate equations
Ψ^+	forward light propagation total phase rotation
Ψ^-	backward light propagation total phase rotation
$\Psi_0(t)$	light source optical field
Ω	light rotating angle
ω	frequency angle

CHAPTER 1

INTRODUCTION

1.1 Fibre Optic System in Power System

Since the invention of optical fibre, especially the first successful factory production of practical optical fibre in the 1970s, the fibre optic industry has been rapidly growing, its practical importance and application potentials are widely recognized, particularly in telecommunications, while the characteristics of EHV electrical power transmission line protection systems and the inherent advantages of optic fibre have attracted wide attention of the researcher in the former to the latter. Back in the mid 1980s, the research of both theoretical projections and the practical applications of optical fibre in power system protection had been actively carried out [26, 59, 61, 62]. These demonstrated the wide awareness of the increasing importance of fibre optic technology in the power engineering community.

An EHV electrical power transmission line protection system essentially requires reliable and high-performance communication channels for data transfer and control. Accurate and economical voltage and current measurement devices are also desirable in order to obtain better monitoring and protection results. At present, many types of communication channels used in power protection systems are to some degree affected by the presence of power system faults. By using rented data communication links from telecommunication authorities, unpredicted problems will be at times caused by the extensive use of electronic signal repeaters and complex switching equipment. These extra telecommunication components not only reduce the reliability of data channels (everyone may have an experience of unclear voice and noisy background on the telephone), but also cause a long time delay. Both noisy channels and a long time delay will affect the performance of a power system protection relay. So direct transmission of power system information over rented communication links is becoming

less feasible.

The characteristics of being immune to electromagnetic interference (EMI), a wide bandwidth and a low attenuation in optical fibre make fibre optic links (FOLs) potentially well suited for power system transmission line protection relaying applications. The obstacle limiting FOL applications is partly technical and partly economical. It is only recently that it has become feasible to develop a fibre optic communication systems for power systems protection due to both the technological advances of fibre research and large scale cost-reductions. Technologically, significant advances have been achieved in the past decade and they have proved that lightwave transmission over FOL is far superior in performance to that which can be obtained over wires and microwave links. When used as a communication medium, FOL has many advantages over conventional media. Typically, optic fibre can support a wider transmission bandwidth (in GHz level), has lower transmission loss per unit length (0.15 ~ 0.5dB/km) [65], and is immune to EMI. In addition, it has small size, light weight and flexibility over metallic cables. These advantages allow optical fibres to be ideally installed along existing power transmission lines and do not suffer from electromagnetic interference. By using FOLs along power transmission lines instead of using microwave links, also reduces the huge costs in setting up microwave communication relay towers. Economically, many experimental fibre optic communication systems have been tried [8, 40], and now there are number of commercial fibre optic communication systems are available.

In recent publications, most new protection schemes have employed FOLs for data transfer [2, 3]. Some practical short distance FOLs for power system data transfer and control have been developed [35, 59, 61], but without electrical signal repeaters, none of them are suitable for long distance data transmission. Repeaters, however, introduce additional problems for power system long-haul transmission line protection relaying. They need a voltage supply at remote locations and may also be influenced by the power environment. Thus the reliability of the FOL is significantly reduced. So a reasonably long spanning optic fibre installed along the power transmission lines without repeaters is an ideal design of a FOL for power system protection relaying.

However fibre optic systems are by nature sophisticated because of the complex properties and behaviour of both the fibre and the light source. It is a demanding and computationally intensive task to determine the system design parameters. Hence a systematic study and a general investigation of a FOL are of great theoretical and practical importance.

Another important application of optical fibre, side along the development of optical fibre as a communication medium, is fibre optic current sensors (FOCSs). The ability of FOCSs to operate under most hostile environmental conditions, the potential of very low cost driven by the large commercial telecommunication and optoelectronic markets, as well as their properties of lightweight and small-size as sensing units, are all valuable assets of FOCSs over conventional current sensing devices.

In EHV power system protection relaying, accurate and real-time measurement of power system voltage and current is necessary. The conventional method for current measurement is based on the ferrous-cored current transducer (CT). Since the CT is placed in the high voltage region, the insulation between the CT secondary and the permeable core which surrounds the current carrying conductor must be extremely high, hence the CT used in the high potential locations is both large and expensive. By using FOCSs, not only will the costs be dramatically reduced, but also their sensitivity and versatility are far superior to those of conventional CTs. It is clear that FOCSs are very attractive devices for the electrical power supply industry.

Although FOL and FOCS systems are both technically and economically attractive, a successful design of a fibre optic system is still a difficult task and full of challenge since there is not a systematic reference available to help determine system design parameters and the general selection of system components. The system configuration and design parameter setting up are all complex and time-consuming. It also demands extensive theoretical knowledge and practical experience of these systems. Actual prototype hardware evaluation is generally cumbersome, expensive, time consuming, and relatively inflexible.

Over the past decade, computer-aided simulation and design techniques have been developed to facilitate the design process of such complex systems. These techniques rely on models of devices and systems, both analysis and simulation, to guide the designer throughout the life cycle of a system. In the context of FOL and FOCS simulation, computer simulation can provide the flexibility of varying system design models and parameters so that the relations between them can be easily and clearly examined. Besides, there are many more benefits from the insights into system performance provided both by the modelling process itself and by the experience gained from simulation experiments, so that an optimization of system performance can be obtained.

There has been some published work on computer simulation of FOLs [14, 15]. But the simulations have been carried out by using a general-purpose software package [18]. This has limited the flexibility of these simulation methods and it is in general difficult to model specific problems in a concise way. Furthermore commercial packages are complex and usually inefficient to interface with other CAD programs such as the CAD program of the transmission line protection scheme [3].

In contrast to the relatively well-established FOL research and application development, FOCSs are still in their infancy, particularly their applications in power systems protection. The problem central to the development of a practical FOCS is the linear birefringence in the fibre. A spun highly-birefringence (SHB) fibre model was developed to solve this problem, but the temperature-dependent problem still remains. A mirror Faraday rotator configuration (MFRC) [49, 50] was suggested to reduce this temperature-related effects. But before a full acceptance of the FOCS with MFRC can be effected, some detailed system analyses and performance evaluations are essential. Unfortunately there are not any accessible results on these aspects.

1.2 Objectives

The overall objective of this thesis is to develop computer simulation systems of both a FOL and a FOCS, so as to provide tools for studying the properties of these systems

extensively, and to investigate further techniques for optical fibre applications in the area of EHV transmission line protection relaying.

A detailed interpretation of the objectives are:

(1) To develop a complete computer simulation system of a FOL. The detailed reasoning and establishment of the various processes of the models are presented. The system is composed of a laser equivalent electrical circuit model, a single-mode fibre model and a receiver model. Comparison and contrast of the system simulation results with available experimental results will be conducted both to verify the system design and to prove the feasibility of the system models. The FOL simulation system performance will be tested by using simulated fault waveforms generated from a CAD fault simulation package [30]. Further evaluation of the system performances in a wider aspect would help examine the relationship among the design parameters of system components, such as light wavelength, fibre loss and noises. Furthermore the world aims to explore the practical impact of the parameters on a FOL design, for the purpose of optimizing a FOL system design for power system protection relaying.

(2) To design and implement a complete laboratory FOL test system. An IMS T414 transputer is used as a central unit on a test and control board (TCB) which can generate test software to coordinate the behaviour of the whole system. The TCB is used to provide an interface between a relaying scheme and a physical FOL. The establishment of this laboratory test prototype lays the base for further investigation of FOL applications on power system protection relaying, and strengthens the simulation model with the support of physical experiments.

(3) To explore the application of FOCS by developing a complete computer simulation system of the latter. The FOCS simulation model consists of a spun fibre model and a mirror Faraday rotator (MFR) model. Also the effects of detailed inferences in these models are presented. Available experimental results are used to verify the system simulation models. Further applications of the FOCS model in a power system relaying scheme are discussed by using simulated fault waveforms generated from a CAD fault simulation package [30]. This would provide a solid base for studying

FOCS applications in power system protection, and furthermore to give general guidance in FOCS system design and considerations.

1.3 The Structure of This Thesis

Chapter 2 provides a general background of both power system protection relaying and a fibre optic system including FOLs and FOCSs. Closely related work on computer simulations of FOLs and FOCSs are examined and summarized. Finally the simulated power system fault waveforms are introduced which is used as testing data for the simulation models in later chapters.

In Chapter 3, a complete computer simulation model of a FOL is developed. The use of pulse code modulation (PCM) for data transfer is established and a system configuration is described. Detailed modelling considerations are discussed and the modelling processes are presented. The simulation system performance and the simulation output waveforms are evaluated and analyzed.

In Chapter 4, the simulation and application of a FOL for power system protection are presented. The simulation results are compared and contrasted with existing laboratory experimental results. Also the simulation model of the FOL is applied into a CAD model of line protection scheme. Furthermore, a complete design of a hardware test system with a transputer based TCB and a physical FOL is described

In Chapter 5, a complete computer simulation model of a FOCS is presented. The model is a combination of a spun fibre model and a MFR model. The system design principles and related parameter considerations are discussed with particular regard to its current measurement range, bandwidth and noise limitations. Two existing laboratory experimental results are used to compare and contrast the simulation results. A FOCS design for EHV power system line protection relaying is discussed and tested by using simulated fault current waveforms.

Chapter 6 summarizes the work presented in this thesis and draws the conclusions.

Further work in this area is suggested; such as, for example, the actual FOL prototype hardware implementation, further FOCS model application in EHV transmission line protection and possibly further development of the simulation systems for general test purpose and as design tools.

It should be mentioned that all tables and figures in a chapter are listed at the end of the chapter, and all detailed reasoning of the simulation models are presented in the corresponding appendix. It should be also noted that the list of symbols and the references are in an alphabetical order, the latter according to name of the first author.

CHAPTER 2

BACKGROUND & RELATED WORK

This chapter is intended to give the reader sufficient background knowledge for the purposes of a better appreciation of the subsequent chapters. However, it is assumed that the reader is familiar with basic EHV line protection schemes and the fundamental principles of fibre optic systems.

In section 2.1, the area of power system protection relaying is described and typical relaying schemes are summarized. Similar tasks are aimed for section 2.2 in the area of fibre optic systems. In section 2.3, some related work in the area of computer simulation of fibre optic communication links and fibre optic current sensors are approached. Fault simulation waveforms are described in section 2.4 for testing fibre optic communication links and an optical fibre current sensor. A summary is given in section 2.5.

2.1 Power System Protection

In an ideal world, no faults would occur and protection systems would be superfluous. In reality, unfortunately, accidents happen, equipment fails, and not all eventualities are covered in any system design. Protection is therefore essential for the safe and secure operation of any electrical power supply network.

In this section, the basic requirements for the protection components in power system engineering are introduced, in particular power transmission line protection relaying.

2.1.1 General Descriptions

A power system can be thought of as a chain in which a few or many power plants and

utility companies are linked together, the links of which are the generators, the power transformers, the switchgears, the power transmission lines, the distribution circuits, and the utilization apparatus. Occasional failure of any link destroys the capacity of the chain to perform the function for which it was intended, and in consequence the failure would have to be removed from the system. In order to detect such failures, power system protective measuring equipments are employed. Power system protection is a measuring technique which monitors the state of the plant and initiates its removal from the system if and when faults occur. It provides: (a) the decision and timing for the removal of faulted plant so as to aid the stability of the rest of the system and (b) a protection function so as to limit damage to plant due to excessive fault current.

In low-voltage distribution systems, surge arresters are used for overvoltage protection, fuses and slow-acting circuit breakers are employed with overcurrent protection. In high-voltage subtransmission and transmission systems, on the other hand, reliable sensors, fast-acting relays, and circuit breakers are needed to detect and clear the fault quickly, so that the stability of the remaining system is secured. In short, the protection, and therefore the stability, and security of a power system, are affected by the ability of the protection devices to detect and respond to system abnormalities like, grounding, overvoltage, overcurrent, undervoltages, overspeeds, unbalanced phases, and reversed flow. A protection system chiefly requires the following components:

- (i) Sensors (transducers) for transferring primary system voltages and currents
- (ii) Protection relays for detecting system abnormalities such as faults
- (iii) Circuit breakers (interrupters) to open (disconnect) the circuit

Besides protecting generators, power transformers, and switchgears, currently detecting faults on transmission line is a very important function of protection devices. Transmission lines are interconnection links between the electrical power plants and separate utility companies. They provide the links for exchange of electric power, contributing to increased efficiency and higher continuity of service. The advantages of interconnections include: (i) Economical interchange, (ii) Sharing of generation

reserves, (iii) Utilization of large and more efficient generation units, (iv) Sharing the large investments required for example by nuclear power plants, and (v) System support during emergencies. In order to maintain these advantages, it is essential that interconnections have high capacity and therefore operate at EHV of 275kV and upwards. The most commonly used voltage on the U.K. EHV system is 400kV, with a trend to higher voltages in many overseas countries. Hence it is required that these interconnections must be highly reliable and their design and protection are thus conducted with utmost care. For example, high-speed tripping is essential for all faults within the protection zone (internal fault) due to EHV, and it is crucial that the link be maintained during fault occurring outside of the protection zone (external faults). In general, the protection must provide coverage for more contingencies than might be justified in other system areas. High-speed simultaneous tripping of all circuit breakers at terminals ends of the protected line for internal faults (i) minimizes line damage; (ii) improves transient stability of the power systems; and (iii) permits high-speed reclosing.

Computers have been widely used in the electrical power engineering field since the 1950s. Rockefeller [53] outlined the feasibility of protecting a substation by using a computer, examined the protection requirements of all types of station equipment into one unified system and suggested the use of minicomputers in power system substations for control, data acquisition, and protection against faults and other abnormal operating conditions. Some of the problems associated with the use of a digital computer for performing all the protection functions in a substation were clearly recognized as well. This has become known as computer relaying. The computer relaying has considerably advanced since the early 1970s. Since then there has been a number of reports on various techniques of performing relaying functions. Recently microprocessor relays have become a much more important research area. The idea of using a single computer for performing all the protection functions has been moving into using individual relaying microprocessors for each major protection function. In 1987 an IEEE Tutorial course [27] focused on the background and development of

microprocessor relays and protection systems. It indicated that the research and development activity has been much more intense in transmission line protection than in the protection of other components of a power system. There are two major reasons for this bias: firstly, in view of the fact that analogue transmission line protection systems cost several times more than the protection systems for other elements, the researchers were of the opinion that microprocessor relays for transmission line protection could cost less than their analogue counterparts; secondly, since the transmission line protection function is more complex than the protection of any other components, most researchers, therefore, concluded that the development of a successful microprocessor based transmission line protection system would also imply that microprocessor relays could be successfully developed for all other protection functions. A number of different tasks were proposed and the most significant ones are: (i) Communications (ii) Man machine interface with a sequence of events reporting and fault reporting, (iii) Automatic reclosure, and (iv) Breaker failure protection.

Currently, line protection schemes can be classified into two categories:

- (i) Unit protection schemes. This scheme operates by comparing the measuring parameters (voltage and/or current) derived from two or more points in a given system. Examples are current differential schemes and phase comparison schemes.
- (ii) Non-unit protection schemes. This scheme operates by measuring the parameters derived from only one point. Examples are overcurrent protection and distance protection schemes.

A differential protection scheme is one of the most commonly used transmission line protection schemes, in particular for long-haul transmission line protection. In this thesis, the main focus is placed on the development and problems with the communication links in the context of differential line protection schemes.

2.1.2 Differential Line Protection Schemes

Many types of digital differential protection schemes for two terminal transmission lines (i.e. plain feeders) and three terminal transmission lines (i.e. teed feeders) have been developed. One method, based on Kirchhoff's current law, is often used to distinguish faults between protective plants. This is known as a current differential relay. The relay operates when the phasor difference of two or more similar electrical quantities exceeds a predetermined threshold. Some relaying schemes based on differential protection principles have been proposed over the last decade [2, 4, 36, 37, 56]. A brief description of the operating principles of some of the existing schemes applicable to EHV line protection are outlined hereafter.

2.1.2.1 Algorithms Based on Phasor Relaying

Kwong et al. [37] proposed a current differential relay for the protection of a teed feeders based on the principle of master and slave terminals. The sampling of the current signals at each end is controlled by a free running clock. An interpolation method was used to predict the actual value of the sample at the slave end corresponding to the same time at the master end by taking into account the propagation delay over the communication channel. The transient embedded current waveforms were sampled by using the one cycle window Fourier method. The algorithm process was achieved by correlating the current data samples with stored samples of reference fundamental, sine and cosine waveforms. The discrete Fourier method gives the vector components I_{\sin} and I_{\cos} of a current signal i , where I_{\sin} is Fourier sine integral of signal i , I_{\cos} is cosine integral of i , and the amplitude $|I|$ is equal to:

$$|I| = \sqrt{I_{\sin}^2 + I_{\cos}^2} \quad (2.1)$$

If I_A , I_B , I_C are the current vector signals measured at the three terminal ends, then the differential current I_{diff} and bias current I_{bias} are:

$$I_{diff} = I_A + I_B + I_C \quad (2.2)$$

$$I_{bias} = \frac{1}{2} (|I_A| + |I_B| + |I_C|)$$

A percentage biased differential characteristic was used and the tripping criterion was:

$$|I_{diff}| > K_b \cdot |I_{bias}| \quad (2.3)$$

where K_b = percentage bias setting.

This relay was designed to work with communication links which had a wide bandwidth of 64kbits/s and above. Eight samples per cycle was used and its average operating time was about 26ms.

2.1.2.2 Algorithms Based on Time Variation

Akimoto et al [4] have developed a percentage differential protection system for teed feeders, in which a separate protection was provided for each phase. The operating quantity is the vector sum of terminal currents (i.e. $|I_1 + I_2 + I_3|$) for a particular phase and the restraining quantity is proportional to the scalar sum of the currents (i.e. $|I_1| + |I_2| + |I_3|$) for the same phase and the operating criterion is given as:

$$|I_1 + I_2 + I_3| - K_1 \cdot (|I_1| + |I_2| + |I_3|) - K_0 > 0 \quad (3.4)$$

where: I_1, I_2, I_3 are terminal current values for the phase being protected. K_1 is the percentage bias ratio. K_0 is a threshold value.

Sanderson et al. [56] improved the performance of the scheme in that the basic operating principle is amplitude comparison as above but the operating and restraining quantities are derived from incremental fault currents following a disturbance, by removing the initial load currents. The operating quantity is the vector summation of the incremental currents for each phase, but the restraining quantity is the maximum of each terminal current for the particular phase being protected. The method is such that for an internal fault, the fault current will exceed the largest of the terminal

currents, but for an external fault condition, the vector sum of terminal current will be less than the maximum of the terminal currents and the operating criterion can be represented as:

$$| dI_1 + dI_2 + dI_3 | > Max (| dI_1 | + | dI_2 | + | dI_3 |) \quad (2.5)$$

where d indicates an incremental current which is the superimposed current due to a fault. The improved scheme utilized communication links for data transmission between the terminals of the teed-feeder and the average operating time is 20ms

2.1.2.3 Algorithms Based on Superimposed Components

The differential schemes based on extracting the fundamental phasor components suffer from inherent time delay in their operation, and those based on amplitude comparison and incremental superimposed component principles lack sensitivity firstly because the restraining quantity is arbitrarily chosen, and secondly by considering the maximum phase load current as the restraining quantity, the relay is prone to failure. However, a relay can be arranged to compare either the total time variation of the differential and bias modal current or their superimposed components, thereby improving the relay performance.

A fault occurrence on a transmission line can be considered as equivalent to superimposing a voltage at the point of fault which is equal and opposite to the prefault steady state voltage. The postfault voltage and current components may be considered as being made up of the prefault steady-state components and fault injected components as follows:

$$\begin{aligned} V_{post} &= V_{pre} + \Delta V_{fault} \\ I_{post} &= I_{pre} + \Delta I_{fault} \end{aligned} \quad (2.6)$$

Superimposed components ΔV_{fault} and ΔI_{fault} are simply the differences between the total time variation of the signals and a projection of their steady-state (pre-disturbance)

values. They contain all the essential information regarding the travelling wave components, if present, whose relative magnitude is considerably enhanced when the prefault signals are removed from the fault generated travelling waves. A protection relay algorithm based on superimposed components of the signal rather than total variations has a number of distinct advantages over the former and they are: (i) faster operation, (ii) higher fault resistance coverage, (iii) immunity to error caused by prefault loading; (i) and (ii) are attained by virtue of the fact that the threshold levels associated with such a relay are lower.

Aggarwal & Johns [2] presented a new high speed current differential protection scheme for application to three-terminal transmission lines. The relay decision process is based on the superimposed components concept. The basic relay operating principles hinges upon a time variation of the differential quantity $D(t)$ and a bias quantity $B(t)$ using the instantaneous values of the modal currents at the master end P and slave ends Q and R of a diagram as given in reference [2]. If $i_p(t)$, $i_q(t)$, $i_r(t)$ are the instantaneous values of the CT secondary current at terminals P, Q and R respectively, then the two quantities $D(t)$ and $B(t)$ at the master P end are given in continuous form by:

$$\begin{aligned} D(t) &= i_p(t) + i_q(t) + i_r(t) \\ B(t) &= i_p(t) - i_q(t) - i_r(t) \end{aligned} \tag{2.7}$$

It can be seen from equation 2.7, a solution given by a typical combination would be such that, under normal operating conditions or external fault conditions, the differential signal $D(t)$ is very small and the bias $B(t)$ is of a relatively large value; conversely, for internal faults, $D(t)$ would be approximately equal to the fault path current, and is large enough to cause tripping.

In its simplest form, the relay would operate for faults when the magnitude of the differential quantity $D(t)$ exceeds a percentage K_B of the bias $B(t)$ by a certain pre-defined threshold value K , i.e.:

$$| D(t) | - K_B | B(t) | \geq K_S \quad (2.8)$$

The relay was implemented and tested by Husseini [23] in laboratory using simulated fault current waveforms which were generated in real time through a local programmable transmission line (PTL). Its operating times for a majority of faults were in the range of 4 to 6 ms. Since this relay requires wide bandwidth data transmission (at least 96kbits/s for two aerial mode signals), a large bandwidth and reliable communication link is essential for the implementation of this type of relay scheme.

2.1.3. Communication Links

From the foregoing, it is apparent that in differential relaying, current differential protection schemes are the most popular type currently in use for power system protection purposes. They are inherently selective, suitable for high-speed operation, and capable of good sensitivity. However, they require the following two operating conditions: (i) the instantaneous current waveforms at the remote and local ends need to be converted into electronic levels at the point where CTs are installed, (ii) digital or analogue data at the remote ends need to be transmitted from the switch yard to remote end for comparison with the local currents within the protection equipment. Since the transmission routes for the data information system are in the vicinity of the power apparatus which generate large electromagnetic noise, it is apparent that there is a high risk of corruption of the electronic low level transmitted data. Hence, a reliable communication link is required for the efficient operation of the developed relay.

Over the years, many types of data channels have been, to some degree, successfully applied in the control and protection of power system transmission networks. These range from electrical channels such as line carriers, pilot-wire and telephone lines, to microwave radio and recently, optical fibres. The choice of one specific channel is

governed by various factors which depend on the type of protection and the requirements of the types of applications and more importantly, the reliability and the security of the systems.

Most of the aforementioned, except optical fibres, are to a certain extent affected by the presence of power system fault transient waveforms, and electrical and electromagnetic interference (EMI). More importantly, they suffer from restricted capacity and are usually only suitable for short distances and lower speed protection because of their high signal attenuation.. This is particularly so for metallic pilot wires and leased telephone circuits due to the effects of induced voltage and ground potential rise. EMI on a data transmission system is thus a major problem from the view-point of system reliability. For long-haul transmission, a large number of repeaters must be introduced along the transmission line and this affects reliability and causes considerable time delays. However the evolution of the fibre optic industry and the advent of reliable and affordable fibre [6] has provided a very attractive alternative. Fibre optic communication channels provide many advantages over conventional channels and they are:

- (i) Large-length bandwidth. Because of its wide bandwidth and low attenuation (less than 0.3dB/km at $\lambda_0 = 1.55\mu\text{m}$ [8]), fibre often is the lowest-cost transmission medium per channel kilometre.
- (ii) Low installation and operating costs. The wide bandwidth and low loss increase repeater spacing , thereby reducing costs.
- (iii) Electromagnetic and other form of interference immunity. Fibre is a dielectric waveguide. It therefore is not affected by, nor does it radiate, electromagnetic energy. It is immune to crosstalk from adjacent (coated) fibres and does not conduct ground currents that would affect the signals.
- (iv) High-quality transmission. As a result of the noise immunity of the fibre transmission path, fibre routinely provides communication quality that is orders of magnitudes better than copper or microwave. The general standard bit-error-rate (BER) for a fibre transmission link is a 10^{-9} minimum, with 10^{-11} or better as the normal.

This is in contrast to the BER 10^{-5} to 10^{-7} for copper and microwave system.

(v) Nonconductor. Fibre does not conduct electricity. It therefore can be installed in applications where shock and explosive hazards exist. It does not conduct lightning and therefore is a means of protecting against outages (due to communication channel failures) in lightning-active regions.

(vi) Small physical size. Several fibres can be installed into an earth wire with little difficulty; therefore fibres can be protected by the earth conductor and installed along power transmission lines.

(vii) Environmental stability. Fibre retains its transmission characteristics where are virtually unaffected by environmental extremes encountered in normal installations. Only extreme cold(-20 to -40 °C) causes an increase in attenuation to various degrees, depending on the cable design. With coax, temperature can have an effect problem on performance. Water has little effect whereas with copper cable, it causes rapid performance degradation.

(viii) More security of communication channels than microwave channels. Because fibre does not radiate a field of electromagnetic energy, it is inherently secure unless physically contacted or distorted. If the waveguide is contacted or distorted such that a portion of the optical energy field propagating in the cladding or core is diverted, then the security can be compromised. In this event, however, the fibre and terminating equipment can be designed to detect the loss of energy or resultant perturbations in the modal patterns and initiate an alarm.

In recent years, a number of FOL applications in power system have been published [25, 35, 59, 60, 61]. A few new transmission line protection schemes [2, 3] are proposed by using FOLs, such as the development of a new high speed 3 terminal line protection scheme and a differential line protection scheme for power system based on composite voltage and current measurements.

2.2 Fibre Optic System

In this section, the basic concepts of fibre optic systems are introduced. Firstly an overview of a historical fibre optic development is given. This is followed by fibre optic classifications, and a listing of some properties of optical fibre. Finally the application of optical fibre in communication links and the application of fibre optic voltage and current sensors in power system are briefly described

2.2.1 Historical Developments of Optical fibres

From Alexander Graham Bell's experiments with his photophone in 1880 up until 1950, optical communications remained in the concept stage. In the early 1950s, Briam at American Optical developed the first optical fibre bundles for image communication. Due to high loss, these were not practical for communications. Attenuation of fibres remained in the 1000dB/km range even into the mid-1960s.

It was not until late 1960, when Maiman at Hughes Research announced the operation of the first laser, that optical communication began to be of more practical importance. The first generation of communication systems were atmospheric, but the atmosphere made a poor communications medium due to scatter and unpredictable weather interference. Interest in fibre as the communication medium began in 1966 when Kao and Hockham at Standard Telecommunications Laboratory predicted that by removing the impurities in glass, 20dB/km attenuations would be achievable, whereby fibre could become a practical communications medium. In 1970, Maurer, Keck and Schultz at Corning Glass Works succeeded in fabricating such low-loss fibres. The fibre-optic revolution began.

The first fibre optic systems in the 1970s were short and used principally for military applications, where harsh electromagnetic environments could benefit from the dielectric properties. The first fibre optic prototype telephone systems were

implemented by the Bell System and General Telephone in 1977. In the same year, Corning Glass Works reported achieving 0.5dB/km attenuation at $\lambda_0=1200\text{nm}$. Systems development based on graded index fibre at 3 to 5dB/km began in 1978 for both military and telephone applications.

The capacity and lower attenuation of single mode fibre were needed in order to make long-haul fibre link applications practical. In 1983, a number of factors came together to revolutionize the fibre industry. The first major production of single-mode fibre was occurring at AT&T Bell Laboratories. The price of single-mode fibre was driven almost overnight from about \$1.50 to less than \$0.50 per metre. Therefore the wide-scale commercial fibre revolution had truly begun.

By 1985, long-wavelength operation at $1.55\mu\text{m}$ had become a practical option, although most systems were still designed for $1.3\mu\text{m}$. From there on, intensive research aimed at the fundamental understanding of the loss mechanisms and dispersion properties of glass fibres pressed forward. Today laboratory samples of fibres with a loss of 0.15dB/km at $1.55\mu\text{m}$ have been reported.

In 1970, Corning Glass Works developed long (hundreds of meters) waveguide fibres with losses of only 20dB/km. This formally started the age of optical waveguide telephony and also began to have an impact in power system. In 1983, Erickson presented a report on fibre optic applications in electrical substations to the IEEE/PES 1983 winter meeting in New York. Two years later, a further tutorial course [26] on fibre optic applications in electrical power systems was conducted. Meanwhile a few practical optical fibre applications in power systems were announced [59, 62], such as development of a PCM current differential relaying system using fibre-optic data transmission. These messages manifested that this rapidly maturing fibre optic technology had become very important to the power engineering community.

2.2.2 Optical Fibres

Optical fibre is a dielectric waveguide that propagates electromagnetic energy principally in the visible and infrared of the electromagnetic spectrum. When this optical energy is modulated, it can be used to transmit information over the length of the fibre.

In this subsection, the classifications of optical fibre are listed in Table 2.1, followed by the basic operation of light beams in a fibre. Finally single-mode fibre properties are described.

2.2.2.1 Classifications

An optical fibre is produced by forming concentric layers of cladding glass around a core region. The core region maintains the low-optical-loss property necessary for the propagation of optical energy. The higher the refractive index, the slower the optical energy propagates. When a high-refractive-index glass core is surrounded by the lower-index cladding material, the light energy is contained within the higher-index core due to the reflection at the interface of the two materials. A parameter Δ corresponding to the wavelength difference refractive index of the core and cladding is described by reference [24] as:

$$\Delta = \frac{(n_1^2 - n_2^2)}{2n_1^2} \approx \frac{n_1 - n_2}{n_1} \quad (2.9)$$

where n_1 is the maximum core refractive index (centre), n_2 the cladding refractive index, and Δ is a measure of the relative difference between a fibre core refractive index n_1 and the fibre cladding refractive index n_2 .

Generally optical fibres are of two types; the single-mode fibre (SMF) and the multi-mode fibre (MMF). Typically $\Delta = 0.002$ for a SMF and $\Delta = 0.02$ for a MMF. A

SMF has a smaller core diameter and can support only one mode of light propagation. The refractive index profile of its core is usually a step-index type. In a MMF, the core diameter is much larger than that of a SMF. The core index profile of a MMF can be either a step-index or a graded-index type. In a graded-index MMF, the core index profile is designed to vary with the radius to meet the requirement for a minimum modal dispersion effect. A plastic lossy coating and a thick jacket usually surround the cladding to prevent damage and to increase the strength of the fibre. A detailed classification of the most commonly used optical fibres are listed in Table 2.1.

In table 2.1, the fibres are arranged in two general categories, SMF and MMF. Under the SMF division, there are subdivisions as (a) simple step-index type SMF, (b) w-index type SMF, (c) triangle-index type SMF. These are ideally suited for long-haul FOLs. The simple step-type-index SMF is also used as fibre optic sensor. The polarisation-controlled SMF are also listed under SMF category as (d) elliptical core fibre and (e) the bow-tie fibre. They have a polarized-maintaining property and are often used for fibre optic sensor applications. Under the MMFs, (f) is the step-index type and (g) the graded-index type. They are often used for short-haul communication links.

2.2.2.2 Basic Operations

Fig.2.1 illustrates the mechanism in the simplest class of fibre design, the step-index type MMF. As the light ray strikes the surface of the fibre, it is refracted slightly toward the centre of the core by an angle that is a function of the glass-to-core interface refractive-index difference. On the inside of the core, it propagates and eventually strikes the core/cladding interface. If the angle is less than the critical angle defined by the refractive-index difference, it reflects the light back into the core and continues to propagate in this fashion. If the light ray strikes the core/clad interface at an angle greater than the critical angle, it passes into the cladding. Since the cladding is coated with some lower-refractive-index plastic buffering material, the light

propagating in the cladding is absorbed and lost.

The critical angle θ_c within the fibre is equivalent to an acceptance angle at the fibre surface. The sine of this angle defines the numerical aperture (NA) of the fibre. NA is therefore a parameter that defines the cone of optical-energy acceptance for the fibre. It is critical to the coupling efficiency and propagation properties of the fibre. The relationship for numerical aperture in a step-index fibre is as follows:

$$NA = \sin\theta_c = K\sqrt{(n_1^2 - n_2^2)} = Kn_1\sqrt{2\Delta} \quad (2.9)$$

Where K is typically 0.94 - 0.98 [24]. The large acceptance angle of step-index type MMF makes it ideal for coupling to large-area light-emitting diodes (LEDs). The major limitation effect on fibre bandwidth, however, is that the propagating rays follow many different path lengths. Rays from a light pulse entering the fibre at one instant in time are spread at the other end since some rays are delayed longer than others. In order to improve the bandwidth of the fibre while maintaining a reasonable NA, a class of MMF called graded index was developed. It possesses the property that, it tends to curve the rays toward the axis of the core. The parabolic core index shows the rays propagating down the axis more than those of a higher angle, therefore equalizing the time it takes any rays to propagate the length of the fibre. But this optimization is wavelength-dependent and bandwidth is limited by practical limitations on profile design and production control. In practice, the graded index is limited to about 1 to 2 GHz-km for production fibre. This is not adequate for long-haul applications. However the answer to this requirement is SMF. If the propagating energy in the fibre can be restricted to one mode, then there can be no differential path distances or time-delay differences between modes. The bandwidth, from the standpoint of waveguide design, would be infinite. Because of only one mode existence, there are no higher mode losses, SMF thus has lower fibre loss than MMF. Both large bandwidth and low loss make SMF to be used for long-haul data transmission.

2.2.3 Single-Mode Fibre Properties

SMF has many positive properties with regard to the way that light travels through it and therefore warranting a better understanding of its properties in order for it to be used in wide applications. In this section, modelling some important fibre optic properties are introduced which will be used in subsequent chapters for modelling both FOLs and FOCSs.

2.2.3.1 Optical Dispersion

Light is affected by the interaction with matter. When the light travels through glass fibre, the refractive index of fibre is altered with light wavelength, thus the refractive index n becomes a function of λ . The variation $dn/d\lambda$ is defined as optical dispersion. The effect of dispersion is such that optical modes propagate down the fibre at different rates and arrive at the receiving end at different times. This has the effect of spreading the signal energy in time. If the signal is a digital pulse, it arrives reduced in peak amplitude and spread in time (pulse broadening) and if the signal is analogue modulated, then the dispersion effect appears as a bandwidth limitation.

2.2.3.2 State of Polarization

The state of polarization (SOP) of the electromagnetic wave is characterized by the orientation of the electrical-field (E-field) vector representing the propagating wave along a transmission path. The wave is said to be linearly polarized if a single E-field vector or the two components along the x- and y-axes, E_x and E_y have the same phase. If the two components along the x- and y- axes are equal in amplitude, but are optically 90° out of phase, then the resultant wave is a circularly polarized light. If the two components along the x- and y- axes are not equal in amplitude, but are optically 90° out of phase, then the resultant wave is an elliptically polarized light. When polarized light passes through a medium possessing birefringence, the output light will have its

SOP changed. The detection of a change of the SOP can be used to build fibre optic current sensors.

2.2.3.3 Birefringence

An idealized SMF allows only one fundamental mode HE_{11} to exist [17]. This is because HE_{11} mode has no cut-off frequency. When a fibre core diameter decreases to form a SMF, the HE_{11} mode is always present in the SMF. In theory, if an ordinary SMF is perfectly constructed so that it is circularly symmetric and laid in a straight line, linearly polarized light launched at the input will maintain this state along the whole length of the fibre to the output. In practice, however, such conditions are not possible. Fibre cannot be made as perfect cylindrical structures so that intrinsic imperfections, as well as external factors such as bends, stress and changes of temperature, produce optical azimuthal inhomogeneities. Linearly polarized input light can be decomposed into linearly polarized orthogonal components with different phase velocities. Thus coupling between the two orthogonal components and random variations in the relative phase velocity cause the SOP to vary along the length of the fibre in an unpredictable way.

In FOCS designs, the SOP of the modes in a fibre must be strictly controlled. A Faraday rotation current sensor normally requires the fibre to have either very low linear birefringence or a high circular birefringence. Three types of birefringence are described below:

(1). Linear Birefringence

Practical SMFs with an asymmetric cross section propagate two orthogonal linearly polarized modes with axes aligned with those of fibre symmetry. These modes propagate unchanged in the absence of length-dependent variations in the fibre, with a difference $\Delta\beta$ (the birefringence) in their propagation constants. The fibre

polarization properties can be modelled [32] as a discrete linearly birefringent element whose retarder $R(z)$ is proportional to fibre length z .

$$R(z) = \Delta\beta \cdot z \quad (2.10)$$

Two commonly used parameters which are useful in describing fibres with length-invariant properties are the normalized linear-birefringence B and the mode beat-length L_p at which the polarization state is periodically repeated:

$$B_l = n_x - n_y = \frac{\lambda}{2\pi} \Delta\beta = \frac{\lambda}{2\pi} \frac{R(z)}{z} \quad (2.11)$$

$$L_p = \frac{2\pi}{\Delta\beta} = \frac{\lambda}{B_l} \quad (2.12)$$

Where n_x and n_y refer to the refractive-indexes for polarized light along the fibre principal x - and y - axes, respectively. In general, B_l comprises both stress anisotropy B_s (e.g. bow-tie fibre) and a waveguide shape components B_w (e.g. elliptical core fibre).

For a low-birefringence fibre, an increase in L_p is desired. However, in a polarization-maintaining fibre (see section 2.2.3.4), to decrease the value of L_p is required (i.e. increase the birefringence) in order to reduce the likelihood of power transfer from the required to the unwanted electric field mode. It is well known from coupled-mode theory that maximum power transfer between electric field modes occurs when the period of external perturbations matches that of L_p . The natural stiffness of the fibre resists perturbations with periods less than about 1mm [47]. Thus if a fibre is required to resist external perturbations, it is wise to select L_p to close to the target 1mm.

(2). Circular Birefringence

The most common cause of circular birefringence is fibre twist [63]. Twist introduces a torsional stress [5]. For a uniform twist rate ξ and absence of linear birefringence,

the fibre can be modelled as a discrete polarization rotation element with rotation $\Omega(z)$ which increase linearly with fibre length

$$\Omega(z) = (g' \xi) z \quad (2.13)$$

where the experimental value $g' = 0.073$ for silica [63]. The two normal modes are now left and right circularly polarized with difference in propagation constants $\Delta\beta_{circ} = 2g'\xi$. The circular birefringence is thus:

$$B_{circ} = \frac{\lambda}{2\pi} \Delta\beta_{circ} = \frac{\lambda}{\pi} g' \xi \quad (2.14)$$

This equation shows that twist fibres introduce circular birefringence.

(3). Elliptically Birefringence

If constant linear and circular birefringence are simultaneously present, the two fibre modes are elliptically polarized. An elliptically birefringent fibre can be fabricated by spinning a high linear birefringence fibre (e.g. a bow tie fibre) during drawing. The resulting fibre has a permanent frozen-in rotation of the birefringent axes. The polarization eigenmodes are elliptically polarized, and the elliptical birefringence is dependent on the linear birefringence of the unspun fibre and the twist rate. The modal birefringence B_e for the elliptically-polarized eigenmodes of the fibre is expressed as [22]:

$$B_e = \frac{\lambda}{2\pi} (\sqrt{(\Delta\beta)^2 + 4(\xi - g'\xi)^2} - 2\xi) \quad (2.15)$$

The above formula implies both linear birefringence and circular birefringence. For a spun fibre no shear stress is present since the fibre has a permanent twist; thus $g'\xi = 0$ [5].

2.2.3.4 Polarization-Maintaining Single-Mode Fibre

Because of asymmetric cross section or external factors such as bends, stress, vibration and changes of temperature, SMF is not truly single mode in that two modes with degenerate polarization states may propagate down the fibre. To remove the degeneracy, a number of SMFs have been designed to propagate a single linear polarization state. A stable state of linear polarization is required for many fibre sensors. To achieve this, it is necessary to reduce the amount of coupling between the two mode components by introducing strong linear birefringence into the fibre. There are a number of approaches to making this fibre and preserving polarization. The simplest method of fabricating a high birefringence fibre is an elliptical core fibre (e.g. waveguide shape birefringence B_w as shown in Table 2.1 (d)). By having a high enough index differential between the core and the cladding regions, light launched with linear polarization aligned along the major axis will be preserved in its polarization state. The disadvantages of this approach are that the small core diameter required makes launching and coupling between optical elements difficult, and the high index of refraction difference between the core and cladding makes the fabrication of low-loss fibre more difficult. To solve these problems, fibres with built-in stress (i.e. stress birefringence B_s) were developed, such as bow-tie fibre [7] as shown in table 2.1 (e). The stress causes an refractive index difference along a major and a minor axis, and light launched along the major axis is preserved in its polarized state.

2.2.3.5 Faraday Effect

The Faraday effect is a well known optical phenomenon which was discovered by Faraday in 1845, and can be exploited in optical fibres to measure magnetic field. If an external magnetic field, H , is applied to a suitable medium such that there is a field component parallel to the direction of linearly polarized light in the medium, it is found that the direction of polarisation of the emergent light has been rotated through an angle F , such that:

$$F = V_H \int_z H dz = V_H \times \frac{I}{\pi D} \times z \quad (\text{rad}) \quad (2.16)$$

$$f = F / z = V_H \times \frac{I}{\pi D} \quad (\text{rad} / \text{m}) \quad (2.17)$$

where F is the total Faraday rotation, f is the unit Faraday rotation, H is the magnetic intensity (A/m), I is the electrical current (A), D is the diameter of the fibre coil (m) and the Verdet constant V_H is found to be [44]:

$$V_H = 2.0 \times 10^{-35} \times \frac{c^2}{\lambda^2} \quad (\text{rad} / \text{A}) \quad (2.18)$$

where c is speed of light. If the fibre length is z , the number of turns of fibre coil is N , then $z = N \pi D$, so:

$$F = V_H N I \quad (\text{rad}) \quad (2.19)$$

This equation clearly shows that the total Faraday rotation is proportional to I and N .

2.2.4 Fibre Optic Links

The guiding properties of fibre optic can provide a link for communicating information between any two ends. With a light source and photo-detectors, a basic FOL can be setup as in Fig.2.2. In Fig.2.2, the light source may be a LED or a LD, the photo-detector may be a silicon PIN or an APD and the fibre optic may be either a SMF or MMF. The process is that of near-linear conversion of detected optical power back to photo-current. At the input is an optical source driver that converts the input signal to a drive current that intensity modulates the source. The optical source then generates the optical energy that is coupled into the fibre. The energy propagates down the fibre and is attenuated to a degree and distorted by optical dispersive properties. The energy exits the fibre at the other end and may be coupled into a photo-detector. The light energy absorbed in the photo-detector is converted to a photo-current. This photo-current is then amplified in the receiver electronics and converted back to the original

signal format at the output.

The question naturally arising is over what distance can effective communication be established using an optical fibre ? Depending on the application and transmission requirements, a fibre link can be constructed of various materials. In power system industry, distances of over 100km are quite common for protection relay communication purposes. Thus ideally, a long-haul fibre optic communication link (100km and above is considered as long-haul) is desirable without the necessity of having to use a repeater.

At present, there are in general three approaches to the design of a long-haul optical fibre system. The first approach is to use a fibre operating at a wavelength of about $1.3\mu\text{m}$ where the dispersion is close to zero (i.e. silica fibres) and to develop the system using LEDs and PIN diodes. This system is relatively inexpensive to install and operate and is very reliable. To maximize the repeater spacing up to 50km, SMF with a loss factor of less than 0.5dB/km and a fibre dispersion of less than a few picoseconds per kilometre nanometre are required; replacing the LED by a laser (driven by a FET circuit) and using an APD as detector followed by a low-noise FET amplifier could boost the repeater spacing even higher.

The second approach is the use of an ultra-low-loss fibre (0.16dB/km) operating at $1.55\mu\text{m}$ wavelength and a precisely graded fibre to minimize the multipath dispersion effect. LED and PIN diodes can again be used to achieve an inexpensive and reliable operation. Again replacing the lasers and detectors as above would increase the bit rates of transmission and repeater spacing. But some related negative factors such as, dispersion, modal noise, would also be increased. Thus the design of precisely graded indexing of the fibre could be done only by sacrificing the attenuation minimized fibre loss and with added cost.

The third approach is to use a fibre designed as in the second approach but to use a

narrow-spectral-width laser source instead, preferably a single-frequency stabilized light source at $1.55\mu\text{m}$ wavelength. The performance of this combination, plus the application of coherent detection method, could be improved by 1-100 times over the second method. The obstacle to this approach is that construction of these laser sources is at present very expensive and the laser is relatively short-lived. Therefore it is not suitable for practical applications as yet.

2.2.5 Measurements

Fibre optic technology entered the telecommunication field only around 1970s, yet, its rapid progression in practical applications is almost unparalleled by any other scientific or technological development in history. Although most current applications of fibre optic technology have been concentrated in the field of telecommunications, the improvements of the techniques and cost reductions in opto-electronic components combined with mass commercial production has led to other developing and emergence of new product areas of fibre optic sensors.

Optical fibres have many advantages over metallic wires when they are employed as communication links. Besides the advantages of low loss and low cost, they are immune to many environmental changes such as the EMI and electrical noise. However, the environment does have some influence on the operating characteristics of optical fibres. For example, temperature, electric or magnetic field, and even the radius of curvature of fibre bending may affect optical fibre performance. Therefore, these effects should be taken into account and avoided, if possible, in telecommunication system. On the other hand, we can also take advantage of the sensitivity of fibre optic to these environmental effects by building sensors to measure these effects. In fact, with a little care, many types of sensors can be built to sense various physical perturbances such as acoustic, magnetic, temperature, and radiations. Indeed, with this dielectric construction, it can be used in environments involving high voltages, high temperatures, electrical noise, chemical corrosion, or other stressing

conditions. The application of fibre optic sensors can be found in large industries, such as aerospace, chemistry, biology, medicine, mechanical and in particular high voltage power system industry. Besides, the cost of fibre optic voltage and current sensors is significantly reduced compared with that of conventional voltage transducers and CTs due to the obviation of very expensive high voltage insulators required in the use of the latter. The main advantage is of course the wide bandwidth in the case of the former.

In the power industry, most optical current/voltage sensor systems in use or under development nowadays are based on the Faraday effect, the Pockels effect or Kerr effect [26]. The Faraday effect is a magneto-optic effect. The application of a magnetic field to a material which exhibits the Faraday effect produces a change in the index of refraction of the material. By designing a device for measuring the difference of the index change, a current sensor is obtained. The Pockels and Kerr effect is electro-optic effect where the change in the index of refraction is proportional to the electric-field E and to the square of the electric field E^2 , respectively. These effects can be used for voltage measurement.

Recently two typical types of sensors have been under development; all fibre sensors and fibre with bulk magneto-optic material sensors as shown in Fig. 2.3(a), (b) and (c), respectively. The fibre with bulk magneto-optic material sensors (see Fig.2.3(b)) were originally proposed by Rogers [54]. Recent work on this type of sensors was presented in [10, 11, 67]. They have the advantages of mechanical stability, freedom of choice of magneto-optic material, and the use of relatively low-cost components such as MMF, LED sources, and PIN photo-detectors. In comparison with all fibre sensors, the disadvantages of the bulk magneto-optic material with fibre sensors are less accurate, large size and sensitive to environment noise.

In an all fibre current sensor, a SMF is used as the sensitive element (see Fig.2.3(a)). Many efforts have been made in the development of this interesting type of sensor [38] [41]. This sensor is in its early development stage. Applications of the sensor have so

far been limited to laboratory instruments and field trials and have so far only been carried out under very carefully controlled conditions.

These and similar sensors use methods either based on Faraday rotation of polarized light in optically active media such as magneto-optic crystal as in Fig.2.3(b), or directly in the glass fibre as in Fig.2.3(a), or based on the change in the SOP of light in birefringent media such as electro-optic crystals exposed to high voltage (Pockels effect) as in Fig.2.3(c), where the polarization changes are converted to light-intensity changes with an appropriate polarization analyzer.

In the case of current sensing with magneto-optic crystals or SMF, light traverses in a magnetic field H and has its plane of polarization rotated (Faraday effect) by an amount F given by $F = V_H \times H \times z$. z is the optical path length in the crystal or the SMF. The H is generated by the electric current I , to be measured in a conductor nearby the crystal or SMF sensing head. The polarization modulation from the Faraday effect is converted to intensity modulation using the polarization analyzer. By properly adjusting the polarization bias between polarizer and analyzer, the detected output light-intensity changes can be made approximately linear with magnetic field H . In the all fibre sensor case, $H \times z$ is approximately equal to NI , where N is fibre coil turns and I the current.

Similarly the sensing method for voltage is based on the Pockel effect. A ferro-electric rather than magneto-optic crystal is used. An electrical voltage in the crystal induces a birefringence, which causes a change in the state of polarization of light travelling in the crystal. The polarization change is converted to an intensity change as in current sensor, using a polarization analyzer.

A major dissimilarity between these two sensing methods is that the Pockel effect is reciprocal while the Faraday effect is not. This means that if light travelling through a ferro-electric crystal is reflected back on itself, the polarization change resulting from

the birefringence cancels and the light exits the crystal in the same polarization state as with which it entered. With a magneto-optic crystal or fibre in a magnetic field (as with other types of optical activity), this cancelling effect does not happen, so the change in polarization is cumulative and not reversible when the light travels in the reverse direction.

2.3 Related Work

In this section, an overview is given of a few typical FOLs and FOCSs that are currently in use or which have been evaluated through the CAD methods. A comparison is made between different system and where possible , some of the existing problems are highlighted.

In the first subsection, three practical FOLs in power system protection, suitable only for short distance FOL are described. A new transmission line protection scheme, assuming an ideal FOL, is described, and the main theme of the thesis is indicated. The followed subsection describes two recent works of FOL computer simulation studies. In the final subsection, FOCS applications in power system are discussed.

2.3.1 Fibre Optic Links for Power System Protection

In EHV power system protection, it is evident that FOL applications have attracted considerable amount of attention; but few systematic studies of practical FOL applications in power system are available. In this respect much work has been done in Japan. One of the earliest practical FOL applications in power system was developed by Takagi et al. [62] specifically for power control and protection. In their system, the FOL was composed of LEDs, step-index MMFs and PIN-photodiodes. The characteristics of these optical components were:

- (i) Light sources was LED operating at light wavelength $0.8\mu\text{m}$, the output power was -15dBm , and supply voltage was $+5\text{V}$.

- (ii) optical receiver was PIN-photodiodes, receiver sensitivity was from -40 ~ -20 dBm for meeting BER = 10^{-9} requirement [17]. Its maximum receiver bandwidth was 4Mbits/s.
- (iii) Fibre cables were MMFs with 0.4 of NA. Fibre losses was less than 10dB/km, fibre bandwidth was 15MHz every km.

In their design of the FOL, the maximum transmission distance without repeaters was 2km, the maximum data bit rate B was 2Mbits/s. Four fibres were used for voltage data, current data, synchronizing data, and a spare one respectively. This was outdoor equipment with operating temperature range $-20^{\circ} \sim 70^{\circ} \text{C}$ and moisture range 40 ~ 100%.

A few years later, Suglyama et. al [59] also developed a practical FOL applied to a PCM current differential relating system for EHV (275kV) power system protection. In their FOL system, LDs were used as light emitting element, MMF with a loss of 2.30dB/km was selected and total application fibre length was 8.5km. The optical receiver used was an APD, a standardized PCM terminal equipment was used for the general use of the optical fibre installed for private communication channels for EHV power system protection. The equipment was connected to a relay by the primary PCM group signal (transmission speed was 1.544Mbits/s) which is the standard form providing 24 multiplex data channels, each channel having a data rate 64kbits/s.

In 1989, Suzuki et al.[61] developed a FOL for a new substation protection and control system in an EHV substation. Since the FOL was applied within the substation, an optical local area network (LAN) was used to connect a digital relay which was located close to the outdoor power apparatus. The data transmission form followed the IEEE 802.4 token passing bus as the LAN protocol. In the FOL, again the light source was an LED at light wavelength $0.85\mu\text{m}$ with output power -13 ~ -15dBm, fibre optic cable was MMF with an average loss of 3dB/km, data transmission speed was 10Mbits/s

In all of the three practical FOL systems, no repeaters were used. Ideally repeaters should not be present in a practical FOL application in power system, so that the FOL can take the EMI advantage and thus provide a reliable communication data link.

Current differential protection scheme needs the support of good FOL in order to be suitable for long-haul transmission line protection. Recently with the availability of FOLs that are capable of transmitting information with a sufficiently large dynamic range over a distance compatible with the requirements of EHV line protection, several new transmission line protection schemes have been proposed. Aggarwal and Johns [2,3] presented two new high speed differential protection schemes for power transmission line protection. The protection schemes have been simulated using CAD techniques. They can provide very fast tripping speeds of about 4-6ms (section 2.1.2.3), but such a high speed tripping signal can only be guaranteed by using wide band FOLs. However almost all the work in this area has assumed an idealised data transmission over FOLs. There has not been any systematic study, performance analysis and evaluation of a FOL from a practical point of view. One of the main themes of the work described in this thesis is thus to contribute to this part of the knowledge.

2.3.2 Computer Simulation of Fibre Optic Links

A system is a collection of interacting elements or components that act together to achieve a common goal. Therefore, the study of FOLs should start with the design, analysis and simulation of the functionality of its components. FOLs are very complex in nature and computer-aided simulation and design provides an ideal platform for the extensive study of these systems. There has been some work published in this area. Personick [48] presented a receiver design for digital fibre optic communication systems. Dogliotti et al. [13] described their work for estimating error probability in fibre optic transmission systems. But it was not until 1984 that the use of CAD techniques in a digital light waveguide system was reported by Duff [14]. He analyzed

each component model and later integrated them into a system. The component and staged performance results were obtained by using a general software package such as SPICE and SYSTID [18]. The system model consisted of: (i) an optical source model in which laser and LED spectrums were modelled as a normalized Gaussian function, (ii) a fibre transfer function which included the effect of fibre loss and source (Laser or LED) spectrum, (iii) receiver PIN and APD models, (iv) receiver noise model. Furthermore a bit error rate performance criterion for the system was described.

From a technical point of view, techniques for the modelling and analysis of digital communication systems fall into three classes. Those based on analytical calculations, those based on time-domain Monte Carlo simulations, and hybrid approaches based on a combination of simulations and analytical calculations. Analytical calculations are computationally fast but are limited in their applications because of the necessary assumptions and approximations needed to model the physical phenomena. Time-domain simulations are more flexible but Monte Carlo simulations of digital lightwave links operating at low error rates require very long input sequences (eg., BER at 10^{-9} needs at least binary data sequences $> 10^9$). Although a discussion of both the simulation methods and time-domain techniques applicable to digital lightwave links was given by Duff [14], no end-to-end simulation results were presented.

Elrefaie et al [15] described a hybrid approach which combined Monte Carlo simulation and analytical techniques. Monte Carlo simulations were used to derive estimates of statistical distributions that were not analytically tractable, and the simulation-derived distributions were combined with other analytically distributions. A time-domain simulation model for the functional blocks in single-model digital lightwave communication links was presented that included:

- (i) LED as optical source, its waveform was modelled by turn-on and turn-off response.
- (ii) SMF as communication links
- (iii) PIN and APD detectors

The simulation process was carried out by using a software package SYSTID. Problems arose from using general electromagnetic wave communication system CAD package SYSTID [18] for specific problems of optical transmission. Some of the special features arising from the optical transmission configuration were not well dealt with and more insight into the system operation could not be obtained. For example, they described the LED optical source by simply using turn-on and turn-off signal pulse response (rise and fall times) model. This may not be true when a laser is employed as the optical source. In fact, an optical envelope output of a signal pulse modulated laser has pulse transient and chirp phenomena [9]. Furthermore communication software commercial packages are complex and usually inefficient to interface with other CAD programs such as power system protection CAD programs.

2.3.3 Fibre Optic Current Sensors

In contrast to the well-established area of fibre optic communication application, FOCSs are still in their infancy. Particularly their applications in power systems. One of the early FOCS applications was presented by Cease & Johnston [10]. It was a magneto-optic current transducer (MOCT). Problems of using conventional oil-filled CTs on EHV and ultra high voltage (UHV) circuits include:

- (i) Potential for catastrophic failure
- (ii) Saturation under fault current conditions
- (iii) Ferro-resonance effects
- (iv) Hysteresis effects
- (v) High voltage if output leads are opened
- (vi) Large/Heavy requiring substantial supports
- (vii) Accuracy limited to 0.3 percent
- (viii) Subject to EMI effects
- (viii) Limited current measurement bandwidth

The benefits of using a MOCT are:

- (i) Does not contain oil, therefore can not explode
- (ii) No saturation under fault current conditions
- (iii) Does not contain iron, therefore no ferro-resonance effects
- (iv) No hysteresis effects
- (v) Output is a fibre optic cable(no charge of open circuit)
- (vi) Small/light weight (sensor weights less than 2 pounds)
- (vii) Accuracy limited by electronics
- (viii) Immunity to EMI
- (viii) Very large current measurement bandwidth

The presented a MOCT configuration is similar to the functional block diagram in Fig.2.3 (b). It is perceived that except for a polarizer and an analyzer, the rest of the optical components used are very much the same as those in a fibre optic communication system. They are: a LED, fibre optic, PIN diode and low noise pre-amplifier, low pass filter. The operating principle of the MOCT is: light emitted by the LED is transported by an fibre optic to the polarizer. After being polarized, the light is injected into the Faraday rotator material, and exited through an analyzer. The analyzer is a polarization rotated 45° from the first polarizer. The net result is that an intensity modulated light beam exits the analyzer. This intensity modulated light is then transported through another fibre optic to a PIN diode for demodulation and results in an output of the amplifier of a voltage signal that is proportion to the current flowing in the conductor. Therefore current is measured. Some measurement results and discussions were conducted.

Although MOCT has greatly improved the sensing performance compared to conventional CT, as Cease & Johnston [10] have pointed out that there is a limitation in the ability of the electronics to reproduce amplitude and frequency information contained in the optical signals from the rotator. But they have failed to give reasons as to why this is so. In fact, irrespective of whether Faraday rotation is induced by a current through a fibre or bulk crystal type (in section 2.2.5), it does affect the

accuracy of sensitivity in measurement because of such factors as fibre bend, vibration and temperature.

MacDougall et al., [41] have presented an all-fibre optic current sensor for power systems. By using polarizing fibre instead of normal polarizer and analyzer, the system costs are reduced. Mathematical models have been used to describe the all-fibre current sensor. The sensor response P is given as follows:

$$P = \frac{2F \sin \sqrt{\Delta \beta^2 + (2F)^2}}{\sqrt{\Delta \beta^2 + (2F)^2}} \quad (2.20)$$

In the all-fibre current sensor, the main optical components of the sensor design are a coil of low birefringence SMF (to be placed around the electrical conductor whose current is to be measured) and two sections of polarizing optical fibre, both of which are spliced to opposite ends of the fibre coil.

When a fibre functions as a sensing element, the fibre must be turned into a coil. Moreover multi-turns and a small diameter of the fibre coil are required as a single turn of the fibre coil does not provide enough detectable Faraday rotation under normal operating conditions. However, multi-turns of fibre introduce birefringence from bending. The equation (2.20) clearly reveals the distorting effect by $\Delta\beta$ (either intrinsic or induced). A more quantitative assessment of this problem can be obtained by analysing the sensor performance in certain operating regions.

A problem central to the development of a practical FOCS device is that of linear birefringence in the fibre, invariably present as a result of intrinsic manufacturing imperfections (elliptical core, anisotropic stress) or induced by bending, vibration and transverse pressure. Thus special fibres designed to overcome these problems were considered. They developed a low-birefringence fibre by using a carefully controlled annealing method [58]. This method is annealing of stress in fibre and provides

improvement of reduced linear birefringence problem. However, although the resultant fibre exhibits very low internal birefringence, it is sensitive to external perturbations such as vibration, coiling and applied stress due to poor polarization-maintaining property (See section 2.2.3.4). In practice, such external perturbation induced birefringence should be taken into account, e.g. vibration occurs when current sensor is operating outdoors and in windy conditions. This vibration-induced birefringence, not like fibre bending, is much more difficult to predict when the sensing coil is prepared.

Huang et al. [22] have presented the theory of imperfect nonconventional SMF. Spun and twisted fibres with various imperfections (such as fibre cross-sectional ellipticity, bending, transverse applied fields) were taken as examples to illustrate the general theory. Spun fibre is made by spinning a fibre during the manufacture drawing process so as impart a rapid built-in rotation of the fibre birefringent axes. Twisted fibre is made by simply twisting a fibre. Theoretically, both spun and twisted fibres are the same, but torsional stress is induced by twisting and the number of turns per meter that the fibre can be twisted to before breakage is about 100 turns [64]. They described the modes in these nonconventional fibres. When $\xi \gg \Delta\beta$, the modes of either twisted or spun fibre are elliptically polarized or quasi-circularly polarized. B_e of the spun fibre was described in equation (2.14) and from which following points can be presented:

(i) If $\xi \gg \Delta\beta$, the spun elliptical birefringence B_e can be extremely small. This highly-spun fibre has full Faraday sensitivity, but almost zero residual birefringence and consequently a lack of resistance to external perturbations.

(ii) If $\Delta\beta$ is high and ξ is small ($\xi \ll \Delta\beta$), spun elliptical birefringence B_e is mainly represented by the $\Delta\beta$. High $\Delta\beta$ fibre has good polarization maintaining property, but very low Faraday rotation sensitivity.

By compromising above two extreme cases of ξ and $\Delta\beta$, Laming & Payne [38] have developed a spun highly-birefringent (SHB) fibre optic current sensor where a large rate ξ is used, thus it allows the fibre to have a high $\Delta\beta$ to be used at the same time

and still keep B_e at a low value. The sufficient residual B_e is present to ensure good resistance to external perturbations (vibration, packaging effects) while maintaining good Faraday rotation sensitivity. This allows very small, multi-turn coils to be wound and enables an extension of the sensitivity of fibre current monitors into the submilliamp region.

A problem of the SHB fibre approach is that the polarization effect of the sensing fibre has a dependence upon thermal stress due to its highly linear birefringence and therefore the magnitude of the induced B_e in the spun fibre is temperature-dependent.

Most recently some signal processing schemes are developed which successfully overcome the temperature-related problems. These schemes make twisted fibre and spun fibre become ideal practical current sensing elements for wide area applications.

These signal processing schemes are:

(i) Reflect-back configuration (RBC) [38]. A mathematical model is presented but not complete as no mirror model has been included for the CAD study of SHB optical fibre current sensor. Also RBC will remain unstable in current reading due to the birefringence changes with temperature.

(ii) Sagnac interferometer configuration (SIC) [12]. It uses a temperature-stable spun elliptical-core FOCS. The scheme is based on a novel Sagnac interferometer constructed with spun birefringent fibre that is largely insensitive to temperature variations while remaining sensitive to Faraday rotation. The principle of removing temperature effects is to distinguish between the effects of temperature and Faraday rotation because the Faraday effect is nonreciprocal and temperature effect is reciprocal. The theoretical analysis is interesting, but with not enough experimental results to support it.

(iii) Mirror Faraday Rotator configuration (MFRC) [49,50]. It is a novel technique, completely passive. It is able to reduce the influence of environmental noise on the measurement of currents or magnetic fields with an FOCS. The method is based on the

use of a mirrored Faraday rotator (MFR) in conjunction with a highly twisted low-birefringence optical fibre. Also the experimental results shown that MFR configuration can greatly reduce reciprocal noise including vibration and temperature.

Highly twisted low-birefringence optical fibre is made the use of the stress-optic effect to only produce a weak circular birefringence, providing the fibre with some polarization-maintaining properties, also twisting the fibre after drawing is difficult when a large twist is required and furthermore results in residual photoelastic rotation [64] which is highly temperature sensitive.

SHB fibres are constructed by drawing a fibre from a spinning linearly birefringent preform. The resulting fibre has much better polarization-maintaining properties than twisted fibre. While unlike the twisted fibre, it is not circularly birefringent but has rotating elliptical birefringence (equation 2.14), so spun highly birefringence optical fibre can be used instead of the twisted low-birefringence optical fibre in the case of FOCS. Before a fully acceptance of the spun highly birefringent fibre current sensor application into power system protection, some detailed study and performance demonstration of the FOCS would be very much helpful. Unfortunately there has not been a report of such results while have been publicly accessible. In this thesis, a systematic CAD study of SHB FOCS with MFR configuration for power system protection is presented in a later chapter.

2.4 Fault Waveform Simulations

In this section, some typical fault waveforms that will be used in the evaluation of FOLs and the testing of FOCS performance in the application of power systems are described.

It is important in the design and development of high speed digital protection systems, that the voltage and/or current waveforms presented at the relaying point can accurately

represent the real signals presiding on a power system network. It is also important to use these waveforms through actual FOL and FOCS under different considerations of system design. The ultimate judgement of a FOL operation or FOCS is to test its performance under field conditions. But due to the nature and the scales of application of such systems, economical and technical constraints are imposed. Therefore, fault simulations for FOL and FOCS testing are of particular importance.

In reference [30], a fault simulation principle was presented. In an off-line digital simulation of faulted EHV transmission lines with particular reference to very-high-speed protection is considered as one of the most appropriate methods for power system modelling. A CAD simulation package for two and three terminal transmission lines has been developed at the University of Bath, UK, with the aim of deriving precise current and voltage information of different EHV power system network configurations before and after a fault. Another approach is to use the Electromagnetic Transients Program (EMTP) software package. In this simulation, modern transmission line theory is used to accurately predict the fault transient behaviour of two-terminal EHV overhead lines. Full advantage is taken of the many years of experience in the development of sophisticated simulation programs. These programs have been developed from the studies of the theory of natural modes developed by Wedephol [66]. A detailed explanation and all digital simulation results of the fault transient phenomena on 2-terminal EHV transmission line are given in Appendix A.

2.5 Summary

In this chapter an attempt has been made to provide adequate background theory, research and development related to plant in power system transmission line protection schemes, fibre optic links and fibre optic current sensors, with an explanation of their basic operating principles. In section 2.1.2, three types of current differential line protection schemes are presented. Those are the algorithms based on phasor, the algorithms based on time variation, and the algorithm based on superimposed

components. It has been shown that the algorithm based on superimposed components has operating times for a majority of faults in the range of 4 to 6 ms, but it requires wide bandwidth data transmission links, therefore a large bandwidth and reliable communication link is essential for the implementation of this type of relay scheme. In section 2.3 a survey is conducted to show how other researchers approached the problem of system modelling. In each case, the advantages, if any, and existing problems of each approach, are described, and further explained why it is needed to develop our own modelling system. In short, the problems with these approaches are one or more of the following:

- (1) in the power system line protection case, algorithms based on superimposed components can provide high speed current differential protection line scheme, while in the research of new high speed current differential protection scheme [2], only an assumed ideal fibre optic link is used in the typical line protection scheme.
- (2) in computer-aided design of a fibre optic communication link case, a general-purpose software simulation package was used. Therefore it was difficult to look at the laser models and difficult to interface with other CAD software programs, e.g. a line protection scheme software program.
- (3) in fibre optical current sensor case, only twisted fibre was used as current sensor sensing head in a MRFC, also no CAD study of a spun fibre optic current sensor with the MRFC has been reported.

In the next three chapters, the detailed simulation methods and models will be presented which are new extensions of the computer simulation models of a FOL and a FOCS. The building up of these models allows us to relatively easily investigate FOL and FOCS application in power system line protection scheme and do not suffer from the problems mentioned above.

Table 2.1 Classification of Optical Fibres

Fiber Type						
Single Mode Fiber			Multimode Fiber			
(SMF)			Polarization Control Fiber		(MMF)	
Simple index (a)	W-Fiber (b)	Triangle (c)	Elliptical core (d)	Bow-tie Fiber (e)	Simple index (f)	Graded index (g)
n-Profile						
(a)	(b)	(c)	(d)	(e)	(f)	(g)
Application						
Long-haul Sensor (a)	Dispersion control (b)	Long-haul (c)	Sensor Polarization control (d)	(e)	Short-haul (f)	Short-haul Dispersion reduced (g)

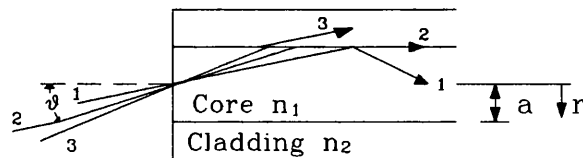


Fig. 2.1 Numerical aperture $\sin \theta_c$ defined for a step-index fibre where θ_c the critical angle, n_1 the core index, n_2 the cladding index and ray 1, 2 and 3 represent three different light angles into the fibre

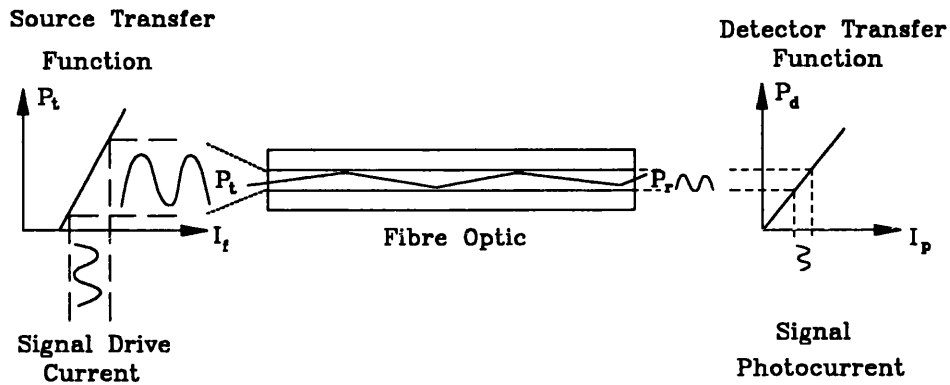


Fig. 2.2 Basic fibre link operation, the electric-optical and optical-electric conversion process. P_t source optical power, P_r received optical power

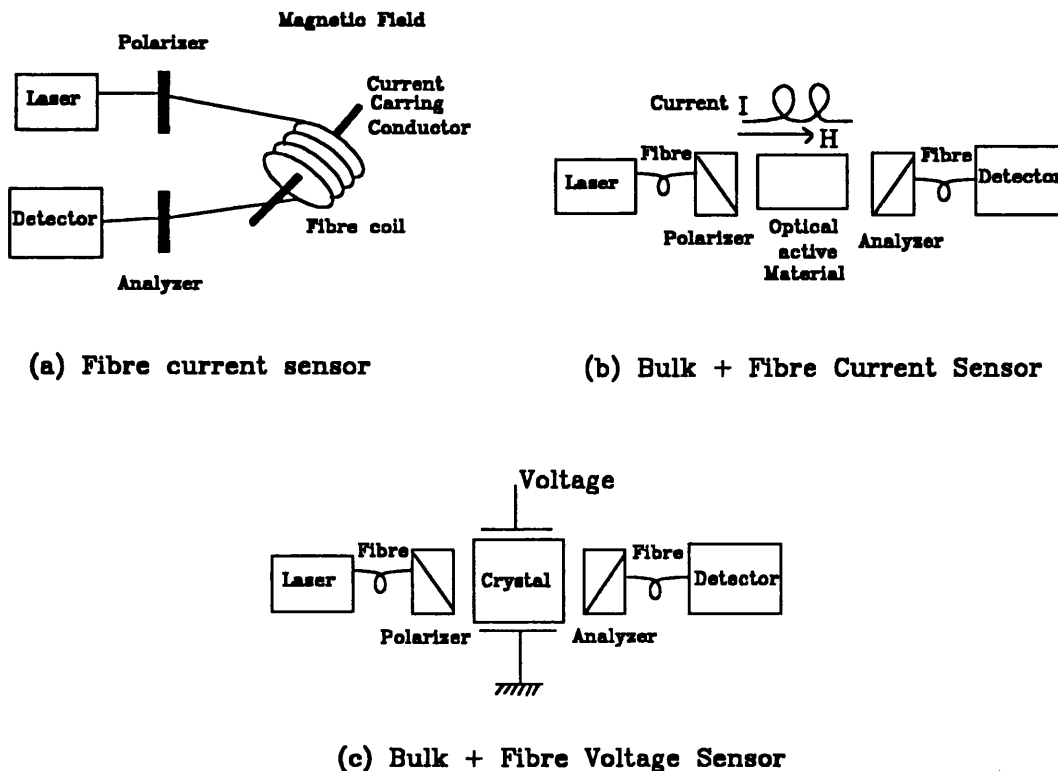


Fig.2.3 Diagram of fibre optic polarimetric current and voltage sensors

CHAPTER 3

FIBRE OPTIC LINKS SIMULATION

3.1 Introduction

FOLs for power system protection relaying are finding widespread use in the Electricity Supply Industry. In this respect, it is important to ascertain the effect of FOLs on the signals transmitted due to the limitations imposed by the various components within the FOLs. However, it is not always physically possible to carry out the experiments in practice, and even so, it was to be with high-cost, and very time-consuming. Fortunately, with the large computation power problem, high speed and extensive availability of computers, computer aided design and simulation provide a flexible alternative.

In this chapter, a complete CAD simulation of a FOL is presented. In section 3.2, the use of pulse code modulation (PCM) for transferring analogue signals to digital non-return-zero (NRZ) binary signals is established, and then a FOL configuration is determined. In section 3.3, the theoretical models of the FOL are described: they are light source spectra, a laser equivalent electrical circuit model, a SMF model and a receiver model. Three main noise models are also considered including shot noise, circuit noise and mode partition noise. In section 3.4, the FOL design considerations are discussed: these include bit error rate (BER) estimation, dispersion power penalty and power budget calculation. These can be used to estimate the maximum link span length. In section 3.5, the simulation process of a FOL is described. Firstly a model of each individual component is simulated and evaluated, then a complete CAD model of a FOL is presented and finally the FOL simulation performance and the simulation signal waveforms received by the PIN diode detector are presented.

3.2 Fibre Optic Link Designing Considerations

In this section, a brief discussion of the main considerations in the selection of FOLs is described. The reasons for using a PCM, LD and SMF are established and besides, each of the components modelled within the FOL configuration are described.

3.2.1 Pulse Code Modulation

A fibre optic is a waveguide in which light propagates. Thus an electrical signal must be modulated into a light wave before it is possible to describe its characteristics when passing through a FOL. There are three basic types of modulation techniques: amplitude modulation (AM), phase modulation (PM) and frequency modulation (FM). In AM, the optical amplitude varies with the electrical signal. In PM or FM, the optical phase varies or frequency with the signal or the derivative of the signal. When a current signal is modulated by a light source, the optical signal generated by the light source can be described by an AM signal. It should be noted that neither PM nor FM are recommended for fibre optic data communication since both APD and PIN photo-detector are optical signal envelope devices, they are insensitive to either light sources 'phase or frequency' variation within the light source.

In a FOL, analogue transmission is not commonly used because of the nonlinear light-versus-current characteristics of optical sources, in particular lasers. For semiconductor lasers, their optical power output is only within the one to several mW range. For an AM light source, a small output power produces a small optical signal. After passing through a FOL, the optical signal power will be attenuated. A small optical signal power level results in a low signal-to-noise ratio (SNR) at the receiver. Digital modulation (on-off keying), on the other hand, is easily accomplished with these sources by the modulation of light source bias current. Simplicity in the modulation of the pulse, coupled with the extremely wide bandwidth of optical fibres have made binary digital transmission the method chosen for the majority of FOLs.

An analogue signal has to be converted to a digital binary signal before it can be transmitted through a digital FOL. One simple and popular method called pulse code modulation (PCM), is often used to convert analogue signals into digital binary signals. A PCM system takes regular recurring samples of the information signal's amplitude; converts (Pulse Amplitude Modulation - PAM) them into binary codes consisting of a series of pulses (ones and zeros) representing the sample's amplitude and then combines a number of these pulses into a single digital bit stream. Because the PCM bit stream has only two states, 'on' (binary one) and 'off' (binary zero), it is insensitive to the non-linearities of the transmission system. PCM signals can be regenerated at a receiver by amplifying the incoming signals, slicing them and re-timing them as long as the receiver can distinguish between 'on' and 'off' states. If no noise or distortion gets added to the transmitted information signals, the PCM signal can be regenerated many times without adversely affecting the quality of the original message signals. This means that PCM signals can be transmitted over a long distance without degrading the quality of the information signals. For power system protection relaying, this is particularly important since it is quite common for fault information to be transmitted over a long distance to the decision devices. PCM type signal have also been employed for a short distance of a FOL application in power system protection relay [59]. Another attractive reason to use PCM application is that, it is easy to use a microprocessor to implement terminal equipment with a time multiplexed digital channel.

In PCM, two common frame structures in the public telephone network are the standard T₁ transmission system (used in US and Japan) and the European system (used in European countries). In the former, the frame time is 125 μ s and it contains 193bits with 24 multiplexed channels, so its transmission data bit rate (B) is 1.544 megabits per second (Mbits/s); in the latter, a primary digital multiplex signal specifies a frame with 32 channels which comprises of 30 data channels, one frame synchronization data channel, and one signalling channel. Each frame has a B of 2.048Mbits/s.

In digital protection relaying systems, some PCM frame structures based on their data information normally differs from the public telephone network. However, from the economical point of view it would be better to choose either the standard T_1 transmission system or the European system since the latter are more readily available. Reference [59] chosen the standard T_1 PCM frame structures.

3.2.2 Link Configuration

A FOL is a type of physical transmission facility where the signal is in the form of a light wave and is transmitted through a cylindrical glass fibre core. Its signal is guided through the fibre from its transmitted point to its detected point, thus the link can be described as an end-to-end data communications link.

As mentioned in chapter 2, Duff [14] and Elrefaie [15] presented some work on computer simulation of FOLs. The first described the general concept with no reference to end-to-end data transmission system simulation results. The second gave some simulation results with a LED as light source, but since the simulation process was carried out by using a general purpose software package, it is difficult to interface with other power system protection CAD programs.

The major components of an end-to-end optical fibre system for power system protection relaying consist of a laser as an optical transmitter, SMF and PIN or APD as optical receiver as shown in Fig.3.1, where a multiplexer (MPL) multiplexes three analogue signals. These analogue signals can be either 3-phase voltages or three-phase currents. The three channel multiplexed signals then go to an analogue-to-digital converter (A/D) to convert into digital data. The use of a MPL is economical since it saves two A/D chips. As long as the A/D converting time is less than $80\mu\text{s}$, it can convert three analogue signal within $250\mu\text{s}$ (4kHz sample rate). It should be mentioned that if the unit protection is of the current differential type, then it is necessary to transmit only three phase current. However, if the protection is based on composite

voltage and current signals, it is necessary to transmit six signals over the FOL. In the latter case, a fast A/D convertor with a converting time less than $40\mu\text{s}$ is required. The parallel A/D data are transferred to PCM data by going through a parallel-to-serial converter (P/S). For a 4kHz sampling data rate a 12bit A/D will produce 48kbits/s PCM data, several phase voltage and current signals can be multiplexed into the standard PCM frame of European system (2.048Mbit/s) or T₁ transmission system (1.544 Mbit/s). Such PCM signals are then injected into an optical transmitter (based on a laser) termed the electrical-to-optical device (E/O). The optical signal goes through a SMF over a certain distance to reach the other end where the receiver is either a PIN or APD photo-detector termed an optical-to-electrical device (O/E). After the O/E, a received optical power is converted into a received current signal. Since the O/E produces shot noise when it receives optical power, shot noise has to be considered at the received current signal to become a noisy current signal. The noisy current signal is amplified by a preamplifier (G) to make its amplitude reach a certain level. Because the preamplifier has circuit noise etc, thus more noise will be added on to the already noisy current signal. Because noise has an infinite bandwidth, a low pass noise filter (NFL) with a bandwidth equal to the transmission data bandwidth has to be implemented. The latter allows only the transmission signals (and some limited noise within this bandwidth) to pass. Finally, the decision circuit (DeC) distinguishes the signal from the noisy current signal and regenerates a noise-free signal. Because of the noise nature of the noisy current signal, the decision circuit can sometimes make a wrong decision. The actual 'on' or 'off' signal becomes 'off' or 'on' signal, and therefore a bit error occurs. In a sequential binary data signals, many bit errors would occur. The ratio of bit error with respect to the sequential data signals is called bit error rate (BER). BER is often used as a parameter for judging a FOL performance. After the decision circuit, a de-multiplexer (DMPL) separates three digital signals which can go through three serial-to-parallel converters (S/P), and finally digital-to-analogue converters (D/A) recover the three original analogue signals. A detail description of all the individual components in Fig.3.1 is given in the following sections.

3.3 Modelling of a Fibre Optic Link

This section is concentrated on the theoretical models of fibre optic link for a communication system in general and for power system protection relays in particular. In section 3.3.1, two unmodulated time averaged laser spectrum models and an equivalent circuit of a laser transfer function model are represented. In section 3.3.2 the SMF transfer functions are described. In section 3.3.3, the models of a receiver with a PIN or an APD photodiode and a FET preamplifier are given and finally, models of shot noise, circuit noise and mode partition noise (MPN) are described.

3.3.1 Optical Source Models

Semiconductor LDs and LEDs are the most important optical sources in current FOL use. The optical output power is usually directly modulated by varying the drive current signal. For PCM, the drive current signal can be sequential non-return-zero (NRZ) binary signal pulses. A source for FOL modelling may be characterized by three parameters, the optical output waveform, the time averaged spectrum (unmodulated source spectrum), and the output noise (source noise). The first two parameters are the most important and in general, the optical output waveform is defined as an impulse response $h_1(t)$ and the optical source spectrum defined as $S(\lambda)$. $h_1(t)$ is regarded as the optical source transient response to a pulse signal at the source driving circuit. For LEDs, it may be simply presented as the a time of turn-on and turn-off response to a pulse signal. For most LDs, it appears as a transient phenomena. The optical source spectrum is often useful when computing fibre loss, fibre dispersion and mode partition noise, etc. Typical time-average spectra for two different semiconductor LDs and an LED are given in Table.3.1. The laser spectra exhibit N-longitudinal modes and a nearly Gaussian gain envelope. Both the laser and LED spectra may be modelled as a normalized Gaussian functions given as:

$$S(\lambda) = \frac{1}{\sigma_0 \sqrt{2\pi}} e^{-(\lambda - \lambda_0)^2 / (2\sigma_0^2)} \quad (3.1)$$

A typical commercial spectral width, σ_0 , of for LED emission is between 20nm and 100nm, and for a typical commercial laser σ_0 is from 2nm to 10nm. The LED has a more stable characteristic than the laser. The lasers also have additional unique noise sources, such as mode partition noise (MPN) and chirping. These require actual laser diode (LD) models. Because the application is for long-haul transmission line protection relaying, laser sources can meet the requirement due to their large optical power, and thus it is necessary to design the LD modes.

The transmitter of the system is modelled as a semiconductor LD intrinsic equivalent electrical circuit operating with an N-longitudinal mode spectrum output over a 1.3 μ m or 1.55 μ m light wavelength range. A common practical N-longitudinal mode semiconductor laser is considered due to economical requirements in the system design, but many advanced lasers which are more expensive would produce even better results since these lasers, for example, distributed-feed-back type LDs operate in single or near single longitudinal mode. For a typical N-longitudinal mode LD, its spectrum $S_{zz}(\lambda)$ without a modulated signal is given as:

$$S_{zz}(\lambda) = \sum_{i=-N/2}^{N/2} a_i S(\lambda - i\Delta\lambda) \quad (3.2)$$

where the amplitude a_i is the amplitude of the i th N-longitudinal mode, $\Delta\lambda$ is the distance between adjacent spectral lines; and $S(\lambda)$ is a Gaussian distribution given by equation (3.1). As long as a_i in equation (3.2) is a Gaussian decay function, the laser spectrum $S_{zz}(\lambda)$ envelope can be regarded as the same as equation (3.1), while for N-longitudinal mode laser, MPN has to be taken into account. MPN will be described in section 3.3.3.4.

In order to describe the LD impulse response function $h_1(t)$, firstly, it is necessary to

use the laser rate equation of a single lasing mode corresponding to a single emission wavelength. This is given by Adams [1]:

$$\frac{dn_e}{dt} = \frac{i}{e} - \frac{n_e}{\tau_e} - A(n_e - N_0) s_p \quad (3.3)$$

$$\frac{ds_p}{dt} = A(n_e - N_0) s_p - \frac{s_p}{\tau_p} + \rho \frac{n_e}{\tau_e} \quad (3.4)$$

Where n_e is the electron density, s_p the photon density, i the injected or pump current (signal), e the electron charge, τ_e the spontaneous emission lifetime, τ_p the photon lifetime, the optical gain $g = A(n_e - N_0)$, A the optical gain parameter, N_0 the minimum electron density required to obtain a positive gain, and ρ the fraction of the spontaneous emission going into the lasing modes.

The solution for both small-signal and large-signal response can be obtained by directly solving the laser rate equations using a numerical method. An alternative method is to analyze the laser rate equations by using equivalent electrical circuit techniques. The latter is used to simulate the LD dynamic operation where the LD is modelled by a parallel RLC electrical circuit. A detailed derivation of the equivalent electrical circuit model related to laser rate equation is given in Appendix B.1. In a later section, simulation results obtained by using the equivalent circuit model will show that the equivalent electrical circuit model can be used as the laser impulse response function $h_1(t)$. The $h_1(t)$ is the inverse Fourier transform of laser transfer function $H_1(\omega)$ which is the ratio of the optical power to signal current. In order to get a comparison result between the laser rate equation solution and the laser equivalent circuit solution, the results need to be examined from a different point of view. The photon density transfer function is represented by $H_{\text{photon}}(\omega)$ which is the ratio of photon density to signal current. Both $H_1(\omega)$ and $H_{\text{photon}}(\omega)$ are given in equation (B.1-24) and (B.1-25) in Appendix B.1 as:

$$H_1(\omega) = \frac{I_L(\omega)}{I_1(\omega)} = \frac{1}{LC D(j\omega)} \quad (3.5)$$

$$H_{\text{photon}}(\omega) = \frac{S_1(\omega)}{I_1(\omega)} = \frac{1}{eG_0 LC D(j\omega)} \quad (3.6)$$

Where $D(j\omega) = (j\omega)^2 + j\omega[R_{sc}/L + 1/RC] + [1 + R_{sc}/R]/(LC)$, $S_1(\omega)$ is the spectrum of the photon density, $I_1(\omega)$ is the spectrum of laser injection current, $G_0 = A(n_e^\circ - N_0)$, n_e° is the steady state of n_e from equation (3.2) and (3.3), and the parameters of the laser equivalent electrical circuit model R , C , R_{sc} , L , are represented as in equation (B.1-20) in Appendix B.1. The laser impulse response $h_1(t)$ thus can be obtained by taking inverse Fourier transform of $H_1(\omega)$.

3.3.2 Single-Mode Fibre Transfer Function

In this section, firstly, the transmission limitations and the negative factors causing the FOL impairments are described and then the SMF impulse response function $h_2(t)$ is presented.

3.3.2.1 Fibre Loss

Fibre loss is attributable by the mechanisms that are related to the effects of fibre material properties (e.g. Rayleigh scattering, impurity absorption), geometrical effects (e.g. micro-bends, core geometry variations), joint effects (e.g. couplers, splices), etc.. The main loss of an optical fibre results from its material effect. This arises from Rayleigh scattering, impurity absorption and etc. The SMF loss coefficient can be modelled by the simplified equation [65]:

$$\alpha(\lambda) = A_L \lambda^{-4} + B_L + C_L(\lambda) + O_L \quad (dB / km) \quad (3.7)$$

where $\alpha(\lambda)$ is the total fibre loss, A_L (dB- $\mu\text{m}^4/\text{km}$) is the Rayleigh loss coefficient, B_L (dB/km) represents wavelength-independent losses, $C_L(\lambda)$ is intended to encompass all other intrinsic wavelength-dependent losses including an absorption loss from water

(OH⁻) contamination, and O_L includes all extrinsic losses such as the fibre coupling loss, and splicing loss.

In equation (3.7), the fibre intrinsic loss is $A_L\lambda^4 + B_L + C_L(\lambda)$ in which the $A_L\lambda^4$ and $C_L(\lambda)$ are the function of the light wavelength λ . The use of a different λ results in a different fibre loss. Two low loss regions are located at around $\lambda_0 = 1.3\mu\text{m}$ and $\lambda_0 = 1.55\mu\text{m}$. Their typical losses are given as following:

- (i) The loss is about $0.37 \sim 0.4\text{dB/km}$ near $\lambda_0 = 1.3\mu\text{m}$
- (ii) The loss is about $0.18 \sim 0.2\text{dB/km}$ near $\lambda_0 = 1.55\mu\text{m}$.

Because of the difference of low fibre loss in these two regions, long-haul FOL design are normally selected for operating at around either $\lambda_0 = 1.3\mu\text{m}$ or $\lambda_0 = 1.55\mu\text{m}$.

For other losses, O_L is considered to be about 0.1dB/km for SMF. Losses in MMF have the same fundamental limitations from Rayleigh scattering and long-wavelength infra-red absorption as SMF. The losses of MMF are generally higher than those of SMF due to high dopant concentrations which result in large compositional fluctuations scattering. Also a MMF has higher sensitivity to microbend losses and particularly of the high-order modes than SMF due to the large core. Because of higher fibre losses, MMFs are only suitable for short distance of FOL.

Typical data for the estimated fibre average loss in practical use are shown in Table 3.4 where SMF total losses are 0.5dB/km at $\lambda_0 = 1.3\mu\text{m}$ and 0.3dB/km at $\lambda_0 = 1.55\mu\text{m}$. For MMF, the average fibre loss would be 1.3dB/km at $\lambda_0 = 1.3\mu\text{m}$.

3.3.2.2 Dispersion

Fibre dispersion $dn/d\lambda$ includes several dispersion components such as material dispersion, waveguide dispersion. In a SMF, material dispersion is the main factor that limits data transmission bandwidth. Material dispersion ($d\tau/d\lambda$) causes light propagation delay differences in a fibre at different λ . The light propagation total delay

is called the group delay $\tau(\lambda)$ which is a function of λ and has Taylor series components $d\tau/d\lambda$ at λ_0 . For the many types of fibres available, all have a slightly different material dispersion which can be measured. The $\tau(\lambda)$ of a type of SMF with a zero dispersion at $1.310\mu\text{m}$ wavelength can be approximated by a three-term polynomial as follows [21]:

$$\tau(\lambda) = a_d + b_d \lambda^2 + c_d \lambda^{-2} \quad (3.8)$$

Where $a_d = -34.74\text{ns/km}$, $b_d = 10.11\text{ns}/(\text{km}\cdot\mu\text{m}^2)$, $c_d = 29.83(\text{ns}\cdot\mu\text{m}^2)/\text{km}$. From this equation, $d\tau/d\lambda = 0$ at $\lambda_0 = 1.310\mu\text{m}$, $d\tau/d\lambda = -0.87\text{ns}/(\text{km}\cdot\mu\text{m})$ at $\lambda_0 = 1.3\mu\text{m}$, $d\tau/d\lambda = 12.65\text{ns}/(\text{km}\cdot\mu\text{m})$ at $\lambda_0 = 1.55\mu\text{m}$.

3.3.2.3 Fibre Transfer Function

In Fig.3.1, the fibre impulse response is presented as $h_2(t)$ in the time domain. Its Fourier transform form is represented by the fibre transfer function $H_2(\omega)$. Two methods of obtaining SMF transfer functions are discussed in this section. One is based on the optical power domain called the baseband fibre transfer function $H_2(\omega)$. The other is based on optical electric field domain to directly calculate the ensemble of the optical power $\langle P(t) \rangle$ in the time domain. The first model assumes that the fibre is a linear system in the optical power domain, which is a valid assumption over the ranges of input bit rates and fibre lengths applicable to current direct detection FOL. It allows attenuation and dispersion dependencies with wavelength λ caused by light source spectrum $S(\lambda)$ to be taken fully into account. Its frequency domain transfer function $H_2(\omega)$ for a modulated optical signal propagating over a fibre length, z , of SMF can be written as follows:

$$H_2(\omega) = \int S(\lambda) A(z, \lambda) e^{-j\omega z (\tau_0 + \frac{d\tau(\lambda)}{d\lambda}(\lambda - \lambda_0) + \dots)} d\lambda \quad (3.9)$$

where:

- (i) $S(\lambda)$ is the light source optical spectral density as a function of λ given by

equation (3.1);

- (ii) z is the fibre length ;
- (iii) $A(z, \lambda)$ is the normalized optical power loss coefficient of the fibre and it is assumed that $A(z, \lambda)$ is a much more slowly varying function over the wavelength range of source spectrum $S(\lambda)$. It can thus be approximated as a constant $A(z, \lambda) = e^{-\alpha(\lambda)z}$ due to the fibre loss being a function of length where $\alpha(\lambda)$ is the fibre total loss as given in equation (3.7);
- (iv) $\tau(\lambda) = \tau_0 + d\tau/d\lambda(\lambda - \lambda_0) + \dots$ is the group delay per unit length for the fibre at λ_0 , where $\tau_0 = n/c$, c is the speed of light, and n the fibre refractive index. τ_0 only causes a delay and has no influence on the shape of the output signal and group delay $\tau(\lambda)$ is given by equation (3.8).

The baseband transfer function of the SMF may be calculated by substituting equations (3.1) (3.7) (3.8) into (3.9), to give:

$$\begin{aligned}
 H_2(\omega) &= A(z, \lambda) \int \frac{1}{\sigma_0 \sqrt{2\pi}} e^{\frac{(\lambda-\lambda_0)^2}{2\sigma_0^2}} e^{-j\omega z \frac{d\tau}{d\lambda}(\lambda-\lambda_0)} d\lambda \\
 &= e^{-\alpha z} e^{-\frac{1}{2} \omega^2 z^2 \sigma_0^2 \left(\frac{d\tau}{d\lambda}\right)^2}
 \end{aligned} \tag{3.10}$$

where $z^2 \sigma_0^2 (d\tau/d\lambda)^2$ interestingly shows the characteristic of the baseband transfer function whose bandwidth is limited due to the $d\tau/d\lambda$ and the fibre length z . The fibre impulse response function $h_2(t)$ is the inverse Fourier transform of $H_2(\omega)$.

For simulation purposes, a method is used to compute the received optical power of a photon-detector in time domain. The general fibre link impulse response $h_2(t)$ is considered to include a light source spectrum effect. The unmodulated light source has the envelope of optical electric field $\Psi_0(t)$. The fibre baseband impulse response is $g_1(t)$ which is obtained by taking the Fourier transform of the dispersive fibre transfer function $G_1(\omega)$ in equation (B.2-4) of Appendix B. When a signal $x(t)$

modulates a light source, then assuming that the modulated optical signal is $m(t)$, we get $m(t) = h_1(t)*x(t)$. By combining the modulated optical signal, $m(t)$, with the unmodulated source optical field, $\Psi_0(t)$, and the fibre baseband impulse response $g_1(t)$, the output signal of a photodiode is given by the ensemble of the optical power $\langle P(z,t) \rangle$ after a distance, z , in the dispersive optical fibre [42] as:

$$\langle P(z,t) \rangle = \left| \int_{-\infty}^{\infty} g_1(\tau) \sqrt{m(t-\tau)} \Psi_0(t-\tau) d\tau \right|^2 \quad (3.11)$$

After making a few assumptions (these are discussed in Appendix B), a convolution form of the linear optical fibre transmission characteristics is obtained by expanding this equation (Appendix B.2):

$$\langle p(z, t) \rangle = h_0 + \int_{-\infty}^{\infty} h_2(\tau) m(t-\tau) d\tau \quad (3.12)$$

The ensemble average of the optical power $\langle p(z,t) \rangle$ after distance, z , in the dispersive optical fibre is a function of h_0 , $h_2(t)$ and $m(t)$, where:

- (i) h_0 is a constant optical power due to the circuit driver bias above the laser threshold.
- (ii) The fibre impulse response $h_2(t)$ can be calculated by taking inverse the Fourier transform of $H_2(\omega)$ in equation (3.10) when the simple source spectrum is given by equation (3.1), or it can be calculated by taking the inverse Fourier transform of equation (B.2-13) which rewritten as:

$$H_2(\omega) = \frac{1}{2\pi} G_1(\omega) * [G_1^*(-\omega) S_{zz}(\omega)] \quad (3.13)$$

where $G_1(\omega)$ is the dispersive fibre transfer function, the $*$ is the notation representing the convolution calculation, $S_{zz}(\omega)$ is the spectrum of the complex envelope of the source which is the Fourier spectrum of the autocorrelation function of the envelope of optical electric field $\Psi_0(t)$ in equation (3.11). In theory, it can be assumed that the spectrum, $S_{zz}(\omega)$, of the complex envelope of the optical source signal is a Gaussian envelope which is given by equation (3.2)

- (iii) The modulated optical signal $m(t) = h_1(t)*x(t)$ and $x(t)$ is PCM pulse signal and $h_1(t)$ is given by taking fourier transform of equation (3.5).

Equation (3.12) is used as the basis of the CAD study of the FOL simulation model. For a simple Gaussian laser spectrum, the inverse Fourier transform of equation (3.10) is used to obtain the fibre impulse response $h_2(t)$. But for an no Gaussian spectrum, such as an N-longitudinal-mode laser is shown in equation (3.2), equation (3.10) requires an integrated calculation process, however equation (3.13) can provide a simple calculation method since the signal processing methods (i.e. FFT and convolution) can be applied to obtain the fibre impulse response $h_2(t)$. In practice, the laser spectrum is a measurable parameter.

3.3.3 Receiver and Noise Models

The purpose of using an optical receiver is to convert a modulated optical signal back to the electrical signal and to recover the electrical signal from whatever information that had been encoded. Most simple photo-detectors are PIN diodes or APDs. They are ideal AM envelope detectors, and are insensitive to phase or small changes in wavelength. With reference to the optical receiver shown Fig.3.1 again O/E can be either a PIN diode or an APD which acts as a square-law detector and has photo-current output that reproduces the envelope of the received optical power signal. The photo-current signal with added noises is amplified by a low-noise preamplifier. The low-pass filter has the minimum bandwidth required to pass the signal and keep noise as low as possible. The final stage in the receiver is the decision circuit which consists of a comparator, with its threshold level set to the centre of the receiver waveforms as shown in Fig.3.3, to give an equal probability of error for decisions on both 'on' and 'off' signal.

3.3.3.1 Photodiodes

A photo-diode (PIN or APD) operates in a reverse-biased mode such that incoming photons are absorbed in a depleted semiconductor to create a photo-current. In the computer simulation of a receiver model, the use of both PIN and APD detectors are considered in which a digital bit stream consisting of '1' and '0' ('on' and 'off' states) is incident at the data bit rate B. The detected average photo-current signal I_{s1} or I_{s0} in the two states resulting from the detection of an optical signal is given by Personick [48]:

$$I_{s,j} = \left(\frac{\eta e}{h\nu} \right) \langle G \rangle p_j \quad j = 0 \text{ or } 1 \quad (3.14)$$

where η is the detector quantum efficiency, h Planck's constant and ν the optical frequency (c/λ), $j = '0'$ or $'1'$ represents signal 'on' or 'off', $\langle G \rangle$ is the average APD gain, however $\langle G \rangle = 1$ when the photo-detector is a PIN photo-diode, and p_j is the average received power during a single bit.

3.3.3.2 Shot Noise

One of the unpredictable aspects of the output current from a photo-diode illuminated by an average optical signal is a phenomenon known as quantum noise or shot noise. The variance of the noise current model of an APD due to shot noise is given by:

$$I_{ns,j}^2 = 2e \left(\frac{\eta e}{h\nu} \right) \langle G \rangle^2 F(G) P_j k_2 B \quad (3.15)$$

Where η , e , h , ν , j , $\langle G \rangle$ and p_j are the same as in equation (3.14), $I_{ns,j}$ is the rms shot noise current, and k_2 the bandwidth factor of the noise low pass filter, B bit rate, $F(G)$ the excess noise factor of the APDs which is related to the mean gain $\langle G \rangle$ and is represented by a simpler approximation $F(G) = \langle G \rangle^x$ [17]; the empirical value x for good Si (silicon) detectors have $x = 0.25$ and good Ge (Germanium) detectors has $x = 0.9$. Equation (3.15) can also be modelled for a PIN detector when $\langle G \rangle$

and $F(G)$ are 1.

3.3.3.3 Circuit Noise

Presently, field effect transistors (EFTs) are mainly used as a front-end amplifier in an optical receiver due to their low-noise. Most receiver circuits available today are a PIN or APD diode with an FET front-end amplifier. The principal noise sources are thermal noise from the FET channel conductance g_m , the photodiode load resistor R_L , gate leakage (dark) current I_d , and FET 1/f-noise corner frequency f_c (defined as the frequency at which 1/f-noise which dominates the FET noise at low frequencies and has a 1/f power spectrum). Fig.3.2 shows a simple diagram of a photo-detector which consists of a photo-diode, a load resistor, and a common-source FET preamplifier. The variance of the equivalent amplifier input noise $I_{nc,j}^2$ is given by Kasper [33] as:

$$I_{nc,j}^2 = \frac{4k_B T}{R_L} k_2 B + 2eI_d k_2 B + \frac{4k_B T \Gamma}{g_m} (2\pi C)^2 f_c k_f B^2 + \frac{4k_B T \Gamma}{g_m} (2\pi C)^2 k_3 B^3 \quad (3.16)$$

where T the absolute temperature, C the total input capacitance, Γ the FET channel noise factor (typical value 1.1), k_2 , k_3 , k_f are the normalized noise-bandwidth integral values and only depend on the input-optical-pulse shape. For rectangular non-return-zero (NRZ) input pulses and output pulses with a full raised-cosine spectrum, their values are $k_2 = 0.562$, $k_3 = 0.0868$ and $k_f = 0.184$. For a rectangular return-zero (RZ) input pulse with a 50% duty cycle, the values are $k_2 = 0.403$, $k_3 = 0.0361$ and $k_f = 0.0984$.

3.3.3.4 Mode Partition Noise

MPN is an important factor when using an N-longitudinal mode laser source and a SMF in a FOL. It is caused by the instant fluctuation of the power distribution among the laser N-longitudinal modes and the differential dispersion-induced fluctuations in

the recovered power. The variance of this noise is given by the following equation [46]:

$$I_{mpj}^2 = \frac{1}{2} k^2 (\pi B)^4 [A_1^4 \sigma_0^4 + 48A_2^4 \sigma_0^8 + A_1^2 A_2^2 \sigma_0^6] \quad (3.17)$$

$$\text{where } A_1 = -\frac{d\tau}{d\lambda} z, \quad A_2 = \left(\frac{d^2\tau}{d\lambda^2} + \frac{2}{\lambda} \frac{d\tau}{d\lambda} \right) z \quad \text{and}$$

where I_{mpj} is the rms mode partition noise, k a statistical factor that varies from 0 to 1. k varying from 0.5 to 0.6 can be used for system design prediction using the present MPN theory, $d\tau/d\lambda$ and $d^2\tau/d\lambda^2$ can be calculated by using equation (3.8).

3.4 Design Considerations

In this section, three important FOL design considerations are described. Firstly, a method for estimating BER of a FOL is described, followed by a discussion of dispersion power penalty in the FOL design and finally a method is outlined to calculate link span distance.

3.4.1 Bit Error Rate Estimation

When the transmitted signal is in digital form, the transmission link performance is generally evaluated by data rate B , bit error rate (BER) and time jitter. When B is relative low, the BER becomes the main factor. Within an optical receiver, the signal is normally treated as analogue prior to threshold detection and regeneration. The regenerator performs the function of determining what logical state ('on' or 'off') is represented by the received signal waveform at a specific sample period. It decodes the received signal by comparing the signal amplitude with a set threshold. The presence of noise at the threshold can cause false crossing and, therefore, bit errors. Because a proper decoding depends on the signal level relative to the noise, there is a direct relationship between BER and SNR at the receiver. The amount of noise present

is a function of receiver bandwidth B_N , which in turn is a function of the data transmission rate B .

BER is defined as the ratio of the number of information bits detected erroneously to the total number of bits transmitted. Transmitted bits are sometimes detected as error because noise can cause the signal to appear on the wrong side of the threshold detector during the sampling period. BER is, therefore, a function of the received SNR.

The relationship is statistical, that is, the probability of an error increases as the probability of the noise level exceeding threshold increases. The relationship for binary encoding (on-off) is shown in Fig.3.3, where a noisy current at the detector is shown with Gaussian distributions for both the binary the 'on' state and the binary 'off' state. Note that the noise distribution is larger for 'on' state than for the 'off'. This is because the added optical power for an 'on' state increases the shot noise (refer to equation (3.15)). The threshold, therefore, must be offset for equal probability of error for the two states. The threshold voltage is related to its equivalent photo-current I_{th} in this diagram.

A rigorous calculation of error probability can be found in various references [29]. A simplified form of BER or error probability P_e is defined by the complementary error function as follows:

$$P_e = \frac{1}{\sqrt{2\pi}} \int_Q^\infty \exp(-y^2/2) dy \quad (3.18)$$

where Q is the mean signal to rms noise ratio, and y the actual signal level to rms noise ratio. If the decision level current I_{th} is chosen under condition of $P_{e0} = P_{e1} = P_e$, then Q can be obtained by:

$$Q = \frac{I_{th} - I_{s0}}{I_{n0}} = \frac{I_{s1} - I_{th}}{I_{n1}} \quad (3.19)$$

where two states; 'on' and 'off' of the average signal current are I_{s1} and I_{s0} , the noise currents are I_{n1} and I_{n0} and the decision level current is I_{th} at photo-detector. Eliminating I_{th} in equation (3.18) gives $Q = (I_{s1} - I_{s0}) / (I_{n1} + I_{n0})$. A value of $Q \geq 6$ is normally required to maintain P_e and hence a BER below 10^{-9} [17].

Writing $r = I_{s0}/I_{s1}$ as the off/on extinction current ratio, and $I_{av} = (I_{s0} + I_{s1})/2$ as the average detected current and thus Q becomes:

$$Q = \left(\frac{1-r}{1+r} \right) \frac{2I_{av}}{(I_{n0} + I_{n1})} \quad (3.20)$$

Referring to the above equation, the average current I_{av} can be obtained from equation (3.14). The square of the noise currents I_{nj} are the total variance of the noise currents. As to noise current sources, they are the laser intensity noise due to the unstable lasing power of a laser, MPN due to fibre dispersion, and the circuit noise and shot noise at the photo-detector. In power system protection relaying, long distance protection signalling needs to be considered with transmission B of only a few Mbit/s. It has been found when B is less than about 150Mbits/s, the laser intensity noise can be neglected. Thus in the FOL study model for power system protection relaying, shot noise (equation (3.15)), circuit noise (equation (3.16)) and MPN (equation (3.17)) need to be considered. The various noise contributions can be added to get the total variance of the noise current as:

$$I_{n,j}^2 = I_{nc,j}^2 + I_{ns,j}^2 + I_{mp,j}^2 \quad j = 0 \text{ or } 1 \quad (3.21)$$

Equations (3.17), (3.19) and (20) can be used to generate the BER curves (as shown in Fig.3.10) by plotting the probability, P_e , of BER as a function of the average receiver power, P_{av} , so that we can estimate the receiver sensitivity that is affected by changing the system parameters.

3.4.2 Dispersion Penalty

Besides, the total fibre loss in a FOL, a dispersion penalty remains a considerable part of the optical power loss since dispersion broadens a transmitted signal pulse resulting in intersymbol interference (ISI) at the receiver decision circuit, in particular for a receiver circuit with no re-equalizer and no time extractor. It is thus necessary to have a realistic estimate of the dispersion penalties in a FOL design. The basic dispersion power penalty is also related to the dispersion normalized pulse broadening $\Delta t/T$, where T is the time slot for one bit, thus data bit rate B is equal to $1/T$. A simple approximation of the power penalty due to dispersion is given by Gimlett [21]:

$$P_d \approx 22 B^2 \Delta t^2 \approx 22 B^2 z^2 \sigma_0^2 \left(\frac{d\tau}{d\lambda}\right)^2 \quad (3.22)$$

where $d\tau/d\lambda = 12.65 \text{ ns}/(\text{km} \cdot \mu\text{m})$ at $1.55 \mu\text{m}$ and $d\tau/d\lambda = -0.87 \text{ ns}/(\text{km} \cdot \mu\text{m})$ at $1.3 \mu\text{m}$ which are calculated by differentiating equation (3.8). As can be seen from equation (3.22), the power penalty increases with the bit rate B and fibre length z . This is a useful estimation tool for FOL feasibility studies. The term of $z^2 \sigma_0^2 (d\tau/d\lambda)^2$ is to measure the power penalty due to the material dispersion.

3.4.3 Link Power Budget

One of the primary objectives in computer modelling of a FOL is to find ways for maximizing repeater spacing while at the same time maintaining a specified performance and providing a power margin to account for unforeseen effects. The most basic form of system design is the power budget, and the most apparent transmission limitations are due to fibre transmission losses and dispersion. Starting with the optical transmission power P_t of the source, and with the power losses due to fibre losses, coupling and splicing losses and etc, are subtracted to compute the P_r of light when arriving at the receiver. This power must exceed the receiver sensitivity power P_{rs} in order to meet the BER performance requirement (10^{-9}). In addition, the losses due to

effects such as dispersion are assigned the equivalent of a power penalty and included in the budget as if they were actual losses. The power margin for FOL reliability design would need to be taken into account. The maximum fibre link length is simply computed as the length when the received power equals the receiver sensitivity adjusted for all power penalties. This calculation is given by the following equation:

$$z = \frac{10}{\alpha} \log \frac{P_t}{P_{rs}} \quad (3.23)$$

This equation is a useful formula to estimate the FOL transmission length z when knowing P_t , P_{rs} and fibre average loss α .

3.5 Fibre Optic Link Simulations

This section describes the simulation processes of a FOL. It starts with a laser transmitter model simulation, fibre optic impulse response model simulation and receiver model simulation. The receiver model includes a noise generator and a decision circuit simulation. The simulation method of the FOL is a hybrid technique which combines all noises calculation and time domain decision circuit.

3.5.1 Laser Source Spectrum Simulation

Two laser source spectrum models have been presented in equation (3.1) and (3.2), respectively. The first source model may be used for single-longitudinal mode laser source, in particular for a LED light source, which has Gaussian shape. Since single or near single-longitudinal-mode lasers are very expensive and have a relative short life time, N-longitudinal-mode lasers are used in many practical FOLs. Some practical light sources are listed in Table.3.1, where the parameters are:

- (i) the LED operating at $\lambda_0 = 1.3 \mu\text{m}$ has the optical output power $60\mu\text{W}$, the spectrum rms width $\sigma_0 = 35\text{nm}$ and a rise/fall time 3.0ns ;
- (ii) the laser operating at $\lambda_0 = 1.3 \mu\text{m}$ has the optical output power 1mW , the N-

- longitudinal-mode Gaussian envelope spectrum rms width $\sigma_0 = 1.1\text{nm}$ and a rise/fall time 0.5 ns ;
- (iii) the laser operating at $\lambda_0 = 1.55\ \mu\text{m}$ has the optical output power 1mW , the N-longitudinal-mode Gaussian envelope spectrum rms width $\sigma_0 = 1.6\text{nm}$ and a rise/fall time 0.3 ns .

In simulation, the laser source spectrum $S_{zz}(\lambda)$ without signal modulation is given in equation (3.2) where if the i th mode amplitude a_i is assumed as a function of $\exp(-i^2D)$, where D is a selected constant. If parameters of the laser spectrum are $N/2 = 5$, $D = 1/8$, $\Delta\lambda = 1\text{nm}$ and $\lambda_0 = 1.55\ \mu\text{m}$, the laser spectrum (in the simulation) can be obtained as illustrated in Fig.3.4. It can be estimated that the laser source rms spectrum width, σ_0 , is approximately 2nm . It is a measurable parameter in a practical system.

3.5.2 Laser Transient Waveform Simulation

The laser rate equations (3.3) and (3.4) can be solved numerically by using 4th order Runge-Kutta method. However, the equivalently electrical circuit model of equation (3.5) or (3.6) is more attractive to the FOL simulation; since it can simply provide an impulse response function $h_1(t)$, the simulation process can be easily carried out in the time domain, also it provides an interface to many other electrical circuit models by using signal processing methods. Referring to equation (3.3) and (3.4), if the laser parameters are chosen as: the laser cavity volume $3 \times 10^{-16}\text{m}^3$, the spontaneous emission lifetime $\tau_e = 3(\text{ns})$, the photon lifetime $\tau_p = 2(\text{ps})$, the optical gain $g = A(n_e - N_0)$ where the optical gain parameter $A = 1.7 \times 10^3\ (\text{s}^{-1})$ and the electron density $N_0 = 1.5 \times 10^8$, the injected signal current pulse 'off' i_{s0} is equal to or just above the laser threshold current i_{th} , the injected signal current pulse 'on' $i_{s1} = 1.3\ i_{th}$ and the fraction of the spontaneous emission ρ is selected at 10^{-4} or 10^{-3} or 10^{-2} , then the results of the laser equivalent electrical RLC circuit model are: the resistance $R = 4.826(\text{ohm})$, the capacitance $C = 0.13824 \times 10^{-9}\ (\text{farad})$, the inductance $L =$

9.6488×10^{-12} (henry), the resistance of the conductance $R_{SE} = 1.6 \times 10^{-3}$ (ohm) (For detail, please see equation B.1-20 in Appendix B).

For a step-current pulse signal, the numerical calculation results of the laser rate equations and the simulation results of the laser equivalent circuit model are shown as curves a, b, c in Fig.3.5 and Fig.3.6, respectively. A comparison study shows that the two solutions have a similar performance when $\rho \geq 10^{-2}$, but diverge significantly as ρ reduces, the reason being that, the laser rate equations are nonlinear and the small-signal laser circuit model is obtained by linearizing the nonlinear rate equations. Large ρ results in small changes in the photo density and in this case, the nonlinear parts of the laser rate equation are small and can be neglected; while for small ρ , a complex large-signal laser circuit model due to the highly nonlinear properties of the device is essential. Fortunately it is desirable to have a large ρ to obtain a square pulse with little spectral chirping in the communication links for power system protection relaying, so that small signal analysis of the circuit model is suitable.

By using the laser equivalent electrical circuit model with the setting of a PCM binary NRZ signal at $B = 150$ Mbit/s, a pulse modulated optical power signal output of the laser at the large $\rho = 10^{-2}$ is shown in Fig 3.7. It shows that laser transient response has a very small rise and fall time and also has a slight shoot over; this phenomenon has to be taken into account when high B is required, but it is not important for low B applications, for example, the power system line protection relaying case. It is necessary to analyze the laser transient phenomena when the FOL employs a laser as a light source, in particular, when the FOL is used in other applications requiring very high bit rate. In our simulation of a FOL, the large $\rho = 10^{-2}$ of the pulse modulated optical power signal output is used.

3.5.3 Fibre Loss Estimations

Fibre loss is a negative factor that limits data transmission distance. Taking some

practical SMF and MMF as references, their characteristics are listed in table 3.2 and table 3.3, respectively. In table 3.2, SMF has a typical total loss of less than 0.45dB/km and dispersion less than 3.0ns/(km.μm) at $\lambda_0 = 1.3\mu\text{m}$, and less than 0.25dB/km and dispersion less than 18.0ns/(km.μm) at $\lambda_0 = 1.55\mu\text{m}$. In table 3.3, MMF at $\lambda_0 = 1.3\mu\text{m}$ has a typical total loss of variations from 0.8 to 3dB/km.

Referring to theoretical fibre loss model (equation (3.7)) with above characteristics of the practical fibres, typically estimated total fibre losses as used for FOL simulation are listed in Table.3.4, where SMF total loss at $\lambda_0 = 1.3\mu\text{m}$ is about 0.5dB/km and total loss at $\lambda_0 = 1.55\mu\text{m}$ is about 0.3dB/km. The MMF has a higher fibre total loss. The results support our decision of selecting SMF for long-haul data transmission due to higher loss of MMFs.

3.5.4 Fibre Transfer Function Simulation

The fibre transfer function represents the quality of FOL. Because in an N-longitudinal-mode laser, light at different wavelengths has different propagation speeds, thus this dispersion phenomenon limits the fibre transmission bandwidth. By using equation (3.10) and selecting parameters; dispersion $d\tau/d\lambda = 1.87\text{ns}/(\text{km}.\mu\text{m})$ at $\lambda_0 = 1.3\mu\text{m}$ or dispersion $d\tau/d\lambda = 17\text{ns}/(\text{km}.\mu\text{m})$ at $\lambda_0 = 1.55\mu\text{m}$, the laser $\sigma_0 = 2\text{nm}$, and fibre length $z = 100\text{km}$, 160km and 180km respectively, the simulated fibre transfer function $H_2(\omega)$ can be obtained, as shown in Fig.3.8. In Fig.3.8, curve d is for $\lambda_0 = 1.3\mu\text{m}$ with a fibre length 100km, and curves 'c', 'b', 'a' are for wavelength $\lambda_0 = 1.55\mu\text{m}$ with a fibre length of 100km, 160km and 180km, respectively. The results show that, for the same fibre length $z = 100\text{km}$, curve 'c' at $\lambda_0 = 1.55\mu\text{m}$ has -3dB bandwidth limitation about 110MHz, curve 'd' at $\lambda_0 = 1.3\mu\text{m}$ has -3dB bandwidth limitation about 680MHz, this shows that the fibre at $\lambda_0 = 1.55\mu\text{m}$ has larger bandwidth limitation than that at $\lambda_0 = 1.3\mu\text{m}$. The results also show that, for the fibre at $\lambda_0 = 1.55\mu\text{m}$, curve 'a' with $z = 180\text{km}$ has -3dB bandwidth limitation about 40MHz and curve 'b' with $z = 160\text{km}$ has -3dB bandwidth limitation about 43MHz.

This clearly shows that for the fibre span distance 180km and fibre at $\lambda_0 = 1.55\mu\text{m}$, transmission B will be limited below 40Mbit/s.

Taking the inverse Fourier transform of equation (3.10), the impulse response of the fibre, $h_2(t)$ is obtained. In order to see how dispersion broadens by a pulse, a simulation for $h_2(t)$ was also done. Assuming that the laser source has $\sigma_0 = 2\text{nm}$, a fibre length $z = 120\text{km}$, the impulse response is plotted in Fig.3.9. In Fig.3.9 (a), the pulse broadens by 1ns, however the pulse broadens by 8ns. Results show that larger dispersion at a laser $\lambda_0 = 1.55\mu\text{m}$ has a larger pulse broadening than that at smaller dispersion at $\lambda_0 = 1.30\mu\text{m}$ after 120km transmission in the fibre. A broadened pulse increases the bit error probability at the receiver decision circuit due to the long tail affecting the adjacent pulse, in particular for a high B. One of the problems is that there is a larger dispersion effect when a laser operates at $\lambda_0 = 1.55\mu\text{m}$. However, it has been shown that in section 3.5.3 that fibre at $\lambda_0 = 1.55\mu\text{m}$ has the advantage of having a lower loss than that at $\lambda_0 = 1.30\mu\text{m}$. There must thus be a compromise between dispersion and fibre loss consideration in design of a FOL.

3.5.5 Dispersion Penalty Evaluation

As it has been described in section 3.4.2 that dispersion power penalty has to be taken into account when designing a FOL. Equation (3.22) represents the relationship between power penalty and material dispersion. It is necessary to quantitatively evaluate the dispersion penalty. In order to have some comparative results, the characteristics of several practical LEDs, and selected lasers are listed in Table.3.5, where for practical LED types, LED-A at $\lambda_0 = 1.3\mu\text{m}$ has $\sigma_0 = 35\text{nm}$, and LED-B $\lambda_0 = 1.529\mu\text{m}$ has $\sigma_0 = 40\text{nm}$. For practical laser types, Laser-A at $1.3\mu\text{m}$ has $\sigma_0 = 1.1\text{nm}$, Laser-B at $1.535\mu\text{m}$ has $\sigma_0 = 1.6\text{nm}$. For selected laser types in the FOL simulation, Laser-C at $1.3\mu\text{m}$ has $\sigma_0 = 2\text{nm}$, Laser-D at $1.55\mu\text{m}$ has $\sigma_0 = 2\text{nm}$. The dispersion power penalty evaluations for different B's with different fibre length are summarized in Table.3.6.

If a design target of dispersion power penalty is assumed at less than 1dB, then by using equation (3.22), an approximate judgement of the performance of FOL designs is given in Table 3.6. In Table.3.6, it has been shown that for laser operating at $\lambda_0 \approx 1.3\mu\text{m}$; with Laser-A, $B = 500\text{Mbit/s}$ and $z = 50\text{km}$ or Laser-C, $B = 40\text{Mbit/s}$ and $z = 100\text{km}$ or Laser-C, $B = 90\text{Mbit/s}$ and $z = 100\text{km}$, the FOL design only has a small $\text{DP} < 0.1\text{dB}$. None of them exceed a 0.1dB power penalty due to $\lambda_0 = 1.3\mu\text{m}$ being near to zero dispersion where $\lambda_0 = 1.310\mu\text{m}$, while for LED-A operating $\lambda_0 \approx 1.3\mu\text{m}$, with $B = 40\text{Mbit/s}$ and $z = 80\text{km}$, the FOL has a dispersion penalty (DP) = 2.27dB, or with $B = 140\text{Mbit/s}$ and $z = 60\text{km}$, it has a $\text{DP} = 1.436\text{dB}$. Their DP s have had 1dB power penalty due to the large source spectrum width and relatively longer distances. These results show that although light source operates at near zero dispersion $\lambda_0 = 1.32\mu\text{m}$ range, it is desirable to use the laser to obtain small power penalty (less than 1dB) for the long fibre spanning distances for data transmission.

In Table 3.6, the DP of a FOL is 2.43dB if the FOL has the LED-B, 80km fibre length, 6 Mbit/s data rate, and operates at $\lambda_0 \approx 1.55\mu\text{m}$, the DP of the FOL is 1.48dB if the FOL data rate is changed from 6Mbit/s to 40 Mbit/s and the fibre length is changed from 80km to 10km, and the DP of the is 1.52dB if the FOL data rate is changed from 6Mbit/s to 90 Mbit/s and the fibre length is changed from 80km to 4.5km. The DP of the FOL is 1.597dB if the FOL has the Laser-B source, 90Mbit/s data rate and 100km fibre length, and the DP of the FOL is 2.13dB if FOL light source is Laser-D. All above dispersion power penalty excess 1dB of the designing target due to the parameters such as high data rate or long distance, therefore, such poor FOL designs should be avoided.

Again for a light source operating at $\lambda_0 \approx 1.55\mu\text{m}$ in Table.3.6, with Laser-B, $B = 90\text{Mbit/s}$ and $z = 50\text{km}$, the DP of the FOL is 0.312dB, and with Laser-D, $B = 40\text{Mbit/s}$ and $z = 100\text{km}$, the DP is 0.43dB. These two FOL designs can meet the less than 1dB penalty requirement, but the former has a high B and short z and the latter has a low B and long z . The latter FOL design is more suitable for an application in

power system protection relaying where long distance transmission is required.

The results in Table 3.6 shows that from the dispersion point of view, it is hoped that the laser operates at near zero dispersion with λ_0 1.32 μm range. However from the fibre loss point of view, the FOL at $\lambda_0 = 1.55\mu\text{m}$ has a lower loss than that at $\lambda_0 = 1.3\mu\text{m}$, thus it is desirable to select a FOL operating at $\lambda_0 = 1.55\mu\text{m}$. But for a higher B or a longer fibre span distance, the dispersion problem is the main limitation for FOL applications. In power system line protection, a long transmission distance is desirable, but not with a very high B, therefore a laser source operating at $\lambda_0 \approx 1.55\mu\text{m}$ is a suitable selection for the FOL designs.

3.5.6 Link Power Budget Calculation

From equation (3.23), it can be seen that the transmission distance z depends heavily on the fibre loss, while only marginally on the P_t and P_r levels. The fibre total loss is quite different when light source operates at $\lambda_0 = 1.3\mu\text{m}$ and $\lambda_0 = 1.55\mu\text{m}$. In section 3.5.3, it was estimated that the fibre loss is $\alpha = 0.6\text{dB/km}$ at $\lambda_0 = 1.3\mu\text{m}$ and $\alpha = 0.3\text{dB/km}$ at $\lambda_0 = 1.55\mu\text{m}$. It can be seen that shifting λ_0 from 1.30 μm to 1.55 μm , the fibre loss is reduced by roughly a fact of 2, and therefore would increase z by the same factor. For example, if P_t is set at 0dBm (1mW) and P_r is set at -50dBm, the fibre spanning distance would be 83km for the light source operating at $\lambda_0 = 1.3\mu\text{m}$, while the fibre span distance 166km for light source operating at $\lambda_0 = 1.55\mu\text{m}$. From the fibre loss point of view, a light source operating at $\lambda_0 = 1.55\mu\text{m}$ is better than one operating at $\lambda_0 = 1.3\mu\text{m}$. However since the dispersion effect at 1.55 μm is greater than that at 1.30 μm , a larger dispersion power penalty would be required for a source at 1.55 μm than that at 1.30 μm . Recalling Table 3.6, for light source at 1.55 μm , $B = 90\text{Mbit/s}$ and $z = 100\text{km}$, the power penalty has reached to 2.13dB. This power penalty is added into power budget evaluation, and the fibre span distance thus is reduced from 166km to 156km. As B increases, more power penalty has to be added into the power budget evaluation, and the fibre dispersive effects become more

important.

3.5.7 Noise Analysis

In section 3.3.3, a photo-receiver model and noise models were described. This section will evaluate these models and give quantitative introduction. For the receiver model of equation (3.14), $e = 1.6 \times 10^{-19}(\text{J})$, Planck's constant $h = 6.63 \times 10^{-34}(\text{J-s})$, light frequency $\nu = c/\lambda$, light speed $c = 3 \times 10^8(\text{m/s})$ and assuming the quantum efficiency $\eta = 1$, and the average APD gain $\langle G \rangle = 10$, the average recovered power $P = -50\text{dBm}$, thus we obtain:

(i) A photo to electrical conversion factor $(\eta e / h\nu) \approx 1.045(\text{A/W})$, and a signal current $I_s = 1.045 \times 10^{-7}(\text{A})$ at $\lambda_0 = 1.3\mu\text{m}$.

(ii) Photo to electrical conversion factor $(\eta e / h\nu) \approx 1.247(\text{A/W})$, and signal current $I_s = 1.247 \times 10^{-7}(\text{A})$ at $\lambda_0 = 1.55\mu\text{m}$.

For shot noise in equation (3.15), assuming that $\langle G \rangle = 10$, the excess noise $F(G) = 5.01$, $\lambda_0 = 1.55\mu\text{m}$, the $k_2 = 0.563$, and $B = 40\text{Mbit/s}$, thus the shot noise limitation $I_{ns} = 7.99 \times 10^{-9}(\text{A})$.

For the thermal noise limitation of equation (3.16), taking the first component for analysis where $I_{nc} = (4k_B T / R_L)^{1/2} k_2 B^{1/2}$, $k_2 = 0.563$. If the temperature $T = 300\text{K}$, $B = 40\text{Mbit/s}$, $R_L = 1\text{k}\Omega$, thus thermal noise current $I_{nc} = 1.4517 \times 10^{-8}(\text{A})$.

For mode-partition noise of equation (3.17), if $k = 0.5$, $B = 40\text{Mbit/s}$, $\sigma_0 = 2\text{nm}$, $L = 100\text{km}$, and $\lambda_0 = 1.55\mu\text{m}$, then $I_{mjp} = 2.7 \times 10^{-12}\text{A}$.

If assumed received power P_r is -50dBm , all the above noise contributions are added and the low pass filter bandwidth, B_N , is designed to be 40MHz in order to allow 40Mbit/s data passing the filter and to eliminate all noise above 40MHz , then the signal-

to-noise ratio, Q , ($Q = P_r / \text{Noise}$) can be calculated to be about 7.5. From the simplification error probability P_e of equation (3.17), $P_e = 10^{-12}$ at good signal-to-noise ratio $Q = 7.5$ which is less than the 10^{-9} requirement, so such a design can be accepted.

3.5.8 Bit Error Rate Curve Simulation

In the design of a digital communication link system, the BER curves can clearly show the performance of the system, therefore it is necessary to simulate FOL BER curves in our design. There are many types of APDs or PINs with FET preamplifier available on the market today, two examples of typical PIN diodes are listed in Table 3.7 at the BER = 10^{-9} requirement. One has a sensitivity of about -51dBm ~ -52.5dB, the other has sensitivity of only around -36.0dBm ~ -38.0dBm at B = 16 ~ 160 Mbit/s. As can be seen among various types of APD or PIN with FET preamplifiers, a practical receiver must be designed to meet a FOL application. In our simulation, a good sensitivity APD and PIN with FET preamplifier have been selected. Their parameters are listed in Table 3.8. where except for the factor that the APD has a diode gain $\langle G \rangle = 10$ and excess noise factor $F(G) = 5.01$ and the PIN has $\langle G \rangle = 1$, excess factor $F(M) = 1$, all other parameters are set the same. The reason of doing this is to get some comparison with results between the APD and PIN performance.

For the APD receiver, its BER curves as a function of the mean received sensitivity optical power are plotted as in Fig.3.10. The BER curves in Fig.3.10 show both the fibre dispersion and distance limitation in the system. Since the average fibre loss is 0.3dB/km at $\lambda_0 = 1.55\mu\text{m}$ and 0.6dB/km at $\lambda_0 = 1.3\mu\text{m}$, for 0dBm transmission power P_t , after 100km fibre distance the received signal power is -60dBm at $\lambda_0 = 1.3\mu\text{m}$ and -30dBm at $\lambda_0 = 1.55\mu\text{m}$. At $\lambda_0 = 1.3\mu\text{m}$ the receiver sensitivity power of curve 'b' and 'd' are about -54.5dBm and -52dBm, and none of them can accept the receiver power -60dBm to keep the BER = 10^{-9} , and they are not suitable for a 100km fibre

span data transmission. At $\lambda_0 = 1.55\mu\text{m}$ the receiver sensitivity power of curve 'a', 'c' and 'e' are -55dBm, -53dBm and -46dBm respectively, they are all less than -30dBm, therefore they can be used for a 100km span data transmission., but curve 'g' has a BER = 10^{-7} at received power -30dBm, so its can not be used for a 100km fibre span data transmission. The results show that although there is less dispersion limitation at $\lambda_0 = 1.3\mu\text{m}$, the higher average fibre loss will limit the fibre transmission distance. In long-haul transmission line power system protection relaying, laser and small average loss fibre operating at $\lambda_0 = 1.55\mu\text{m}$ are preferred.

3.5.9 Decision Circuit Simulation

As described in section 2.3.3, a hybrid approach is used, which combines an analysis calculation method with a time-domain decision circuit model, to carry out the FOL simulation. The method is to calculate all possible noise contributions under a Gaussian approximation at a specified time interval; the calculated rms noise value is then used into a noise generator, so that received signal with added noise can then be obtained. One simulation result is shown in Fig.3.11, where the FOL parameters are: laser at $\lambda_0 = 1.55\mu\text{m}$, $\sigma_0 = 2\text{nm}$, $z = 180\text{km}$, $\alpha = 0.3\text{dB}$, and calculated BER = 1.3×10^{-2} . Thus noisy signal waveforms are sent to the receiver decision circuit. The decision circuit has a set specific sample time period with a setting decision threshold level. As soon as a received pulse signal with added noise waveform comes into the decision circuit, it determines if the pulse signal level at the sample time period is above its decision threshold level or not. If so, the decision circuit will regenerate a pulse 'on', otherwise a pulse 'off'. As clearly seen, for such noisy signal in Fig.3.11, even for optimum decision level setting at optimum sample point, there are still many level crossing points during decision period due to noise, therefore bit error occurs. This time decision circuit is also able to simulate a time jitter which causes the circuit sample point change with the jitter noise.

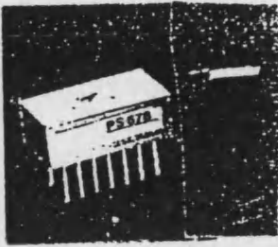

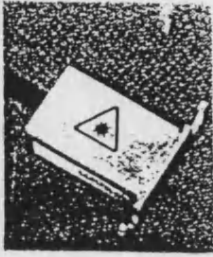
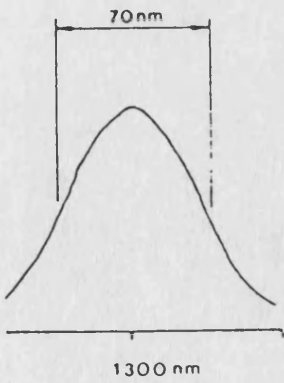
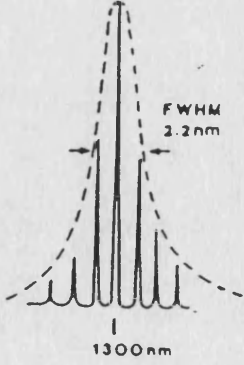
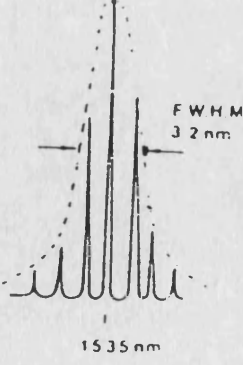
In order to carry out the FOL simulation more realistically, at certain time intervals

the simulation program recalculates all noise distributions due to some FOL parameter changes. The recalculated rms noise value thus re-excites another noise generator, so the received signal with different added noise contributions can be simulated. All simulation processes discussed above are repeatedly carried out until the simulation time has been met the design requirement.

3.6 Summary

In this chapter, a complete computer-aided simulation and modelling system of FOLs is presented. A laser equivalent electrical circuit model, a fibre optic transfer function model and a receiver model are described. The simulation results are both qualitatively and quantitatively evaluated where possible. It also shows how to calculate the overall noise contributions that excites a noise generator, and how a decision circuit recovers and determines the original current signal from the noisy receiving signal. The performance of a FOL is simulated in the time domain.

Table 3.1 Light Source *

Source	LED	Laser	Laser
Model	LH42-19 	LC53-17 	LC71-18 
Wavelength λ	1.30 μ m	1.30 μ m	1.535 μ m
Pigtail to fibre Core/cladding	50/125 μ m	8/125 μ m	8/125 μ m
Power output	60 μ W	1.0mW	1.0mW
Rise/Fall time	3.0ns	0.5ns	0.3ns
Laser threshold	N/A	90 ~ 160(max) mA	30 ~ 50(max) mA
Drive current	150 mA	30mA	25 ~ 40(max) mA
Operating Temperature	-20° ~ +65°C	+25° ~ +50° C	-20° ~ +70°C
Spectral width (F.W.H.M)	70nm	2.2nm	3.2nm
Spectra	Gaussian type	Longitudinal-mode	Longitudinal-mode
			

* "Product Guide - Optical Electronic/Positioning", UK CATALOG No.90.1, Speirs Pobertson Limited, 1992

Table 3.2 Characteristic of single-mode fibres

Specification No.	P2509**	P2510**	P2511**
Attenuation (dB/km) $\lambda = 1.285\mu\text{m}$ $= 1.30\mu\text{m}$ $= 1.55\mu\text{m}$	≤ 0.45 - ≤ 0.30	≤ 0.40 - ≤ 0.25	≤ 0.36 - ≤ 0.22
Dispersion ns/(km. μm) at $\lambda = 1.26 \sim 1.35\mu\text{m}$ $= 1.285 \sim 1.33\mu\text{m}$ $= 1.55\mu\text{m}$	≤ 6.0 ≤ 3.0 ≤ 18.0	≤ 6.0 ≤ 3.0 ≤ 18.0	≤ 6.0 ≤ 3.0 ≤ 18.0
Zero dispersion wavelength λ (μm)	1.304 ~ 1.324	1.304 ~ 1.324	1.304 ~ 1.324

Table 3.3 Characteristic of multi-mode fibres

Core/cladding (μm)	50/125**	62.5/125**	100/140*
Attenuation (dB/km) $\lambda = 0.85\mu\text{m}$ $\lambda = 1.30\mu\text{m}$	2.4 0.8	3.2 1.2	4 ~ 5 3 ~ 4
Bandwidth (MHz.km) $\lambda = 0.85\mu\text{m}$ $\lambda = 1.30\mu\text{m}$	400 600	160 500	100 ~ 700 100 ~ 700
Numerical Aperture (NA)	0.2 ± 0.015	0.275 ± 0.015	0.29

Table 3.4 Typical estimated fibre loss in practical use

Light wavelength λ	Single-Mode** (core/cladding/coating)(μm) (8 /125/250)		Multi-mode ** (core/cladding/coating) (μm) (50/125/250)	
	Intrinsic $A_L+B_L+C_L$	others O_L	Intrinsic $A_L+B_L+C_L$	others O_L
1.3 μm	0.4	0.1	1.0	0.3
1.55 μm	0.2	0.1	-	-

* "Product Guide - Optical Electronic/Positioning", UK CATALOG No.90.1, Speirs Pobertson Limited, 1992

** "The fibre Optic Component & Accessary Catalogue", 4th Edition, AURIGA(Europe)PLC, UK, 1993

Table 3.5 Characteristics of LEDs and Lasers

Source	Model	Centre wavelength (nm)	RMS spectral width σ (nm)
LED-A	LH42-19 *	1300	35
LED-B	QL 1520 *	1529	40
Laser-A	LC53-17 *	1300	1.1
Laser-B	LC81-18 *	1535	1.6
Laser-C	Simulation type	1300	2.0
Laser-D	Simulation type	1550	2.0

* "Product Guide - Optical Electronic/Positioning", UK CATALOG No.90.1, Speirs Pobertson Limited, 1992

Table 3.6 Power penalty for inter-symbol-interference (ISI)

Bit rate Mbit/s	Light source	Light centre wavelength (nm)	Fibre length (km)	Dispersion penalty (dB)
40	LED-A	1300	80	2.27
140	"	1300	60	1.436
6	LED-B	1529	80	2.43
40	"	"	10	1.48
90	"	"	4.5	1.52
500	Laser-A	1300	50	<0.1
90	Laser-B	1535	"	0.312
90	"	"	100	1.597
40	Laser-C	1300	"	<0.1
90	"	"	"	<0.1
40	Laser-D	1550	"	0.43
90	"	"	"	2.13

Table 3.7 Features an InGaAs photo-detector PIN diode and GaAs FET preamplifier

Specification	PT series receivers*	PS series receivers*
Wavelength	$\lambda = 1300\text{nm}$	$\lambda = 1300\text{nm}$
Sensitivity at BER = 10^{-9}	-51.0 ~ -52.5 dBm	-36.0 ~ -38.0dBm
Line data rate	16 ~ 160Mbit/s	16 ~ 160Mbit/s
Dynamic range	27.0 ~ 29.0 dB	25.0 dB
The conversion factor	0.65 ~ 0.85 A/W	0.65 ~ 0.85 A/W
Total leakage current	20.0 nA	40.0 nA
Operating temperature	-20 ~ +80° C	-20 ~ +80° C

* "Product Guide - Optical Electronic/Positioning", UK CATALOG No.90.1, Speirs Pobertson Limited, 1992

Table 3.8 Features of following detectors; a photo-detector PIN diode and a APD diode with FET preamplifier used in the simulation

Simulation Photodiode Types	APD	PIN
Diode gain $\langle G \rangle$	10	1
Excess noise factor $F(G)$	5.01	1
Diode load resistance R_L	1×10^6 ohms	1×10^6 ohms
FET trans-conductance g_m	30×10^{-3} mhos	30×10^{-3} mhos
Total FET capacitance C_T	1.1 pF	1.1pF
FET channel noise factor Γ	1.1	1.1
FET 1/f-noise frequency I_c	20 MHz	20 MHz
FET gate dark current I_d	50 nA	50 nA
Operating temperature T	300 Kelvin	300 Kelvin
Noise bandwidth factor I_2, I_3	0.563, 0.0868	0.563, 0.0868
Noise bandwidth factor I_f	0.184	0.184
The conversion factor $\eta e/h\nu$	0.9 A/W	0.9 A/W

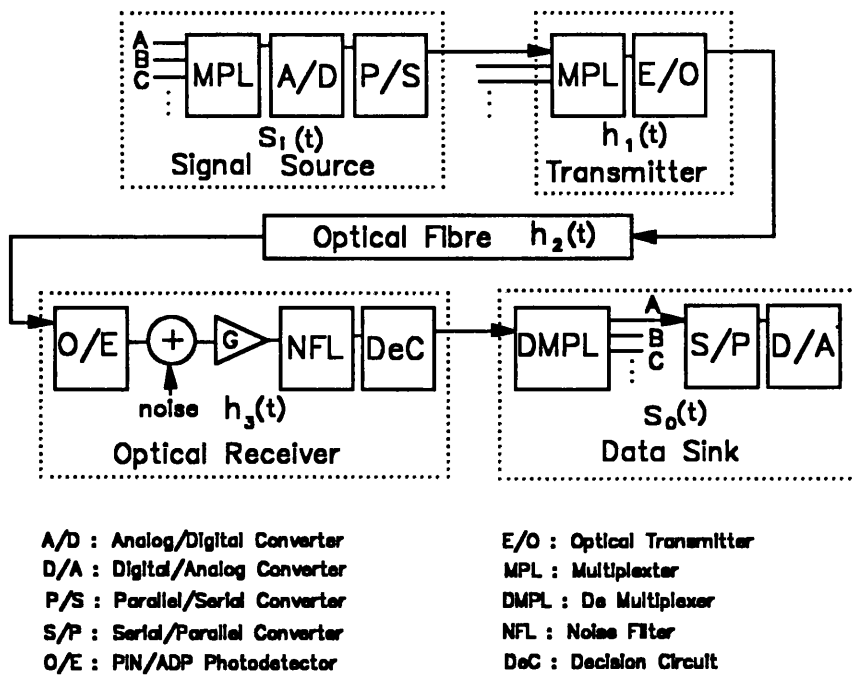


Figure 1. Digital Transmission System Model

Fig.3.1 Digital transmission fibre optic link model

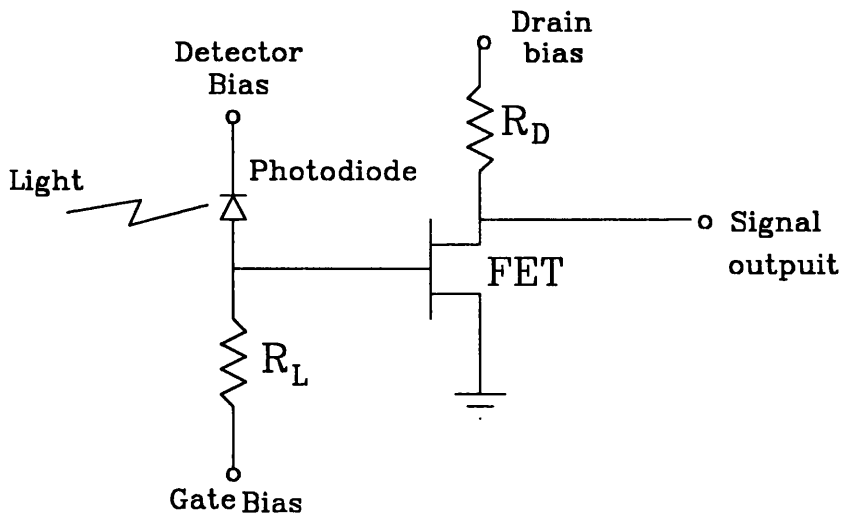


Fig.3.2 Common photo-receiver with FET preamplifier

R_L is the photo-diode load , R_D is the FET preamplifier resistor

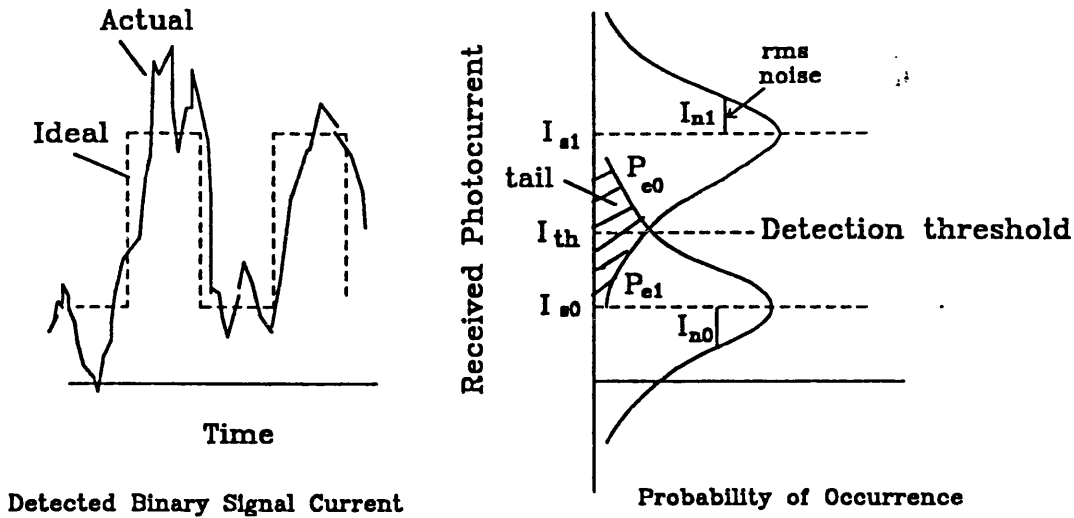


Fig.3.3 Error probability for binary states. I_{n1} the mean photocurrent for a signal 'on', I_{n0} the mean photocurrent for a signal 'off', I_{th} decision threshold level, I_{n1}^2 rms signal variance due to noise for a binary 'on', I_{n0}^2 rms signal variance due to noise for a binary 'off', P_{e0} probability that a 'on' was detected when a 'off' was sent, and P_{e1} probability that a 'off' was detected when a 'on' was sent.

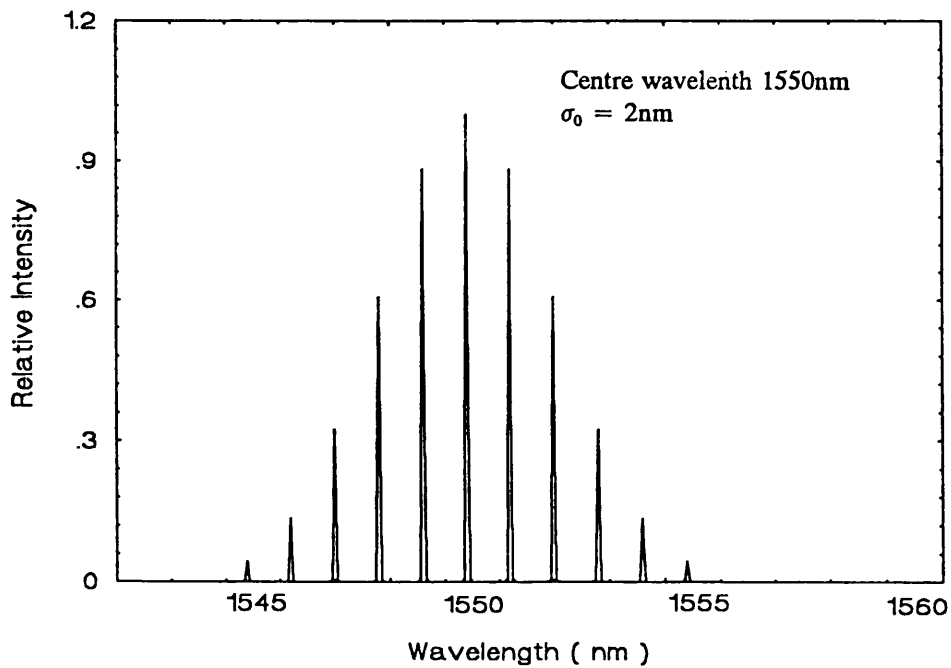


Fig.3.4 Unmodulated spectrum of the laser at light operating wavelength $\lambda_0=1.55\mu\text{m}$, FWHM=2nm

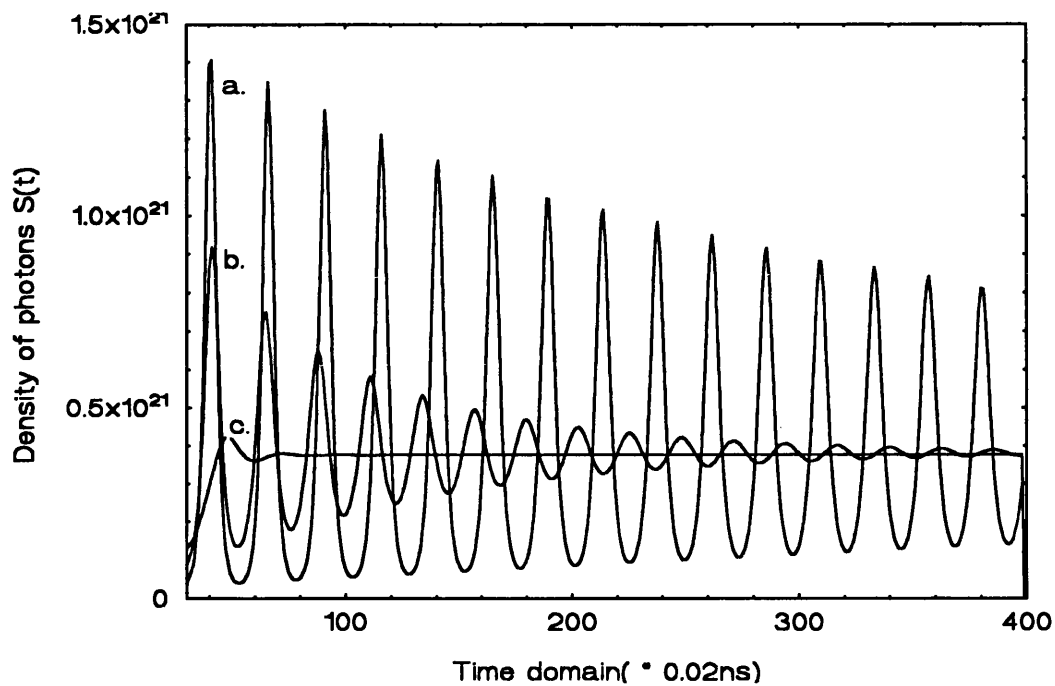


Fig.3.5 Numerical solution to the laser, where curve a, b and c correspond to $\rho=10^{-4}$, $\rho=10^{-3}$ and $\rho=10^{-2}$

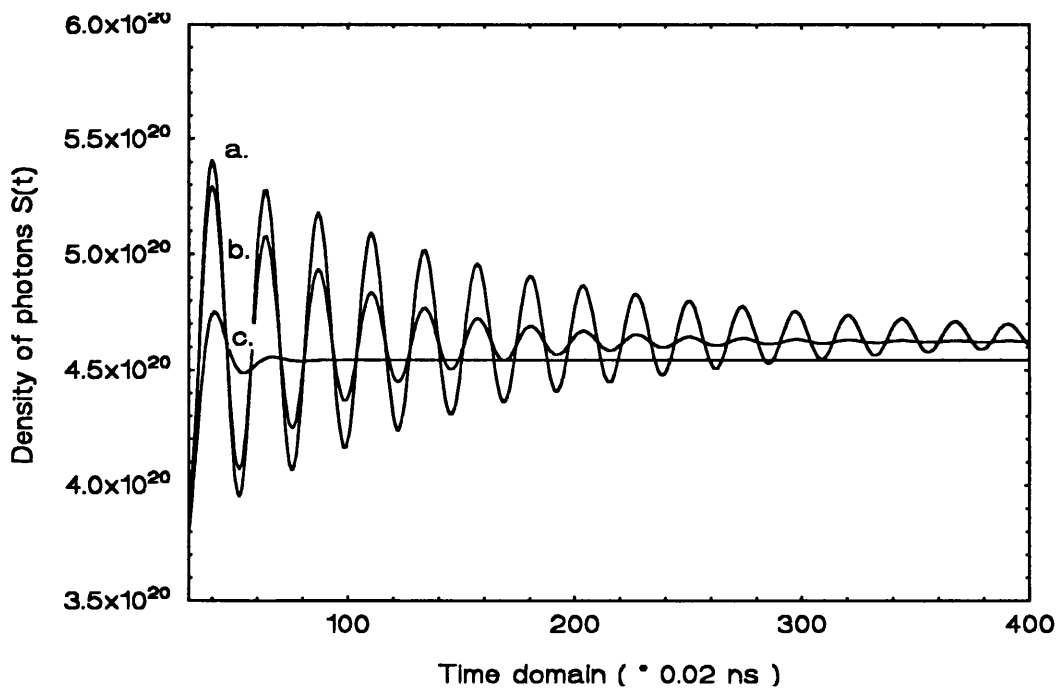


Fig 3.6 Equivalent circuit model solution to the laser, where curve a, b and c correspond to $\rho=10^{-4}$, $\rho=10^{-3}$ and $\rho=10^{-2}$

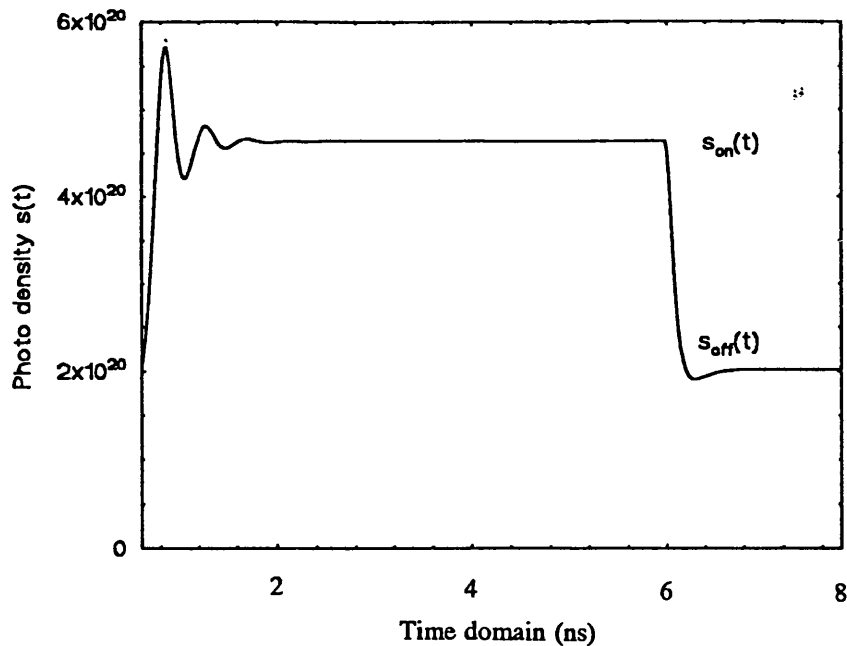


Fig.3.7 A pulse modulated output signal of the laser, photdensities of the $s_{on}(t)$ and s_{off} are correspond to binary state 'on' and 'off' respectively

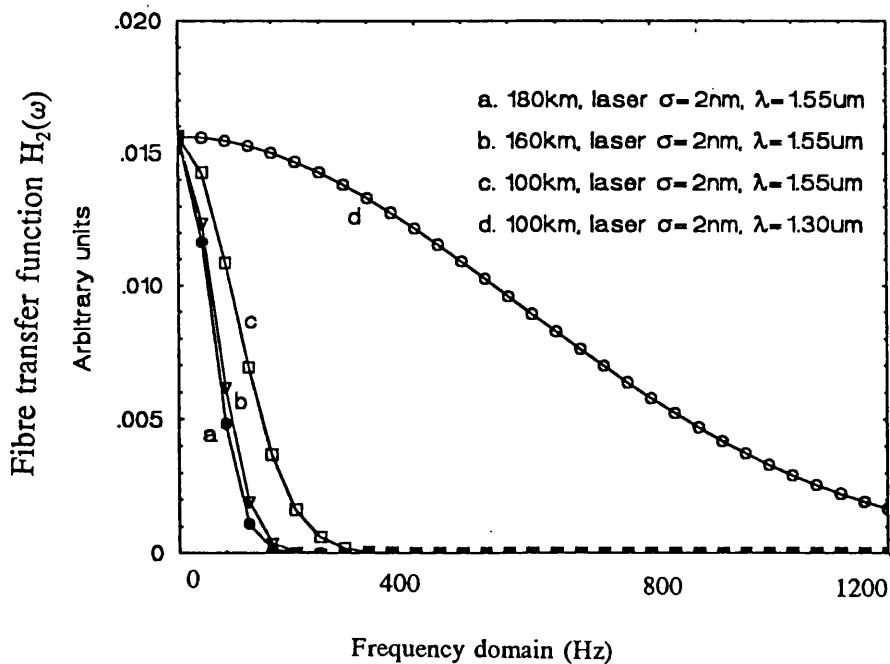


Fig.3.8 Transmission bandwidth chacteristics of the fibre transfer function $H_2(\omega)$

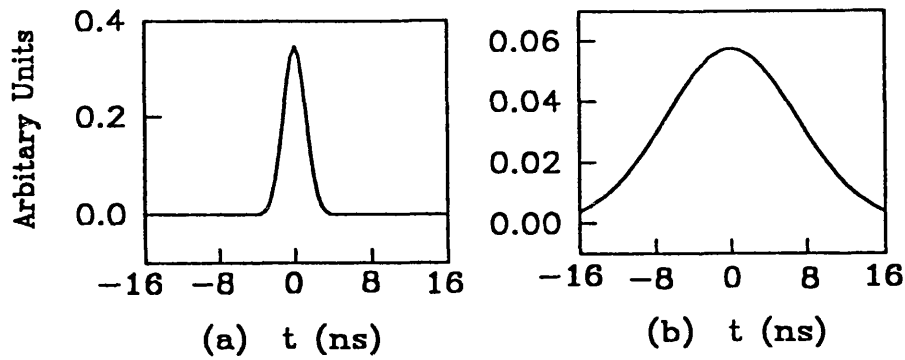


Fig.3.9 Fibre Impulse Response Function $h_2(t)$
 (a) For laser with $\lambda_0=1.30\mu\text{m}$, $\sigma_0=2\text{nm}$, $z=120\text{km}$
 (b) For laser with $\lambda_0=1.55\mu\text{m}$, $\sigma_0=2\text{nm}$, $z=120\text{km}$

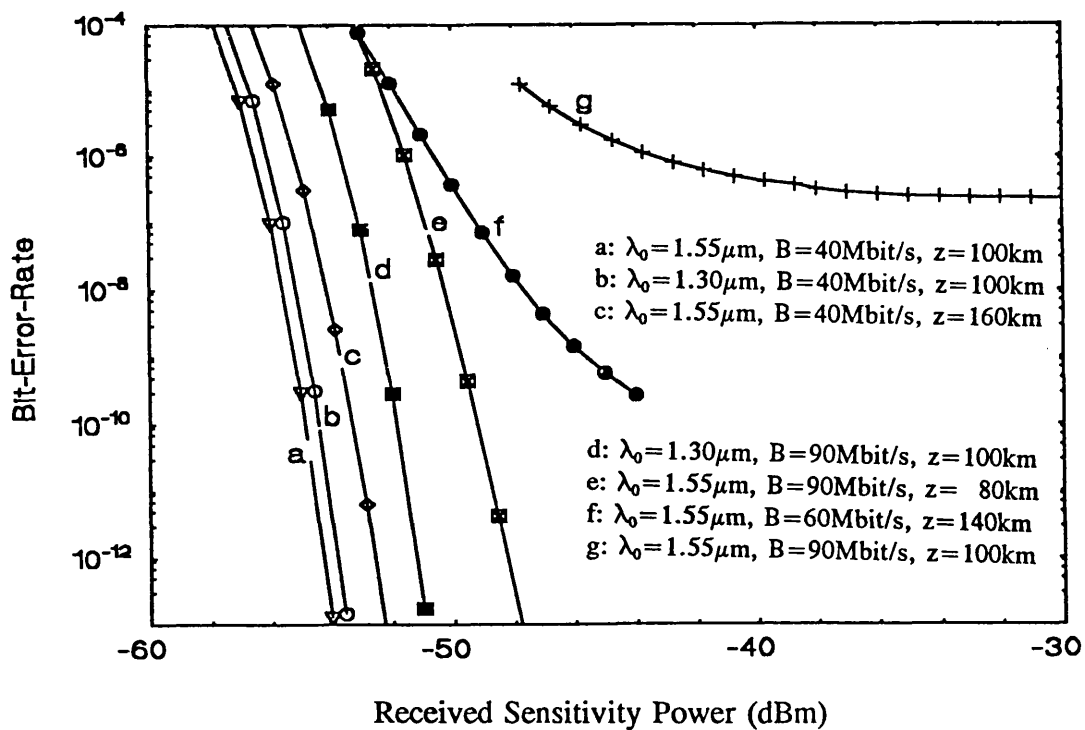


Fig.3 10 Bit-error-rate (BER) as a function of mean received sensitivity optical power P_r

Received Power

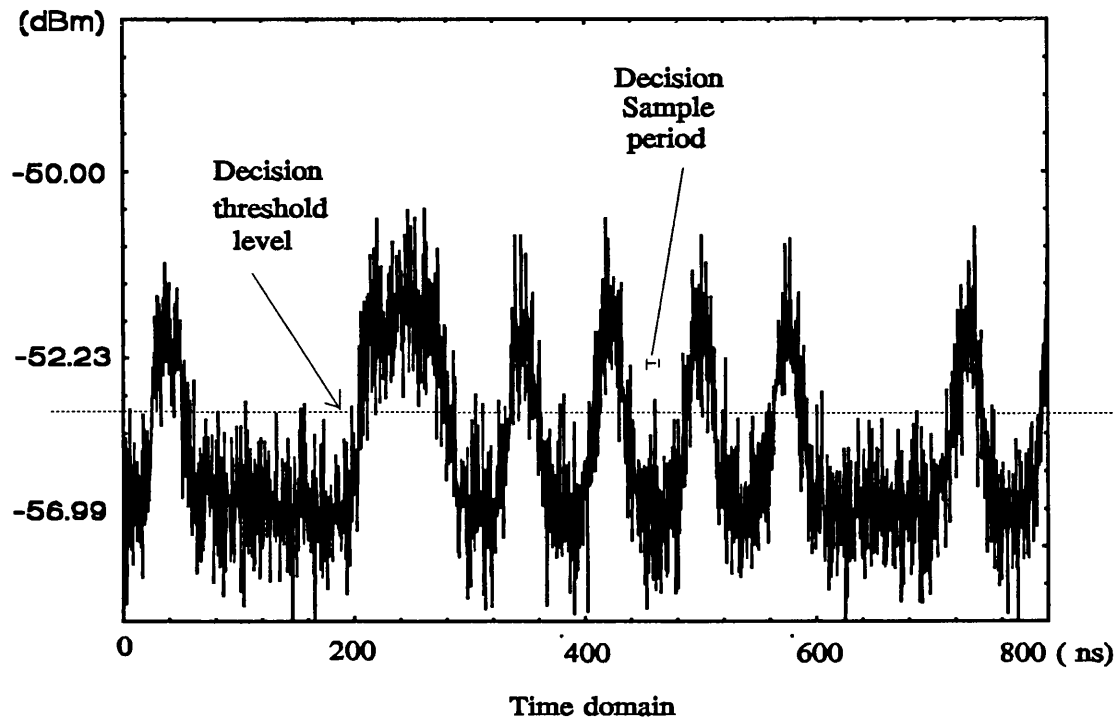


Fig.3.11 Signal received by the PIN diode with added noise under the operating conditions:

laser $P_t = 0\text{dBm}$, $\lambda_0 = 1.55\mu\text{m}$,

$B = 40\text{Mbits/s}$, $\alpha = 0.3\text{dB/km}$,

$z = 180\text{km}$, calculated $\text{BER} = 1.3 \times 10^{-2}$

CHAPTER 4

FIBRE OPTIC LINKS APPLICATIONS

4.1 Introduction

Because of the technological advances of optical fibres and digital communications systems, digital teleprotection systems [19], which are both faster and more reliable than current analogue systems, are attracting active attention in power system protection relaying. In Chapter 3, a complete CAD model of a FOL has been detailed. In this Chapter, examples of the FOL simulation model applications in power system protection are presented. The design of a hardware FOL testing board is described. Besides, some of the important aspects on software implementation and hardware consideration are discussed.

In section 4.2, the simulation of a FOL for power system protection is presented. Then the simulation results are compared with available laboratory experimental results. In section 4.3, the FOL simulation model is applied to a developed line protection scheme, and hence a complete CAD model of the line protection scheme with an actual FOL simulation model is developed. In section 4.4, the design of a transputer-based test and control board (TCB) is described, where the TCB can be used to connect a physical current differential relay and FOL, and therefore a concrete test for the FOL performance can be carried out.

4.2 Fibre Optic Links Simulation Test

This section starts with description of encoding multi-channel analogue voltage and current signals into PCM data. The PCM data are then transmitted through the FOL

simulation model. In order to see clearly how the PCM data are affected by the FOL, the noisy PCM data at the receiver side are analyzed. Finally, the received PCM data are converted back into the original analogue signals. A current waveform is taken as an example to show how the simulation work is carried out in the CAD program study of the FOL.

4.2.1 The Simulation Process

Laser, SMF and receiver models together with the possible noise mechanisms have been presented in Chapter 3. By combining them, a FOL simulation program for computing the link reception performance is developed. Equation (3.12) is a simulation of the FOL in the time domain. FFT and convolution methods are applied to develop the $h_2(t)$ function. The modulated optical envelope power signal $m(t)$ of the laser is obtained from the laser equivalent circuit model. Under a linear assumption, all the noise contributions are added to obtain the total rms noise current. In order to take into account the distorted waveforms at a receiver, the time decision circuit designed (the quasi-analytical BER estimation method as described in previous section 3.5.9) is applied to produce a realistic BER performance. For the purpose of applying the FOL simulation program in power system line protection, six channel waveforms (three phase voltages and three phase currents) of 4 cycles are converted into PCM data sequences which form the input of the laser equivalent circuit model. The coupling transmission optical power P_t between the laser output and optical fibre input is adjusted to 0dBm. The simulation of the FOL operating at both $\lambda_0 = 1.3\mu\text{m}$ and $\lambda_0 = 1.55\mu\text{m}$ are considered. The average fibre loss is set to be 0.3dB/km at $\lambda_0 = 1.55\mu\text{m}$ and 0.6dB/km at $\lambda_0 = 1.30\mu\text{m}$. In order to get the best system performance, the optimal values of both the decision threshold level (setting the equal probability of the binary "one" and "zero") and decision timing sample period (middle area in a pulse) at receiver end have been calculated before the noise is added. The B value is chosen to be 40Mbit/s. Finally both the calculation and measurement of BER are performed to obtain comparison results.

4.2.2 Available Laboratory Experimental Results

Blank et al. [8] presented a long span optical transmission experiments at 34 Mbit/s and 140Mbit/s. In one of the experiments, a 34Mbit/s transmission system trial was conducted over 176km of standard-index SMF. The transmitter used a commercial $1.55\mu\text{m}$ N-longitudinal-mode laser (NDL5003) with laser threshold current of 60mA at 17°C and a mean launch power P_t of +2dBm. The transmission path consisted of 176.2km step-index fibre with 32 splices, where average spliced-loss of 0.234dB/km was obtained, with the three connectors adding a further 3dB attenuation. The receiver sensitivity of -53.0dBm at $1.55\mu\text{m}$ was provided by a commercial Ge APD and trans-impedance preamplifier. A 0.7dB penalty was incurred due to reduced APD quantum efficiency at $1.55\mu\text{m}$ wavelength.

In the above mentioned experiment, the spectral width of the typical N-longitudinal-mode laser was 3nm (rms) and the fibre dispersion at $1.55\mu\text{m}$ was $18\text{ns}/(\text{km}\cdot\mu\text{m})$. These led to dispersion-limited systems at line data rate of 34Mbit/s and a span length of 176km. Practical spans of 100km to 150km could therefore be provided (for more details of the explanations and discussion see reference [8]).

In the following section, the simulation results of the FOL simulation program is used to compare with the above experimental results.

4.2.3. Simulation Results and Discussions

Because of the flexibility of the CAD techniques, a number of system performance results of the simulated fibre optic digital system may be obtained. In Chapter 3, the simulation results, in the forms of the BER curve, the laser impulse response $h_1(t)$, the fibre transfer function $H_2(\omega)$, and the receiver signal waveforms with added noise, have been discussed. The actual fault waveforms converted into PCM NRZ binary data through the FOL simulation program may be carried out as follows:

Fig.4.1(a) represents a single a-phase line-earth voltage fault waveform which is generated from a configuration of two busbars at 140km distance between end P with a generator capacity of 5GVA and end Q with a generator capacity of 20GVA in Fig.A.3 of Appendix A. The fault is set at 50 km from end P with zero fault impedance. Six channel waveforms, three phase voltages and three phase currents over 4 cycles, are converted into PCM data by using 12bit A/D converters, then multiplexed into 40Mbit/s NRZ binary data sequences. This PCM NRZ binary data set forms the input of the FOL simulation program. The optical envelope power PCM with 36-bit binary data at the laser output corresponding to the A/D coding view area is illustrated in Fig.4.1(b). The laser with σ_0 of 2nm operates at $\lambda_0 = 1.30\mu\text{m}$. The transmitting power P_t is 0dBm. A Selected APD has a gain of $\langle G \rangle = 20$, a noise figure $F(G) = 8.1$, and other parameters are as given in Table (3.8), so the APD sensitivity is about -55dBm. After 100km data transmission, the received PCM data with added noise is shown in Fig.4.1(c). After time domain decision circuit and D/A converters, the recovered waveform is obtained as shown in Fig.4.1(d). In Fig.4.1(c), it can be seen that PCM binary signals are very noisy due to a fibre loss of 0.6dB/km at $\lambda = 1.30\mu\text{m}$ and a 100km transmission distance. Fig.4(c) also shows that it is highly possible to make a wrong decision at the decision circuit. The BER of the FOL is about 7.26×10^{-3} . In such an improper FOL design, the received waveforms have distortions which could severely affect the performance of many unit protection algorithms.

If the laser operating wavelength is changed from $1.30\mu\text{m}$ to $1.55\mu\text{m}$, the fibre loss becomes 0.3dB/km, thus a longer distance of data transmission would be expected. Considering a fibre span of 160km, the signal received at the PIN diode, Fig.4.2 shows the result of the binary data pulse with added noise at the input of the decision circuit. It looks as if little errors have occurred during the data transmission testing. Its calculation of BER at the receiver is 7.19×10^{-16} which is well below 10^{-9} required threshold. Therefore such a FOL design can be used for practical data transmission over a 160km span and high quality data transmission can be produced.

If the fibre length is only changed from 160km to 180km and other parameters stay the same as above (e.g., $\lambda_0 = 1.55\mu\text{m}$ and PIN diode), the received PCM data are plotted in Fig.4.3. It shows very noisy received data. There are many cross points when the decision circuit level is set at the symmetric level of the received data, thus high BER would occur after the decision circuit. In fact, the calculated BER is 1.3×10^{-2} which fails to meet the requirement of 10^{-9} . If using an APD instead of a PIN detector, the received PCM data is plotted in Fig.4.4. It shows that the received data have been improved and it is difficult to see any cross points at all when the decision circuit level is set at the symmetric of the received data. In fact, the BER is improved from 1.3×10^{-2} to 1.03×10^{-10} after using the APD instead of the PIN.

The simulation results show that the most applicable FOL has span length over 160km under following FOL configuration parameters; $P_t = 0\text{dBm}$, B bellows 40Mbit/s, laser's $\sigma_0 = 2\text{nm}$ at $\lambda_0 = 1.55\mu\text{m}$, the fibre dispersion is $17\text{ns}/(\text{km} \cdot \mu\text{m})$, APD received sensitivity power is -55dBm . When comparing these simulation results with the experimental results in section (4.2.2), it is clearly evident that there is close correspondence between the two results. But the simulation results are slightly better than the experimental results due to better FOL setting parameters in the simulation than that in the experiment such as σ_0 of 2nm over 3nm, P_r of -55dBm over -53dBm . Moreover, theoretical simulation models produce better results even under the same FOL setting parameters because some ideal assumptions are adopted in the simulation process.

4.3 Fibre Optic Links Model for Line Protection Schemes

In this section, the FOL simulation model application into a line protection scheme is presented. Firstly, examples of calculating channel/modem time delay for some practical data transmission through telephone channel modems or fibre links are given, followed by testing of a typical line protection scheme.

4.3.1 Channel/Modem Time Delay

In Chapter 2, three different line protection schemes are described; they have an average tripping time of 26ms, 20ms and 4 ~ 6ms respectively. The tripping time is the time required by the scheme to detect a fault. The schemes should also include the channel/modem time delay, thus the channel/modem time delay can directly affect the performance of the schemes. The channel/modem time delay is defined as the time taken for a channel status change at the input of one protection unit to reach the output of the remote protection unit. The delay, varying from unit to unit, depends on many factors, such as data bit rate and protocol, number of protection channels, transmitter and receiver processing time, internal circuit propagation delay, communication channel propagation delay. Some major aspects of data transmission delay are:

(i) Most telephone channels are analogue, so that digital data transmission through these channels must use modems. Two typical modems are in use today that have B of 300bit/s and 1200bit/s due to the bandwidth limitation of the telephone channels (4KHz per channel). If one sample data information set requires 12 bits, the transmission line delay caused by the modem will be 40ms for $B = 300\text{bit/s}$ and 10ms for $B = 1200\text{bit/s}$. These figures show that it is impossible for a line protection scheme to have 4 ~ 6ms tripping speed by using these modems as data transmission mechanism. Some private data channels may have modems operating at bit rate 4800bit/s, yet it still requires a 2.5ms data change time. If adding a channel propagation delay of 0.53ms for 160km (light speed used), another 0.5ms for additional delay such as A/D and D/A converting time, the total channel/modem time delay is about 3.53ms. So the time delay will affect the overall optimal tripping time of 4 ~ 6ms of the line protection scheme.

(ii) The FOL can provide very large bandwidth, reliable and secure channels. These advantages make FOL an ideal candidate as data transmission links. Because of large bandwidth, FOL has a smaller channel/modem time delay than conventional channels.

A typical Fibre optic channel propagation delay is $\tau_0 = n/c$, where c is the light speed and n is the glass fibre refraction index ($n = 1.5$). This gives a 0.8ms channel delay for a distance of 160km. For power system protection relaying, 48kbit/s bit rate per channel is often used to meet the transmission fault information requirement. At the B of 48kbits/s, each message of 12 bits takes approximately $12/4800 = 0.25$ ms to transmit. An additional delay of 0.5ms has to be added. This includes the A/D and D/A converting time, etc. Thus the channel/modem time delay is up to 1.6ms (a maximum message converting delay of approximately $0.25 +$ channel propagation time 0.85 ms $+$ additional design consideration delay 0.5 ms). Because FOLs can provide larger transmission bit rate per channel than 48kbit/s, a B of 64kbits/s of a channel is commonly used, therefore the message converting time is reduced from 0.25ms to 0.187ms. The channel/modem time delay reduces from 1.6ms to 1.54ms. It shows that channel/modem time delay of a FOL can be less than 2ms. Thus a high speed line protection scheme is possible when it uses of FOLs as the communication links in the system.

4.3.2 Fibre Optic Links Model Testing

Aggarwal & Johns [3] developed a new differential line protection scheme for power system protection relaying using composite voltage and current measurements. The operation of this protection scheme involves deriving differential signals that are functions of both the voltages and currents measured at each end of the circuits. This approach avoids the need for relay bias to compensate for capacitance spill currents, thus providing sensitivity to lower level fault currents.

In this line protection scheme, an ideal FOL was assumed. The channel/modem time delay was assumed to be 3ms. In order to investigate how an actual FOL would affect the system performance, the previously developed FOL simulation model is applied to the scheme. A complete CAD model of the line protection scheme is thus developed. The block diagram of the line protection scheme CAD model, including the FOL

model, is shown in Fig.4.5. It shows the FOL model within the dashed lines.

The line protection scheme is based on master and slave principles using the FOL model as a means of communication between the ends and had been designed with a view to considerably simplifying the digital hardware requirements and reduce the bandwidth requirements for signal transmission over the FOL. Both voltage and current signals are proportional to the aerial mode voltages and currents. By means of a phase/modal transform, the modal signal S_{pk} (at the slave end P) and S_{qk} (at the master end Q) at both ends can be obtained, respectively. The suffix $k = 2$ or 3 is used to represent the two aerial modes. The modal signal S_{pk} is transmitted through the FOL to the master end Q. The operation of the relay involves a comparison of the modal signals S_{pk} and S_{qk} at the end Q. In theory the signals at both ends should be exactly the same for all "healthy" conditions (i.e. $S_{pk} = S_{qk}$). However, due to quantisation, transducer errors, etc, it is necessary to apply a small voltage threshold level (T_h) to the difference. Thus, in its simplest form the relay would give a trip output signal if $|S_{pk} - S_{qk}| \geq |T_h|$. For more details about relay operating principles, refer to reference [3].

By using voltage and current waveforms of Fig.A.4(c) in Appendix A, a testing of the line protection scheme is carried out. The fault waveforms are typical voltage and current fault waveforms at both the slave end P and the master end Q. The transmission distance is 140km. An internal fault is assumed at 50km to end P, the fault being at the maximum of the prefault a-phase-earth with zero earth impedance. Both ends of three channel voltage and current fault waveforms are measured to transfer modal signals. The S_{p2} and S_{p3} at end P are plotted in Fig.4.6(a), and the S_{q2} and S_{q3} at end Q are plotted Fig.4.6(b). By comparing Fig.4.6(a) with Fig.4.6(b), it can be seen that the measurements of S_{pk} and S_{qk} differ both in phase and magnitude, producing large discernable differences between the two signals for both mode signals S_{q2} and S_{q3} . Because the relay for the line protection scheme is located at the master end Q, the modal signals at end P must be transmitted over the FOL model. After the

aerial mode composite signals i.e., S_{p2} and S_{p3} are transmitted through the FOL, a comparison of the modal signals is thus made by a comparison device at the master end Q. The comparison results are differential modal signals $|S_{p2} - S_{q2}|$ as plotted in Fig.4.7(a) and (b). Fig.4.7(a) shows the differential modal signal $|S_{p2} - S_{q2}|$ after the signal S_{p2} passes through a FOL model in which laser operates at $\lambda_0 = 1.55\mu\text{m}$ and the fibre optic length is 140km. It clearly shows no bit errors occurring. The threshold level T_h is at a relatively low level. As soon as the differential modal signal $|S_{p2} - S_{q2}|$ exceeds the threshold level T_h , trip signals are generated. It can be seen that the threshold is quickly exceeded and a trip decision is asserted approximately 12ms after fault inception. Here the operating time of 12ms has included the 2ms channel/modem delay. Fig.4.7(b) shows the differential modal signal $|S_{p2} - S_{q2}|$ after the signal S_{p2} passes through a FOL model in which laser operates at $\lambda_0 = 1.30\mu\text{m}$ and the fibre optic length is 100km. It clearly shows that the tripping signals have many spikes due to a large bit error rate. However, for this internal fault, the relay still gives a correct decision. A problem could nonetheless arise for an external fault where a distortion in receiving signals due to high bit rate errors could threaten relay stability. Therefore the latter FOL design considered here is unsuitable for data transmission in the line protection scheme.

The above test results help us to conclude that with a properly designed FOL, the differential line protection scheme based on composite voltage and current measurements for power system protection relaying can be put into practical use and with the expected performance results. However, an improperly designed FOL would result in operational failure of the line protection scheme as a high bit error may occur.

4.4 Test and Control Board

In this section, the design of a complete FOL laboratory testing system is described. A partially implemented hardware system is presented. Further work is indicated.

4.4.1 General Considerations

PCM is a kind of source coding technique. By using PCM, time division multiplexing data channels can be easily implemented at terminal equipment. The technique of multiplexing data channels is to ensure that the transmission medium is operated at its most economical information rate. NRZ is line coding, but directly interprets the PCM binary data. By using a line coding technique, channel effects can be avoided. By combining the source and line coding techniques, PCM NRZ binary data are thus used for data transmission over the FOL simulation model. In practice, if a long sequence of 'on' pulses of PCM NRZ data exists, accumulated dc level (average optical power is not the same during the same specific sample time period) may occur due to the long continuous 'on' pulses and thereafter causing results in the following 'off' pulse to be interpreted as a 'on' pulse, so that accumulated dc component is error prone. Also the NRZ does not provide transmitter timing information, while many FOL receiver circuits may need a time extractor. In order to improve data quality in a FOL, other line coding (or channel coding) techniques may be used for efficient data communication and to ensure that the transmitted signals in the FOL have the following features:

- (i) No relative dc component,
- (ii) With embedded timing information to ensure that the distant receivers can extract a reliable clock to time their decision making processes,
- (iii) Addition of sufficient redundant codes to enable the bit error rate of each transmission link to be monitored.

Channel properties are directly related to the characteristics of line coding. One of common line coding techniques used in a FOL is return-zero (RZ) binary data. It reproduces a binary pulse into two pulses, one is 'on' or 'off' and the other is 'off' or 'on', so that it can guarantee that 'on and 'off' pulses (average optical power) are the same during the same specific sample time period, thus with relatively little dc component. It also contains data timing information. Timing information is essential

for a high bit rate transmission FOL that needs a time extractor at its receiver. Since RZ has double pulses than those in NRZ signals with the same information, it needs a double data transmission bit rate. This double increasing B is the main disadvantage of the RZ line coding. However it is possible to add some sufficiently redundant codes (i.e. scrambling line coding techniques) to enable the transmission pulses to have very little relative dc component, timing information and a slightly increased bit rate. To find a suitable data format for a FOL in power system line protection, experimental studies for a particular FOL application in power system protection are needed.

In order to test and evaluate the performance of a physical FOL in power system protection relaying, the setting up considerations of a complete FOL laboratory test system have been made. The block diagram of the test system is shown in Fig.4.8(a). The physical FOL in the diagram includes a transmitter with a laser as its light source, optical fibre as transmission link, fibre splices, fibre couplers and a receiver with a PIN diode or APD. The TCB is shown within a dash line in which an IMS T414 transputer is used to act as an intelligent unit.

A transputer is a microprocessor with its own local memory and inherent data communication links. The links are asynchronous and with their own communication protocols. They can easily connect one transputer to another. A transputer can be used in both a single processor system or a network to build high performance concurrent systems. A network of transputers and peripheral equipments can be easily constructed by using point-to-point communications. These characteristics of a transputer are particularly valuable in the design of the TCB which can not only test data transmission performance in a physical FOL, but also are easily connected to a power system protection relay, so that the relay performance through the FOL can be tested.

4.4.2 Hardware Design

In power system protection, normally several PCM data channels are needed to transfer fault data and trip data signals. European standard primary PCM terminal equipment has a bit rate of 2.048 Mbit/s which can provide 30 data channels, one frame word and one signalling word. If more than 30 data channels are needed, 4 primary PCM systems are multiplexed into secondary PCM system. The secondary PCM system has a data bit rate of 8.192Mbit/s. It can provide 120 PCM data channels, and therefore more data information (e.g., channel error detecting signals, trip signals, tele-metering and voice signals) can use the PCM channels for transmission.

The hardware functions are to collect remote data from one end of a relay and then to transmit these data over the FOL to the local end where detecting devices and switching equipments are present. By utilizing a 32-bit high performance and fast processing speed IMS T414 transputer [28], a TCB for testing the FOL is built up. The TCB can store and process data signals sampled from any protection unit, it can also easily encode and decode the data into and from the PCM and multiplex data channels over FOL. It also provides a synchronise link with three selectively typical bit rates of 5Mbit/s, 10Mbit/s or 20Mbit/s respectively. This designed synchronous link is different from the transputer inherent links. It allows data errors to happen during the data transmission process over the FOL, thus the FOL performance testing can be carried out.

Fig.4.8(b) shows the TCB configuration. It consists of an IMS T414 with 256kbytes of random access memory (RAM) and data transmitter and receiver. The 256kbytes of RAM are divided into two parts, one is for PCM data transmission and the other is for receiving data. The transmitter codes the PCM data into line coding format and then transmits them into the FOL. The received data at the receiver are stored into the receiving RAM. A comparison unit in the TCB then compares the received data with the original transmission data, thus enabling the data transmission bit errors to be

detected. In order to access and monitor the TCB, a transputer development system (TDS) is employed. TDS is an integrated development system. It consists of a plug-in IMS B004 board into an IBM PC. The IMS B004 is an IMS T800 transputer with 2Mbytes of RAM. The TDS supports some appropriate development software and OCCAM programming language for developing a transputer network, thus TCB based on the transputer thus can be developed. The testing results of the FOL data transmission performance can be stored in the TCB and the TDS is able to monitor these results which can be shown on the screen of a PC. Because the line coding format can be implemented by software, different line coding techniques thus can be investigated by using the TCB.

4.4.3 Software Considerations

TDS supplies a complete OCCAM software development environment. A programmer can edit, compile and run OCCAM programs entirely within TDS. OCCAM programs can be developed on TDS and then configured to be run on the TCB with the code being loaded onto the TCB from the TDS. TDS can also be used to generate programs for the TCB that operate completely independently of TDS. Two aspects of software developments are:

(i) Program design for concurrent process: In TCB hardware design, most of the TCB functions are implemented by using the software on the transputer. It is obviously necessary to concurrently run, for example, the data signal converting process, transmitting process, receiving process, and comparing process. The high level OCCAM programming language conveniently supports the declaration of concurrent algorithms and their implementations on a transputer or a network. OCCAM enables an application to be described as a collection of processes, where each process executes concurrently, and communicates with one another through internal and external channels. Each process describes the behaviour of a particular aspect of the implementation, and each channel the connection between all of the processes. To gain

a maximum benefit from the transputer architecture, the TCB can be programmed in OCCAM. This provides the advantages of a high level language, concurrent processes, the maximum program efficiency and the ability to conduct low level operations (for example, low level transputer instructions) of the TCB, so OCCAM programming language is selected to implement all test functions on the TCB.

(ii) Program monitoring on the TDS: In the TCB, a program is able to encode or decode the data signals which then are transmitted over to and received from the FOL. In order to analyze the data transmission performance of the FOL, it is very important to have a facility to monitor the result of the data transmission on the TCB. By using TDS monitoring programmes, the keyboard input data can be sent in a parallel mode to screen for monitoring and to TDS for data processing. The TDS then transmits the processed data to the TCB. Also the monitor programmes allow the data format strings can be edited on the TCB before sending to the application units (i.e. FOL), and then the application results can be monitored on the screen.

4.4.4 Results

The complete hardware implementation of the TCB was tested. By using the TDS transputer network test program, the implemented TCB can be diagnosed and tested to get rid of possible mistakes such as wrongly connected cables, poor connections, electrical noise, poor designs. A set of test results are given in Table 4.1 where MT* is an identification symbol for local transputer, 0* is an identification symbol for remote transputer. In T4 full test (line 1 - line 8), line 7 shows that the link 0 on the remote transputer (0*) is connected to link 2 on the local transputer (MT*), the MT* type is T414b and its internal clock is 17MHz. In the network test (line 9 - line 13), line 13 shows that the remote transputer 0* is the T414b on the TCB, and it has 256k memory. If any memory error and links error on the TCB are found, it will be reported in a similar table as Table 4.1. The test results have proved the correctness of the transputer on the TCB hardware design and implementation.

A task monitor program (i.e., a pipeline sorting example) is programmed as an application on the TCB. The task monitor program has two parts, one is a monitor program and the other is a task program, they run parallelly in TDS and TCB. The task monitor program can sort a sequence of characters into alphabetical order; firstly a sequence of random alphabets are input from the keyboard via TDS to the TCB, then the task program on the TCB sorts the random alphabetical into an order, and at the same time the simple monitor program runs on the TDS to monitor the task program running. Finally the result can be sent to the PC monitor. This monitor program can also be extended to implement the monitoring bit error performances of the FOL.

Further work in hardware aspects is to connect the TCB with a physical digital current differential relay and a physical FOL. This would allow the data from the relay to go through a practical FOL. Further work in software aspects is to generate more application programs running on the TCB, so that the results of data transmission performance over the FOL can be studied in more detail.

4.5 Summary

This Chapter is mainly concerned with the practical applications of the FOL to power system protection. Firstly, the FOL model is applied into the CAD model of a line protection scheme [3], thus a complete CAD model for line protection scheme with the detailed FOL simulation model is obtained. Then, a complete hardware configuration with a partial implementation is described. An IMS T414 transputer is used as an intelligent control unit. It has the ability to connect a real relay with concrete fibre optic communication links, thus many practical issues relating to the application of a FOL can be further investigated.

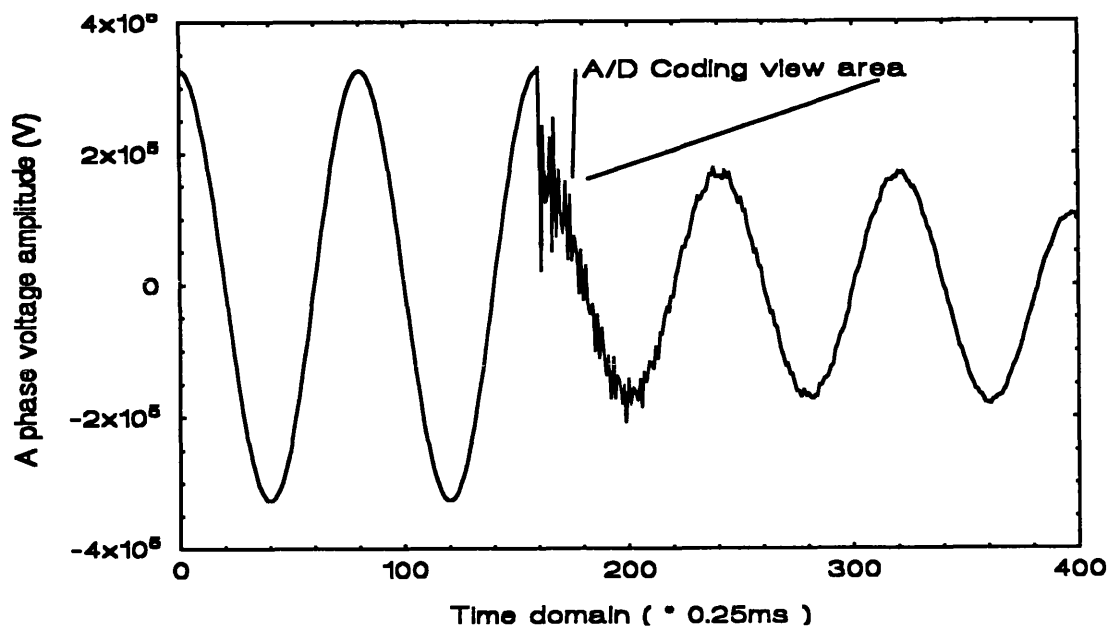


Fig.4.1 (a) A typical single phase line-earth voltage fault waveform at relaying terminal P end (the system configuration is shown in Fig.A.5.(b), Appendix A)

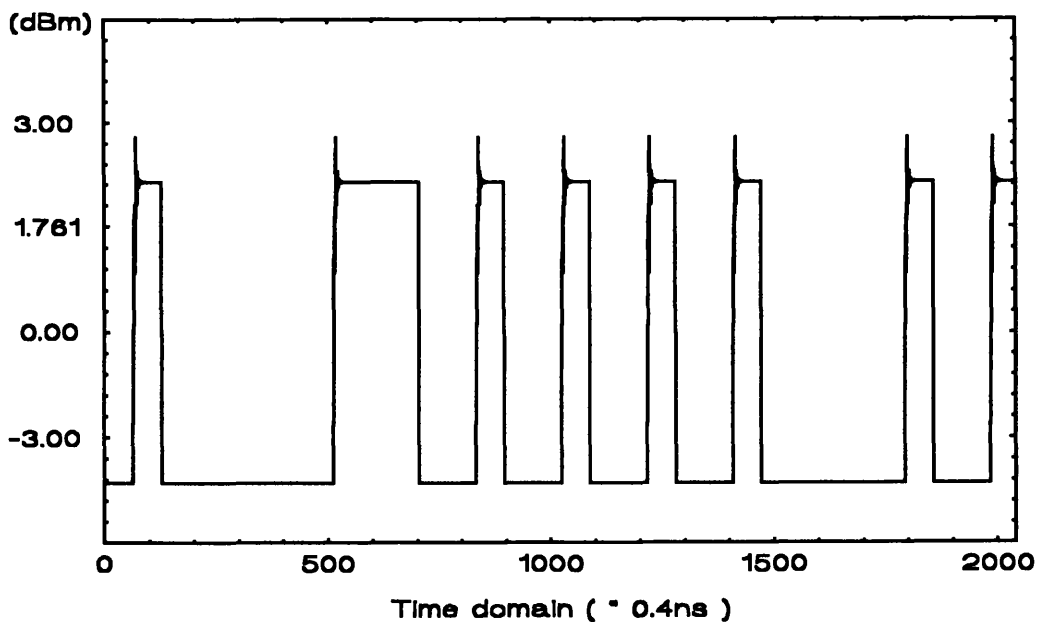


Fig.4.1 (b) Modulated envelope optical NRZ signal at the laser output
 $B = 40\text{Mbit/s}$, and $P_t = 0\text{dBm}$

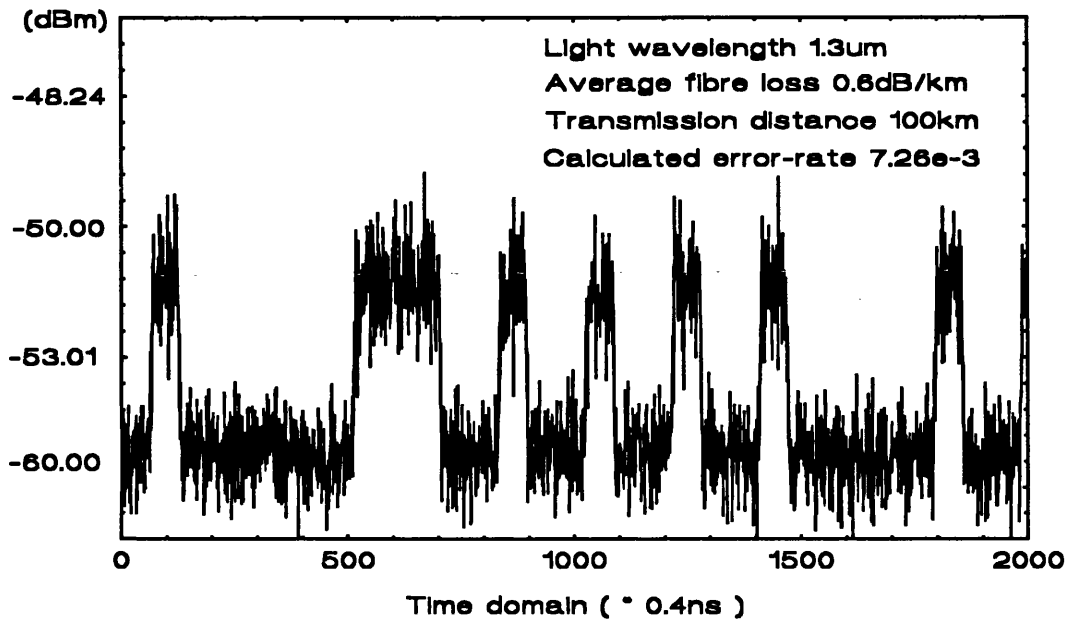


Fig.4.1 (c) Signal received by the APD with added noise, fiber length=100km

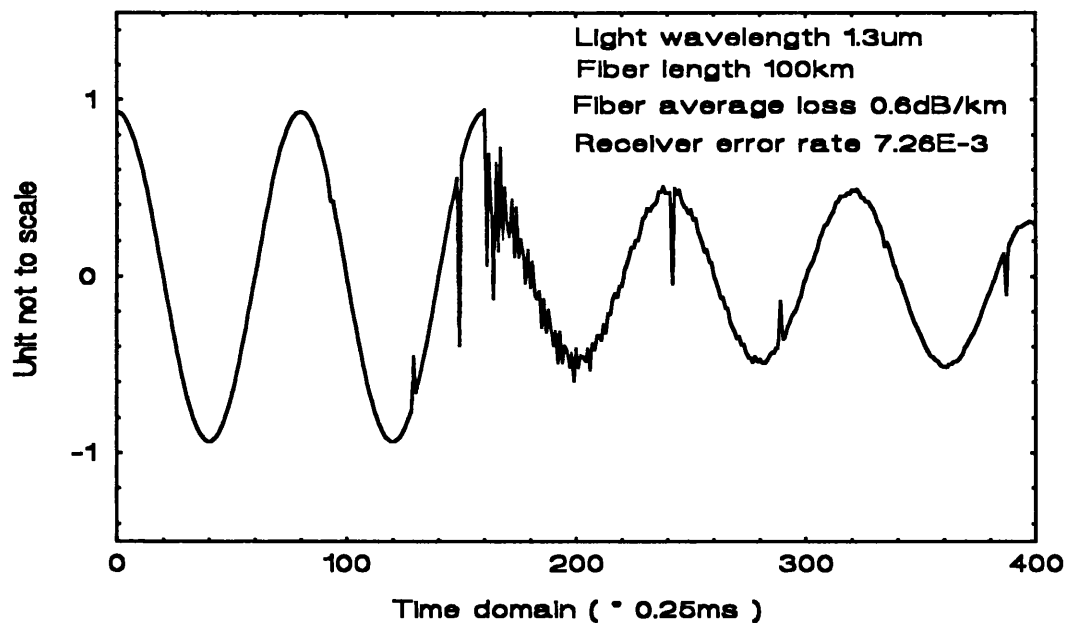


Fig.4.1 (d) Reception analogue waveform after decision circuit and D/A converter

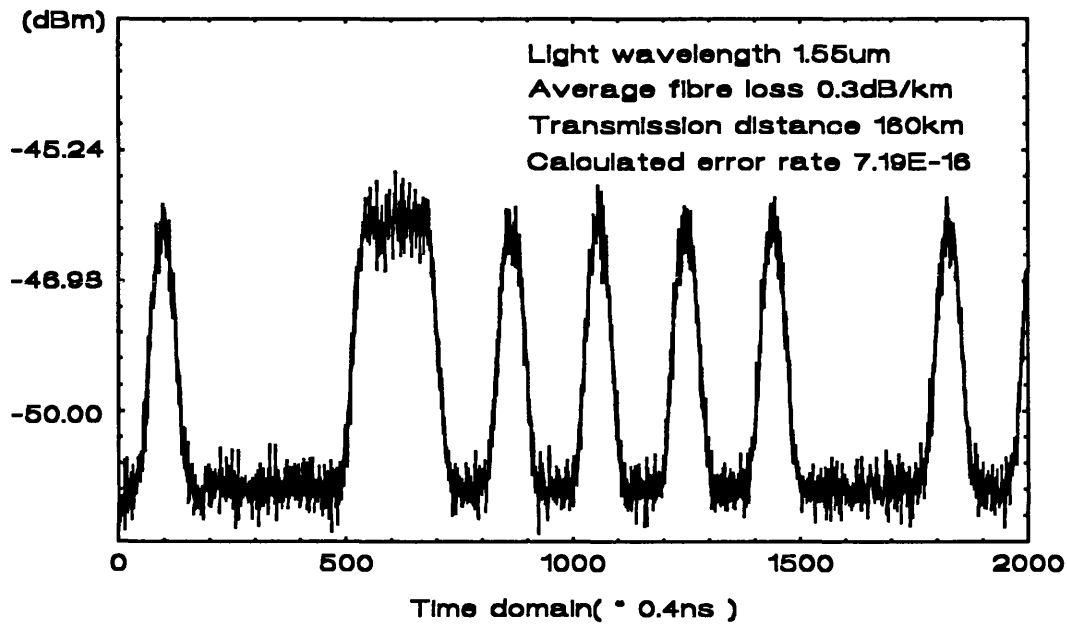


Fig.4.2 Signal received by the PIN with added noise
 $z = 160\text{km}$, $\lambda_0 = 1.55\mu\text{m}$, $\text{BER} = 7.26 \times 10^{-16}$

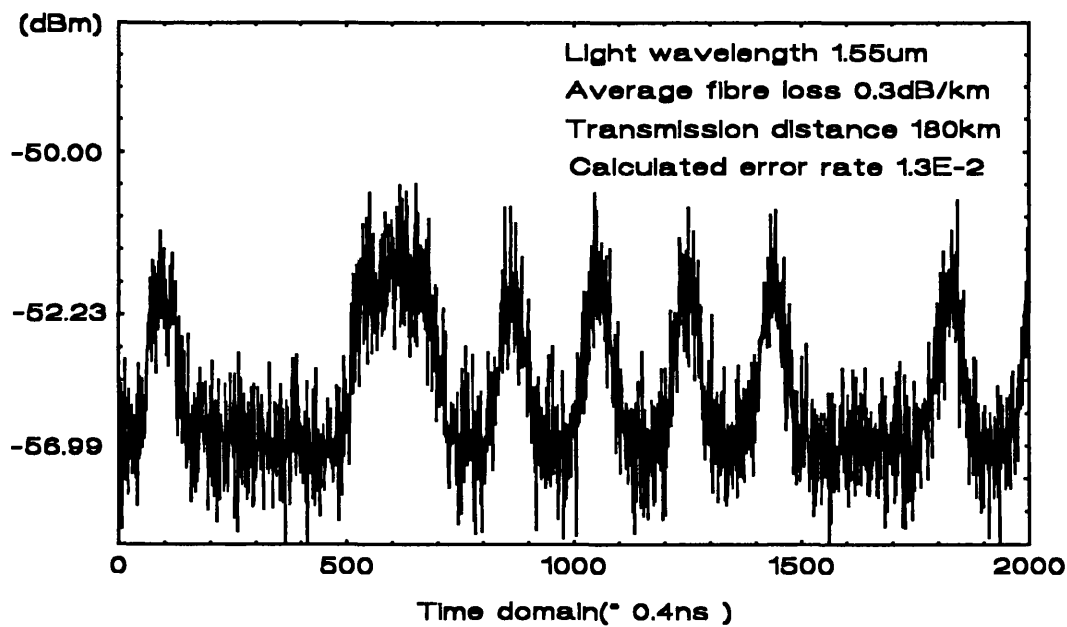


Fig.4.3 Signal received by the PIN with added noise
 $z = 180\text{km}$, $\lambda_0 = 1.55\mu\text{m}$, $\text{BER} = 1.3 \times 10^{-2}$

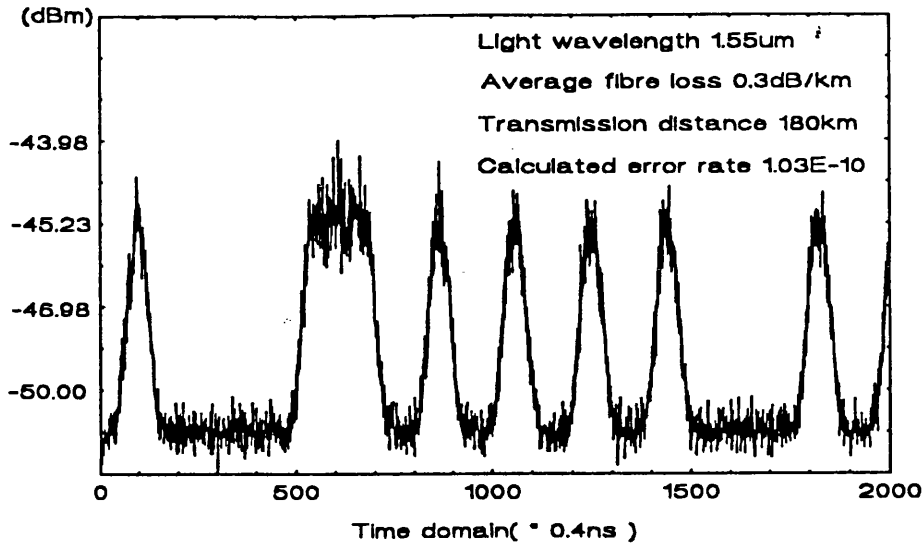


Fig.4.4 Signal received by the APD with added noise
 $z = 180\text{km}$, $\lambda_0 = 1.55\mu\text{m}$, $\text{BER} = 1.03 \times 10^{-10}$

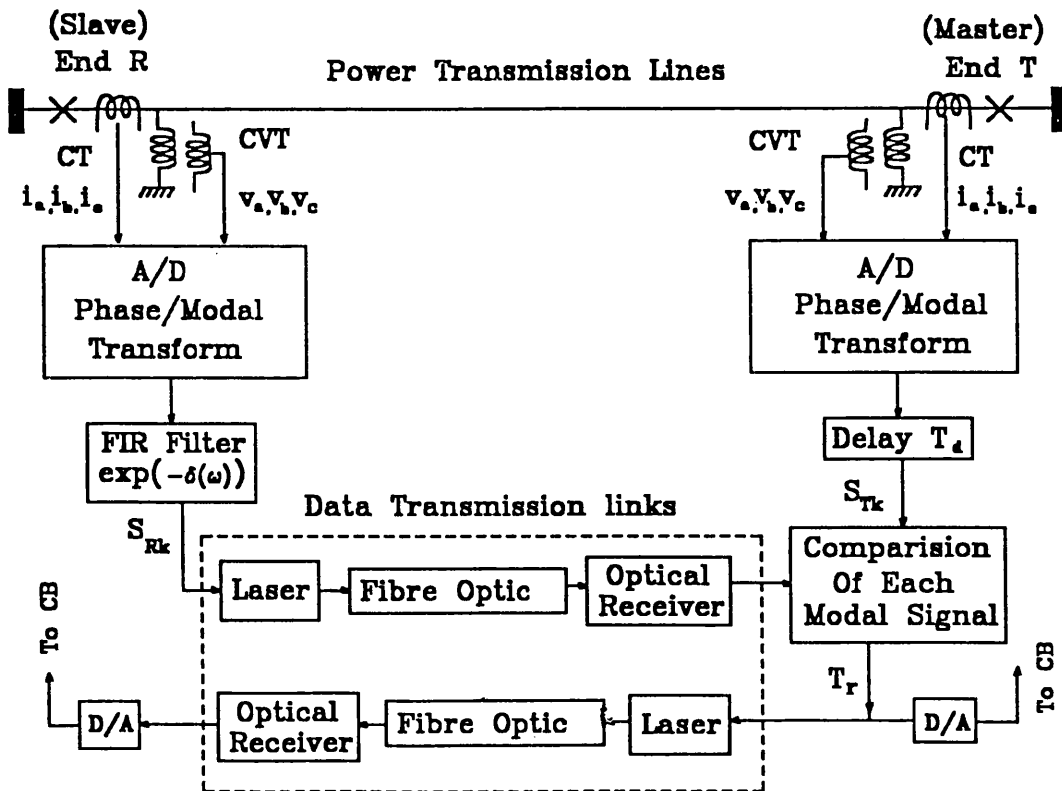
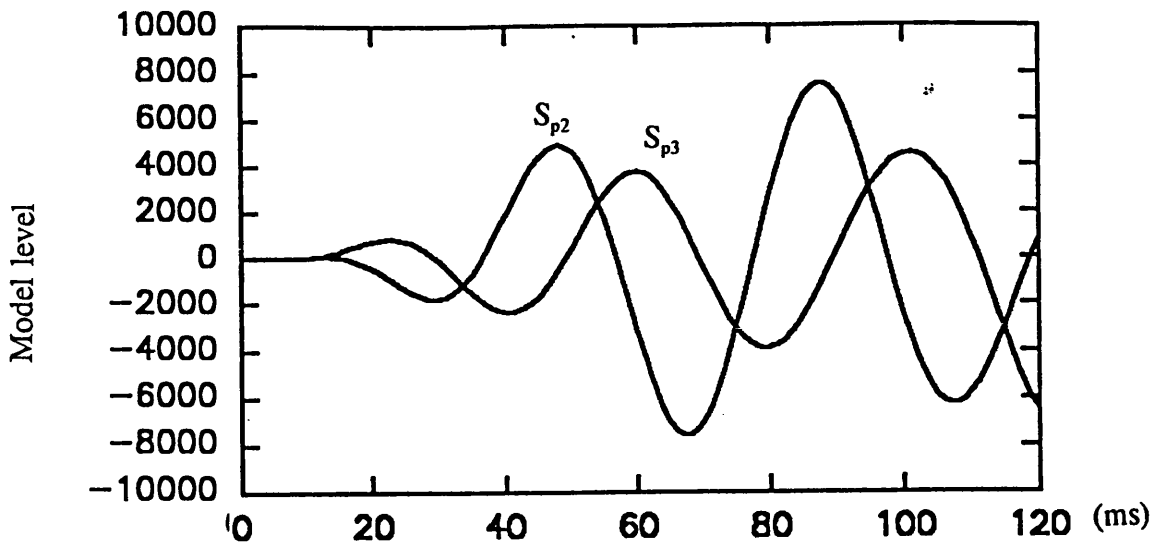
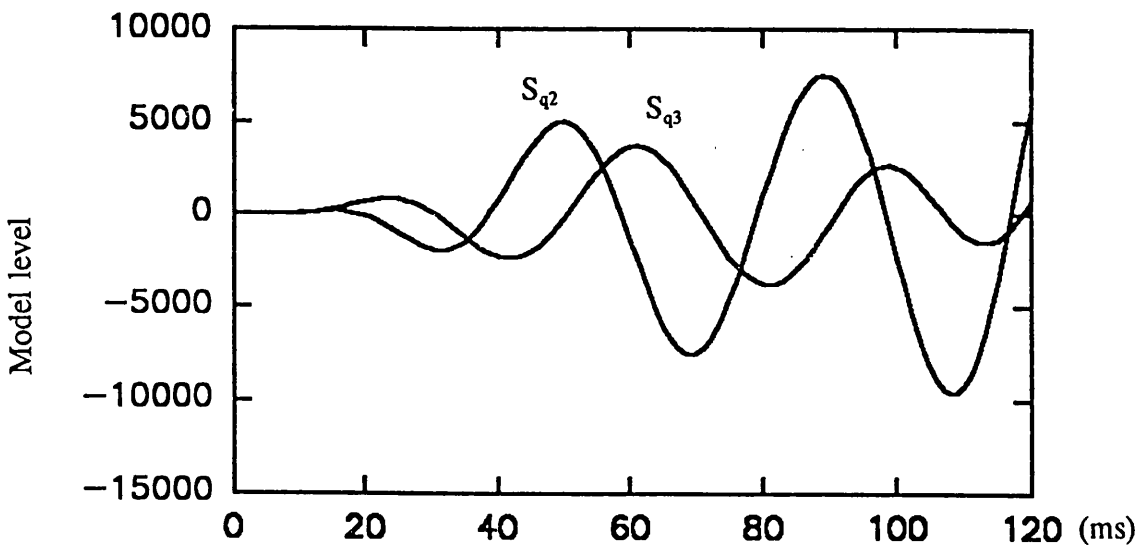


Fig.4.5 A block diagram of the line protection scheme with added the FOL model

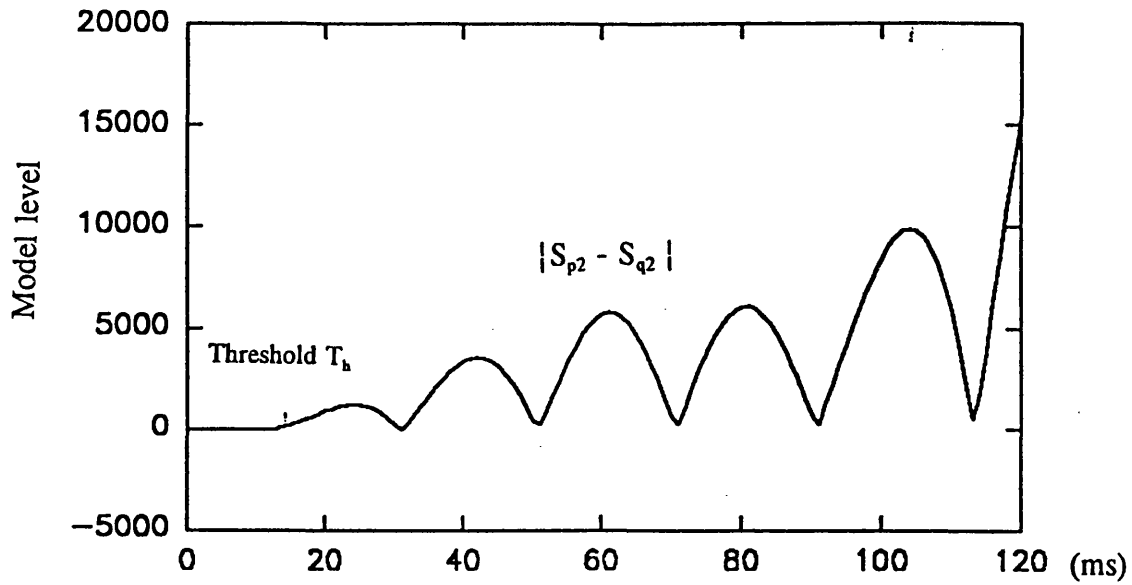


(a) Aerial mode signals at end P

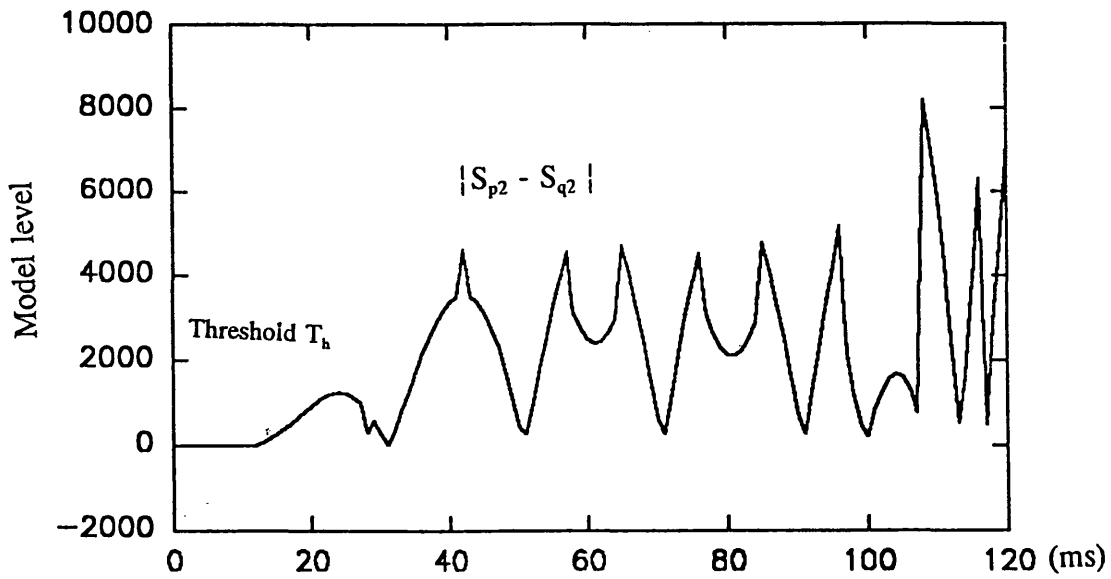


(b) Aerial mode signals at end Q

Fig.4.6 Aerial mode signals at ends P & Q

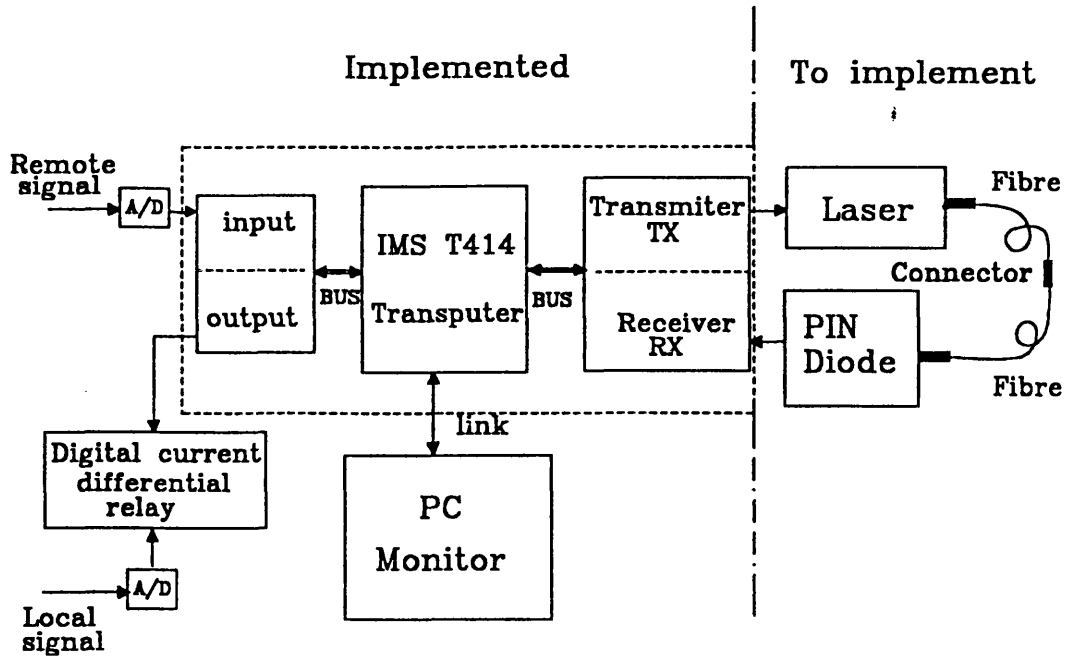


(a) Trip signal at FOL channels with no bit-errors

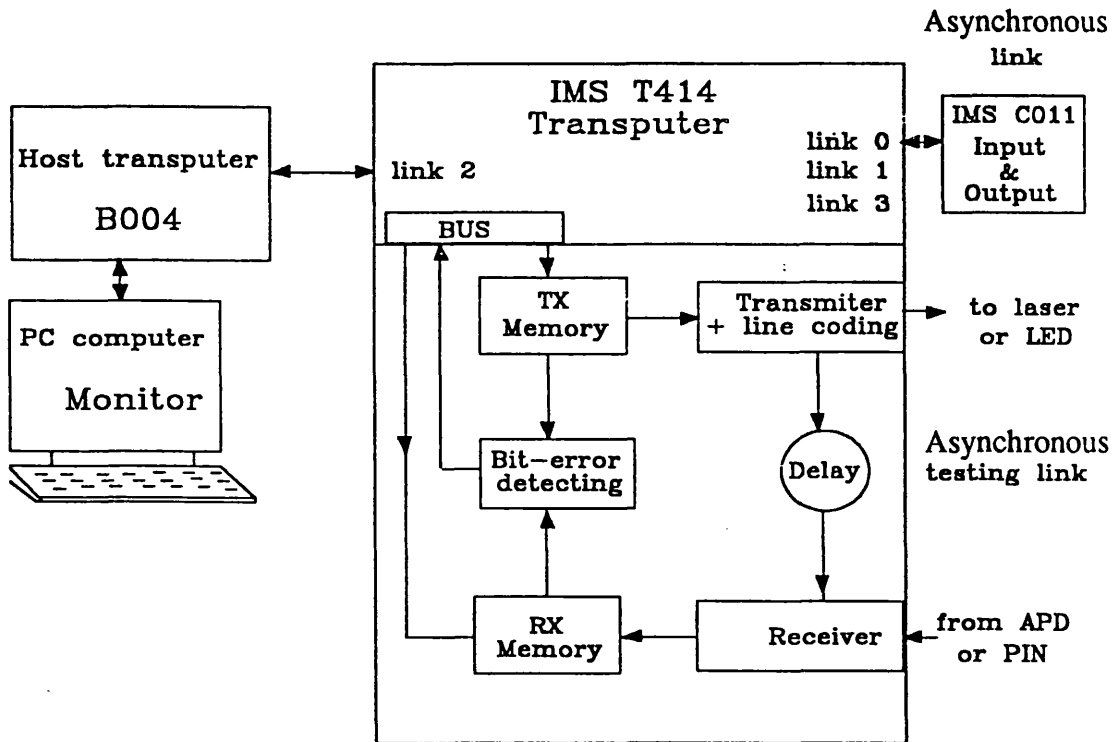


(b) Trip signal at FOL channels with bit-error rate $\approx 10^{-3}$

Fig.4.7 Trip signal $|S_{p2} - S_{q2}|$ (\geq Threshold level T_h)



(a) The block diagram of the complete fibre optic test system



(b) Partially implemented hardware testing board

Fig.4.8 A complete fibre optic test system

Table 4.1 Results of the TCB testing

line 1	T4 Full Test								
line 2	Loading and matching network ...								
line 3	Boot Booted by				Analysed				
line 4	Id	Link	Id	Link	Type	Speed	or Reset	Line	
Line 5	--	----	--	----	----	----	-----	----	
line 6	MT*	--	--	--	Host	---	Reset	ok	
line 7	0*	0	MT*	2	T414b	-17	ok	ok	
line 8	The total number of transputers found is 2								
line 9	Testing network ...								
line 10	Id	Type	Tested	Error	Id	Link0	Link1	Link2	Link3
line 11	--	---	-----	-----	-----	-----	-----	-----	-----
line 12	MT*	Host	----	-----	-----	---	0* 0	---	
line 13	0*	T414b	256k	ok	MT* 2	0000	0000	0000	
line 14	Testing will repeat - type <any> to exit								

CHAPTER 5

OPTICAL FIBRE CURRENT SENSORS SIMULATION

5.1 Introduction

In this chapter, a complete CAD study of FOCS modelling and its performance evaluation are presented. The FOCS model is a combination of a spun fibre model and a MFR model. The latter is introduced to overcome the temperature and vibration noise related side-effects. The performance of the simulated model of the FOCS is evaluated with particular regard to its current measurement range, bandwidth and noise limitations. In particular, a FOCS for EHV line protection is discussed and tested by using simulated fault current waveforms.

This Chapter starts by introducing the state of the art of the FOCS development, followed by an analysis of the design principles and considerations of related design parameters. Two sets of laboratory experimental results are also used to compare and contrast the computer simulation results with those from an actual test. The FOCS performance is fully evaluated based on the simulation results and some conclusions are reached.

5.2 The State of the Art of Fibre Optic Sensors

For most of the power system line protection schemes, current measurement is the most crucial step toward a successful operation of the protection. In EHV transmission line protection, electric currents are measured on line of several kilovolts such as a 400kV EHV line. A common conventional method for current measurement is based on the ferrous cored CT which typically steps down the current by a factor of 1000 ~ 2000 producing a current of a few amperes at secondary, and which is then measured

by conventional electronic method. Since the CT is placed in the high voltage region, the insulation between the CT secondary and the permeable core which surrounds the current carrying conductor must be extremely high, hence the CT used in EHV transmission line is both large and expensive. Also the conventional CT has a saturation problem under certain fault conditions, in particular when the fault currents are offset. There are limitations on the bandwidth which can pose problems with protection relay based on non-power frequency measurements such as of the travelling wave types.

Recently, there has been an upsurge in the development of FOCS for power system protection relaying. The attractiveness of FOCSs has increased with the introduction of digital protection relays that require signals only in the mW power range, in contrast to those supplied by the electromagnetic CTs which have secondary outputs of either 5A or 1A. The latter have then to be scaled down to the hardware level. At present, conventional CTs are still extensively used in both solid-state and microprocessor-based relays which have to have special interfacing modules for converting the secondary quantities from the electromagnetic CTs into levels suitable for the electronic circuitry.

FOCSs, coupled with fibre-optic cabling in order to provide the link from EHV switchyard to the control house (thus immunising the low level signals against electromagnetic interference), provide an attractive alternative. Other inherent advantages of the FOCS are: (i) A fibre is dielectric and thus does not require the usual costly and bulky oil-filled electrical insulation tower, with its tendency to explode if breakdown occurs, (ii) lack of saturation effects, (iii) lower weight and smaller size, (iv) components cost, driven by large commercial fibre optic telecommunication system and opto-electronic market, are reducing considerably with the extensiveness of the applications of these systems, (v) the FOCS is able to detect transient electrical faults owing to its high measurement bandwidth (limited only by the optical transit time of the light within the fibre).

Since the early demonstrations of the principle of optical fibre current monitoring by Papp et al.[51] and Smith [57], there has been active research and development aimed at understanding the polarization properties of the fibre [5, 47, 55, 64], at developing optical signal processing schemes [34] and at engineering such FOCSs for power systems line protection applications [10, 11, 41]. A FOCS consists of a light source, a polarizer, an analyzer and either a magneto-optic material placed near to current-carrying conductor or alternatively a coil of fibre wound around a current-carrying conductor. As described in section 2.2.3.5, the Faraday effect causes a rotation of a light polarization which is proportional to the current of the magnetic field when the light propagates in the fibre. Analysis of the output plane of the light polarization, therefore, can provide a measurement of the current. Unfortunately, problems of fibre bending, linear birefringence (the latter varies with temperature and vibration), severely limit the performance of ordinary FOCSs and challenge the invention of new generation of FOCSs.

The problem central to the development of a practical FOCS is to deal with the linear birefringence in the fibre which is invariably present as a result of intrinsic manufacturing imperfections, e.g. elliptical core, anisotropic stress [45], or induced by bending [64]. The linear birefringence interferes with the Faraday-induced rotation and, even if present in small amounts, makes it nearly impossible to measure the Faraday-induced rotation. The working rule of measuring Faraday rotation is that the maximum usable fibre length is one half its beat length L_p due to the periodic Faraday rotation property along the fibre length. Typical fibres have a L_p of a few metres when they are straight, or a few centimetres when packaged or wound in small coil. Thus, whatever the length of the fibre employed in the current sensor coil, the presence of linear birefringence will reduce the effective fibre interaction length to less than a metre. Moreover, package effects are environmentally unstable and this results in a variation in interaction length with time.

Birefringence is formed by two polarized light electric fields when they differently

propagate in their fast or slow axes respectively. Early work to overcome the birefringence problem was aimed at producing a low-birefringence fibre by spinning the preform during fibre drawing to average the fast and slow axes of the fibre. This technique for producing low birefringence spun fibre [5] has been widely used in experimental and prototype current monitors, however, the coiled fibre suffers from bend-induced birefringence [64] which will greatly reduce the current sensitivity due to small Faraday rotation quenched by the presence of bend-induced linear birefringence.

It has long been realized that it is an indispensable requirement for measuring Faraday rotation to induce sufficient circular birefringence [63] into the fibre to swamp the bend- and packaging-induced linear birefringence. Circular birefringence can be introduced into the fibre by either twisted fibre or spun fibre. The central idea of the large induced circular birefringence swamping into linear birefringence, is to regard the fibre as being composed of untwisted birefringence sections, each having a length of one quarter of a twist period and rotated with respect to each other by $\pi/2$ radians. Thus, an interchange of fast and slow light wave propagation occurs at the junction between the sections, and the birefringence of the first section is exactly cancelled by the second one and so on. Along the fibre length, the total birefringence will slightly oscillate around zero with a small magnitude which depends on the birefringence of the individual sections. Therefore a very low birefringence fibre is produced.

A problem with the twisted fibre is that, the number of turns per metre of a fibre is limited to about 100 before breakage, thus posing difficulty to produce a large circular birefringence. A practical maximum twist-rate for a cabled fibre is about 50 twists/m which can produce a relatively low circular birefringence, thus the minimum coil size which can be wound is restricted to 20-cm diameter. The problem with the FOCS design still exists since the fibre remains sensitive to the introduction of bend birefringence.

Stone [58] tried to overcome the bending problem by annealing coiled fibre to remove the bend-induced birefringence. However, removal of the fibre coating and subsequent high temperature annealing tends to weaken the fibre, making it difficult to produce a small multi-turn device. Moreover, the approach does not remove the vibration sensitivity.

Since low linear birefringence fibre is very sensitive to external perturbations such as vibration, coiling (i.e. bend) and applied stress, special fibres designed to overcome these problems are of particular interest. One solution to the problem is to excite only one polarized mode in a fibre to obtain a highly linear birefringence fibre, that is, the polarization-maintaining fibre. For the Faraday-effect current sensor, however, such an approach is unsuitable since the presence of highly linear birefringence in the fibre quenches the small Faraday rotation once the fibre length exceeds half of the polarization beat length L_p . Thus, the interaction beat length between the fibre and the magnetic field (Faraday sensitivity) is very small (in millimetre range) for the polarization-maintaining fibre.

In order to overcome the two aforementioned critical problems (in either low linearly birefringent fibre or highly linear birefringent fibre (e.g. Bow-tie fibre as shown in Table 2.1), a new type of spun fibre which exhibits a high-birefringence was developed [39], SHB fibre. By choosing appropriate fibre parameters and fibre-drawing conditions, a predominately-circular birefringence can be frozen in the fibre. In consequence, both circular-birefringence and linear-birefringence co-exist in the fibre to form elliptically birefringence (section 2.2.3.3). Large quasi-circular birefringence ensures good Faraday sensitivity, and highly linear-birefringence guarantees a high resistance to external perturbations. SHB fibre can be regarded as a compromise between the polarization-maintaining fibre and the true circularly birefringent fibre which has good electric-current response. It allows small-diameter multi-turn coils to be wound around a current-carrying conductor without paying special attention to the induced birefringence. Fibre coils, having hundreds of turns with a diameter as small

as one centimetre, are easily constructed, thus making fibre sensors sensitive to even very low electric currents.

A disadvantage of the SHB fibre approach for FOCS is that the precursor fibre depends its linear birefringence on thermal stress and therefore the magnitude of the induced elliptical birefringence in the SHB fibre is temperature-dependent. There are some signal processing schemes which have successfully overcome the temperature problem. They are (i) Reflect Back Configuration (RBC), (ii) Sagnac Interferometer Configuration (SIC), (iii) Mirror Faraday Rotator Configuration (MFRC). Laming et al. [38] presented a mathematical model of RBC current monitor for a CAD study of spun fibre current sensor. Their model was not complete as a mirror model was not shown. Also RBC sensors will still present very unstable current reading due to the birefringence changes with temperature. Clarke [12] presented a theoretical analysis for SIC, but there were not enough experimental results. Pistoni et al. [49,50] concluded, based on laboratory experimental results, that MFRC can greatly reduce reciprocal noises including vibration, temperature, etc., but as to the limitations of physical experiments, the study was not systematic and there is thus no complete CAD study for FOCS with MFRC which has hitherto been reported.

5.3 Fibre Optic Current Sensors Theory and Design

5.3.1 Spun Fibre Model

Generally speaking, it is feasible to make the assumption that in a birefringent fibre (e.g. elliptically fibre core), only two orthogonally polarized modes exist. Spun fibres are obtained by spinning such a conventional birefringent fibre during the drawing process. A typical spun fibre cross section construction is shown in Fig.5.1, and the corresponding coordinate system is shown in Fig.5.2, where the right hand rectangular coordinate system x , y and z represents air medium; light propagation is along the z axis. The initial light electric field E is linearly polarized at an angle φ to the x axis.

Rectangular principal right hand coordinate system x' , y' and z' are spun fibre medium. θ is the orientation angle between air medium and spun medium coordinate system. ξ is fibre spinning rate and assumed to be a constant. For a low spinning rate, ξ can be 20-40 turns per metre (turns/m), while for high spinning rate, ξ can reach 610 turns/m (1220π rad/m) or more. $\Omega(z)$ is the light rotating angle after propagating a z distance.

Jones [31] published his work of an operator for calculating optical system elements; this is the well-known Jones matrix. By using the Jones matrix, a retarder and a rotator for linear birefringence fibre are obtained as given in Appendix C.1. Using a plane-wave approximation, McIntyre & Snyder [43] analyzed the properties of an isotropic twisted fibre by modelling it as a stack of rotated birefringent plates and employing a coupled-mode theory, the details of which are shown in Appendix C.2. Also an analytical expression for the two orthogonally polarized fields in the fibre was represented as a function of the fibre birefringence, spinning rate and the fibre length.

With reference to Fig.5.2, in which it is assumed that an initial orientation angle is equal to $\theta(0)$ (the orientation angle at fibre $z = 0$). After light propagates a distance z ($z > 0$), the orientation angle becomes $\theta(z)$. By introducing the solution of twisted plane medium (McIntyre & Snyder ,1978) to spun fibre in Appendix C.2, and processing this result with Jones matrix operator, a spun fibre model may be represented as:

$$\begin{bmatrix} E_x(z) \\ E_y(z) \end{bmatrix} = \begin{bmatrix} \cos\theta(z) & -\sin\theta(z) \\ \sin\theta(z) & \cos\theta(z) \end{bmatrix} \begin{bmatrix} \cos\gamma z + j\frac{\Delta\beta}{2\gamma}\sin\gamma z & \frac{\xi}{\gamma}\sin\gamma z \\ -\frac{\xi}{\gamma}\sin\gamma z & \cos\gamma z - j\frac{\Delta\beta}{2\gamma}\sin\gamma z \end{bmatrix} \times \begin{bmatrix} \cos\theta(0) & \sin\theta(0) \\ -\sin\theta(0) & \cos\theta(0) \end{bmatrix} \begin{bmatrix} E_x(0) \\ E_y(0) \end{bmatrix} \quad (5.1)$$

$$\gamma = \frac{1}{2} \sqrt{\Delta\beta^2 + 4(\xi + f)^2} \quad (5.2)$$

$$\text{where } \Delta\beta = \frac{\beta_x - \beta_y}{2}, \quad f = \frac{5.79 \times 10^{-19}}{\lambda^2} \frac{I}{D} \quad (\text{rad / m})$$

f is the unit Faraday rotation as given by equation (2.17) in section 2.2.3.5.

Furthermore, assuming $\theta(0) = \theta$, $\theta(z) = \theta + \xi z - \Omega'(z)$, $2\phi(z) = \theta(z) + \theta(0)$ and $\Omega(z) = \theta(z) - \theta(0)$. (For detailed expansion, please see equation (C.3-4) in Appendix C.3.), a simplified form of the matrix is obtained:

$$[E(z)] = [K(z)] [E(0)] \quad (5.3)$$

The column matrix form $[E(0)]$ has two polarized elements $E_x(0)$ and $E_y(0)$, $[E(z)]$ has its own two polarized elements $E_x(z)$ and $E_y(z)$. $[E(0)]$ is the initial electric field and z the transmission distance in $+z$ direction, $[K(z)]$ is the square matrix for fibre transfer function which is represented as following:

$$[K(z)] = \begin{bmatrix} B_2 + jB_1 & -K_2 + jK_1 \\ K_2 + jK_1 & B_2 - jB_1 \end{bmatrix} \quad (5.4)$$

Where $B_2 = \cos \gamma z \cos \Omega(z) + \xi/\gamma \sin \gamma z \sin \Omega(z)$

$$B_1 = \Delta\beta / 2\gamma \sin \gamma z \sin 2\phi(z)$$

$$K_2 = \cos \gamma z \sin \Omega(z) - \xi/\gamma \sin \gamma z \cos \Omega(z)$$

$$K_1 = \Delta\beta / 2\gamma \sin \gamma z \cos 2\phi(z)$$

For a spun fibre [22], the $K_2 = 0$, therefore, $\cos \gamma z \sin \Omega(z) - \xi/\gamma \sin \gamma z \cos \Omega(z) = 0$, so that the following is established:

$$\Omega(z) = \tan^{-1} \left(\frac{\xi}{\gamma} \tan \gamma z \right) + n\pi \quad (5.5)$$

Since $\theta(z) = \theta + \xi z - \Omega'(z)$, $\Omega(z) = \theta(z) - \theta(0)$, $2\phi(z) = \theta(z) + \theta(0)$ and $\theta(0) = \theta$, thus:

$$\Omega'(z) = \xi z - \tan^{-1} \left(\frac{\xi}{\gamma} \tan \gamma z \right) + n\pi \quad (5.6)$$

$$\phi(z) = \frac{1}{2} \tan^{-1} \left(\frac{\xi}{\gamma} \tan \gamma z \right) + \frac{m\pi}{2} + \theta \quad (5.7)$$

m, n are integers and θ is the initial orientation of the local slow axis of the fibre.

A similar conclusion appeared in [5, 38], but there were no detailed inferences. Furthermore, reflected conjugate mirror model was not represented in reference [38].

5.3.2. Faraday Rotator Model

As mentioned in section 2.2.3., the SOP of the light wave in a fibre can be changed by the Faraday effect when the fibre (or fibre sensor head) is exposed to a magnetic field and the quantitative relation between the current of the magnetic field and the polarization changes is as shown in equation 2.15. In a FOCS design, the principle is to measure the current indirectly by measuring the induced Faraday rotation, and another introduced method is to use a permanent 45° Faraday rotator followed by a mirror for a RBC to form a MFRC. The MFRC can eliminate the influence of any medium birefringence changes (e.g. temperature effect on spun fibre) on the final SOP of the propagating light beam. It behaves like a mirror where the returning light beam is always orthogonally polarized with respect to the incoming light beam. Pistoni et al. [49,50] published some experimental results of FOCS under the MFRC. These results gave some basic idea and sensing impression of how to use a permanent 45° Faraday rotator effectively in order to eliminate the influence of medium birefringence changes. In this CAD study of a FOCS, a permanent 45° Faraday rotator is also considered. Furthermore, it is aimed to conduct a systematic study of taking advantage of the flexibility of CAD methods.

A mathematical Faraday rotator model is considered as a starting point herein. In the rectangular coordinate system, light is assumed through a Faraday rotator with a permanent 45° Faraday rotation angle. Thus at forward (+z direction) light propagation path , the Faraday rotator matrix [68] is :

$$[F + 45^\circ] = \begin{bmatrix} \cos 45^\circ & \sin 45^\circ \\ -\sin 45^\circ & \cos 45^\circ \end{bmatrix} = \begin{bmatrix} \sqrt{2} / 2 & \sqrt{2} / 2 \\ -\sqrt{2} / 2 & \sqrt{2} / 2 \end{bmatrix} \quad (5.8)$$

At backward light propagation path with -z direction , it is:

$$[F - 45^\circ] = \begin{bmatrix} \cos 45^\circ & -\sin 45^\circ \\ \sin 45^\circ & \cos 45^\circ \end{bmatrix} = \begin{bmatrix} \sqrt{2} / 2 & -\sqrt{2} / 2 \\ \sqrt{2} / 2 & \sqrt{2} / 2 \end{bmatrix} \quad (5.9)$$

The MFR model of equation (5.9) will be used in the FOCS modelling.

5.3.3 Phase Conjugate Mirror

A phase conjugate mirror (M) is used as a light reflector. The purpose of using such a mirror is to compensate for linear birefringence variations caused by temperature etc. (any reciprocal variations) in a FOCS. The effect of a true (scalar) phase conjugate mirror which renders the complex conjugate of each Cartesian coordinate of a vector, would, by definition, be the transformation [68]:

$$\begin{bmatrix} a \\ b \end{bmatrix} \rightarrow \begin{bmatrix} a^* \\ b^* \end{bmatrix} \quad (5.10)$$

This is true when using a rectangular coordinate system and the same z axis for the incident wave and reflected wave. Since the conjugate wave always travels in the direction opposite to that of the incident wave, we represent the conjugate wave in its reflected frame by changing the sign of the x (or y) component. The effect of phase conjugation in the rectangular coordinate system is then represented symbolically by $[M]^*$:

$$[M]^* \begin{bmatrix} a \\ b \end{bmatrix} = \begin{bmatrix} -a^* \\ b^* \end{bmatrix} \quad (5.11)$$

where it is assumed that the reflected light is with a changed sign of the x component.

5.3.4 Design and Configuration

Most FOCS measurement schemes use a configuration which involves launching linearly polarized light into the fibre and analysing the SOP of the light output. In the case of an isotropic or pure circularly birefringent fibre, the output is plane polarized and rotated by the Faraday effect. For the SHB fibre which is quasi-circularly birefringent, it can be regarded as being composed largely of a rotator element, but with a small retarder component. The output SOP will then be, in general, nearly plane-polarized with a degree of polarization ellipticity which depends on how close to circular birefringence the fibre birefringence is.

Since the SHB fibre is obtained by spinning a fibre with thermal stress-induced linear birefringence, it is also temperature-dependent. The following current sensor scheme was developed to compensate for the varying polarization orientation and ellipticity which results from the temperature-sensitive elliptical birefringence.

A basic configuration of the FOCS is shown in Fig.5.3, in which a MFR is set at the end of the fibre. This FOCS configuration was once used as a method of compensating for the temperature and vibration related side-effects in the twist-induced circular birefringence experienced in a current monitor.

In Fig.5.3, the LD is used as a light source. The lenses are used for focusing the light beam on a proper position of the optical components, and the light beam goes through a 45° polarizer with respect to the fibre linear birefringence axes (β_x at its x-axis and β_y at its y-axis). Assuming the polarized electric field is E_m , therefore the

polarized electric field $E_{x0} = E_m \cos 45^\circ$ at x-axis, and $E_{y0} = E_m \sin 45^\circ$ at y-axis. After the initial polarized light E_m goes through the beam splitter (BS), half of the polarized optical light energy goes to the Wollaston prism (WP) which is oriented at the same 45° angle with respect to the polarizer, and another half of the polarized optical light energy enters into one end of the spun fibre. After WP, there are two photo-detectors. The photo-detectors detect intensity of two orthogonally polarized modes E_x and E_y , separated by the WP. The sensor output response formula, P [57], is:

$$P = \frac{I_1 - I_2}{I_1 + I_2} = \frac{E_x^2 - E_y^2}{E_x^2 + E_y^2} \quad (5.12)$$

In Fig.5.3, MFR consisting of a M and a permanent 45° Faraday rotator, is set at the other end of spun fibre. It presents a retracing spun optic fibre circuit to suppress the effect of any reciprocal birefringence (e.g. linear and circular birefringence present in the fibre). The MFR guarantees that a light beam which returns in its polarization state will always be linear and orientated at 90° (orthogonal) to the launch state. The singular nature of the MFR matrix representation can be derived from equations (5.8) , (5.9) and (5.11) :

$$[MFR] = [F^{-45^\circ}] [M]^* [F^{+45^\circ}] = \begin{bmatrix} 0 & -1 \\ -1 & 0 \end{bmatrix} \quad (5.13)$$

Now let us see how the light beam SOP operates in the spun fibre when the MFR is employed, assuming that fibre length is z , and the $+$ and $-$ represent a light propagation to $+z$ and $-z$ direction, respectively. Let an initial propagated polarized electric fields be $E_x^+(0)$ and $E_y^+(0)$. When passed through the spun fibre length z , the Faraday rotation induced by a current will modify these fields $E_x^+(0)$ and $E_y^+(0)$ to be $E_x^+(z)$ and $E_y^+(z)$. The $E_x^+(z)$ and $E_y^+(z)$ are then reflected by MFR to become initial backward propagation polarized electric fields which represents as $E_x^-(0)$ and $E_y^-(0)$. When $E_x^-(0)$ and $E_y^-(0)$ return through the spun fibre path with distance $-z$, Faraday rotation induced by the current further modify electric field which then become $E_x^-(-z)$ and $E_y^-(-z)$. By using equations (5.4) and (5.13), total return electric fields thus

become:

$$\begin{bmatrix} E_x(2z) \\ E_y(2z) \end{bmatrix} = [K(-z)] [MFR] [K(z)] \begin{bmatrix} E_x(0) \\ E_y(0) \end{bmatrix} \quad (5.14)$$

where $[K(z)]$ is derived from equation (5.4), $[MFR]$ is derived from equation (5.13) and $[K(-z)]$ is the elements in the reverse direction of $[K(z)]$. The return electronic fields $E_x(2z)$ and $E_y(2z)$ will be divided by the BS and go into the WP. Again after WP, two photodiodes can detect the returned electric fields separated by WP. The current outputs of the photodiodes can be transformed into the sensor response formula P of equation (5.12).

In the case of detecting initial polarized electric fields, $E_x^+(0)$ and $E_y^+(0)$, $E_x^+(0)$ is equal to $E_{in}\cos45^\circ$ and $E_y^+(0)$ is equal to $E_{in}\sin45^\circ$. The WP will separate $E_x^+(0)$ and $E_y^+(0)$ into two photo-detectors, respectively. Since $E_x^+(0) = E_y^+(0)$, so the detected signal $P = 0$.

In the case of detecting the return electric fields, $E_x(2z)$ and $E_y(2z)$ in equation (5.14) are used to put into equation (5.12). If the Faraday rotation modify the $E_x(2z)$ and $E_y(2z)$, the detecting signal P can sense a double Faraday rotation. However, if any reciprocal noise modify the $E_x(2z)$ and $E_y(2z)$, the detecting signal P can sense little reciprocal noise due to the reflected path of the fibre with MFR. The detailed explanation of the MFR eliminating any reciprocal noise can be found in [49].

5.4 Simulation Results Analysis

5.4.1 Available Laboratory Experimental Results

In this section, two sets of the available laboratory experimental results are used in order to compare and contrast previous physical experimental results with those obtained from a computer simulation FOCS model.

Firstly, let us consider the $\Delta\beta$ variations with temperature. A set of experimental results based on RBC of spun fibre current sensor was described by Laming & Payne [38]. The FOCS experimentally determined response P for a loosely wound, 30-turn fibre coil with nominal unspun high $\Delta\beta = 1234\pi$ rad/m (beat length $L_p = 2\pi/\Delta\beta = 1.62\text{mm}$) and spun fibre $\xi = 1219\pi$ rad/m (spin pitch $L_s = 2\pi/\xi = 1.64\text{mm}$). The total fibre length z was $\sim 10\text{m}$ and a single-longitudinal mode semiconductor laser operating at light wavelength $\lambda_0 = 780$ nm was used to inject light into the fibre with the fibre orientation angle $\theta \approx 110^\circ$. The experimental result for the response is shown in Fig. 5.4. It shows the sensor signal response, P, varying with the sensor temperature.

Secondly, let us look at a MFR inserted into a whole FOCS. A set of vibration-insensitive test results based on a MFRC with twisted fibre was given by Pistoni et al. [50]. In the experimental setup, the laser diode emitting at light wavelength $\lambda_0 = 675\text{nm}$ (Toshiba TOLD 9200) was launched into a single-mode twisted low-birefringence fibre 10 metres long. The ξ is 40 turns/m, and $\Delta\beta = 0.17$ rad/m. The external vibration excited at the frequency of 55Hz was made by a mini-shaker. The vibration amplitude was set in order to produce a total birefringence modulation equivalent to 50 micro radians at the output. The experimental results are given in Fig.5.5. Fig.5.5(a) show a power spectrum of the signal induced by a current of 50A rms at 50Hz in the presence of the vibration noise at 55Hz. Fig.5.5(b) shows a power spectrum of the signal detected by the MFR's FOCS. The results show that only 50Hz current signal has significant amplitude and the effect of the vibration noise (55Hz) is reduced by 30dB leading to a residual noise that does not affect the current signal (50Hz).

5.4.2 Simulation Results Evaluation and Comparative Study

In this section, the simulation results based on the FOCS simulation model are presented and analyzed. They are compared with the experimental results as discussed

in section 5.4.1. Furthermore, in order to be able to conduct a comparative study with the experimental results, some necessary adjustments are made to the designed model discussed in section 5.2.

Firstly a $[M]^*$ (in equation 5.11) instead of a $[MFR]$ is used in equation 5.14, so that the sensor becomes a RBC scheme as described in the experiment corresponding to the first set of experimental results in section 5.4.1. All parameters of the RBC scheme are thus set the same as those used in the laboratory experimental. They are: the spun fibre length is 10m, the fibre has $L_p = 1.62\text{mm}$ ($\Delta\beta = 1234\pi$ rad/m) and $L_s = 1.64$ mm ($\xi = 1219 \pi$ rad/ m). Finally the optical current responses based on the model of equation 5.12 are simulated. The optical current response P is plotted against a $\Delta\beta$ change from 1235π to 1233π for the fibre orientation angle at fibre input $\theta = 110^\circ$ as shown in Fig. 5.6.

By comparing the simulation results in Fig.5.6 with the first set of experimental results in Fig.5.4, it is clearly evident that the simulation results are in close correspondence with the experimental results. This verifies this simulation results and moreover, it proves the accuracy of our analysis of the theory underlying the designing principle and also suggests that equation 5.12 and equation 5.14 can be used in a CAD study of the FOCS model.

In the RBC scheme, the response P varies widely with $\Delta\beta$ variation and is dependent on fibre orientation angle θ . Fig 5.7 shows the P to $\Delta\beta$ variations at four different fibre orientation angle θ cases. When the fibre orientation angle $\theta = 0^\circ$ or 45° , the P mean values are near to zero with $\Delta\beta$ variation is from 1235π to 1233π , but the two response phase difference is 90° . Again when $\theta = 22.5^\circ$ or 67.5° and $\Delta\beta$ variation is from 1235π to 1233π , the sensor response P mean values are near -0.2 or +0.2 respectively. From experimental and simulation results shown in Fig.5.4, Fig.5.6 and Fig.5.7, it is also clear that, although FOCS with the RBC scheme as a method for compensating the thermal variations in the SHB current sensor, the P still varies

considerably with $\Delta\beta$ variations. Since the $\Delta\beta$ variation may be caused by many perturbation factors such as temperature and vibrations, so special birefringence control equipment is required. In order to overcome the side-effect caused by reciprocal noise which causes $\Delta\beta$ changes, e.g. the variation, a MFR is taken into account in our CAD study of FOCS model.

The simulation processes of a MFRC FOCS is carried out in the next simulation stage. The FOCS design parameters are unspun fibre high $\Delta\beta = 1234\pi$ rad/m ($L_p = 2\pi/\Delta\beta = 1.62\text{mm}$) and $\xi = 1219\pi$ rad/m ($L_s = 2\pi/\xi = 1.64\text{mm}$), the total fibre length $z = 10\text{m}$. By using equation (2.16), the Faraday rotation F can be calculated. With the fibre length 10m and fibre coil 12 turns, a relatively small current of 50A rms and its induced Faraday rotation F are plotted in Fig.5.8(W1) and (W3) respectively, and their corresponding spectrum analysis are plotted in Fig.5.8(W2) and (W4) respectively. Further, by choosing the fibre length 10m and fibre coil 30 turns, a larger current of 1.06kA rms and its induced Faraday rotation F are plotted in Fig.5.9(W1) and (W3) respectively, and their corresponding spectrum analyses are plotted in Fig.5.9(W2) and (W4) respectively.

The above results show the quantitative Faraday rotation waveforms corresponding to current waveforms. In the case of a small current waveform (current rms = 50A), the Faraday rotation (about 0.005 rad) is rather small. The latter is further limited by several noises. The question now is how small a Faraday rotation can be detected by the FOCS? The answer will be given in the next section. In the case of large current (current rms = 1.06kA), the maximum Faraday rotation (about 0.37 rad) should be within $\pm \pi/2$, since Faraday effect is circular rotation with a cycle $\pi/2$. Normally sensor response P is a nonlinear function of the Faraday rotation F , a good linear range would be required to be within $\pm \pi/6$ (0.5236 rad or 30°). Fig.5.9(W3) shows the 50Hz current signal of 1.06kA rms corresponding to nearly $\pm 0.37\text{rad}$, therefore detectable P should stay within linear range. This limits the maximum measurement range of the FOCS. Details of the measurement range and small current sensitivity in

the FOCS simulation model will be discussed in the next section.

The following simulation processes evaluate the simulation model by adding both Faraday rotation and reciprocal noise to it. Firstly, consider vibration noise which can be modelled as if causing a rotation Θ (rad) which is assumed to be a sinusoid signal and its frequency is at 100Hz. The vibration rotation amplitude is adjusted to a certain value which is compatible with Faraday rotation. With reference to the previously mentioned spun fibre model, it can be assumed that the polarized electric fields are changed by both the Faraday rotation and the vibration rotation after light travels a distance z in the spun fibre. Note that the Faraday rotation is a non-reciprocal signal and vibration rotation is a reciprocal signal. According to the concept of reciprocal and non-reciprocal signal, if a positive sign (+) is assumed for both Faraday phase rotation and vibration phase rotation, when light beam is propagating in a forward direction down a fibre. However light beam is propagating in a backward direction from a fibre, the sign of vibration phase rotation is still positive and the sign of Faraday phase rotation must be negative. Thus the total rotation phase Ψ should be $\Psi^+ = \Theta^+ + f^+$ when the light beam is forward propagated down a fibre, and $\Psi^- = \Theta^- - f^-$ when it is backward propagation; f is unit Faraday rotation, Θ is reciprocal noise (i.e., vibration) rotation, sign + represents forward (+z direction) light propagation in the fibre, and sign - is backward (-z direction) light propagation in the fibre. We can thus substitute Ψ^+ into the square fibre transfer function matrix $[K(z)]$ of equation (5.4), and Ψ^- into the fibre transfer function matrix $[K(-z)]$ which is the reversing matrix of $[K(z)]$. Now by using the CAD model, the forward light propagation rotation Ψ^+ and the sensor detected signal response P and their corresponding spectrum analyses are plotted as in Fig.5.10(W5) - (W8).

Fig.5.10(W5) and (W6) show the forward light propagation rotation Ψ^+ waveform and its spectrum respectively. It can be seen that Ψ^+ has two frequencies, one corresponds to a 50Hz Faraday rotation F (F is induced by a current of 1.06kA rms in Fig.5.9(W3) and (W4)). the other is a 100Hz vibration rotation which is modelled as a sinusoid

waveform. When both the total Ψ^+ and Ψ^- are put into the FOCS simulation model, the sensor response P is obtained. P and its spectrum are shown in Fig.5.10(W7) and (W8). Some important points are discussed below:

(i) In Fig.5.10(W5), it shows Ψ^+ waveform which contains Faraday rotation and reciprocal noise. Its spectrum is plotted in Fig.5.10(W6). Comparing Fig.5.10(W5) with Fig.5.9(W3), the distortion in waveform of Fig.5.10(W5) due to the 100Hz sinusoid signal amplitude is clearly evident.

(ii) Fig 5.10(W7) is sensor detected P corresponding to the input signal waveform in Fig.5.10(W5). Fig.5.10(W8) shows the spectrum of the waveform in Fig.5.10(W7). It is clearly evident there is little difference in waveform distortion between the original Faraday rotation in Fig.5.9(W3) and the sensor detected waveform in Fig.10(W7). This means that sensor detected signal waveform in Fig.5.10(W7) is recovered from the distorted signal in Fig.5.10(W5) into nearly original current waveform in Fig.5.9(W3). When comparing their corresponding frequency spectra as shown in Fig.5.9(W4) and in Fig.5.10(W8), respectively, the latter shows small fluctuations, but these are of very much reduced magnitude and arise due to nonlinear sensor detection. However it can be said that there is close correspondence between the two.

(iii) By comparing the 50Hz and 100Hz components in Fig.5.10(W6) with that in Fig.5.10(W8), it can be estimated that the difference between two components is about 10dB in Fig.5.10(W6), and it is about 45dB in Fig.5.10(W8). Thus the 100Hz component is reduced by about 35dB in Fig.5.10(W8) compared to that in Fig.5.10(W6). This amount of amplitude reduction at 100Hz leads to a residual amplitude in the case of a simulation that does not affect the current signal.

(iv) By comparing the spectra in Fig.5.10(W6) and (W8) with the experimental results in Fig.3.5(a) and (b), it is clear that the CAD simulation results of a 35dB noise reduction meets the experimental results quite well. The simulation results show a 5dB

margin better than that in experiments.. This is reasonable due to the theoretical assumptions used in the CAD study model. In practice both predictable and unpredictable factors may affect the performance of the current sensor, and further investigation, such as design of a practical sensor device, is needed in this area.

In practice, reciprocal noise exists within a large frequency range. A question arising is whether the FOCS simulation model still able to eliminate those noise effects? Now let us consider two frequencies of 100Hz and 150Hz. Reciprocal noise at these frequencies is added on to the total phase rotation Ψ^+ of forward light propagation and Ψ^- of the backward light propagation. Both Ψ^+ and Ψ^- include a Faraday rotation signal induced by a current of 1.06kA rms in Fig.5.9(W3). The simulation results of the sensor response are as plotted in Fig.5.11(W5)-(W8). The results in Fig.5.13(W5)-(W8) clearly indicate that the same amount of a 35dB noise reduction at both these frequencies is achieved. It can thus be concluded that any frequency of reciprocal noise can be reduced to a certain level, leading to a residual noise which has little influence on the current measurement in the FOCS.

In summary, the analysis results and comparison with the laboratory experimental results have proved that the FOCS simulation model developed herein is feasible in producing FOCS design models for practical devices.

5.5 Fibre Optic Current Sensor Simulations Performance Evaluation

5.5.1 Measurement Range

Referring to equation (2.19), a detectable Faraday rotation F , ($2F = 3.34 \cdot 10^{-4} N I$ (degree) at $\lambda_0 = 790\text{nm}$ or $2F = V_H N I = 5.2 \cdot 10^{-4} N I$ (degree) at $\lambda_0 = 633\text{nm}$), is given. For an ideal fibre sensor detecting case, $\Delta\beta = 0$; since the sensor response $P = \sin(2F)$ as given in equation(2.20), thus the detectable F range should be less than 45° . A good linearity range of F may be between 0 and 30 degree. Based on the

formula of $P = \sin(2F)$, the sensor measurement range can, therefore, be calculated.

In the MFRC FOCS simulation model, the ratio $(I_1 - I_2) / (I_1 + I_2)$ of the sensor detector is a nonlinear function of Faraday rotation, so there is not a forward straight way of calculating the Faraday rotation. However, the developed CAD study of the FOCS simulation model can be used to evaluate the polarization behaviour of a spun fibre with MFRC and also to measure Faraday rotation indirectly. Furthermore, the intrinsic nonlinear part of the sensor can be easily investigated.

In this CAD design of the FOCS, the fibre length is 10m, the fibre coil turn number is 100. A Faraday rotation, induced by a current varying from -4000A to +4000A, is used as the input to the FOCS, the sensor responses to this indirect current input with respect to several fibre orientation angle θ are shown in Fig.5.12(a), where curves 'a', 'b', 'c' and 'd' correspond to $\theta = 0^\circ, 22.5^\circ, 45^\circ$ and 67.5° , respectively. It shows that curves 'b' and 'd' need a bias current to enable P to have a symmetric response to the input current. For an easy reading of this bias current value, curve 'b' is shifted +0.1 and curve 'd' shifted -0.1, then the absolute sensor response P for the fibre orientation angle $\theta = 0^\circ, 22.5^\circ, 45^\circ$ and 67.5° is plotted correspondingly as curves 'a', 'b', 'c' and 'd' in Fig.5.12(b). They clearly show that the sensor response P is close, in shape, to the ideal performance, $P = \sin(2F)$, but because of the nonlinear property of the spun fibre sensor, and there has not been an established formula for the calculation of the input current, the FOCS current measuring range can only be estimated with regard to the simulation curves in Fig.5.12(b). Referring to curves 'a' and 'c' in Fig.5.12(b), it can be seen that as the current increases towards $\pm 1.0\text{kA}$, the nonlinear components increase. This limits the maximum current measurement range of the 100 turn fibre sensor to $\pm 1.0\text{kA}$. In practice, a good linearity can be obtained for a Faraday rotation angle less than 30° , so that a good linearity range can approximately give a maximum current measurement of 400A.

Since the Faraday rotation F is a function of fibre length and fibre coil turns, in order

to increase the sensor response to current signals, either increasing fibre length, or decreasing fibre coil turns, or a combination of both would be good starting points. Next in this section, a simulation study for the first two situations are carried out. The results are shown in Fig.5.13 and Fig.5.14.

Fig.5.13 shows how the sensor response P to current range varies with the increment of fibre length, in which the fibre orientation angle $\theta = 0^\circ$, the fibre turns is fixed 100 turns and curves 'a', 'b' and 'c' corresponds to fibre length 10m, 15m and 20m. The results show that as fibre length increases, the sensor response to current range is only slightly better and this is so because the linear measurement range is only slightly increased. Fig.5.14 shows how the sensor response, P , to current range varies with of the decrement of the fibre coil turns, in which fibre orientation angle $\theta = 0$, the fibre length is 10m and curves 'a', 'b', 'c' and 'd' correspond to fibre turns of 10, 30, 50 and 100 respectively. The results show that as the fibre coil turn decreases, the sensor response P to current range significantly increases. Curve 'd' has the same measurement range of about $\pm 1.0\text{kA}$ as curve 'a' in Fig.5.12(b) due to the same parameter setting in the FOCS simulation model. The curves 'a', 'b' and 'c' have a current measurement range of around $\pm 7.5\text{kA}$, $\pm 3.5\text{kA}$ and $\pm 2.0\text{kA}$, respectively, so that the variation of fibre coil turns mainly affects the FOCS measurement range. In the FOCS design, these factors need to be considered carefully.

5.5.2 Operation Bandwidth

FOCS has very large current measurement bandwidth. Its operational bandwidth is only limited by the fact that the instantaneous value of current changes during the time taken for the light to propagate through the fibre coil. Thus, the light emerging from the coil of length z at an instant in time t , will have accumulated an optical rotation given by the integral of the current over the time of propagation of the portion of light. This time is from $(t - \tau)$ to t where $\tau = 2z \times n/c$, the light travelling time in the fibre distance z , n/c is light speed in the fibre, n is the refractive index and 2 is the factor

of the forward and backward light propagation in the fibre. Thus the Faraday rotation induced by a sinusoidal current of unit amplitude and angular frequency is given by:

$$F(\omega) = \int_{t-\tau}^t F_0 \sin(\omega t') dt' \quad (5.15)$$

where F_0 is zero modulation Faraday rotation. Integrating above equation we obtain:

$$F(\omega) = F_0 \tau \sin\left(\omega t - \frac{\tau}{2}\right) \frac{\sin\left(\frac{\omega \tau}{2}\right)}{\frac{\omega \tau}{2}} \quad (5.16)$$

Equation (5.16) shows that the optical signal has a constant time delay of τ and its amplitude varies with the frequency as a sine function $\sin(\omega\tau/2)/(\omega\tau/2)$. When $(\omega_{3dB}\tau/2) = 1.392$ (rad), the response $[\sin(\omega_{3dB}\tau/2)/(\omega_{3dB}\tau/2)]$ is down to 0.707, this can be defined as f_{3dB} of the sensing coil in hertz. Therefore $f_{3dB} = 0.443/\tau = 0.443*c/(2z*n)$. The index $n = 1.5$ for silica glass. If the sensor response bandwidth is required to be $f_{3dB} = 4.43\text{MHz}$, then the fibre length z is required to be equal to or less than 10m. If $f_{3dB} = 1\text{MHz}$, fibre length can be extended to 44m. The result shows that the FOCS has much larger bandwidth than a conventional CT (the bandwidth of the latter is of less than 10kHz).

5.5.3 Noise limitations

The sensitivity and dynamic performance ranges of the FOCS depend upon Faraday rotation in the fibre coil, the optical wavelength and the capacity of the noise eliminating mechanisms, such as the shot-noise detection capability of the optical sensor. The Verdet constant $V_H = 2.0 \times 10^{-35} (c/\lambda)^2$ [44] is inversely proportional to the square of λ . The Faraday effect in a current sensor is typically a few tenths of a degree per kilo ampere.

In the case of small signals, the response, P , of the model is calculated as:

$$P = \frac{I_1 - I_2}{I_1 + I_2} \approx 4F \quad (5.17)$$

where F is the Faraday rotation $= V_H N I_m$ (see equation 2.19). If any noise appears in the signal detecting circuit, the actual light power at PIN photodiodes must be equal to or greater than the noise. Thus the minimum current I_{min} can be calculated. In equation (5.17), $P \approx 4F$ is, however, a normalized value having a double Faraday rotation due to forward and backward light propagation through the fibre path, so that an actual light power intensity at the detector can be determined when calculating the measurable current I_m . Now assuming that $P_0/2$ is the average optical intensity at the PIN diodes and P_d is the light power intensity at the PIN diodes, and the current is small, then the light power intensity P_d at the PIN diodes is given by:

$$P_d = \frac{P_0}{2} (1+r 4F) \quad (5.18)$$

where r is the ratio of the detected power received by the sensor to the ideally detected power due to the effects of the spun fibre and MFR.

Three main kinds of noise were discussed in Chapter 3 in the context of fibre optic communication systems: mode-partition noise arising from fibre dispersion, circuit noise and shot noise at photo-detector circuits. The modelling and analysis methods for those noise mechanisms developed in that context can be applied the CAD study of FOCS models with varied emphases. In a FOCS, only two major sources of noises need to be considered. They are thermal noise in the detector load resistor, and shot noise due to the process of converting photo power into an electronic current, whereas the phase noise, due to the laser source and fibre dispersion, is rarely a problem because of the small path differences between the orthogonally polarized modes in the FOCS. For an easy estimation of the noise level, let us simplify the noise models in Chapter 3. Ignoring the DC component in equation (5.18), the received current I_r produced by the detector due to the rms Faraday signal thus is:

$$I_s = \eta P_d = \eta \frac{P_0}{2} (4 r V_H N I_m) \quad (5.19)$$

where η is the quantum efficiency of the photo-detector. Shot noise is affected by average received power P_0 and will be add to this signal current. A rms shot noise current per unit bandwidth B therefore is:

$$\left(\frac{I}{\sqrt{B}} \right)_{s n} = (2e\eta P_0)^{\frac{1}{2}} \quad (5.20)$$

In the receiver circuit, if the circuit load resistor is R at temperature T , thermal noise will be produced. The thermal noise current per unit bandwidth B is thus as following:

$$\left(\frac{I}{\sqrt{B}} \right)_{T n} = (4k_B T / R)^{\frac{1}{2}} \quad (5.21)$$

The minimum resolvable signal current per unit bandwidth B must be equal to or greater than the sum of shot noise and thermal noise. Combining equation (5.19) (5.20) and (5.21), thus we have:

$$\left(\frac{I_s}{\sqrt{B}} \right)_{\min} = \left(\frac{2\eta r P_0 V_H N I_m}{\sqrt{B}} \right)_{\min} \geq \sqrt{\left(\frac{I}{\sqrt{B}} \right)_{s n}^2 + \left(\frac{I}{\sqrt{B}} \right)_{T n}^2} \quad (5.22)$$

Equation (5.22) is used to calculate the minimum detectable current I_m .

If the shot noise is limited to $(2 \eta r \cdot P_0 \cdot V_H N I_m / B^{1/2})_{\min} \geq (I / B^{1/2})_{s n} = (2 e \eta P_0)^{1/2}$, then the minimum detectable current I_m is represented as:

$$\left(\frac{I_m}{\sqrt{B}} \right)_{\min} \geq \frac{1}{r V_H N} \left(\frac{e}{2\eta P_0} \right)^{1/2} \quad (5.23)$$

In the thermal noise limit, $(2 \eta r \cdot P_0 \cdot V_H N I_m / B^{1/2})_{\min} \geq (I / B^{1/2})_{Tn} = (4K T / R)^{1/2}$, the detectable current I_m is obtained as:

$$\left(\frac{I_m}{\sqrt{B}} \right)_{\min} \geq \frac{1}{2\eta r P_0 V_H N} \left(\frac{4k_B T}{R} \right)^{1/2} \quad (5.24)$$

Now let us take an example by referring curve 'a' in Fig.5.14, where fibre length is 10m and fibre coil turns are 10. Assuming that the source power output is 1mW (0dBm), then after travelling through BS (see Fig.5.3), the light power is reduced by 3dB; after being reflected by MFR and then travelling through BS, another 3dB reduction occurs with a similar 3dB reduction after WP; taking about 1dB coupler loss into account, the total loss is assumed to be 10dB, so that the average signal power $P_0/2$ at detector is 0.1mw. The rest of the parameters are set at: r , the power ratio is 0.4, η the quantum efficiency 0.5A/W and T the temperature is 300K. Inputting all above parameters settings into equations (5.20) and (5.21), the minimum detectable signal current are obtained as:

- (i) shot noise limit = 1.7mA / Hz^{1/2}
- (ii) thermal noise 55.6/R^{1/2}mA /Hz^{1/2}

Discussions:

(i) Equations (5.20) and (5.21) show that both shot noise and thermal noise can be reduced if either power P_0 or fibre coil turns are increased. If N changes from 10 turns to 100 turns, then the shot noise will be reduced from 1.7mA/Hz^{1/2} to 0.17mA/Hz^{1/2} and thermal noise will be reduced from 55.6/R^{1/2} mA /Hz^{1/2} to 5.56/R^{1/2}mA /Hz^{1/2}.

(ii) Thermal noise can also be reduced by using large load resistor R . If it is required that sensor thermal noise be less than its shot noise, then R should be larger than 1.1k Ω ($R \geq 1.1k \Omega$). In other words, thermal noise under a large R condition can be

neglected in comparison with shot noise.

(iii) For a large signal response, a small number of fibre turns are required. When fibre coil has 10 turns and fibre length 10m, the sensor can provide a large current response up to 7.5kA (Fig.5.14) within good linearity measuring range, while shot noise limits this only 1.7A for 1kHz measuring bandwidth requirement.

When comparing this result (1.7A ~ 7.5kA) of the FOCS measurement range with the most recent result (250A ~ 3.0kA) of bulk-Faraday-cell optical current transformers [67], it shows that all fibre current sensors have a larger measurement range than the fibre sensor with a bulk magneto-optic material.

5.5.4 Sensitivity

Good sensitivity to Faraday rotation is also an essential requirement for a good FOCS. However, there is conflict with the requirements between good sensitivity to Faraday rotation and polarized-maintaining fibre. Low birefringence has a good sensitivity to Faraday rotation, but it is also sensitive to external noise such as vibration; while polarized-maintaining fibre is insensitive to both Faraday rotation and noise effects. In order to be able to compare these two extremes, a SHB fibre is used in the FOCS simulation model.

For a spun fibre, the sensitivity increases with ξ . A spin ratio is defined as fibre beat length over spin pitch (L_p / L_s) [5]. Unlike linearly-birefringent fibres, the interaction length of a spun fibre is no longer limited to a quarter of the beat length. For a spun fibre, when $\xi \gg \Delta\beta$, sensor response P will be equal to $\sin(2F)$. This is identical to the response of a perfectly isotropic fibre with full Faraday rotation sensitivity but almost zero residual birefringence and consequently lack of resistance to external perturbations. For an unspun highly birefringent fibre, it has very low Faraday rotation sensitivity, but good polarization maintaining property owing to its short beat-length.

Since spun fibre birefringence is an elliptical birefringence, a sufficient residual elliptical birefringence is present to ensure good resistance to external perturbations and at the same time maintaining good Faraday rotation sensitivity.

In the FOCS simulation examples, spun fibre $L_p = 1.62\text{mm}$ ($\Delta\beta = 1234\pi$) and $L_s = 1.64\text{mm}$ ($\xi = 1219\pi$), so the spin ratio $L_p/L_s = 0.9878$ corresponding to the relative sensitivity about 80 % [39]. It clearly shows that, in an ideal case, the Faraday sensitivity is 1, with an extremely low resistance to external noise, while the FOCS simulation model with SHB has high resistance to noise and still maintains a good 80% Faraday rotation sensitivity.

5.5.5 Testing With Typical Fault Waveforms

In this Chapter, the FOCS simulation models are presented and their performance characteristics are discussed. This section is concerned with an application of FOCS into power system transmission line protection. The nature of the application domain has determined that the FOCS must be able to respond to large fault current correctly. This involves detailed design considerations of many factors, coordination and adjustment of many sensitive parameters. In practice, it is not an easy task and is time-consuming as well as being costly.

CAD methods of FOCS simulation, design and testing have provided an ideal alternative. Here an example of FOCS design is described. A typical fault current waveform (Fig.A.5(b) in Appendix A) is used in the FOCS simulation model. The sensor response to the fault current is thus obtained. In order to clearly see the relationship between original fault signal and sensor detected signal, a-earth fault current is represented in Fig.5.15(W1). It shows that the fault current range varies approximately from +4kA to -4kA. Its corresponding spectrum is analyzed as shown in Fig.5.15(W2).

Three cases of FOCS design considerations are used in the discussion. The FOCS parameters are set as: spun fibre $L_p = 1.62\text{mm}$, $L_s = 1.64\text{mm}$, $z = 10\text{m}$, $\lambda_0 = 790\text{nm}$, and $\theta = 0$. The sensor response P to actual fault current waveform for three different fibre coil turns of 50, 30 and 20 are shown in Fig.5.15(W3), (W5) and (W7), respectively. The spectrum analyses of Fig.5.15(W3), (W5) and (W7) are plotted in Fig.5.15(W4), (W6) and (W8) correspondingly.

In the first case of FOCS design simulation, the fibre coil turn number is 50. The FOCS response to the typical fault current and its spectrum analysis are plotted in Fig.5.15(W3) and (W4) respectively. It clearly shows the presence of one significant distortion component. This can be explained with reference to curve 'c' in Fig.5.14; its measurable current range is within $\pm 2.2\text{kA}$, so that the designed FOCS is not suitable for responding to a current of $\pm 4.0\text{kA}$. If such designed FOCS is put into a practical use, it will generate distortions in the FOCS response signals.

In the second case of the FOCS design, the fibre coil turn number is 30. This design has a measurable current range of about $\pm 4.2\text{kA}$ as shown by curve 'b' in Fig.5.14, but some area of this range is nonlinear. Fig.5.15(W5) shows the sensor response to current, and its spectrum analysis is shown in Fig.5.15(W6). It is fairly hard to distinguish the waveform differences between Fig.5.15(W1) and Fig.5.15(W5). However, by comparing the spectrum in Fig.5.15(W2) with that in Fig.5.15(W6), it can be seen that the FOCS responses have a distinguishable nonlinear component at near 150Hz.

In the third case of FOCS design, the fibre coil turn number is 20. It has a response in the current range about $\pm 7.5\text{kA}$ (as given in Fig.5.14). The FOCS response to the typical fault current and its spectrum analysis are plotted in Fig.5.15(W7) and (W8) respectively. By analysing the waveforms in Fig 5.15(W7) and (W8), it can be seen that neither distorted signal component nor nonlinear effect component is apparent. The sensor response matches its input current very well and this is because the designed

sensor operates in its linear range and produces the best expected results.

The aforementioned is only a simple illustration of how the design parameters of the sensor would affect its sensing performance. In practice, power system protection is itself a complex function with its essential parameters having large operational variations. With the advantages of being flexible, time-saving and cheap cost, the FOCS simulation model provides a useful tool for the modelling and analytical study of the FOCS design in practice. Further investigations in this direction are of potential importance in power system protection relay.

5.6 Summary

In this Chapter, a complete CAD modelling of FOCSs is conducted in the detailed application context of power system transmission line protection. A spun fibre model and a MFR model are presented. It also shows how MFR can eliminate the considerably reciprocal noise which significantly remains in the FOCSs design when using convectional method. This is because MFR, inserted into a retracing fibre optic circuit, suppresses the effect of any reciprocal birefringence present in the fibre, giving an output SOP always orthogonal to the input one.

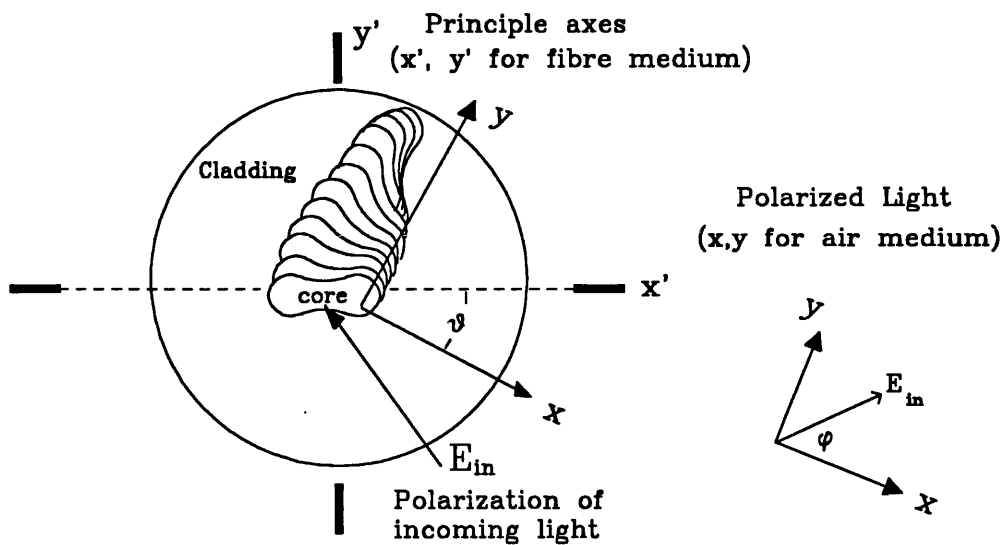


Fig. 5.1 Section of spun fibre shows the orientation angle θ between the principle axes x' , y' and the air medium axes x , y when a polarized light (with polarization angle ϕ) enters the fibre

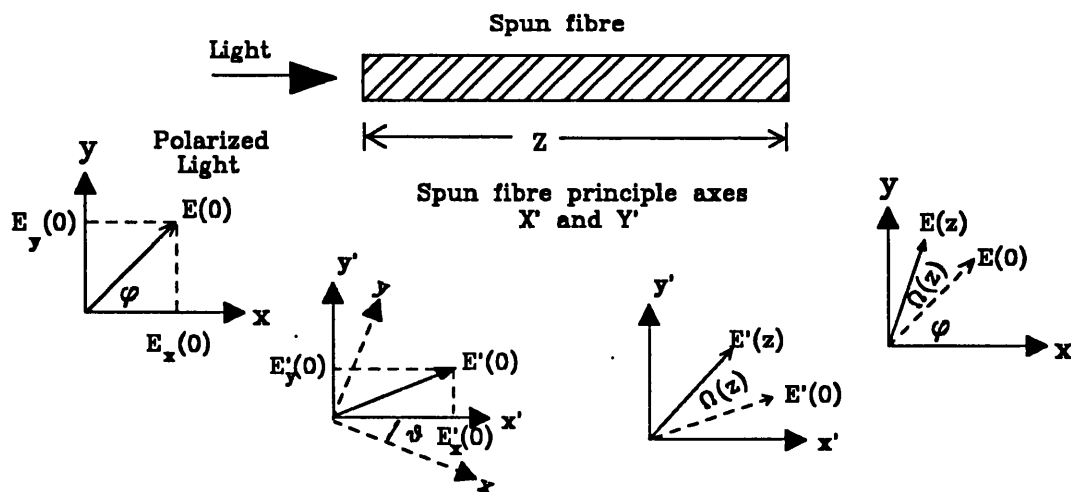


Fig.5.2 Coordinate system for spun fibre medium, light polarization state rotates $\Omega(z)$ after z distance. where θ the orientation angle, ϕ the polarization angle

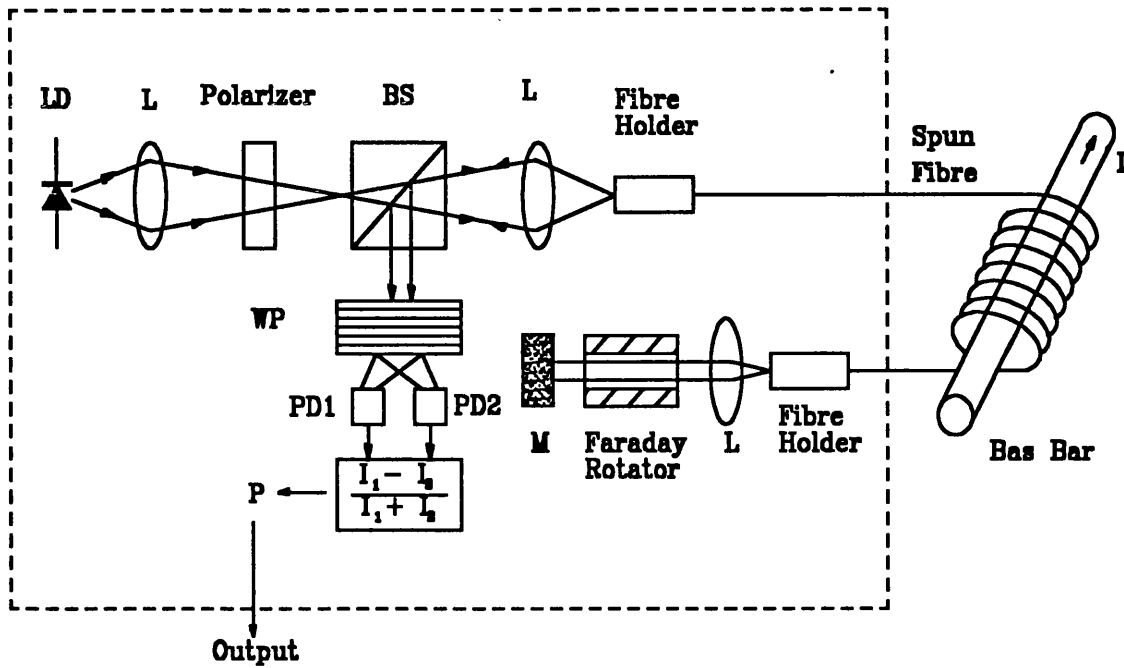


Fig. 5.3 Fibre optical current sensor based on the joint use of a MFR and spun highly-birefringent fibre. Where LD the laser diode, BS the beam splitter; L's the lenses; WP the Wollaston prism; PDs the photodiodes; M the phase conjugate mirror

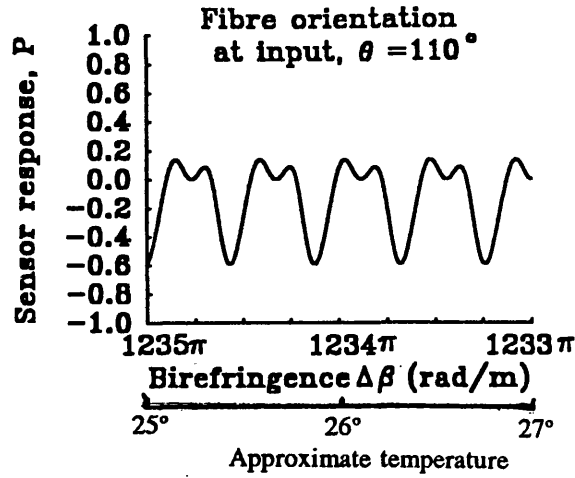


Fig. 5.6 Simulation sensor response P curve for an SHB current sensor having spin rate $\xi = 1219 \pi$ rad/m plotted against birefringence various in unspun birefringence

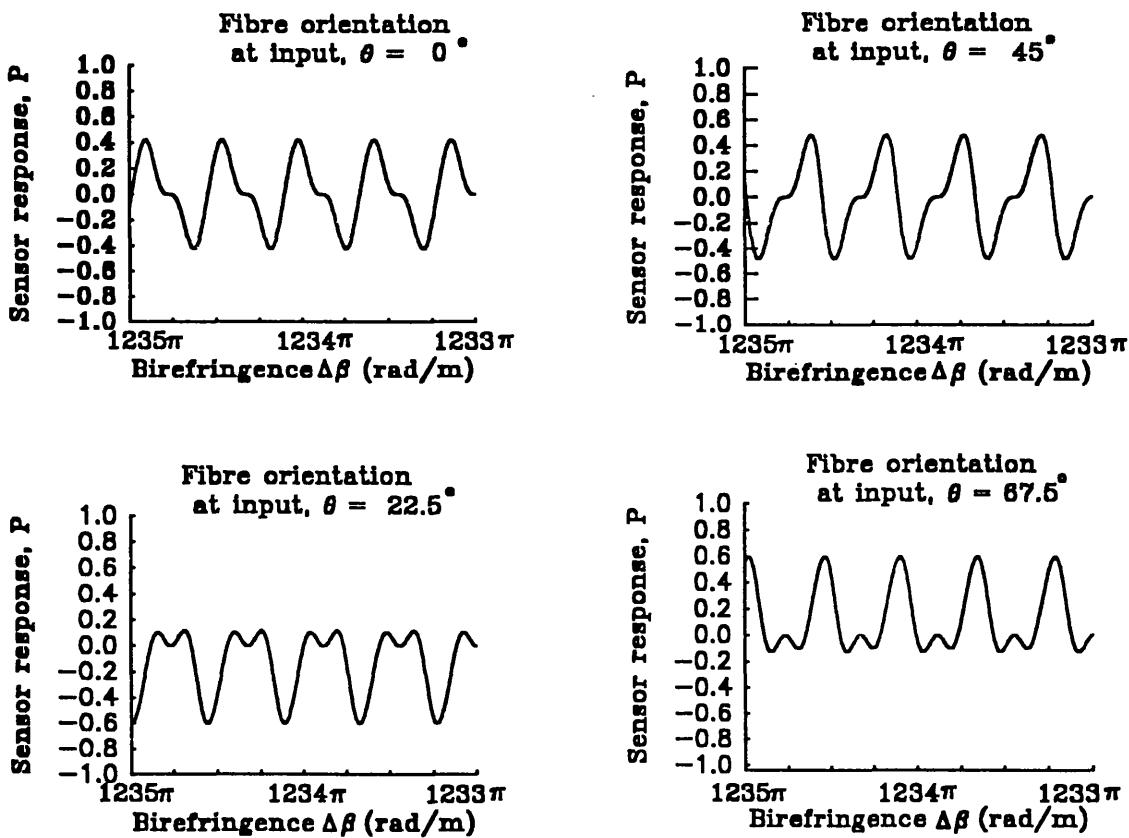


Fig.5.7 Simulation response P curves for an SHB fibre optic current sensor having spinning rate $\xi = 1219\pi$ rad/m plotted against $\Delta\beta$ variations with different fibre orientation at input θ .

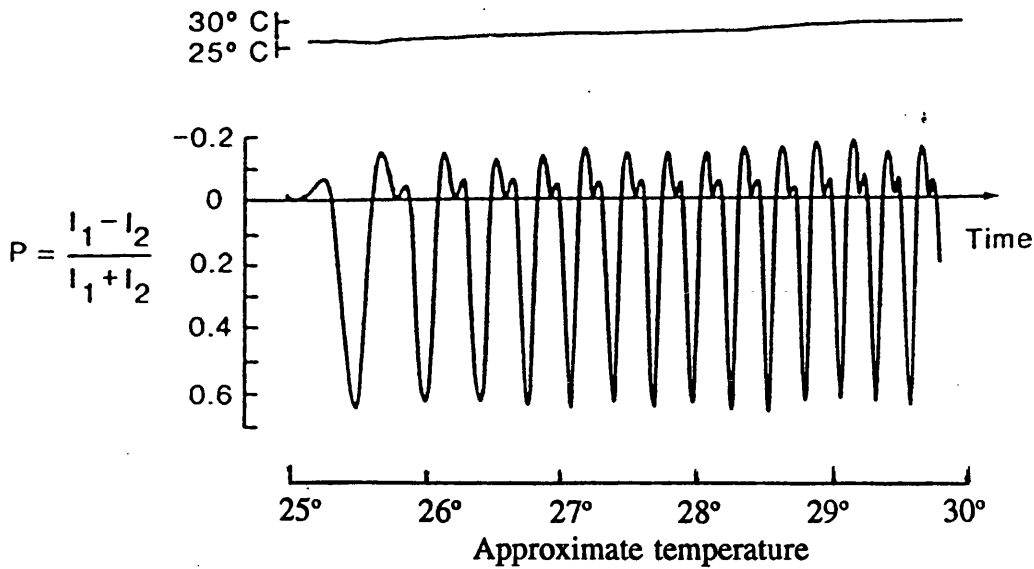


Fig. 5.4 Experimental response P (i.e., equation 5.12) curves obtained while varying the sensor temperature.

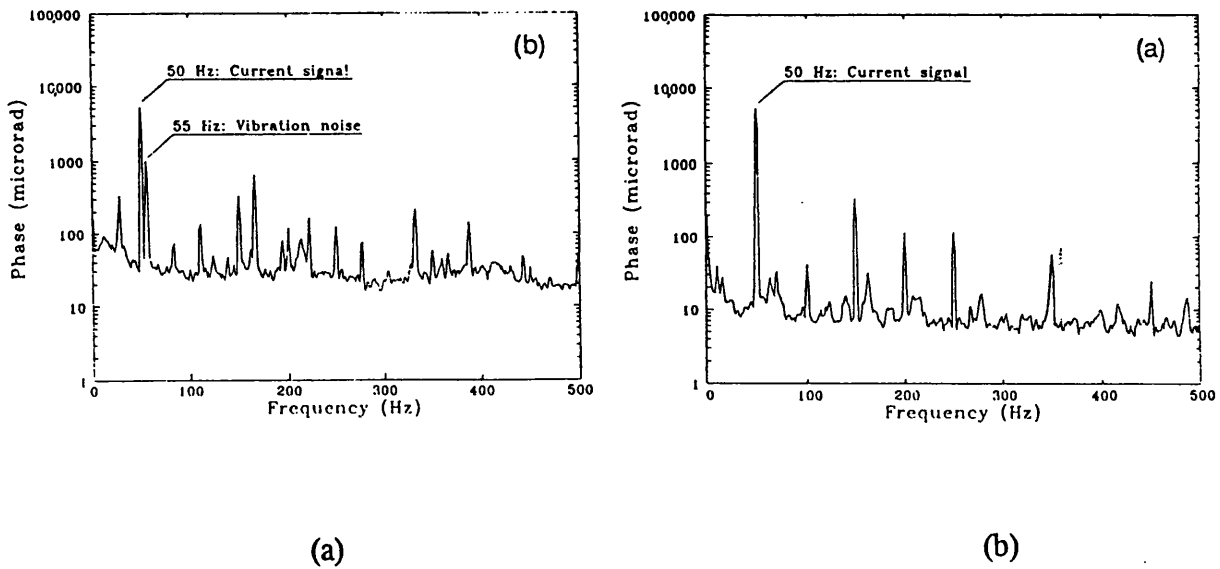


Fig.5.5 (a) Experimental power spectrum of the signal current at 50Hz and vibration noise at 55Hz (b) power spectrum of the signal detected by a FOCS with a MFR (only 50Hz signal existing)

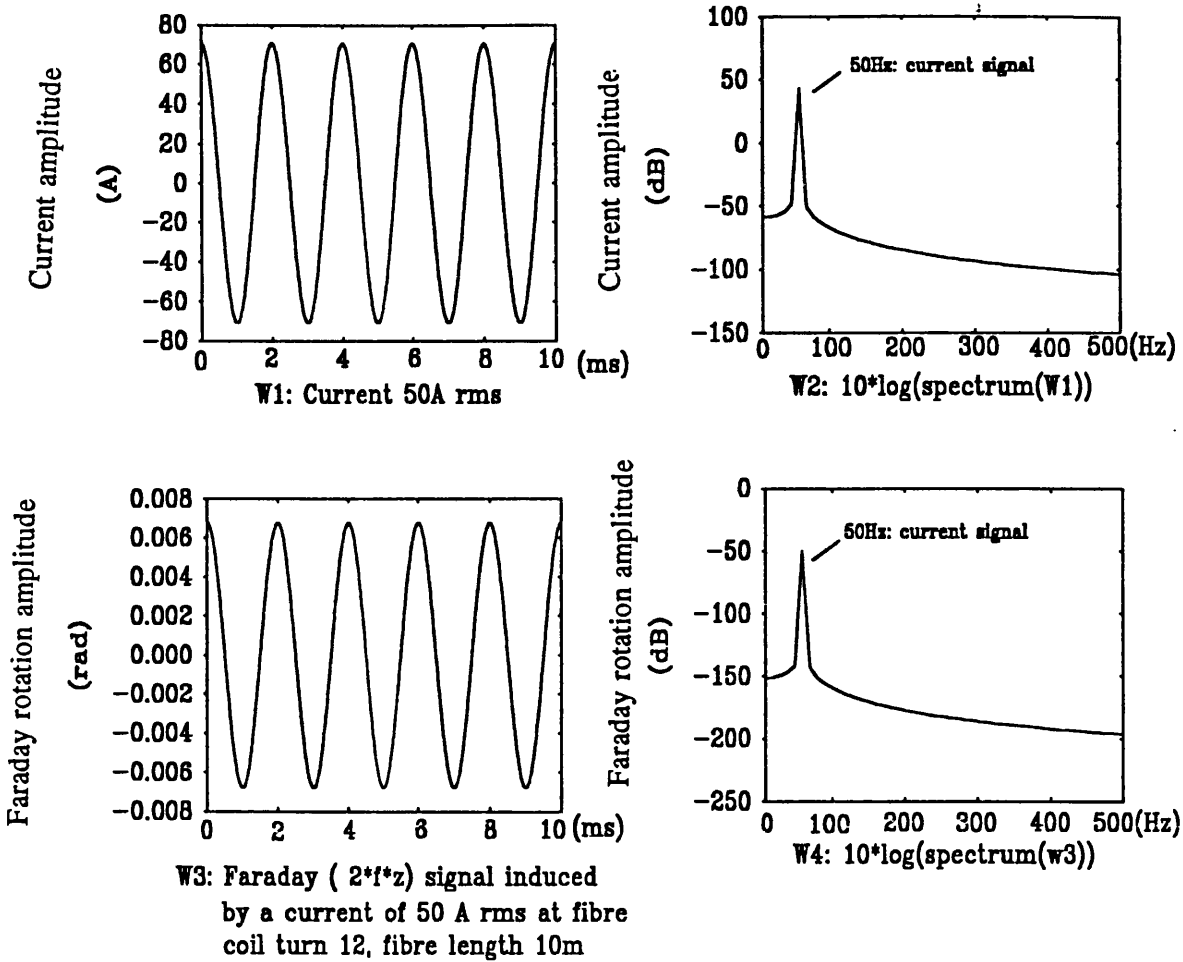


Fig.5.8

- W1: A current signal of 50A rms.
- W2: Spectrum of the current signal in W1
- W3: Faraday angle signal induced by the current signal in W1 the fibre length 10 meter and fibre coil 12 turns
- W4: Spectrum of the Faraday angle signal in W3

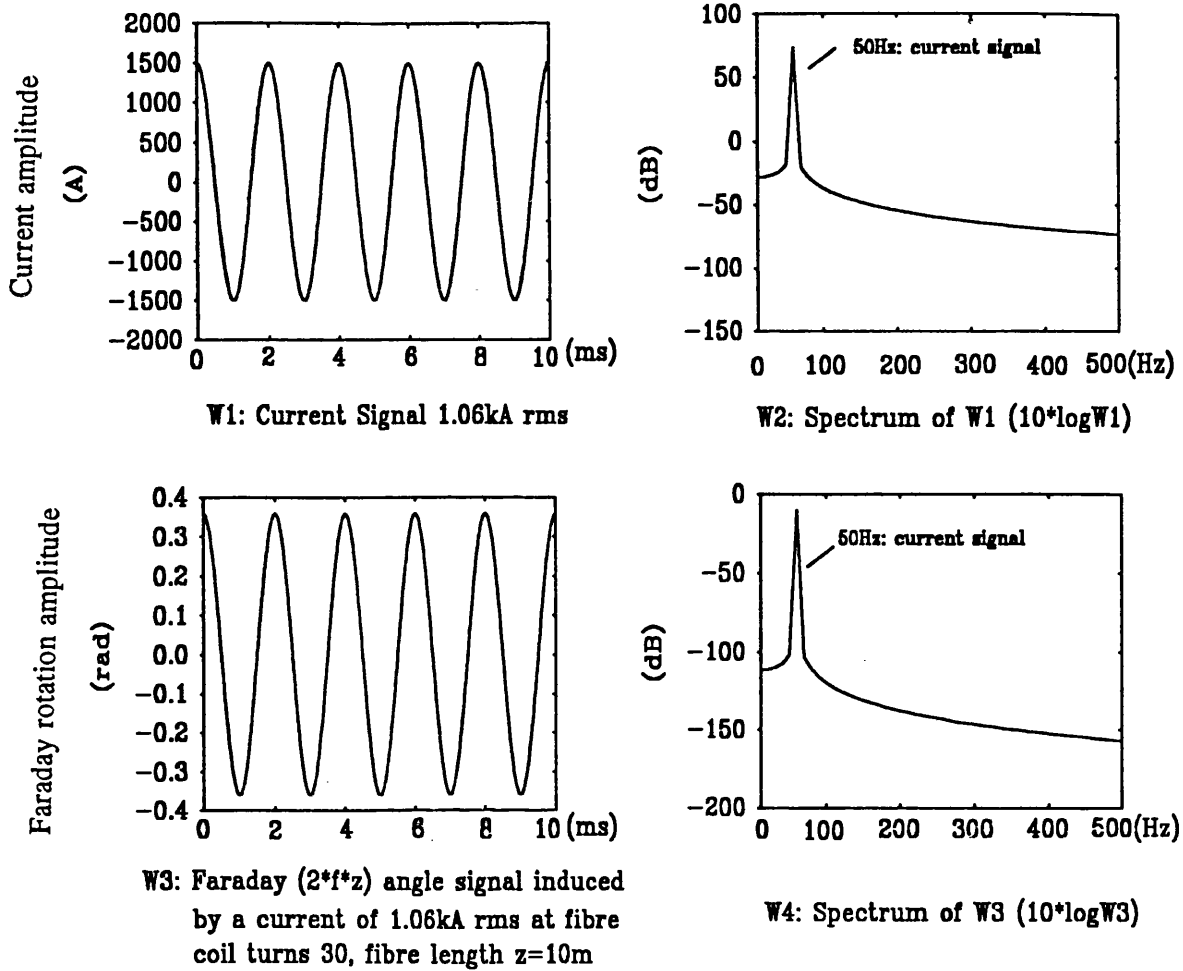


Fig.5.9 W1: A current signal of 1.06kA rms.
W2: Spectrum of the current signal in W1
W3: Faraday angle signal induced by the current signal in W1, the fibre length 10 meter and fibre coil 30 turns
W4: Spectrum of the Faraday angle signal in W3

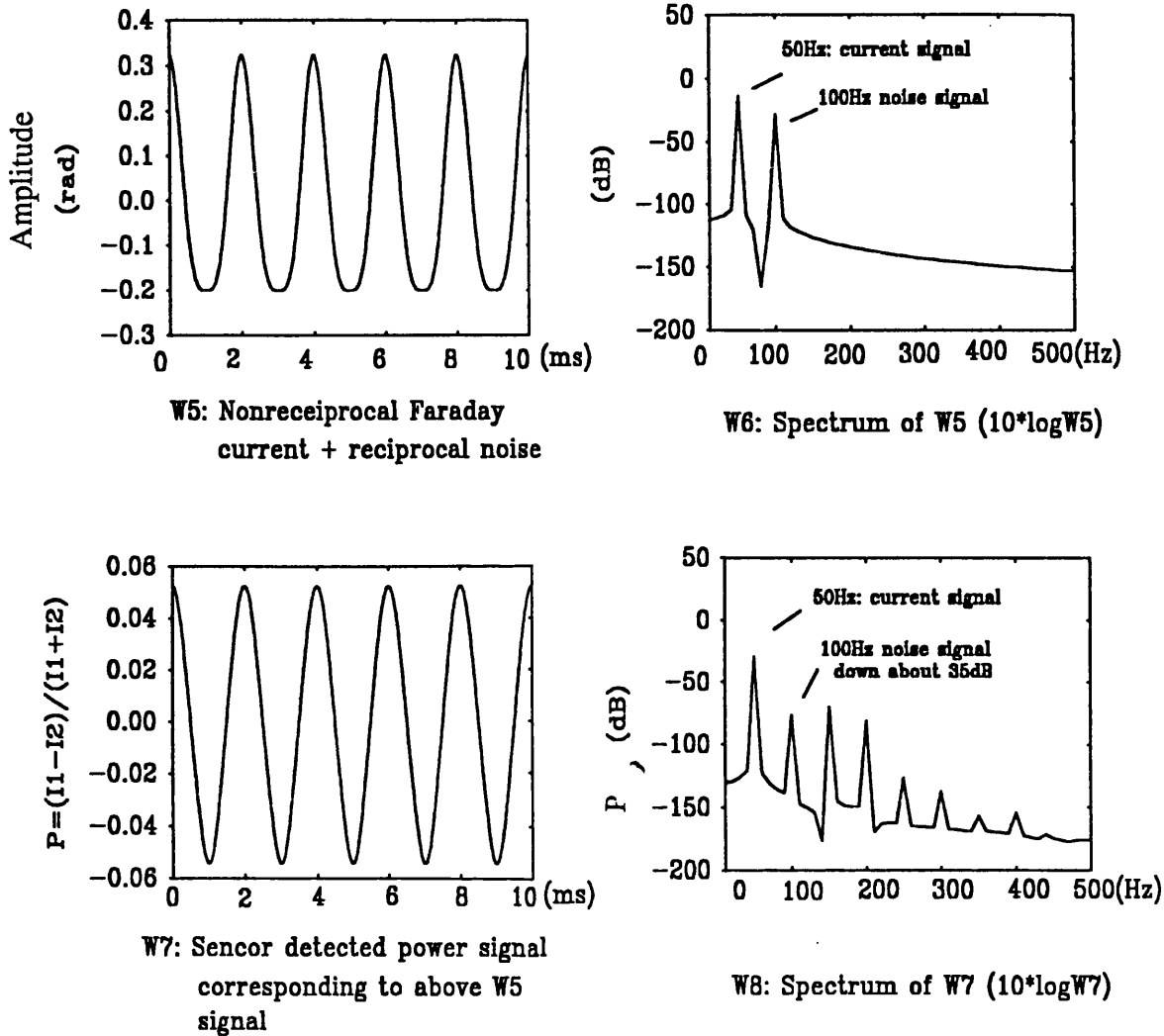


Fig.5.10 W5: A signal of Faraday rotation at 50Hz and reciprocal noise signal at 100Hz
 W6: Spectrum of W5
 W7: Sensor detected power signal corresponding to the waveform in window W5
 W8: Spectrum of W7

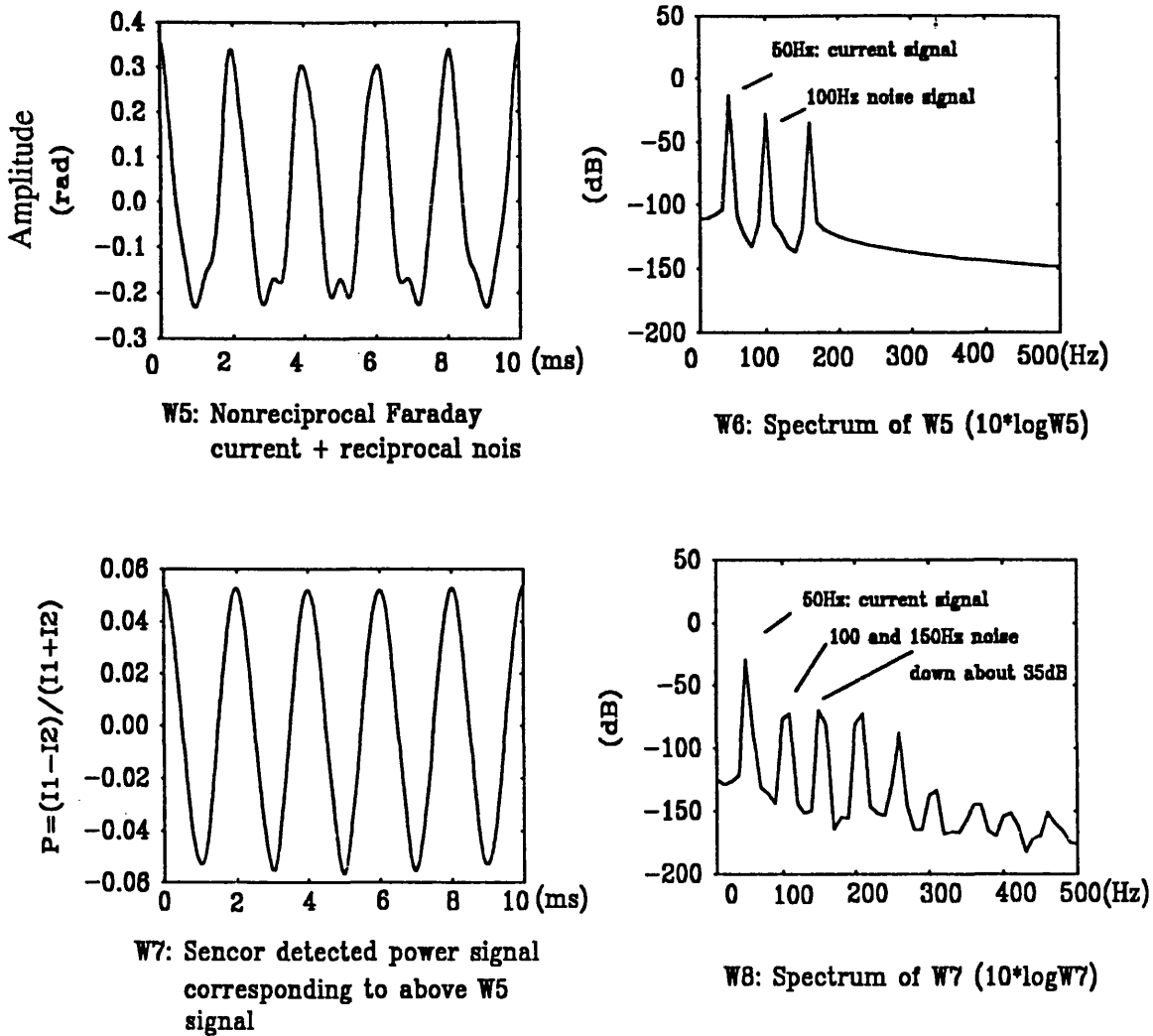
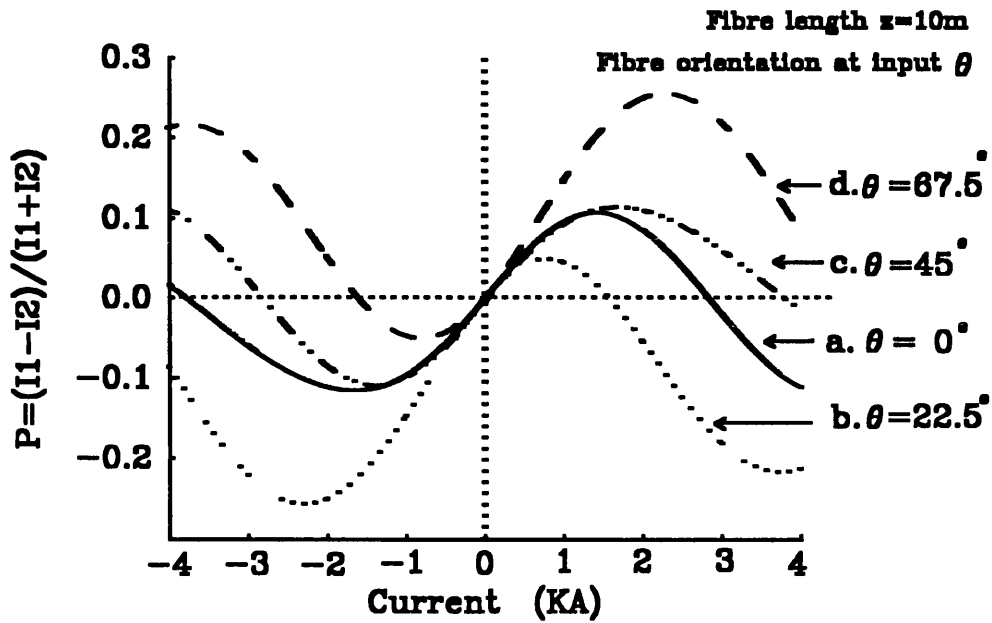
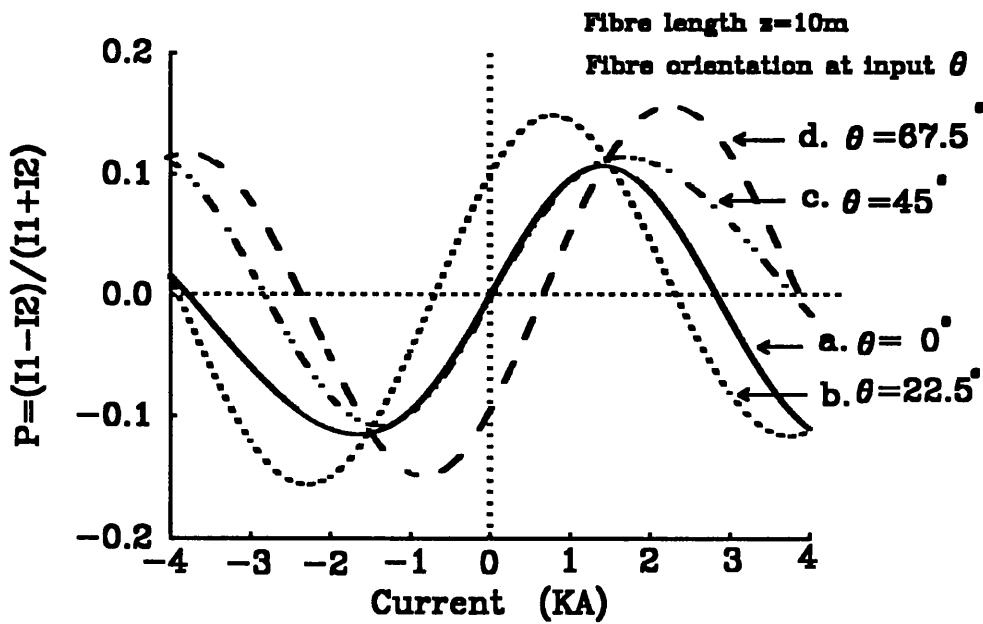


Fig.5.11 W5: Faraday rotation at 50Hz and reciprocal noise signal at 100Hz and 150Hz
 W6: Spectrum of W5
 W7: Sensor detected power signal corresponding to the waveform in window W5
 W8: Spectrum of W7



(a) Actual simulation sensor response P as a function of current



(b) Relative sensor response P as function of current

Fig.5.12 Sensor response P as function of current

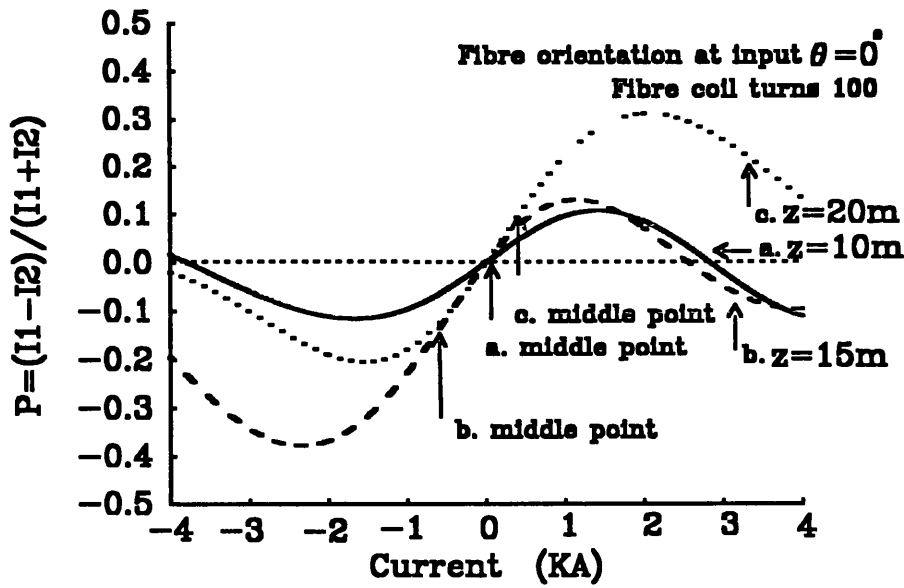


Fig.5.13 Sensor response P to current range.
Three different fibre length cases are $z = 10, 15$ and 20m

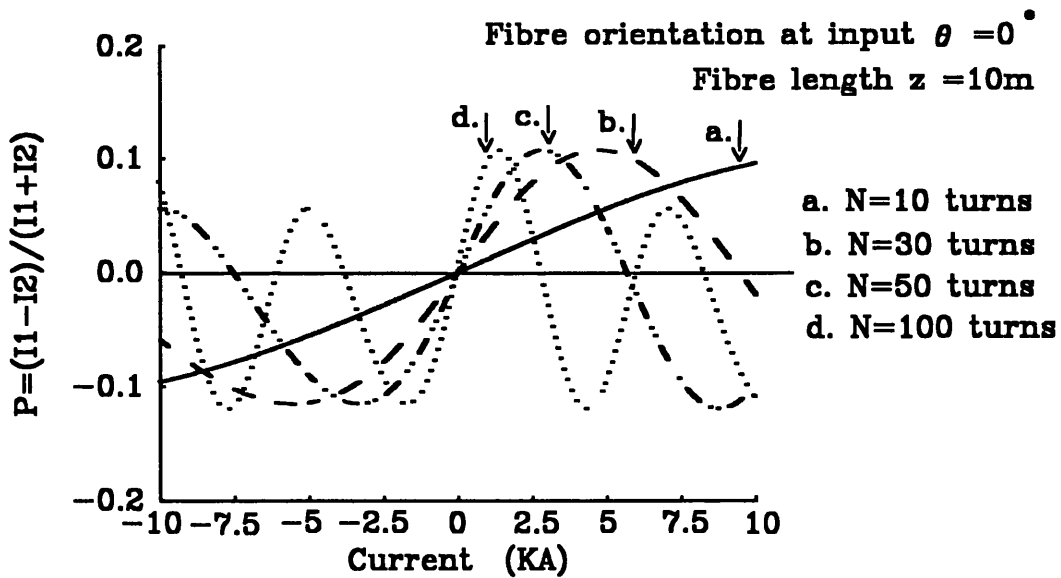
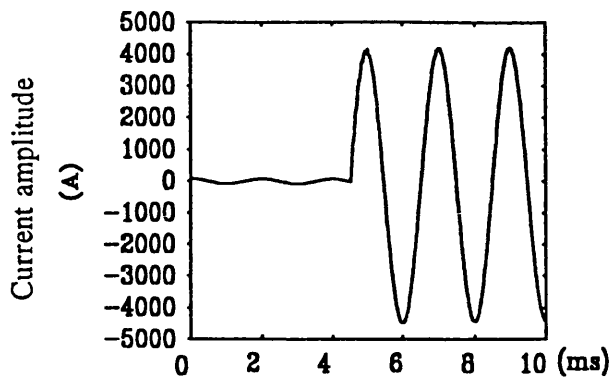
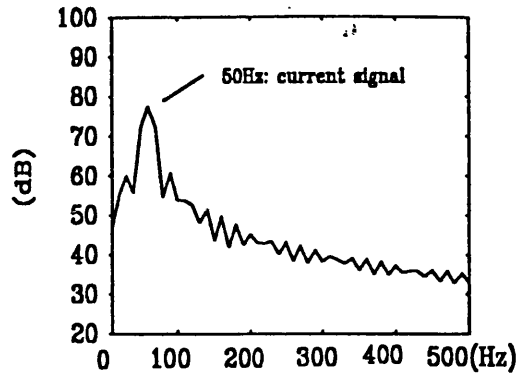


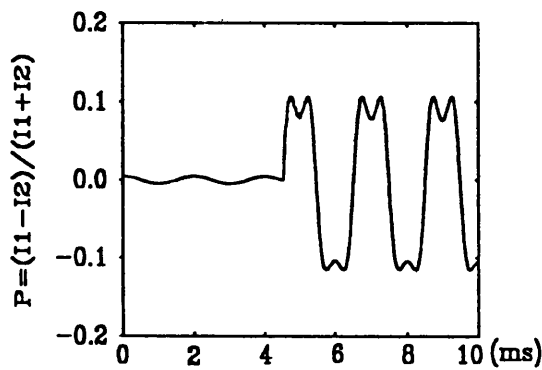
Fig.5.14 Sensor response P to current range.
Four different fibre coil turns are 10, 30, 50 100turns



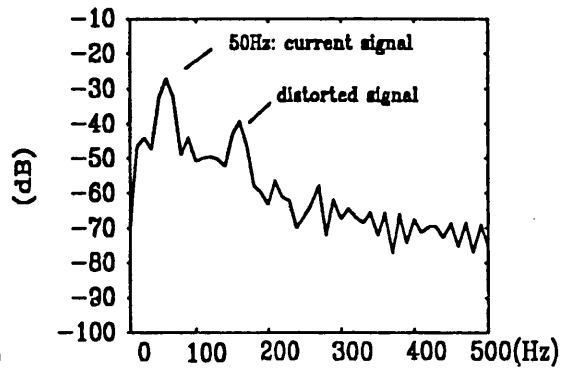
W1: A typical fault current signal as shown FigA.5(b) in Appendix A



W2: Spectrum of W1 ($10 \cdot \log W1$)



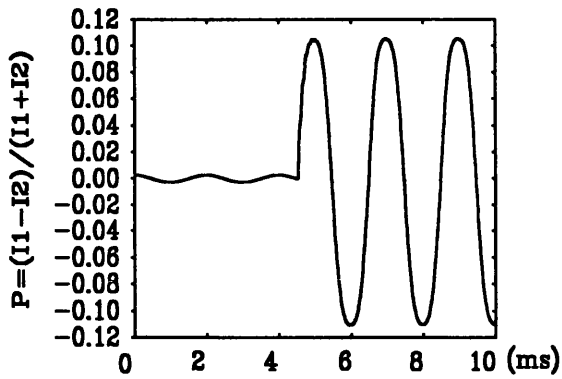
W3: Sensor detected power signal corresponding to above W1 signal at fibre length $z=10\text{m}$ fibre turns=50.



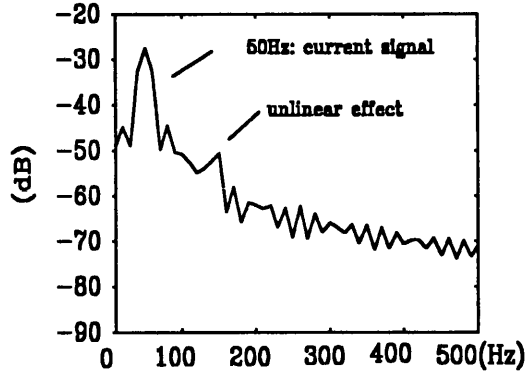
W4: Spectrum of W3 ($10 \cdot \log W3$)

Fig.5.15

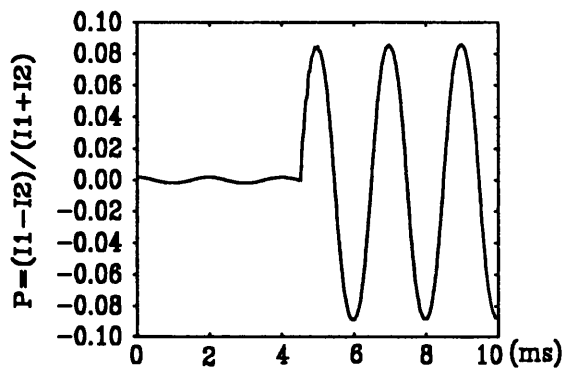
- W1: A typical fault current signal (the same as shown in Fig.A.5(b))
- W2: Spectrum of the window W1.
- W3: Sensor detected power signal corresponding to that typical current in window W1, the sensor fibre length 10m and fibre coil 50 turns.
- W4: Spectrum of W3.



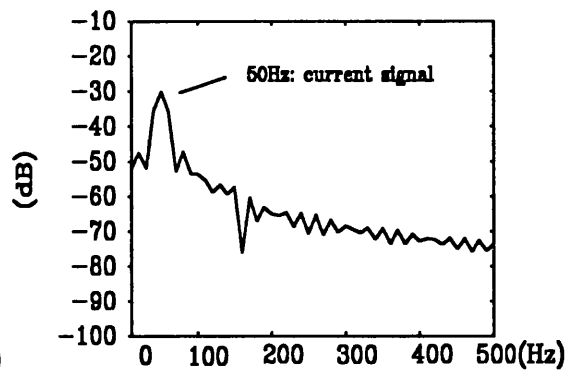
W5: Sensor detected power signal corresponding to above W1 signal at fibre length $z=10m$ fibre turns=30.



W6: Spectrum of W5 ($10 \cdot \log W5$)



W7: Sensor detected power signal corresponding to above W1 signal at fibre length $z=10m$ fibre turns=20.



W8: Spectrum of W7 ($10 \cdot \log W7$)

Fig.5.15 W5: Sensor detected power signal corresponding to that typical current in window W1, the sensor fibre length 10m and fibre coil 30 turns.
 W6: Spectrum of W5.
 W7: Sensor detected power signal corresponding to that typical current in window W1, the sensor fibre length 10m and fibre coil 20 turns.
 W8: Spectrum of W7

CHAPTER 6

CONCLUSIONS AND FURTHER WORK

This chapter summarizes the work presented in this thesis and draws several conclusions. Further work along different lines of the research subjects is suggested. The summary is conducted in three parts: section 6.1.1, fibre optic links CAD simulation system modelling, analysis and performance evaluations; section 6.1.2, practical examples of the fibre optic link applications into power system protection relaying; section 6.1.3, fibre optic current sensor CAD simulation system modelling, analysis and performance evaluations.

6.1 Summary of Work

6.1.1 Fibre Optic Links

In Chapter 3, firstly, a typical N-longitudinal mode laser spectrum envelope is assumed as a Gaussian shape. The laser is modelled by an equivalent electrical circuit model which is derived from laser rate equations under small signal modulation conditions. When PCM current signal pulses are injected into a laser, the laser transient output waveforms are expected to be near square pulses if the selected laser has a large fraction of spontaneous emission ρ . The simulation results of the circuit model of a laser with a large ρ , is in good agreement with the results of laser rate equation model. So it proves that the circuit model is a successful replacement of the laser rate equation model in a FOL simulation.

Two SMF transfer functions are described, one is based on optical power domain and the other on optical field domain. The first assumes that the fibre is a linear system in the optical power domain, so that the fibre transfer function can be obtained by integrating dispersive fibre power transfer function with source spectrum. For a simple

Gaussian source spectrum, the simple fibre transfer function is obtained. The second model can deal with practical measurement light sources. When the spectrum envelope is assumed as Gaussian form, both of them produce the same simulation results. If source spectrum envelope is not Gaussian, the former model is computationally intensive. However, the latter model can use Fourier transform to obtain fibre transfer function, thus it is more convenient and practical.

The receiver model and noise models are also presented. The receiver model is a APD with FET preamplifier. The APD gain is $\langle G \rangle$. The noise models are shot noise, circuit noise and mode-partition noise. All of them are proportional to data bit rate. The FOL performances are evaluated by testing its BER which is directly affected by noises. The simulations and performance evaluations of all individual models are carried out. The results of these models are given in corresponding sections. BER estimations of the FOL are also conducted.

Finally, a method for evaluating the decision circuit for the FOL simulation is presented. It is a hybrid of the calculation method and the time domain simulation. The calculation method is to obtain all noise contributions, so that the signals with added noise can be simulated. The time domain method is to simulate the FOL for data transmission spontaneously.

In summary, the light source output power, fibre loss, fibre dispersion and various type of noise at the receiver side are the main factors limiting the FOL spanning distance. A laser is capable of a higher optical power than does a LED. The fibre loss at $\lambda_0 = 1.55\mu\text{m}$ is more than that at $\lambda_0 = 1.30\mu\text{m}$. Fibre dispersion at $\lambda_0 = 1.55\mu\text{m}$ is higher than that at $\lambda_0 = 1.30\mu\text{m}$. Receiver sensitivity is proportional to data bit rate, thus the higher the data bit rate the more the noise limitations to the FOL spanning distance. For a FOL design, a balance of all above parameters must be taken into consideration.

For a longer span of the FOL at a relative lower data bit rate ($\leq 90\text{Mbit/s}$), a laser operating at $\lambda_0 = 1.55\mu\text{m}$ with either APD or PIN is an acceptable design.

6.1.2 Practical Applications of the Fibre Optic Links

In Chapter 4, simulated fault waveforms are used as test data in order to test the performance of the FOL model. The simulation results are presented as waveforms at the output of different components on the FOL model. They are PCM data waveform at the output of the laser, PCM data waveform received by PIN photodiode with added noise, and the waveform converted from the recovered PCM data waveform. The results show that with an improper design of the FOL, the data waveforms at the receiver are severely distorted. However, the FOL performance can be improved by changing the optical fibre wavelength from $\lambda_0 = 1.3\mu\text{m}$ to $\lambda_0 = 1.55\mu\text{m}$. By comparing the improved simulation results with the experimental results, it is evident that the simulation results are close to the experimental ones. Hence it confirms the correctness of the design of the FOL simulation model.

The FOL model is also applied to a CAD model of a line protection scheme. The FOL model is tested with fibre lengths 100km and 140km corresponding to the operating wavelengths $\lambda_0 = 1.3\mu\text{m}$ and $\lambda_0 = 1.55\mu\text{m}$ respectively. When the laser operates at $\lambda_0 = 1.55\mu\text{m}$, during many test trials, the results show that there are no observable bit errors. So it is feasible to say that the FOL shown little side-effects on the performance of the line protection scheme [3]. However, when the laser operates at $\lambda_0 = 1.30\mu\text{m}$, the results show seriously distorted waveforms at receiver. Such a FOL design is not acceptable as a data transmission medium over a 100km spanning distance. It concludes that the following FOL design parameters: a SMF, a laser operating at $\lambda_0 = 1.55\mu\text{m}$, and a PIN or an APD photodiode are essential for a long spanning distance of 140km for power system line protection.

A complete FOL laboratory test system consideration is presented. Transputer-based TCB is implemented. Sample test programs such as monitoring programs are generated. By using such a TCB, the actual operating performance of the FOL can be obtained. This has laid a solid base for physical laboratory testing of the digital

differential relay scheme with a physical FOL, so that real-time power system protection relaying experiments with concrete FOL can be carried out.

6.1.3 Fibre Optic Current Sensors

In Chapter 5, the spun fibre model is derived by combining the Jones matrix and a twisted medium model. The Jones matrix provides an operator for calculating optical system elements. Furthermore by using the Jones matrix principle, and a permanent 45° Faraday rotator model, with an added phase conjugate mirror model, a complete MFR model can be constructed.

Two sets of available laboratory experimental results are used for a comparative study and verification of the FOCS simulation results. The first one uses a RBC scheme that gives sensor responses varying with the sensor temperature. By comparing them with the simulation results obtained from the FOCS simulation model, it is shown that the simulation results are in good agreement with the experimental ones. The second experiment uses the MFRC scheme to show that MFR can reduce vibration noise by about 30dB, while the simulation results show a total noise reduction of about 35dB which is about 5dB better than the experimental results due to the theoretical FOCS model.

Aspects of design considerations for the application of EHV power transmission line protection are also discussed. A typical simulation fault current waveform is used to test the FOCS performance and the conclusions are:

- (i) Compared with conventional CT, the bandwidth of FOCS is very large, i.e. for 10 fibre, the bandwidth of FOCS can be 4.43Mhz (calculation from equation (5.16)), while the bandwidth of conventional CT is about 10kHz.
- (ii) For a large signal response, small number of fibre turns are required, i.e for measuring 50 A rms current , the fibre turn number can be 100, while for measuring 1.06kA rms current, the fibre turn number has to be reduced from

100 to 30.

- (iii) Noise factors restrain the range of small signals. Two significant noises are thermal noise and shot noise. For a large detector load, the thermal noise becomes very small compared with shot noise.

In summary, the shot noise limits the sensor response to low level currents and the fibre coil turns limit large current range. As the fibre coil number of turns increase, the shot noise decreases, but the sensor response to current range decreases. Sometimes a compromise between low and high level current need to be committed in order to maintain a proper sensor response range. In Chapter 5, a systematic CAD study of FOCS modelling, design and performance analysis are carried out. This should provide an extensive base for further study in this field with the hope that with its further application-domain related issues investigated, profound effects on practical design and application would emerge.

6.2 Conclusions

The objective of this research work is using CAD techniques to build up fibre optic link models and fibre optic current sensor models and, therefore, to conduct an extensive study of the behaviour of optical fibres in these two application fields and related practical issues. The motivation is originated by the inherent properties of optical fibres, the advantages over a conventional medium as communication links and their advantages over conventional current transformers as sensing devices. Power system transmission line protection relaying is chosen as a main application domain because of the potential importance of using a FOL as a communication media and the profound advantages of using a FOCS as current measurement devices. In the field of power system protection relaying, existing fibre optic application systems are inadequate in providing system performance evaluations, such as data bit rate limitations, noise limitations, current measurement ranges, measuring bandwidth, for an optimum system design. CAD techniques provide a flexible and economical

alternative for building up FOL and FOCS simulation models to investigate these parameters in detail. These models also provide a useful tool for both theoretical experiments and practical designs. For such purposes, in this research, a FOL simulation model and a FOCS model are implemented in FORTRAN programming language, and an extensive study is conducted.

In power system protection communication systems, repeaters, if present in a FOL, can introduce extra problems and reduce fibre link reliability. So a FOL design with no repeaters is worth pursuing. Long-haul transmission systems require that the fibre span be as long as possible without the need for any repeaters. The simulation system performance analyses and evaluations have demonstrated that by a better coordination of system design parameters, a FOL with a reasonably long spanning distance can be obtained.

It is beneficial to use the laser circuit model for simulation since it provides a laser transfer function. The performance evaluation shows that fibre dispersion is the main factor to limit the fibre transmission bandwidth. For the same laser source and fibre length, the fibre operating at large fibre dispersion $\lambda_0 = 1.55\mu\text{m}$ has less fibre transmission bandwidth than that operating at small fibre dispersion $\lambda_0 = 1.30\mu\text{m}$. Also fibre has a lower loss at $\lambda_0 = 1.55\mu\text{m}$ than that at $\lambda_0 = 1.30\mu\text{m}$. Since long-haul power transmission line protection schemes require a long distance data transmission link but a lower data bit rate (normally less than 100Mbit/s), a laser source operating at $\lambda_0 = 1.55\mu\text{m}$ is a near optimum selection. But as noise is proportional to the data bit rate, a FOL with a higher data bit rate has more strict noise limitation. A FOL operating at $\lambda_0 = 1.55\mu\text{m}$ is capable of transmitting low bit rate data over 160km without any repeaters. In a practical FOL design, the power margin needs to be considered in link power budget calculation. As a typical example, taking an average 0.3dB/km fibre loss, a 10dB power margin will reduce the fibre length by about 40km, while it is still able to send data over a 100km long spanning distance.

In the line protection scheme simulation process, it is shown that if the laser operates at $\lambda_0 = 1.30\mu\text{m}$, after 100km data transmission, the received signals are highly distorted; however, if the laser operates at $\lambda_0 = 1.55\mu\text{m}$, few bit errors occur. It indicates that with a laser operating at $\lambda_0 = 1.55\mu\text{m}$, a SMF, a receiver with either a PIN or an APD, the resulting FOL design is closer to the optimum case for the line protection scheme.

The designed TCB can be used to connect a current differential relay scheme and a FOL. It acts as an interface between the relay and the FOL. Besides, with the capacity of TDS, it can also be used to test the performance of the FOL under different line coding, so as to determine a proper line coding for a particular application.

In a FOCS, the fibre-induced linear birefringence affects the sensor performance. High birefringence fibre is less sensitive to this effect, but insensitive to Faraday rotation and hence not suitable for making sensing devices. SHB fibre is used to balance these two sides of the fibre properties, and a MFR is introduced to eliminate its temperature and other reciprocal noise effects. A CAD FOCS simulation model based on this principle is developed. With the support of available physical laboratory experimental data, the simulation results draw the conclusion that the FOCS model can be used to study a practical FOCS device. The MFR significantly reduces reciprocal noise (by about 30dB) hence eliminating the influences of reciprocal noises. The simulation results have also demonstrated that a FOCS has a much larger measuring bandwidth than that of a conventional CT.

This thesis describes a comprehensive CAD simulation of both a FOL and a FOCS with their particular applications in power system protection relaying. Both of these simulation models can provide tools for analysing and designing practical system. Equally importantly, the insight into system performance is provided both by the modelling process itself and by the experience gained from the simulation experiments.

6.3 Suggestions of Further Work

6.3.1 A Complete Prototype for Fibre Optic Links Test

In Chapter 4, a complete FOL laboratory test system is designed. It consists of three parts: a current differential relay, a physical FOL and a transputer-based TCB. With a 32-bit high-performance IMS T414 transputer as a microprocessor, the TCB has much more potential in further hardware and software developments.

The first step toward further hardware implementation is to build the connection among the TCB, the digital current differential relay and the proposed FOL. This would enable data from the relay to go through the FOL, so that real data testing can be carried out. This needs further software support so that the TCB will be able to monitor and evaluate real data transmission of the FOL. Hence this would help to verify the CAD FOL simulation system performance and provide further guidance to the FOL design engineers.

Other possible aspects for expansion of the work in this direction need more consideration and consolidation of the related issues and the details of application-orientation. Firstly, the RAM can easily be expanded from 256kbytes to 1Mbytes on the board; secondly two or more TCBs can form a transputer network which is more powerful in intelligent control; besides, data channels can be multiplexed for large data flow and handling, fourthly, the TCB board can be used to test the performance of the FOL with different line code programming. These may originate another independent research subject.

6.3.2 Applications of Fibre Optic Current Sensor

A CAD simulation system of a FOCS is developed. Typical fault current waveforms are used to test the FOCS performance. A first step towards further work is to apply

the FOCS model into some practical applications in power systems or other related areas. A typical example would be to a line protection scheme. By using the FOCS to replace the conventional CT, the performance of the line protection scheme can be further investigated with the hope that the system performance can be evaluated to a deeper level.

6.3.3 Testbed Generation

In this research, a comprehensive simulation system for FOL and FOCS are developed and detailed system performances are studied. The application orientation has been mainly on power system protection relaying. A general-purpose testbed would be able to developed based on the developed FOCS models. In this direction, more advanced CAD techniques need to be employed to provide more user-friendly and intelligence-based interfacing.

REFERENCES IN ALPHABETICAL LISTING

- [1] Adams, M. J "Rate Equations and Transient Phenomena in Semiconductor Lasers", *Opto-Electron*, Vol.5 pp. 201-215, 1973
- [2] Aggarwal, R. K. & Johns, A. T. "The Development of a New High Speed 3-Terminal Line Protection Scheme", *IEEE Transaction on Power Delivery*, Vol. PWRD-1, No. 1, pp. 125-134, January 1986
- [3] Aggarwal, R. K. & Johns, A. T. "A Differential Line Protection Scheme for Power Systems Based On Composite Voltage and Current Measurements", *IEEE Transaction on Power Delivery*, Vol.4, No. 3, pp. 1595-1601, July 1989
- [4] Akimoto, Y., Matsuda, T., Matsuzawa, K., Yamaura M., & Kondow R. Matsushima T. "Microprocessor Based Digital Relays Application in TEPCO", *IEEE Transaction on Power Apparatus and System*, Vol. PAS-100, pp. 2390-2398, May 1981.
- [5] Barlow, A.J, Ramskov-Hansen, J. J. & Payne, D. N "Birefringence and polarisation mode-dispersion in spun single-mode fibres", *Appl. Opt.*, Vol. 20, No. 17, pp. 2962-2968, Sept. 1981
- [6] Bhata, A.L. "Economics of Lightwave over Conventional Communication Methods", *EHO 225-3/85*, IEEE. PES, 1985
- [7] Birch, R.D., Varnham, M.P., Payne, D.N. & Okomoto, K "Fabrication of a stree-guiding optical fibre", *Electron. Lett.*, 19, pp.866-867, 1983
- [8] Blank, L. C., Bickers, L., & Walker, S. D. "Long Span Optical Transmission Experiments at 34 and 140 Mb/s", *Journal of Lightwave Technology*, Vol. Lt-3, No. 5, pp. 1017-1031, 1985
- [9] Boers, P. M., Vlaardingerbroek, M. T. & Danielsen, M. "Dynamic Behaviour Of Semiconductor Laser", *Electronic Letters*, Vol.11, No.10, pp.206-208, May, 1975
- [10] Cease, T. W. & Johnston, P. "A Magneto-Optic Current Transducer", *IEEE Transactions on Power Delivery*, Vol. 5, No. 2, pp. 548-555, April 1990
- [11] Cease, T. W. & Driggans, J. G. & Weikel, S. J. "Optical Voltage and Current Sensor Used in a Revenue Metering System", *IEEE Transactions on Power Delivery*, Vol. 6, No. 4, pp. 1374-1379, October 1991
- [12] Clarke, I. G. "Temperature-Stable Spun Elliptical Optical fibre Current Transducer", *Optical Letters*, Vol.18, No.2 pp.158-160, January 15, 1993

- [13] Dogliotti, R., Levinson, A. & Pirani, G. "Error Probability in Optical Fibre Transmission Systems", IEEE Trans. on Information Theory, vol.IT-25, No.2, pp.170-178, March, 1979
- [14] Duff, D. G. "Computer-Aided Design of Digital Lightwave Systems", IEEE Journal On Slected Areas In Communications, Vol. SAC-2, No.1, pp.171-185, January 1984
- [15] Elrefaie, A. F., Townsend, J. K., Romeiser, M. B. & Shanmugan, K. S. "Computer Simulation of Digital Lightwave Links", IEEE Journal On Slected In Communications, Vol.6, No.1, pp.94-105, January 1988
- [16] Englert, T., Chowdhury, B. & Grigsby, E. "A Laboratory Investigation of Electro-Optic Kerr Effect for Detection of Electric Transmission Line Faults", IEEE Transactions on Power Delivery, Vol. 6, No. 3, pp. 979-95, , July 1991
- [17] Etten, W. V. & Plaats, J.V.D. "Fundamentals of Optical Fibre Communications", *Prentice Hall International UK Ltd.*, chap.10, pp.185-195 or pp.267
- [18] Fashano, M. & Strodbeck, A.L. "Communication Systems Simulation and Analysis with SYSTID", IEEE J. Select. Areas Commun., Vol. SAC-2, pp.8-28, Jan. 1984
- [19] Fischer, D. & Madge, R. "Digital Teleprotections Units. A Technology Overview", IEEE Transactions on Power Delivery, Vol.7, No. 4, pp.1769 - 1774, October 1992
- [20] Galloway, R.H., Shorrocks, W.B. & Wedepohil, L. M. " Calculation of Electrical Parameters for Short and Long Polyphase Transmission Lines", Proc. IEE, Vol. 111, No.2, pp.2051-2059, 1964
- [21] Gimlett, J.L. , Stern, M., Curtis, L., Young, W.C., & Cheung, N.K. "Dispersion Penalties for Single-Mode Fibre Transmission Using 1.3 μm and 1.5 μm LEDs", Electron Lett., vol.21, pp668-670, Aug, 1985
- [22] Huang, H.C. & Qian, J.R. "Theory of Imperfect Nonconventional Single-Mode Optical Fibres" , In Optical Waveguide Sciences, Martinus Nijhoff, The Hague, pp.57-68, June 1983
- [23] Hussein, A. H. "Design & Testing of a New Microprocessor-Based Current Differential Protection Scheme For Teed Circuits", Ph.D Thesis, University of Bath, UK, 1991
- [24] Hoss, R.J. "Fibre Optic Comuncations Design Handbook", Prentice-Hall, Inc, pp.4, 1990
- [25] IEEE Report, "Fibre Optic Channels For Protective Relaying", IEEE

Transactions on Power Delivery, Vol.4, No. 1, Januray 1989

- [26] IEEE Tutorial Course "Fibre Optic Applications in Electrical Power Systems", 84 EH0225-3-PWR, 1985
- [27] IEEE Tutorial Course "Microprocessor Relays and Protection Systems", 88 EH0269-1-PWR, 1987
- [28] INMOS Limited " Transputer Technical Notes " Prentice Hall, New York, London and etc. 1989.
- [29] Jeruchim, M. C."Techniques for Estimating the Bit Error Rate in the Simulation of Digital Communication Systems", IEEE J. on Selected Areas in Communications, Vol. SAC-2, No.1, pp 153-170, Jan. 1984
- [30] Johns, A. T. & Aggarwal, R. K. "Digital Simulation of Fault EHV. Transmission Lines with Particular Reference to Very-High-Speed Protection", Proc. IEE, Vol.123, No.4, pp.353-359, April 1976
- [31] Jones, R. C., "A New Calculus for the Treatment of Optical Systems I.; Description and Discussion of the Calculus", Journal of Optical Society of America, Vol. 31, pp. 488-503, July 1941
- [32] Kapron, F.P., Borrelli, N.F., & Keck, D.B. "Birefringence in Dielectric Optical Waveguides", IEEE J. Quantum Electron., Vol QE-18, pp.222-225, 1972
- [33] Kasper, B. L. "Optical Fibre Telecommunication II - Receiver Design", Academic Press, INC, pp689-707, 1988
- [34] Kersey, A. D. & Jackson, D. A. "Current Sensing Utilising Heterodyne Detection of the Faraday effect in Single-Mode optical fibre", J. Lightwave Technol., Vol. LT-4, no.6, pp.640-643, June,1986
- [35] Kirkham, H., & Johnston, A.R. "Optically Powered Data Link For Power System Applications", IEEE Transactions on Power Delivery, Vol.4, No.4, pp.1997-2004, 1989
- [36] Kitagawa, M, Andow, F., Yamaura, M, & Okita, Y. "Newly Developed FM Current-Differential Carrier Relaying System and Its Field Experiences", IEEE Trans., Pas-97, pp. 2272-2281, November 1978
- [37] Kwong, W.S. , Clayton, M. J. & Newbould, A. " A Microprocessor-Based Current Differential Relay for Use With Digital Communication Systems", GEC Measurements Limited, UK IEE. 3rd INT. Conf, No. 249, pp.65-69, 1985
- [38] Laming, R.I. & Payne, D.N "Electric Current Sensors Employing Spun Highly

- Birefringent Optical Fibers", *Journal Of Lightwave Technology*, Vol.7, No.12, pp.2048-2094, December 1989
- [39] Li, L., Qian, J.R, & Payne, D.N "Miniature Multi-Turn Fibre Current Sensors", *Journal of Optical Sensor*, Vol.2 No.1, pp.25-33, 1987
- [40] Malyon, D. J. & McDonna, A. P. " A 102km monomode fibre systems experiment at 140Mbit/s with an injection locked I-52 laser transmitter", *Electron Lett.* Vol.18, No.11, pp.445-447, 1982
- [41] MacDougall, T. W. & Lutz, D. R. & Wandmacher, R. A. "Development of a Fibre Optical Current for Power Systems", *IEEE Transactions on Power Delivery*, Vol. 7, No. 2, April 1992, pp. 848-852.
- [42] Marcuse, D "pulse distortion in single-mode fibres", *Applied Optis*, pp.1653-1661, 15 May 1980.
- [43] McIntyre, P. & Snyder, A. W. "Light Propagation in Twisted Anisotropic Media: Application to Photoreceptor", *Journal of Optical Society of America*, Vol. 68, No. 2, pp. 149-157, February 1978
- [44] Noda, J. & Hosaka, T. & Sasaki, Y. & Ulrich, R. "Dispersion of Verdet Constant in stress-Birefringent Silica Fibre", *Electronics Letters*, 25th October 1984, Vol. 20, No. 27, pp. 906-908.
- [45] Norman S. R. , Payne D.N., Adams M.J., & Smith A.M. "Fabrication of single-mode fibres exhibiting extremely low polarisation birefringence", *Electron. Lett.*, Vol.15, pp.309-311,, 1979
- [46] Ogawa, K. "Analysis of Mode Partition Noise in Laser Transmission Systems", *IEEE Journal of Q.E.*, Vol, QE-18, NO5, pp849-855, May 1982
- [47] Payne, D. N., Barlow, A.J. & Hansen, J.J.R "Development of low- and High-Birefringence Optical Fibres", *IEEE J. of Quantum Electronics*, Vol. QE-18, No.4, pp.477-487, April, 1982
- [48] Personick, S. D. "Receiver Design for Digital Fibre Optic Communication Systems I and II ", *The Bell System Tech. J.* Vol,52, No.6, pp843-885, July-August, 1973
- [49] Pistoni, N.C. & Martinelli, M. "Polarization Noise Suppression In Retracing Optical Fiber Circuits", *Optics Letters*, Vol. 16, No. 10, pp.711-713, May 15, 1991
- [50] Pistoni, N. C. & Martinelli M. "Vibration-Insensitive Fiber-Optic Current Sensor", *Optics Letters*, Vol.18, No.4 pp.314-316, February 15, 1993
- [51] Papp, A & Harms, H. "Magnetooptical Current Transformer. I: Principles",

- Appl. Opt., Vol.19, No.22, pp.3729-3734, 1980
- [52] Riganto, H., Prutzer, H., Weinhold, B., & Schindele, F. "HV Line Differential Protection With Digital Data Transmission Using Light Fibre Optic Transmission System", Cigre paper No. 34-35, September 1982
- [53] Rockefeller, G. D. "Fault Protection with a Digital Computer", IEEE Trans. on Power Apparatus and Systems, Vol. 88, No. 4, pp.438-461, April, 1969
- [54] Rogers, A.J. "Optical Technique for Measurement of Current at High Voltage", Proc. IEE, Vol.120, No.3, pp.261-267, 1973
- [55] Ross, J. N. "The rotation of the polarisation in low birefringence monomode optical fibres due to geometric effects", Optical Quantum Electron., Vol.16, pp.455-461, 1984
- [56] Sanderson, J.V.H, & Al-Fakhri, B. "Improved Performance of Modern Differential Protection For Teed Feeders- Simulation Studies", 3rd International Conference On Power System Protection, IEE.,m No.249, pp. 70-74, 1985
- [57] Smith, A. M. "Polarization and magneto optic properties of single-mode optical fibre", Applied Optics, Vol. 17, No. 1, pp. 52-56, January 1978
- [58] Stone, J. "Stress Optic Effects, Birefringence and Reduce Birefringence by Annealing in Fibre Fabry-Perot Interference", Journal of Lightwave Technology, Vol.8, No.12, pp. July 1988
- [59] Sugiyama, T., Kano T. Hatata M., & Azuma S. "Development of a PCM Current Differential Relaying System Using Fibre-Optic Data Transmission", IEEE Transactions on Power Apparatus and Systems, Vol. PAS-103, pp. 152-159, January 1984
- [60] Sun, S.C & Ray, R.E "A Current Differential Relay System Using Fibre Optics Communications", IEEE Transactions on Power Apparatus and System, Vol. PAS-102, No.2, pp.410-419, February 1983
- [61] Suzuki, M, Matsuda, T, Ohashi N, & Sano, Y. "Development of Substation Digital Protection and Control System Using Fibre-Optic Local Area Network", IEEE Transactions on Power Delivery, Vol.4, No.3, pp.1668-1675, July 1989
- [62] Takagi, T. Yamakosi, Y. Kudo, H. Miki, Y. Tanaka, M. & Mikoshiba, K. "Development of An Intrastation Optical-Fibre Data Transmission System For Electric Power Systems", IEEE Transactions on Power Apparatus and Systems, Vol. PAS-99, No. 1, pp.318 -327, 1980
- [63] Ulrich, R. & Simon, A. "Polarisation Optics of twisted single-mode fibres", Appl. Opt., Vol.18, No.13, pp2241-2251, July 1979

- [64] Ulrich, R. , Rashleigh, S.C. & Eickhoff, W. "Bending-induced birefringence in single-mode fibres", Opt. Lett., Vol.5, No.6, pp.273-275, June 1980
- [65] Walker, S. S. "Rapid Modelling and Estimation of Total Spectral Loss in Optical Fibres", J. Lightwave Tech. LT-4 pp.1125-1134
- [66] Wedepohl, L. M. "Application of Matrix Methods to the Solution of Travelling_Wave Phenomena in Polyphase Systems", Proc. IEEE, Vol. 110, No.12, pp.2200-2212, December 1963
- [67] Yamagata, Y. , Oshi, T. Katsukawa, H. Kato, S. & Sakurai, Y "Development of Optical Current Transformers and Application to Fault Location Systems for Substations", IEEE Transactions on Power Delivery, Vol. 8, No. 3, pp.886-872, 1993
- [68] Yariv, A. "Operator Algebra for Propagation Problems Involving Phase Conjugation and Nonreciprocal Elements", Applied Optics, Vol. 26, No. 21, 1 November 1987, pp. 4538-4540.

APPENDIX A

DIGITAL SIMULATION OF FAULT WAVEFORMS

A.1 Basic Principle

Any multiconductor line section is defined by its series impedance matrix per unit length Z corresponding shunt admittance Y . Each element of Z varies with frequency and is determined by the conductor types, the geometry and the nature of the earth plane [30].

The theory of natural modes, developed by Wedepol [66], enables a solution to the system voltage steady-state equations given by equation (A-1) to be transformed into a series of independent differential equations of the form of equation (A-2)

$$\frac{d^2 \bar{V}}{dx^2} = ZY \bar{V} \quad (\text{A-1})$$

(A-2)

$$\bar{V} = \exp(-\psi x) \bar{V}_i + \exp(\psi x) \bar{V}_r$$

where $\Psi = Q \gamma^{-1} Q^{-1} Z$, Q is voltage eigenvector matrix, γ is propagation constant matrix.

Matrix function theory permits easy evaluation of the hyperbolic functions, the polyphase surge impedance and admittance necessary for a solution of the problem. For example, the polyphase surge admittance matrix is given by:

$$Y_0 = (Q \gamma^{-1} Q^{-1} Z)^{-1} \quad (\text{A-3})$$

A.1.1 Transmission Line Transfer-Matrix Function

A faulted transmission system essentially consists of a network of cascaded sections as Two-port transfer matrices are particularly useful in the solution of such a problem. For example, with reference to Fig.A.1, the transfer admittance matrix representing a line section up to the point of fault is given by equation (A-4), and this can be used in combination with the corresponding matrices representing the fault discontinuity and the line section between the fault and the receiving busbars, to yield a relationship between the currents and voltages at either end of the line

$$\begin{bmatrix} I_1 \\ I_2 \end{bmatrix} = \begin{bmatrix} Y_{11} & Y_{12} \\ Y_{21} & Y_{22} \end{bmatrix} \begin{bmatrix} V_1 \\ V_2 \end{bmatrix} \quad (\text{A-4})$$

where $Y_{11} = Y_{22} = Y_0 \coth(\Psi x)$, and $Y_{21} = Y_{12} = -Y_0 \operatorname{cosech}(\Psi x)$,

A.1.2 Source-Side Network Matrix

The source network considered here at each terminating busbar is a general source model comprising of some local generation and a number of infeeding parallel lines, each with its own generation. All the generations are based upon arbitrarily defined short circuit levels. This is shown in Fig.A.2

In Fig.A.2, [YS] is an equivalent source admittance matrix at each terminating busbar and this is then used in combination with the corresponding transmission line admittance matrices of equation (A-4) to form the full fault transient model.

A.1.3 Frequency-Transform Technique

The transient phenomenon associated with any disturbance, such as a fault, represents a wide frequency variation and it is therefore necessary to be able to evaluate the transient response over the whole frequency spectrum. The inverse Fourier transform

forms the basis of the method by which the frequency spectrum is used to determine the corresponding time variation of any voltage or current interest. A modified half-range form of the basic Fourier integral as given in equation (A-5) is used.

$$f(t) = \text{Real} \left[\exp \frac{(\alpha t)}{\pi} \int_0^{\Omega} \delta f (\omega - \psi \alpha) \exp(j\omega t) d\omega \right] \quad (\text{A-5})$$

$$\text{where } \delta = \frac{\sin(\pi \omega / \Omega)}{(\pi \omega / \Omega)}, \quad \alpha = \text{frequency shift constant}$$

A.2 Single-Circuit Plain Feeder

A general plain feeder as shown in Fig.A.3 represents the system devised to investigate the fault transient phenomena on 2-terminal EHV transmission lines. In Fig. A.3,

The behaviour of a plain feeder system under faulted conditions is dependent upon the fault point position along line length and the generator capacities at two terminals. The simulation includes the facility to any fault point. To provide these facilities, the system is represented by 3-node model as shown in Fig.A.4.

A general relationship for the system with a fault point between p and q, for example, can be defined as:

$$\begin{bmatrix} I_f \\ I_p \\ I_q \end{bmatrix} = \begin{bmatrix} Y_{11} & Y_{12} & Y_{13} \\ Y_{21} & Y_{22} & Y_{23} \\ Y_{31} & Y_{32} & Y_{33} \end{bmatrix} \cdot \begin{bmatrix} V_f \\ V_p \\ V_q \end{bmatrix} \quad (\text{A-6})$$

The elements of the admittance matrix in equation (A-6) are calculated from Fig A.4 as following:

$$\begin{aligned} Y_{11} &= Y_{22_{pf}} + Y_{11_{fq}} & Y_{12} &= Y_{21_{pf}} & Y_{13} &= Y_{12_{fq}} \\ Y_{21} &= Y_{12_{pf}} & Y_{22} &= Y_{11_{pf}} + Y_{ps} & Y_{23} &= 0 \\ Y_{31} &= Y_{21_{fq}} & Y_{32} &= 0, & Y_{33} &= Y_{22_{fq}} + Y_{qs} \end{aligned}$$

It should be noted that each element in equation (A-6) represents a 3 x 3 sub-matrix for a 3-phase system.

A.2.1 Prefault Calculation

The current constraint applied to the general relation is $I_f = 0$, where the voltage V_p and V_q are defined by a consideration of the system loading condition, thus we have equation (A-7) as given below:

$$\begin{bmatrix} I_p \\ I_q \end{bmatrix} = \begin{bmatrix} Y_{22} & Y_{23} \\ Y_{32} & Y_{33} \end{bmatrix} \begin{bmatrix} V_p \\ V_q \end{bmatrix} \quad (\text{A-7})$$

From equation (A-7), therefore, I_p and I_q are attained. I_p and I_q are then used to define V_f from the inversion of equation (A-6). The defined node voltages, combined with the two port admittance relations are then used to define all the prefault currents of interest.

A.2.2 Fault Transient Component Calculation

In fault case, the sources $I_p = I_q = 0$ referenced from equation (A-6), so that the system can then be reduced to a fault point relation as given by:

$$\begin{bmatrix} V_f \\ V_p \\ V_q \end{bmatrix} = \begin{bmatrix} Z_{11} & Z_{12} & Z_{13} \\ Z_{21} & Z_{22} & Z_{23} \\ Z_{31} & Z_{32} & Z_{33} \end{bmatrix} \cdot \begin{bmatrix} I_f \\ 0 \\ 0 \end{bmatrix} \quad (\text{A-8})$$

Where $Z = Y^{-1}$

For a three-phase system, we can see three-phase impedance at fault point is thus given:

$$\begin{bmatrix} V_{fa} \\ V_{fb} \\ V_{fc} \end{bmatrix} = \begin{bmatrix} Z_{aa} & Z_{ab} & Z_{ac} \\ Z_{ba} & Z_{bb} & Z_{bc} \\ Z_{ca} & Z_{cb} & Z_{cc} \end{bmatrix} \cdot \begin{bmatrix} I_{fa} \\ I_{fb} \\ I_{fc} \end{bmatrix} \quad (\text{A-9})$$

Now considering a single-phase-earth fault involving the 'a' phase, the two healthy phase fault path current I_{fb} and I_{fc} are zero. V_{fa} is the know quantity and is the transform of a suddenly applied sinusoidal voltage of the form $-V_{fa0} \sin(\omega_0 t + \beta) h(t)$, i.e. is simply equal and opposite to the prefault voltage at the point of fault. Thus:

$$I_{fa} = \frac{V_{fa}}{Z_{aa}} \quad (\text{A-10})$$

The current I_{fa} in equation (A-10) is substituted in equation (A-9), then the system transient voltages for the fault condition are obtained.

A.3 Typical Fault Studies

The results presented here are achieved by faulting some typical 400kV two terminal applications with difference generator capacities. Different line length of 128km, 140km and 160km have been selected and fault point varies along the transmission line.

Fig.A.5, Fig.A.6 and Fig.A.7 show some typical voltage and current waveforms observed at the relaying point for different fault positions, different source capacities, etc. It is apparent from the various waveforms that: the transient fault voltage and current waveforms have significant high frequency signal components. These high frequency components can be used to distinguish a faulty transmission line from a healthy transmission line, so protection algorithms often need large bandwidth fault signals. Typically, the required bandwidth per channel is about 4KHz. A three phase transmission line requires 4 to 6 channels for transferring fault transient fault waveforms. Fault transient waveforms thus set a bandwidth requirement for the communication link for transmitting waveforms from the local to the remote ends.

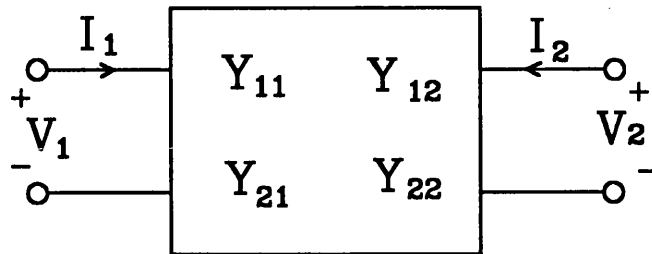


Fig. A.1 A general two-port network

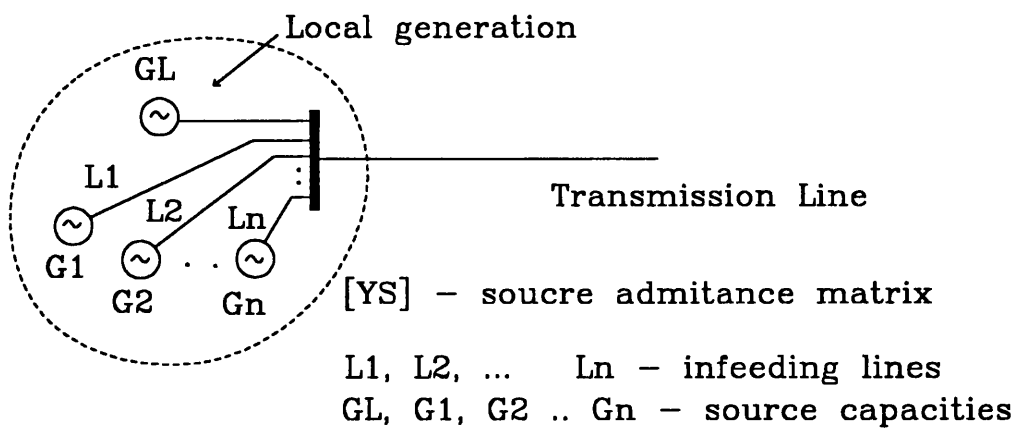
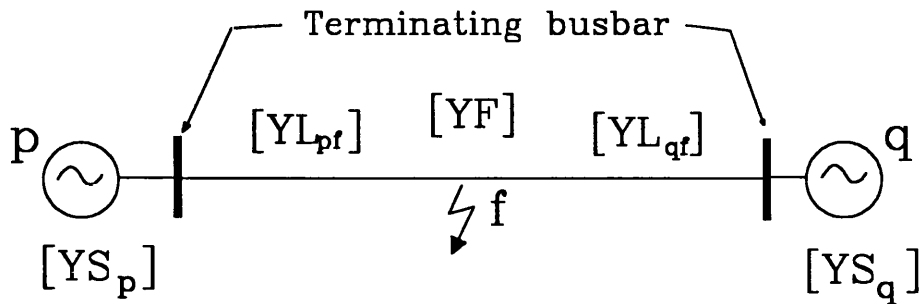


Fig. A.2 General source network



where f is fault occur point, $[YF]$ is the admittance matrix of fault network, YL_{pf} , YL_{qf} are length admittance matrices of feed paths, and $[YS_p]$, $[YS_q]$ are equivalent source admittance matrices at the terminating busbars.

Fig.A.3 Single circuit two terminal system

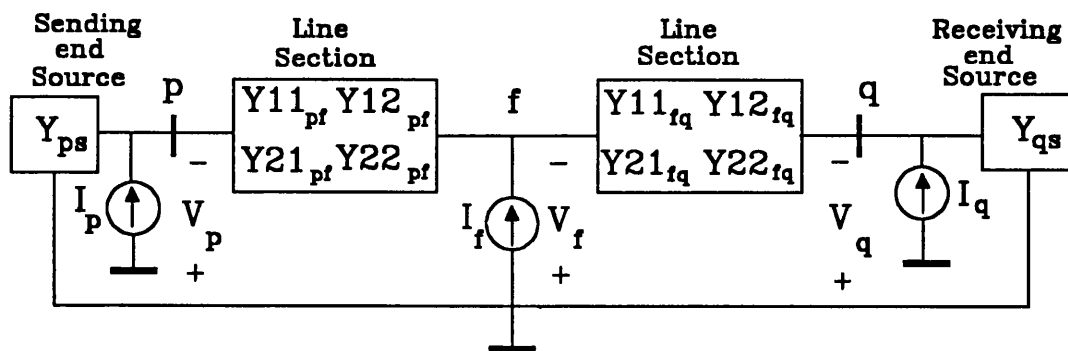


Fig. A.4 Admittance format for the single-circuit plain feeder

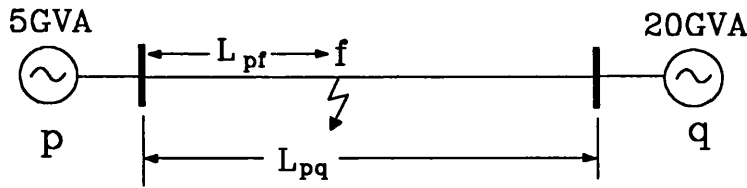
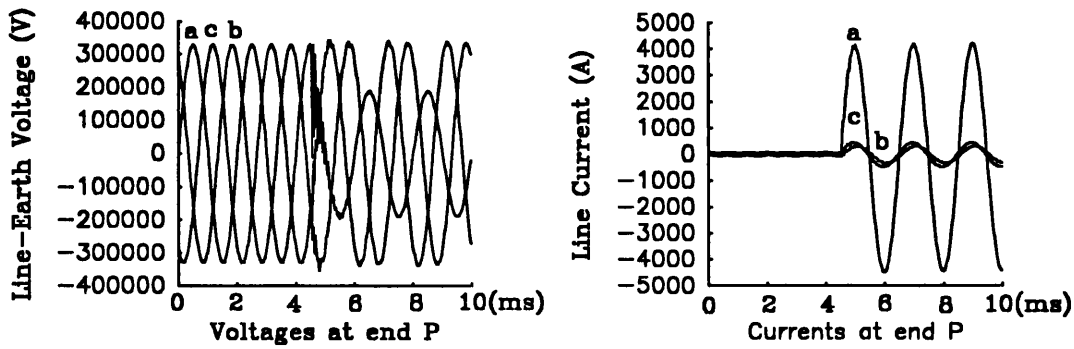
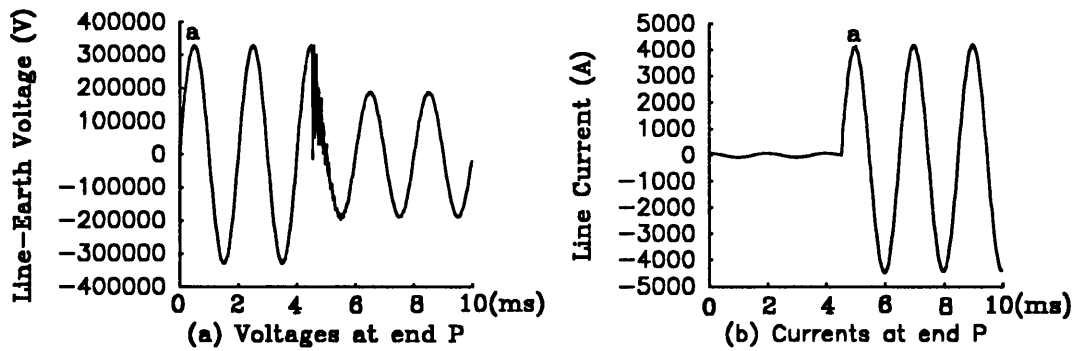


Fig.A.5 (a) System configuration with generator capacities 5GVA and 20GV
Transmission distance L_{pq} and Fault distance L_{pf} to end P

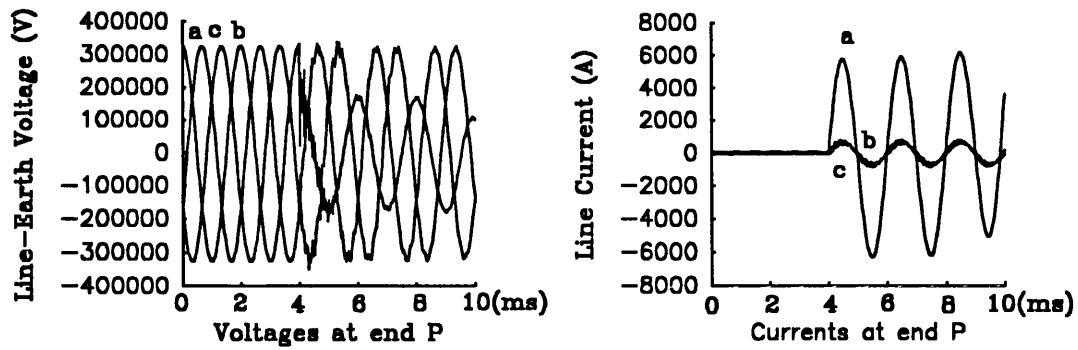


Three phase voltages and currents at end P

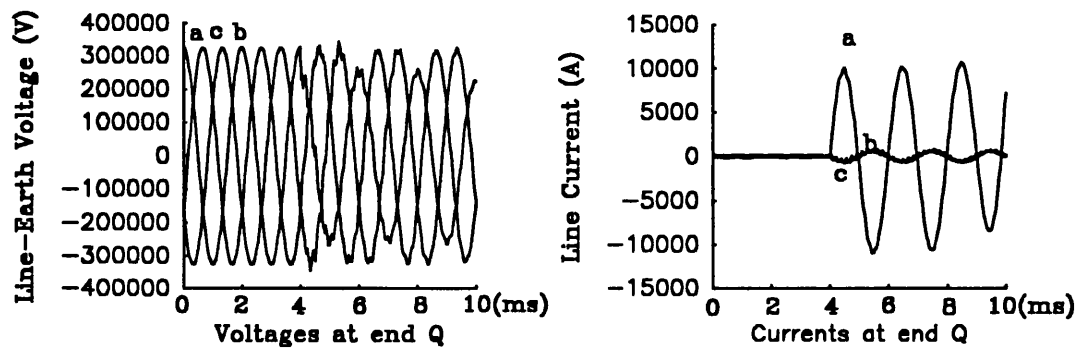


Single phase voltage and current at end P

Fig.A.5 (b) $L_{pq} = 160\text{km}$, $L_{pf} = 70\text{km}$,
phase a to earth fault at $V_a 90^\circ$ with fault to earth impedance 0

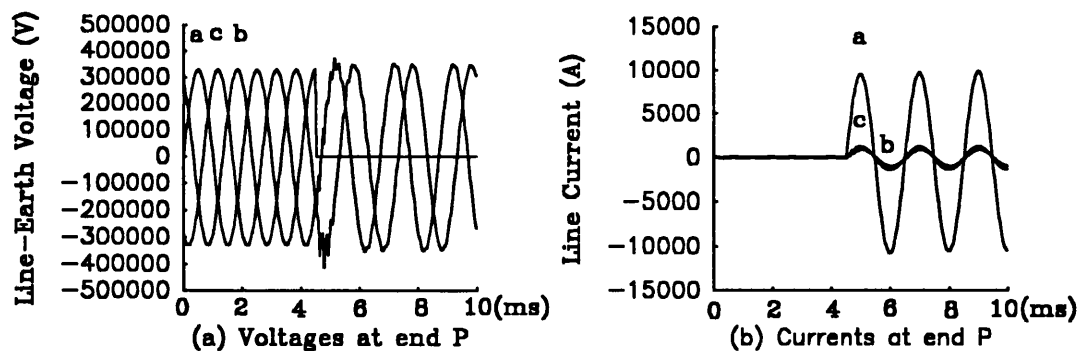


Three phase voltages and currents at end P



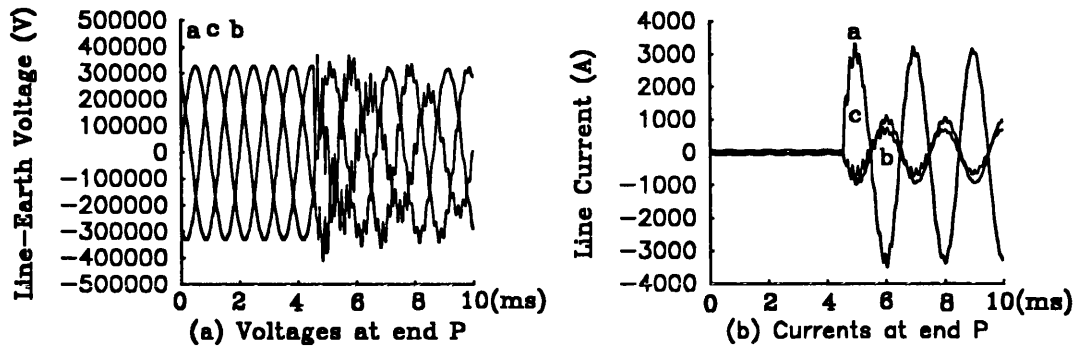
Three phase voltages and currents at end Q

Fig.A. 5 (c) $L_{pq} = 140\text{km}$, $L_{pf} = 50\text{km}$,
 phase a to earth fault at $V_a 90^\circ$ with fault to earth impedance 0

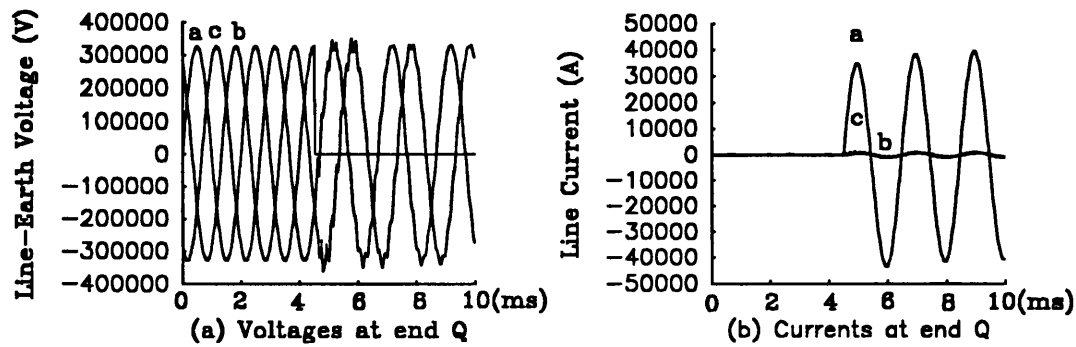


Three phase voltages and currents at end P

Fig.A.5 (d) $L_{pq} = 0\text{ km}$, $L_{pf} = 160\text{ km}$, (fault at end P)
 phase a to earth fault at $V_a 90^\circ$ with fault to earth impedance 0



Three phase voltages and currents at end P



Three phase voltages and currents at end Q

Fig.A. 5 (e) $L_{pq} = 160\text{km}$, $L_{pf} = 160 \text{ km}$, (fault at end Q)
 phase a to earth fault at $V_a 90^\circ$ with fault to earth impedance 0

Fig.A.5 (b)-(e) Show effect of parameter variance on faulty-phase transient waveforms with system configuration of Fig.A.5(a)

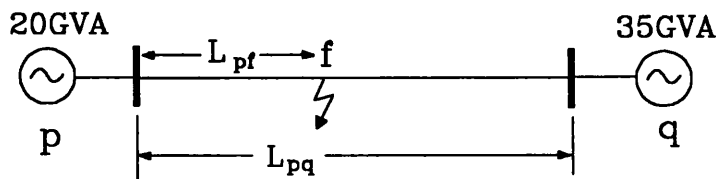
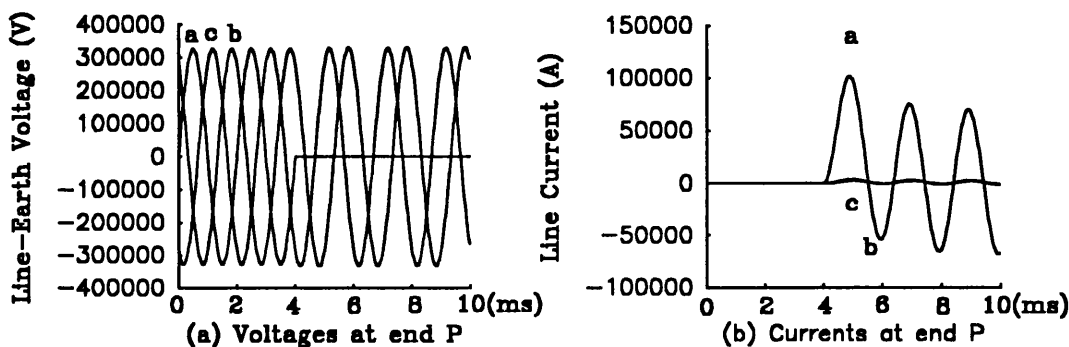
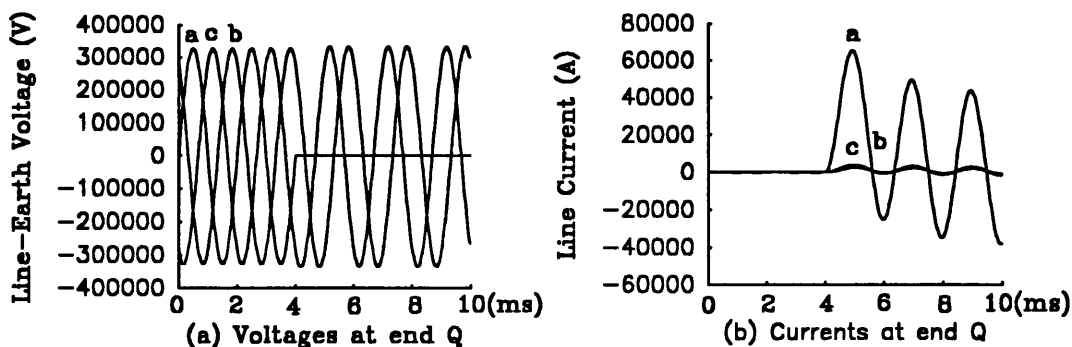


Fig.A.6 (a) System configuration with generator capacities 20GVA and 35GV Transmission distance L_{pq} between P and Q, and Fault distance L_{pf} to end P



Three phase voltages and currents at end P

Fig.A. 6 (b) $L_{pq} = 0$ km, $L_{pf} = 128$ km, (fault at end P)
phase a to earth fault at $V_a 0^\circ$ with fault to earth impedance 0



Three phase voltages and currents at end Q

Fig.A. 6 (c) $L_{pq} = 128$ km, $L_{pf} = 128$ km, (fault at end Q)
phase a to earth fault at $V_a 0^\circ$ with fault to earth impedance 0

Fig.A. 6 (c)-(d) Show faulty-phase transient waveforms at a fault point either end P or end Q with system configuration of Fig.A.6(a)

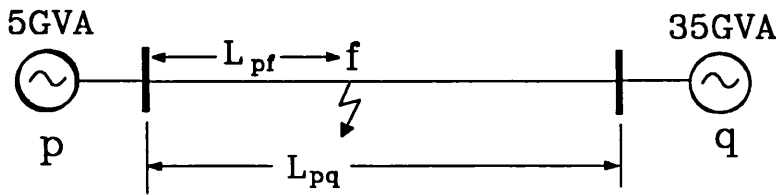
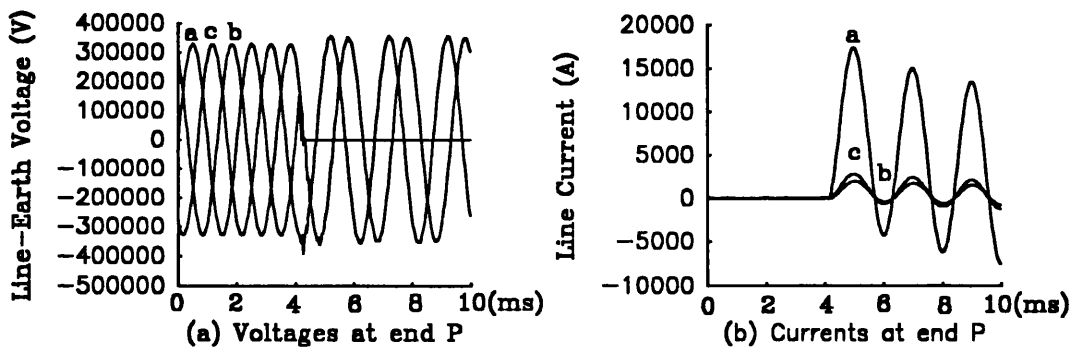
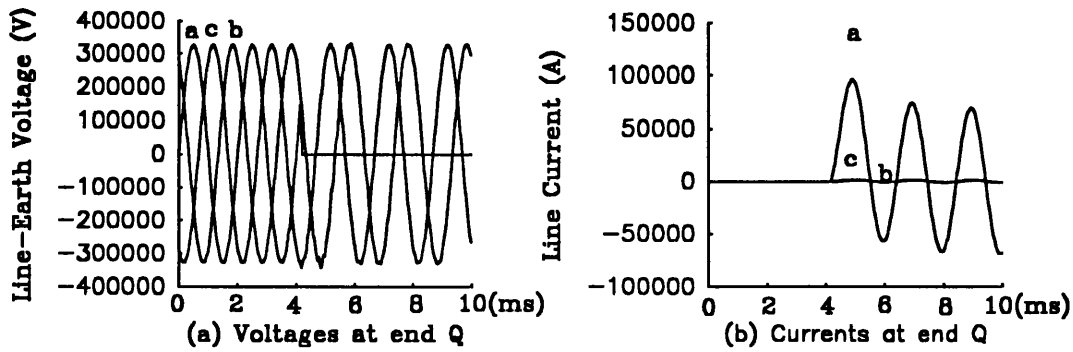


Fig.A.7 (a) System configuration with generator capacities 5GVA and 35GV Transmission distance L_{pq} between P and Q, and Fault distance L_{pf} to end P



Three phase voltages and currents at end P

Fig.A. 7 (b) $L_{pq} = 0$ km, $L_{pf} = 128$ km, (fault at end P)
phase a to earth fault at $V_a 30^\circ$ with fault to earth impedance 0



Three phase voltages and currents at end Q

Fig.A. 7 (c) $L_{pq} = 128$ km, $L_{pf} = 128$ km, (fault at end Q)
phase a to earth fault at $V_a 30^\circ$ with fault to earth impedance 0

Fig.A. 7 (c)-(d) Show faulty-phase transient waveforms at a fault point either end P or end Q with system configuration of Fig.A.6(a)

APPENDIX B

DETAILED INFERENCES OF LASER & FIBRE MODELS

B.1 Laser Characteristics

B.1.1 Laser Rate Equations

A laser diode is a kind of pn-junction semiconductors combined with an optical resonator. The pn-junction forms a diode which operates in the forward direction. The injected current carriers (i.e., carrier density) recombine at the pn-junction giving rise to the emission of photons. If the carrier density increases within the pn-junction, it finally yields the laser emission. Laser characteristic may either be described by a field equation (Maxwell's equation) or the rate equation [1]. A simple method of representing laser characteristic is the laser rate equation. The laser rate equation of a single lasing mode corresponding to a single emission wavelength thus is represented as:

$$\frac{dn_e}{dt} = \frac{i}{e} - \frac{n_e}{\tau_e} - A(n_e - N_0) s_p \quad (\text{B.1-1})$$

$$\frac{ds_p}{dt} = A(n_e - N_0) s_p - \frac{s_p}{\tau_p} + \rho \frac{n_e}{\tau_e} \quad (\text{B.1-2})$$

where n_e is the electron density, s_p is the photo density, i is the injected or pump current, e is the electron charge, τ_e is the spontaneous emission lifetime, τ_p is the photo lifetime, the optical gain $g = A(n_e - N_0)$, A is the optical gain parameter, N_0 is the minimum electron density required to obtain a positive gain, and ρ is the fraction of the spontaneous emission going into the lasing modes.

There is a pair of coupled differential equations which describe the density of injected

current carriers n_e and the density of stimulated photons s_p in a laser optical resonator.

The equations are valid for laser diodes with the following assumptions:

- (1) The laser operates in a single mode above the threshold, i.e. $n_e \geq N_0$.
- (2) The optical resonator is ideal and has a homogeneous population inversion and the density of carriers and photons are homogeneous.
- (3) The stimulated photon gain per unit of time is a linear function of the carrier.
- (4) Noise is excluded from consideration

B.1.2 Steady State Analysis

Since a injected current i must be great than a threshold current i_{th} for a laser to output optical power. If a given dc injected current drives the laser, after lasing transient time, both electron carrier density n_e and photo density s_p tend to be stable. The analysis of steady state of the laser thus is necessary. Under steady state analysis condition, it should take $d/dt = 0$, thus equation (B.1.-1) and (B.1-2) become:

$$\frac{i^o}{e} - \frac{n_e^o}{\tau_e} - A(n_e^o - N_0) s_p^o = 0 \quad (\text{B.1-3})$$

$$A(n_e^o - N_0) s_p^o - \frac{s_p^o}{\tau_p} + \rho \frac{n_e^o}{\tau_e} = 0 \quad (\text{B.1-4})$$

where i^o , n_e^o and s_p^o are the steady state values of injected current, electron density and photo density, respectively. Expanding equations (B.1-3) and (B.1-4), the following two equations are obtained:

$$n_e^o = \frac{s_p^o(1 + AN_0\tau_p)}{\tau_p(A s_p^o + \rho/\tau_e)} \quad (\text{B.1-5})$$

$$\frac{i^o}{e} = \frac{1-\rho}{\tau_e} n_e^o + \frac{s_p^o}{\tau_p} = \frac{i_{th}}{e} + \frac{s_p^o}{\tau_p} \quad (\text{B.1-6})$$

If $A \times s_p^o \gg \rho/\tau_e$, this is true in a laser design, so the laser threshold current. i_{th} can

be calculated by:

$$\frac{i_{th}}{e} = \frac{1-\rho}{\tau_e} (N_0 + \frac{1}{g\tau_p}) \quad (\text{B.1-7})$$

The equation (B.1.-5), (B.1-6) and (B.1-7) are used to calculate laser steady state values i^o , n_e^o , s_p^o and i_{th} .

B.1.3 Small Signal Modulation

In fibre optic links, the information is carried in the form of pulse-code modulation, so knowing the dynamic behaviour of a injection laser is necessary. If a step-current pulse is applied, the carrier density increase and eventually exceeds the N_0 . For $n_e > N_0$, a rapid increase of the photon number s_p occurs. Since increased s_p consumes current carriers, so that the carrier density decreases again until it falls below N_0 . For $n_e < N_0$ the photon density rapidly decreases down to very low levels until the carriers recover and the carrier density increases again. The process is repeated and yields a ringing transient phenomena. In order to study this phenomena more in detail, it is useful to investigate the rate equations by a small signal analysis.

Small signal modulation can be regarded as the signal being superimposed on its mean values. Assuming that a small signal current is Δi , thus the injected current can be taken as :

$$i = i^o + \Delta i \quad (\text{B.1-8})$$

where i^o is the mean value (i.e., steady state value). For a small modulation amplitude $\Delta i \ll i^o$ the rate equations may be linearized. It also affects small variations of n_e and s_p around their mean value n_e^o and s_p^o , and they can be represented by:

$$n_e = n_e^o + \Delta n_e \quad (\text{B.1-8})$$

$$s_p = s_p^o + \Delta s_p \quad (\text{B.1-9})$$

If equation (B.1-7), (B.1-8) and (B.1-9) are inserted into the rate equation (B.1-1) and (B.1-2), and the high order $\Delta n_e \Delta s_p$ component are neglected, thus the small signal analysis equations are obtained as follows:

$$\frac{d\Delta n_e}{dt} = \frac{\Delta i}{e} - \left(\frac{1}{\tau_e} + A s_p^o\right)\Delta n_e - G_o \Delta s_p \tag{B.1-10}$$

$$\frac{d\Delta S_p}{dt} = \left(\frac{\rho}{\tau_e} + A s_p^o\right)\Delta n_e - \rho \frac{n_e^o}{s_p^o \tau_e} \Delta s_p \tag{B.1-11}$$

where $G_o = A (n_e^o - N_o)$ the photo gain.

B.1.4 Electrical Equivalent Circuit of a Laser diode

It may be noted that equation(B.1-10) and (B.1-11) are similar differential equations to a parallel RLC circuit. In fact, the laser diode can be modeled by a parallel equivalent RLC circuit as shown in Fig.B.1

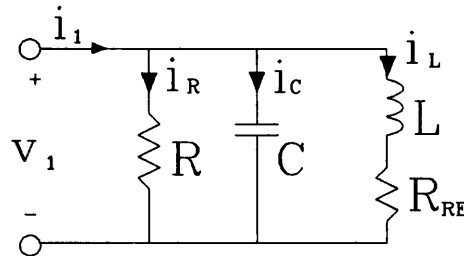


Fig.B.1 A parallel RLC circuit

The above laser equivalent RLC circuit can be described by using differential equations, thus the v_1 and i_L are represented by:

$$\frac{dv_1}{dt} = \frac{i_1}{C} - \frac{v_1}{RC} - \frac{i_L}{C} \tag{B.1-12}$$

$$\frac{di_L}{dt} = \frac{v_1}{L} - \frac{R_{SE}}{L} i_L \tag{B.1-13}$$

Because the laser diode is a pn-junction semiconductor with an optical resonator, the relation between p-n diode junction voltage and current density thus can be given by:

$$n = N^o e^{\frac{v_1}{mV_T}} = N^o \left(1 + \frac{v_1}{mV_T} + \frac{1}{2!} \left(\frac{v_1}{mV_T} \right)^2 + \dots \right) \quad (\text{B.1-14})$$

where N^o is the saturation current density and assumed to be close to the electron density n^o , m 1 or 2 is the empirical value, $V_T = k_B T/e$ the junction temperature voltage, e electron charge, k_B Boltzman constant, T the junction temperature.

If ignoring high order in equation (B.1-14), and assuming that the small signal voltage v_1 at diode junction is proportional to Δn_e , and the current i_L at circuit is promotional to photo density change Δs_p , thus following equations are obtained:

$$n_e \approx n^o + n^o \frac{v_1}{mV_T} = n^o + \Delta n_e \quad (\text{B.1-15})$$

$$v_1 = mV_T \Delta n_e \quad (\text{B.1-16})$$

$$i_L = e A (n^o - N_o) \Delta s_p = e G_o \Delta s_p \quad (\text{B.1-17})$$

Substituting equation (B.1-16) and (B.1-17) into equations (B.1-12) and (B.1-13), they become:

$$\frac{d\Delta n_e}{dt} = \frac{n^o i_1}{mV_T C} - \frac{\Delta n_e}{RC} - \frac{n^o e G_o}{mV_T C} \Delta s_p \quad (\text{B.1-18})$$

$$\frac{d\Delta s_p}{dt} = \frac{mV_T}{e G_o n^o L} \Delta n_e - \frac{R_{SE}}{L} \Delta s_p \quad (\text{B.1-19})$$

By comparing equations (B.1-18) and (B.1-19) with equations (B.1-10) and (B.1-11), the laser electrical equivalent circuit parameters can be thus obtained as:

$$\begin{aligned}
 C &= \frac{e}{mV_T} n^o, & L &= \frac{mV_T}{en^o G_o (A S_p^o + \rho/\tau_e)} \\
 R &= \frac{mV_T}{en^o (A S_p^o + \rho/\tau_e)}, & R_{SE} &+ \frac{\rho mV_T}{e\tau_e S_p^o G_o (A S_p^o + \rho/\tau_e)}
 \end{aligned}
 \tag{B.1-20}$$

The equation (B.1-20) is for calculating the laser equivalent circuit parameters. They are obtained from the parameters in laser rate equations (B.1-1) and (B.1-2) which describe the interplay between the optical intensity (or total number of photons) and the injected currents.

B.1.5 Laser Equivalent Transfer Function

The basic components of a fibre optic communication links simulation system are light source, optic fibre, and photo-detector. Thus an accurate representation of those characteristics in the form of transfer functions is required. If a light source is a laser, it can be modeled by a laser equivalent transfer function.

By taking Fourier transform, the equation (B.1-12) and (B.1-13) become:

$$j\omega V_1(\omega) = -\frac{1}{RC} V_1(\omega) + \frac{1}{C} I_1(\omega) + \frac{1}{C} I_L(\omega) \tag{B.1-21}$$

$$j\omega I_L(\omega) = \frac{1}{L} V_1(\omega) - \frac{R_{SE}}{L} I_L(\omega) \tag{B.1-22}$$

Thus the impedance function and transfer function of the laser can be obtained as following:

$$Z_{laser}(\omega) = \frac{V_1(\omega)}{I_1(\omega)} = \frac{j\omega L + R_{SE}}{LC D(j\omega)} \tag{B.1-23}$$

$$H_{laser}(\omega) = \frac{I_L(\omega)}{I_1(\omega)} = \frac{1}{LC D(j\omega)} \quad (\text{B.1-24})$$

$$\text{where } D(j\omega) = \left((j\omega)^2 + j\omega \left(\frac{R_{SE}}{L} + \frac{1}{LC} \right) + \frac{1}{LC} \left(1 + \frac{R_{SE}}{R} \right) \right)$$

Since it was assumed that $i_L = e G_0 \Delta s_p = e G_0 s_1$ where s_1 represents small photo signal density and $S_1(\omega)$ is its spectrum, therefore the photo density to injected current transfer function is given by:

$$H_{photo}(\omega) = \frac{S_1(\omega)}{I_1(\omega)} = \frac{1}{eG_o LC D(j\omega)} \quad (\text{B.1-25})$$

This equation is used as the laser transfer function.

B.2 Fibre Transfer Function Characteristic

B.2.1 Baseband Fibre Transfer Function

When the current of a semiconductor laser is modulated, the optical signal generated by the laser can be described by an amplitude-modulated signal. The transfer function of the fibre optic behaves like a bandpass filter which can be written as [17]:

$$G(\omega) = G_1(\omega - \omega_o) + G_1^*(-\omega - \omega_o) \quad (\text{B.2-1})$$

where $G_1(\omega)$ is the equivalent baseband characteristic.

For single-mode fibre systems, the transfer function of the fibre can be rewritten as:

$$G(\omega) = \exp \left[-\frac{\alpha(\omega)}{2}L - j\frac{\beta(\omega)}{2}L \right] \quad (\text{B.2-2})$$

where $\alpha(\omega)/2$ is the fibre loss, $\beta(\omega)/2$ is the phase propagation constant and L fibre length. In the relevant frequency region the fibre loss $\alpha(\omega)$ at ω_o is assumed to be a constant α , thus the equivalent baseband characteristic becomes:

$$G_1(\omega) \approx e^{-\frac{\alpha}{2}L} e^{-j\frac{L}{2}(\beta_0 - j\beta'_0\omega - j\frac{\beta''_0}{2}\omega^2)} \quad (\text{B.2-3})$$

where β'_0 β''_0 are the first and secondary phase propagation constant coefficients, and can be represented by time form as following:

$$\beta'_0 = \left. \frac{d\beta}{d\omega} \right|_{\omega_0} = \tau_0 \quad (\text{B.2-4})$$

$$\beta''_0 = \left. \frac{d\beta^2}{d\omega^2} \right|_{\omega_0} = \frac{\lambda_0^2}{2\pi C} \frac{d\tau}{d\lambda} \quad (\text{B.2-5})$$

where τ_0 is the delay of the optical signal in the fibre, and $d\tau/d\lambda$ is fibre dispersion parameter, λ_0 is the optical carrier wavelength and c is light velocity in vacuum.

If putting equation (B.2-5) and (B.2-6) into (B.2-7), a fibre equivalent baseband characteristic form related to time thus becomes:

$$G_1(\omega) = e^{-\frac{\alpha}{2}L} e^{-j\frac{\omega}{2}L(\tau_0 + \frac{d\tau}{d\lambda}\lambda)} \quad (\text{B.2-6})$$

If considering a source spectrum $S(\lambda)$, thus the light source and dispersive transfer function $G_1(\omega)$ give a fibre transfer $H(\omega)$ as following:

$$H(\omega) = \int S(\lambda) e^{-\alpha L} e^{-j\omega L(\tau_0 + \frac{d\tau}{d\lambda}\lambda)} d\lambda \quad (\text{B.2-7})$$

This equation is a simpler model of an optical fibre transfer function.

B.2.2 General Fibre Transfer Function

In practice a light source spectrum is a random process, therefore its autocorrelation function should be used to obtain a general fibre link transfer function $h(t)$. Assuming following conditions are established: the general fibre link transfer function normally

includes a light source and a fibre, the light source has the envelope of optical electric field $\Psi_0(t)$ which is a random process, the fibre baseband transfer function is $g_1(t)$ obtained by taking Fourier transform for equation (B.2.-4) and a injected current signal $m(t)$ inputs the general fibre transfer function, then the output signal of a photodiode is given by the ensemble of the optical power $\langle P(z,t) \rangle$. After distance z in the dispersive optical fibre [42], it is given by follows

$$\begin{aligned} \langle P(z,t) \rangle &= \left| \int_{-\infty}^{\infty} g_1(\tau) \sqrt{m(t-\tau)} \Psi_0(t-\tau) d\tau \right|^2 \\ &= \int_{-\infty}^{\infty} \int_{-\infty}^{\infty} g_1(\tau_1) g_1^*(\tau_2) \sqrt{m(t-\tau_1)} \sqrt{m(t-\tau_2)} \Psi_0(t-\tau_1) \Psi_0^*(t-\tau_2) d\tau_1 d\tau_2 \end{aligned} \quad (\text{B.2-8})$$

From this equation it can be seen that the output signal of the fibre optic link is also a stochastic process. Further assumptions are made as following:

- (i) The signal $m(t-\tau_1) \approx m(t-\tau_2)$ for time difference $\tau_1 - \tau_2 \neq 0$.
- (ii) $R_{zz}(\tau_1-\tau_2) = \Psi_0(t-\tau_1)\Psi_0^*(t-\tau_2)$ is the autocorrelation function of optical electric field process $\Psi_0(t)$.

Thus equation (B.2-8) becomes:

$$\begin{aligned} \langle p(z,t) \rangle &= \int_{-\infty}^{\infty} \int_{-\infty}^{\infty} g_1(\tau_1) g_1^*(\tau_2) \left[\frac{1}{2}m(t-\tau_1) + \frac{1}{2}m(t-\tau_2) \right] R_{zz}(\tau_1-\tau_2) d\tau_1 d\tau_2 \\ &= \frac{1}{2} \int_{-\infty}^{\infty} \left[\int_{-\infty}^{\infty} g_1^*(\tau_2) R_{zz}(\tau_1-\tau_2) d\tau_2 \right] g_1(\tau_1)m(t-\tau_1)d\tau_1 \\ &\quad + \frac{1}{2} \int_{-\infty}^{\infty} \left[\int_{-\infty}^{\infty} g_1(\tau_1) R_{zz}(\tau_1-\tau_2) d\tau_1 \right] g_1^*(\tau_2)m(t-\tau_2)d\tau_2 \end{aligned} \quad (\text{B.2-9})$$

Note that the second term of this equation is the complex conjugate of the first term,

$\langle p(z,t) \rangle = \int_{-\infty}^{\infty} h(t) m(t-\tau) d\tau$, this equation become:

$$\langle p(z,t) \rangle = \int_{-\infty}^{\infty} h(t) m(t-\tau) d\tau \quad (\text{B.2-10})$$

It can be seen that the system is approximately linear with:

$$h(t) = \left| g_1(\tau) \int_{-\infty}^{\infty} g_1^*(\rho) R_{zz}(\tau - \rho) d\rho \right| \quad (\text{B.2-11})$$

Taking Fourier transform, equation (B.2-11) becomes:

$$H(\omega) = \frac{1}{2\pi} G_1(\omega) * [G_1^*(-\omega) S_{zz}(\omega)] \quad (\text{B.2-12})$$

where * is the notation for convolution calculation, $S_{zz}(\omega)$ is the spectrum of the complex envelope of the source which is the Fourier spectrum of the autocorrelation function $R_{zz}(t)$. In theory, it can be assumed that the spectrum $S_{zz}(\omega)$ of the complex envelope of optical source signal (random process) is Gaussian envelope.

Results of both models of equations (B.2.-7) and (B.2-12) are the same under the same Gaussian spectrum. If source spectrum is not Gaussian, the former model is computationally intensive and computed transfer function is usually saved for use, simulation runs do not require changes to spectrum and fibre length z. However, the later model can use Fourier transform to obtain fibre transfer function, the spectrum $S_{zz}(\omega)$ is a measurable parameter, thus the model is easier and more practical.

APPENDIX C

DETAILED INFERENCES OF SPUN FIBRE MODELS

C.1 Jones Matrix

When light passes through an optical plate or a glass fibre, the state of polarization and sometimes the intensity of the light will be changed. Jones [31] devoted to a description of the new calculus for the treatment of optical systems. It represents the effect of any optical element on the light as linear operator acting upon the electric vector of the light wave. The operator is expressed in the convenient form of a two-by-two matrix, whose four matrix elements are in general complex. An explanation of the operator is given as follows:

Assuming that a right-handed rectangular coordinate reference system, x , y and z represent the air medium, the light propagation direction is considered to be along the $+z$ axis, the z axis is perpendicular to the plane of a plate x and y . Also assuming that a right-handed rectangular principal coordinate system x' , y' and z' represent the plate medium, the light propagation in the plate medium is considered to be along $+z'$, and z' axis is in the same direction as z axis. Furthermore, let two principal axes of the i th retardation plate be indicated by x' and y' . Assuming that the positive x' and y' axes have the same relative orientation as the positive x and y axes, then define the orientation of the i th element by stating the angle θ measured counterclockwise from the positive x axis to the positive x' axis. In x , y and z coordinate system, two polarized components at any fixed point along the z axis may be written in the usual complex form:

$$\begin{aligned} E_x &= A_x \exp j(\epsilon_x + \omega t) \\ E_y &= A_y \exp j(\epsilon_y + \omega t) \end{aligned} \tag{C.1-1}$$

where A_x and A_y are the electric wave amplitude and ϵ_x , ϵ_y are the permittivity and are real. If $\epsilon_x - \epsilon_y$ is an integral multiple of π , the light is plane polarized; otherwise, elliptically polarized.

At the plate medium, if we know the x' and y' components at $z = 0$ ($E_x(0)$ and $E_y(0)$) of the electric vector as the light enters the plate, then corresponding components of the light as it emerges from the other side of the plate are:

$$\begin{aligned} E'_x(d) &= E'_x(0) \exp j\beta'_x z \\ E'_y(d) &= E'_y(0) \exp j\beta'_y z \end{aligned} \quad (\text{C.1-2})$$

Where β'_x and β'_y are the propagation constant in the plate medium, d is the thickness of the plate. If orientation θ is the angle measured counterclockwise from the positive x axis to the positive x' axis, we have the relations:

$$\begin{aligned} E'_x(0) &= E_x(0) \cos\theta + E_y(0) \sin\theta \\ E'_y(0) &= -E_x(0) \sin\theta + E_y(0) \cos\theta \end{aligned} \quad (\text{C.1-3})$$

Then the Jones matrix notation is:

$$\begin{bmatrix} E'_x(d) \\ E'_y(d) \end{bmatrix} = \begin{bmatrix} \cos\theta & -\sin\theta \\ \sin\theta & \cos\theta \end{bmatrix} \begin{bmatrix} \exp(j\beta'_x d) & 0 \\ 0 & \exp(j\beta'_y d) \end{bmatrix} \begin{bmatrix} \cos\theta & \sin\theta \\ -\sin\theta & \cos\theta \end{bmatrix} \begin{bmatrix} E_x(0) \\ E_y(0) \end{bmatrix} \quad (\text{C.1-4})$$

Further Assuming $\Delta\beta = (\beta'_x - \beta'_y) / 2$ and $\beta_s = (\beta'_x + \beta'_y) / 2$, then Equation (C.1-4) becomes:

$$\begin{bmatrix} E'_x(d) \\ E'_y(d) \end{bmatrix} = e^{j\beta_s d} \begin{bmatrix} \cos\theta & -\sin\theta \\ \sin\theta & \cos\theta \end{bmatrix} \begin{bmatrix} \exp(j\Delta\beta d) & 0 \\ 0 & \exp(-j\Delta\beta d) \end{bmatrix} \begin{bmatrix} \cos\theta & \sin\theta \\ -\sin\theta & \cos\theta \end{bmatrix} \begin{bmatrix} E_x(0) \\ E_y(0) \end{bmatrix} \quad (\text{C.1-5})$$

This equation shows that light propagation difference $\Delta\beta$ in a linear optical plate

changes state of polarization of $E_x(z)$ and $E_y(z)$. It is useful matrix for any linear optical system treatment. In this thesis, a spun fibre model is obtained based on this equation.

C. 2 Light Propagation in Twisted Anisotropic Media

In the situation of a twisted light transmission medium, light waves propagate along the $+z$ axis or $-z$ axis direction, and the two axes $x(z)$, $y(z)$ (the optical axes of the untwisted medium, now the axes of the polarization ellipses of the normal modes) rotate as the medium twists. At any position $+z$ or $-z$ in the medium, the field can be resolved into two plane waves, one with electric field $E_x(z)$ parallel to $x(z)$ and the other with electric field $E_y(z)$ parallel to $y(z)$. Twisting of the medium causes these two plane waves to interchange energy (couple) as they propagate. Using coupled-mode theory and with an assumed linear twist rotator $\Omega(z) = \xi z$, there are the coupled-mode equations [43]. The two directional equations are:

(i) $+z$ direction with counterclockwise angle measurement

$$\frac{dE_x(z)}{dz} - j \beta_x E_x(z) = \xi E_y(z) \quad (\text{C.2-1})$$

$$\frac{dE_y(z)}{dz} - j \beta_y E_y(z) = -\xi E_x(z) \quad (\text{C.2-2})$$

where β_x and β_y are the propagation constant in the plate medium. one solution of above equations, for example, by Laplace transform method, is given as below:

$$\begin{bmatrix} E_x(z) \\ E_y(z) \end{bmatrix} = e^{j \beta_x z} \begin{bmatrix} \cos \gamma z + j \frac{\Delta \beta}{2} \sin \gamma z & \frac{\xi}{\gamma} \sin \gamma z \\ -\frac{\xi}{\gamma} \sin \gamma z & \cos \gamma z - j \frac{\Delta \beta}{2} \sin \gamma z \end{bmatrix} \begin{bmatrix} E_x(0) \\ E_y(0) \end{bmatrix}$$

$$\text{Where } \beta_s = \frac{\beta_x + \beta_y}{2} \quad , \quad \Delta\beta = \frac{\beta_x - \beta_y}{2} \quad (\text{C.2-3})$$

$$\gamma = \frac{1}{2} \sqrt{\Delta\beta^2 + 4\xi^2}$$

(ii) -z direction with counterclockwise angle measurement

$$\frac{dE_x(-z)}{dz} + j\beta_x E_x(-z) = -\xi E_y(-z) \quad (\text{C.2-4})$$

$$\frac{dE_y(-z)}{dz} + j\beta_y E_y(-z) = \xi E_x(-z) \quad (\text{C.2-5})$$

A solution of these equations, again by using Laplace transform method, is giving as:

$$\begin{bmatrix} E_x(-z) \\ E_y(-z) \end{bmatrix} = e^{-j\beta_s z} \begin{bmatrix} \cos\gamma z - j\frac{\Delta\beta}{2}\sin\gamma z & -\frac{\xi}{\gamma}\sin\gamma z \\ \frac{\xi}{\gamma}\sin\gamma z & \cos\gamma z + j\frac{\Delta\beta}{2}\sin\gamma z \end{bmatrix} \begin{bmatrix} E_x(0) \\ E_y(0) \end{bmatrix}$$

$$\text{Where } \beta_s = \frac{\beta_x + \beta_y}{2} \quad , \quad \Delta\beta = \frac{\beta_x - \beta_y}{2}$$

$$\gamma = \frac{1}{2} \sqrt{\Delta\beta^2 + 4\xi^2} \quad (\text{C.2-6})$$

Equation (C.2-3) or Equation (C.2-6) is to calculate two plane light wave energy interchanging as they propagate in the positive direction or negative direction in a fibre respectively.

C.3 Spun Fibre Model

By applying above solutions of twisted medium [43], for example, to spun fibre, and processing this result with Jones matrix operator, and if orientation $\theta(0)$ is the angle

measured counterclockwise from the positive x axis to the positive x' axis at initial fibre distance $z = 0$, and $\theta(z)$ is the angle measured counterclockwise from the positive x axis to the positive x' axis at fibre distance z, a spun fibre model thus be obtained as follows:

$$\begin{bmatrix} E_x(z) \\ E_y(z) \end{bmatrix} = \begin{bmatrix} \cos\theta(z) & -\sin\theta(z) \\ \sin\theta(z) & \cos\theta(z) \end{bmatrix} \begin{bmatrix} \cos\gamma z + j\frac{\Delta\beta}{2\gamma}\sin\gamma z & \frac{\xi}{\gamma}\sin\gamma z \\ -\frac{\xi}{\gamma}\sin\gamma z & \cos\gamma z - j\frac{\Delta\beta}{2\gamma}\sin\gamma z \end{bmatrix} \times \begin{bmatrix} \cos\theta(0) & \sin\theta(0) \\ -\sin\theta(0) & \cos\theta(0) \end{bmatrix} \begin{bmatrix} E_x(0) \\ E_y(0) \end{bmatrix} \quad (\text{C.3-1})$$

where $E_x(0)$ and $E_y(0)$ are the electric field at fibre distance $z = 0$, and $E_x(z)$ and $E_y(z)$ are the electric field at fibre distance z. To Further calculate, we have:

$$\begin{bmatrix} E_x(z) \\ E_y(z) \end{bmatrix} = \begin{bmatrix} \cos\gamma z \cos(\theta(z)-\theta(0)) + \frac{\xi}{\gamma}\sin\gamma z \sin(\theta(z)-\theta(0)) + j\frac{\Delta\beta}{2\gamma}\sin\gamma z \cos(\theta(z)+\theta(0)) \\ \cos\gamma z \sin(\theta(z)-\theta(0)) - \frac{\xi}{\gamma}\sin\gamma z \cos(\theta(z)-\theta(0)) + j\frac{\Delta\beta}{2\gamma}\sin\gamma z \sin(\theta(z)+\theta(0)) \\ -\cos\gamma z \sin(\theta(z)-\theta(0)) + \frac{\xi}{\gamma}\sin\gamma z \cos(\theta(z)-\theta(0)) + j\frac{\Delta\beta}{2\gamma}\sin\gamma z \sin(\theta(z)+\theta(0)) \\ \cos\gamma z \cos(\theta(z)+\theta(0)) + \frac{\xi}{\gamma}\sin\gamma z \sin(\theta(z)-\theta(0)) - j\frac{\Delta\beta}{2\gamma}\sin\gamma z \cos(\theta(z)+\theta(0)) \end{bmatrix} \begin{bmatrix} E_x(0) \\ E_y(0) \end{bmatrix}$$

$$\text{Where } \Delta\beta = \frac{\beta_x - \beta_y}{2}, \quad \gamma = \frac{1}{2} \sqrt{\Delta\beta^2 + 4(\xi+f)^2}$$

$$f = \frac{5.79 \times 10^{-19}}{\lambda^2} \frac{I}{D} \quad (\text{rad / m}) \quad (\text{C.3-2})$$

f is the unit Faraday effect corresponding to the measuring current I and the fibre coil diameter D.

Assuming that $\theta(0) = \theta$, $\theta(z) = \theta + \xi z - \Omega'(z)$, $2\phi(z) = \theta(z) + \theta(0)$ and $\Omega(z) = \theta(z) - \theta(0)$, where θ the initial orientation angle, ξz the spinning rate along z, $\Omega'(z)$

the external rotation angle (i.e. Faraday effect), $\Omega(z)$ the total rotation angle difference, $2\phi(z)$ the principle axis orientation at distance z , so we have:

$$\begin{bmatrix} E_x(z) \\ E_y(z) \end{bmatrix} = \begin{bmatrix} \cos\gamma z \cos(\Omega(z)) + \frac{\xi}{\gamma} \sin\gamma z \sin(\Omega(z)) + j \frac{\Delta\beta}{2\gamma} \sin\gamma z \cos(2\Phi(z)) \\ \cos\gamma z \sin(\Omega(z)) - \frac{\xi}{\gamma} \sin\gamma z \cos(\Omega(z)) + j \frac{\Delta\beta}{2\gamma} \sin\gamma z \sin(2\Phi(z)) \\ -\cos\gamma z \sin(\Omega(z)) + \frac{\xi}{\gamma} \sin\gamma z \cos(\Omega(z)) + j \frac{\Delta\beta}{2\gamma} \sin\gamma z \sin(2\Phi(z)) \\ \cos\gamma z \cos(\Omega(z)) + \frac{\xi}{\gamma} \sin\gamma z \sin(\Omega(z)) - j \frac{\Delta\beta}{2\gamma} \sin\gamma z \cos(2\Phi(z)) \end{bmatrix} \begin{bmatrix} E_x(0) \\ E_y(0) \end{bmatrix} \quad (\text{C.3-3})$$

For succinctness, put above coupled mode equations in simple matrix form:

$$[E(z)] = [K(z)] [E(0)] \quad (\text{C.3-4})$$

Where $[E(0)]$ the column matrix with two elements $E_x(0)$ and $E_y(0)$, $[E(z)]$ the column matrix with two elements $E_x(z)$ and $E_y(z)$ of $[E(0)]$, and $[K(z)]$ is a square matrix of the following form:

$$[K(z)] = \begin{bmatrix} B_2 + jB_1 & -K_2 + jK_1 \\ K_2 + jK_1 & B_2 - jB_1 \end{bmatrix} \quad (\text{C.3-5})$$

Where $B_2 = \cos \gamma z \cos \Omega(z) + \xi/\gamma \sin \gamma z \sin \Omega(z)$
 $B_1 = \Delta\beta / 2\gamma \sin \gamma z \sin 2\phi(z)$
 $K_2 = \cos \gamma z \sin \Omega(z) - \xi/\gamma \sin \gamma z \cos \Omega(z)$
 $K_1 = \Delta\beta / 2\gamma \sin \gamma z \cos 2\phi(z)$

In the simple case where the spun fibre feature is longitudinally invariant, K_2 and ξ can be regarded as constants. For a spun fibre [22], the $K_2 = 0$, therefore, $\cos \gamma z \sin \Omega(z) - \xi/\gamma \sin \gamma z \cos \Omega(z) = 0$, so it becomes:

$$\Omega(z) = \tan^{-1} \left(\frac{\xi}{\gamma} \tan \gamma z \right) + n\pi \quad (\text{C.3-6})$$

Further other parameters are:

$$\Omega'(z) = \xi z - \tan^{-1} \left(\frac{\xi}{\gamma} \tan \gamma z \right) + n\pi \quad (\text{C.3-7})$$

$$\phi(z) = \frac{1}{2} \tan^{-1} \left(\frac{\xi}{\gamma} \tan \gamma z \right) + \frac{m\pi}{2} + \theta \quad (\text{C.3-8})$$

where m and n are integers and θ is the initial orientation of the local slow axis of the fibre.

Following the same manner, we can have two electric wave mode fields along $-z$ direction whose simple matrix expression is:

$$[E(-z)] = [K(-z)] [E(0)] \quad (\text{C.3-9})$$

In this thesis equation (C.3-4) and (C.3-9) are used to set up a model for the FOCS with a MFR.

PUBLISHED WORK

The following papers are based on the work of fibre optic communication links described in this thesis. Copies of Papers 1 and 2 are enclosed.

1. Aggarwal R.K. and Li H.Y. "Computer Modelling of a Fibre Optic Communication Systems for Power System Protection Relaying", Presented at the 27th UPEC, UK, pp.679-683, September 1992
2. Li H.Y and Aggarwal R.K. "An Improved Modelling Technique of a Fibre Optic Digital System For Power System Protection Relaying", IEE APSCOM-93, Hong Kong, pp. 252-256, December, 1993

Computer Modelling of a Fibre Optical Communication System for Power System Protection Relaying

R.K. Aggarwal & H. Y. Li

School of Electronic and Electrical Engineering
University of Bath, BA2 7AY, UK

Abstract – Computer modelling techniques and analysis methods for simulating a complete fibre optical direct-detection system are reviewed. These include a low-pass equivalence model of a light source transmitter, models of a single-mode fibre and a light receiver. Models for system degradations, particularly emphasising the effect on signals received due for example to such parameters as fibre length, fibre bandwidth, detector noise are discussed. An optical fibre transmission mode, especially a decision circuit mode is simulated for assessing the performance of the model using realistic fault transient signals, similar to those encountered on Power systems in practice, and which are required to be transmitted for protective relaying.

1 INTRODUCTION

In less than 15 years, fibre optics has emerged from an engineering feasibility study to become the dominant telecommunication bit-transport mechanism. For example, the UK currently has 70% of all its long-haul traffic conveyed by fibre system. Owing to the advantageous features of an optical fibre transmission system, which are electromagnetic interference (EMI) immunity, low loss, large capacity, low weight and small physical size, practical optical fibre systems have emerged in electrical power system [1].

In any practical design of a fibre optical system, since there are many types of optical components and different application purposes of the optical fibre system, in order to minimize the cost of a fibre optical system design, it is important to have an accurate knowledge of the optical fibre characteristics, particularly in terms of intrinsic fibre loss (due for example to scattering and absorption) and dispersion (modal and chromatic), together with the effect on signals of transmitters and receivers. Furthermore, other losses associated with splicing and connectors are also essential. The foregoing factors are crucial for drawing up an Optical Budget as the later allows a specification of the maximum distance over which signals can be faithfully transmitted (without the need for any repeaters), certainly well within the sensitivity limit of the receiver and also equally importantly, without excessive distortion due to dispersion.

The primary objective in computer modelling of a fibre optical communication system design is to maximize repeater spacing while maintaining a specified error performance and providing a power margin to account for unforeseen effects. The most basic form of system design takes the form of a power budget, and the most obvious transmission limitations are due to fibre transmission loss and dispersion. Starting with the optical power P_t available from the source, power losses due to coupling, splices, fibre loss, margin, etc, are subtracted to compute the power arriving at the receiver P_r . This power must exceed the receiver sensitivity in order to meet the bit-error-rate performance. In addition, the loss in receiver sensitivity due to effects such as dispersion are assigned a power penalty and included in the budget as if they were actual losses. The maximum system length is simply computed as that length at which the received power must equal to the receiver sensitivity adjusted for all power penalties. This calculation is given by equation (1):

$$L = \frac{10}{A} \log \frac{P_t}{P_r} \quad (1)$$

Where P_t is the power launched by the transmitter into the fibre, P_r is the receiver power, A is the total losses and L is the loss-limited

transmission distance. From equation (1), it can be seen that the loss-limited transmission distance depends strongly on fibre losses, but only marginally on transmitter and receiver power levels. Moving the operating wavelength from 1.30 μm to 1.55 μm reduces the loss by roughly a factor of 2, and thereby would increase L by the same factor. However since the dispersion effect at 1.55 μm is greater than that at 1.30 μm , more transmitter power P_t at 1.55 μm will be required than that at 1.30 μm to meet an increase in L by the same factor. This added transmitter power required to accomplish this is called the dispersion power penalty, an important parameter in optical fibre system design. As the data bit rate is increased and longer fibre length is required, dispersive effects in the fibre become more important.

In a power system protection relaying, particularly of the unit type, long distance data links would be expected to be used. In this case, a pulse code modulation (PCM) system would be considered to convert actual fault transient analogue signals to digital signals. A sampling rate of one phase current would be chosen at typically 4 KHz and a 12 bit A/D converter would be used to obtain 48 kbit/s. Several phase current and voltage signals, and some control information signals in the relay can be multiplexed to meet standard frame bit rate of 2.048 Mbit/s in European system or 1.544 Mbit/s in T₁ transmission system.

In this paper, one standard frame bit rate of 1.544 Mbit/s is considered as a primary group signal for one digital reply protection system [1]. Four primary group signals are multiplexed and converted to the optic secondary group signal with bit rate of 6.312 Mbit/s as the simulation data bit rate through the computer modelling of a fibre optical communication system for power system applications. Higher transmission bit rates than 6.312 Mbit/s are also presented.

2 SIMULATION MODELS

The major components of an end-to-end optical fibre system for power system protection relaying consist of optical transmitter, optical fibre and optical receiver as shown in Figure 1. Some other simulation models have been described in [2].

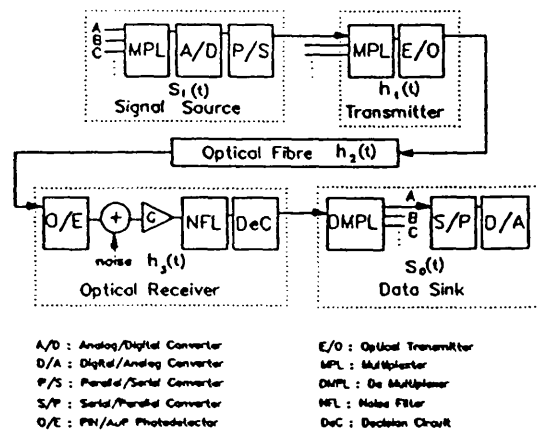


Figure 1. Digital Transmission System Model

An input electrical signal $S_1(t)$ from data source is a type of pulse format, such as NRZ, RZ, PAM, etc. This signal directly modulates a

optical transmitter. The output of the optical signal from the transmitter is coupled into an optical fibre cable. At a receiver, the optical detector converts optical receive power into electrical current with an addition of some noises, such as circuit noise, shot noise and etc. The noisy received waveform is filtered by a low pass noise filter or equalizer. Finally, the decision circuit gives the output of digital data signal, and the analogue signal $S_a(t)$ is the output of the D/A converter. The detail description of the above models in Figure 1 is given in the follows.

2.1 Data Source

A variety of data sources and line codes is used to modulate the optical transmitter. In a simple and practical case, an NRZ line code format is chosen to test the performance of the computer simulation system. Both random data sequence and realistic fault transient signals are used as the input data $S_i(t)$. The random generator is simulated by an uniform distribution sequence with binary digits, which is an ideal case of the NRZ line code, or the realistic fault transient signals are converted into a binary digital sequence. A simulation length of data sequence is chosen by five cycles of power signal.

2.2 Optical Transmitter

Semiconductor lasers and LED's are the most important optical sources. Two important characteristics of optical transmitter are the optical output waveform and the optical carrier or spectrum. In the first case, the optical output waveform depends on the speed of response of the driving circuitry to pulse an optical source, which is presented as a time of turn-on and turn-off response. The rise and fall time response can be presented by an impulse response $h_i(t)$, which can be defined by the parameters of the transmitter. In the second case, the transmitter optical carrier or spectrum modulates electrical signal to optical signal and also is one of the inputs needed to calculate the single-mode fibre transfer function. Both the laser and LED spectrum may be modelled as a normalized Gaussian function given as:

$$S(\lambda) = \frac{1}{\sigma_0 \sqrt{2\pi}} e^{-(\lambda - \lambda_0)^2 / (2\sigma_0^2)} \quad (2)$$

With rms spectral width σ_0 and centre wavelength λ_0 . A typical spectral width of LED emission is in the range between 20 nm to 100 nm, and a typical laser spectral width is from 2 nm to 10 nm. The LEDs have more stable characteristics than Lasers. The lasers also have additional unique noise sources, such as mode partition noise, chirping and reflection. These require specific application models. Here only laser sources are considered to meet a long distance application of transmission system.

2.3 Single-Mode Fibre Transfer Function

The transfer function is presented as $h_2(t)$ in time domain which has been shown in Figure 1. Its frequency domain $H_2(f)$ for a modulated optical signal propagating over a length L of single-mode fibre may be written as follows [3]:

$$H(f) = \int S(\lambda) A(L, \lambda) e^{-j\omega L \tau(\lambda)} d\lambda \quad (3)$$

where $S(\lambda)$ is the transmitter optical spectral density as a function of λ , $A(L, \lambda)$ is the optical power loss coefficient of the fibre, and $\tau(\lambda)$ is the group delay per unit length for the fibre. To evaluate equation (3), it is assumed that the fibre loss $A(L, \lambda)$ is a much more slowly varying function over the wavelength range of $S(\lambda)$. It can thus be approximated to a constant term $A = e^{-\alpha L}$ due to fibre loss as a function of length, and that $S(\lambda)$ may be modelled by a Gaussian distribution with centre wavelength λ_0 and the rms spectral width σ_0 as given in equation (2), and the group delay $\tau(\lambda)$ with a partial Taylor series expanded about λ_0 as shown below:

$$\tau(\lambda) = \tau(\lambda_0) + \frac{d\tau}{d\lambda} (\lambda - \lambda_0) + \frac{1}{2} \frac{d^2\tau}{d\lambda^2} (\lambda - \lambda_0)^2 + \dots \quad (4)$$

If multi-longitudinal-mode lasers are considered with Gaussian envelope spectrum, the above second-order dispersion term $d^2\tau/d\lambda^2$ can be neglected in calculating fibre dispersion [4]. In equation (4), the $\tau(\lambda_0)$ can be omitted, since it only causes a delay and has no influence on the shape of the output signal. Thus the low-pass equivalent model of the single-mode fibre transfer function may then be calculated substituting (2), (4) into (3), and:

$$H_2(f) = A \int \frac{1}{\sigma \sqrt{2\pi}} e^{-\frac{(\lambda - \lambda_0)^2}{2\sigma^2}} e^{-j\omega L \frac{d\tau}{d\lambda} (\lambda - \lambda_0)} d\lambda \\ = e^{-\alpha L} e^{-\frac{1}{2} \omega^2 L^2 \sigma^2 \left(\frac{d\tau}{d\lambda}\right)^2} \quad (5)$$

Where the term of $L^2 \sigma^2 (d\tau/d\lambda)^2$ is interested, since it shows characteristic of lowpass filter which is bandwidth limited due to material dispersion $d\tau/d\lambda$ and the fibre length. There are many types of fibres available today which have slightly different material dispersions that can be measured. The group delay $\tau(\lambda)$ of a type of single-mode fibre with a zero dispersion at 1.310 μm wavelength can be approximated by a three-term polynomial as follows [5]:

$$\tau(\lambda) = a + b\lambda^2 + c\lambda^{-2} \quad (6)$$

Where $a = -34.74 \text{ ns/km}$, $b = 10.11 \text{ ns/km} \cdot \mu\text{m}^2$, $c = 29.83 \text{ ns} \cdot \mu\text{m}^2/\text{km}$

The term of $L^2 \sigma^2 (d\tau/d\lambda)^2$ is effectively the dispersion penalty. However, the basic dispersion power penalty is also related to the dispersion normalized pulse broadening $\Delta t/T$, where T is the time slot for a bit rate $B = 1/T$ [5]. The letter is given as:

$$P_d = 22 B^2 \Delta t^2 = 22 B^2 L^2 \sigma^2 \left(\frac{d\tau}{d\lambda}\right)^2 \quad (7)$$

with rms spectral width σ of the laser sources, and $d\tau/d\lambda = \text{ps/km} \cdot \text{nm}$ at 1.55 μm wavelength and $d\tau/d\lambda = 3.2 \text{ ps/km} \cdot \text{nm}$ at 1.310 μm wavelength, which are calculated by differentiating equation (6). As can be seen from equation (7), the power penalty is increased with bit rate B and fibre length L . The impulse response as calculated by equation (5) for two examples of laser sources is plotted in Figure 2.

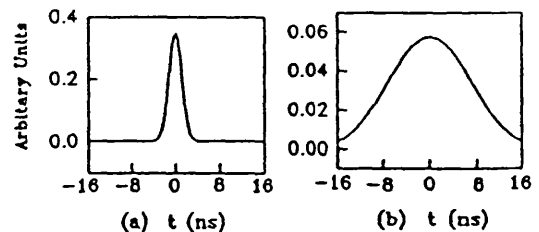


Fig 2 Fibre Impulse Response Function
(a) Laser source $\sigma=4\text{nm}$, $\lambda=1.30 \mu\text{m}$, $L=80\text{km}$
(b) Laser source $\sigma=4\text{nm}$, $\lambda=1.55 \mu\text{m}$, $L=80\text{km}$

Where we assume the laser sources have transmitter power $P_t = 0 \text{ dBm}$ and receiver sensitivity $P_{\text{min}} = -40 \text{ dBm}$. The loss is 0.5 dB/km at 1.30 μm and 0.3 dB/km at 1.55 μm . From equation (1), therefore the budget limitation is 80 km at $\lambda=1.30 \mu\text{m}$ and 133 km at $\lambda=1.55 \mu\text{m}$.

2.4 Receiver model

At an optical receiver, the first element is a photosensitive detector.

converts photons to electrons. This can be either a PIN (positive-intrinsic-negative) diode or an APD (avalanche photodetector). In the computer simulation receiver model, an APD is considered in which digital bit stream consisting of '1' and '0' ('on' and 'off' states) is incident at the bit rate B. The detected signal $i_{o1}(t)$ or $i_{o0}(t)$ in the two states is the average current given [6] by:

$$i_{o,j}(t) = \left(\frac{\eta e}{h\nu}\right) \langle M \rangle P_j(t) \quad j = 0 \text{ or } 1 \quad (8)$$

Where $(\eta e/h\nu)$ is the response of a detector with quantum efficiency η to the incident photons of energy $h\nu$, $\langle M \rangle$ is the average APD gain (in PIN, the $\langle M \rangle = 1$), and $P_j(t)$ is the average power received during a single bit. The bit error rate results from the noise current σ_j associated with the signal $i_{o,j}$. Assuming the Gaussian statistics, the bit error rate is given by:

$$P(E) = \frac{1}{\sqrt{2\pi}} \int_0^\infty \exp(-x^2/2) dx = \frac{1}{2} \operatorname{erfc}\left(\frac{\rho}{\sqrt{2}}\right) \quad (9)$$

Where $\operatorname{erfc}(x)$ denotes the complimentary error function and

$$\rho = \frac{D - i_{o0}}{\sigma_0} = \frac{i_{o1} - D}{\sigma_1} \quad (10)$$

The decision level D is chosen to yield equal P(E) in the two states. Eliminating D in equation (10) gives $Q = (i_{o1} - i_{o0})/(\sigma_0 + \sigma_1)$. A value of $Q \geq 6$ is required to maintain P(E) below 10^{-9} bit error rate. Writing $r = P_0/P_1$ as the off/on extinction power ratio, and $P_{av} = (P_0 + P_1)/2$ as the average detected power and Q becomes:

$$Q = \left(\frac{1-r}{1+r}\right) \left(\frac{\eta e}{h\nu}\right) \langle M \rangle \frac{2P_{av}}{(\sigma_0 + \sigma_1)} \quad (11)$$

The noise current σ_j gets contributions from several noise sources, where the noise sources are considered include circuit noise, shot noise, laser intensity noise, reflection-induced noise, mode-partition noise, and chirp induced noise. In the power system protection relaying, there a long distance relaying would be considered with less than 150 Mbit/s bit rate. The performance of optical fibre systems which employ direct modulation of laser diodes is limited by three main factors 1) attenuation, 2) bandwidth of the fibre, and 3) mode partition noise. In our simulation models, the circuit noise, shot noise, mode-partition noise and intersymbol interference (ISI) power penalty due to fibre dispersion are considered.

A. Circuit Noise

Circuit noise is the contribution to the output noise from the receiver circuit amplifier and the bias circuit. Most receiver circuits available, are a PIN/APD photodetector with an FET front-end amplifier and the variance of the noise current at a noise lowpass filter equivalent bandwidth B_N (due to the amplifier and bias resistor referred to the input) is given by [7]:

$$\sigma_{c,j}^2 = \frac{4KT}{R_L} I_2 B_N + 2eI_d I_2 B_N + \frac{4KT}{g_m} (2\pi C)^2 f_c I_f B_N^2 + \frac{4KT}{g_m} (2\pi C)^2 I_2 B_N^2 \quad (12)$$

Where g_m is the transconductance of the FET preamplifier, C is the total input capacitance, R_L is the load resistance. The I_d is the dark current. ζ is the FET 1/f noise figure, Γ is the FET channel noise factor = 1.1. I_1, I_2, I_f are normalized noise-bandwidth integral and depend only on the input-optical-pulse shape. The noise figure F(M) is given as follows:

$$F(M) = \frac{K}{\langle M \rangle} + \left(2 - \frac{1}{\langle M \rangle}\right) (1-K) \quad (13)$$

Where K is the ionization ratio of the majority and minority carriers.

B. Shot Noise

The variance of the noise current due to shot noise is given by [8]

$$\sigma_{s,j}^2 = I_{in}^2 B_N - 2e i_{o,j} \langle M \rangle F(M) I_2 B_N - 2e \left(\frac{\eta e}{h\nu}\right) \langle M \rangle^2 F(M) P_j(t) I_2 B_N \quad (14)$$

Where I_{in} is the injected photocurrent, $\langle M \rangle$ is the mean avalanche gain for the photocurrent, F(M) is the excess noise factor from (13).

C. Mode-partition noise

Mode partition noise (MPN) is an important factor when using laser source and single-mode fibre as a system. This noise is caused by the instant fluctuation of the power distribution among the laser N-longitudinal modes and the differential dispersion-induced fluctuations in the recovered power. The Noise-Signal-Ratio is given by [9]

$$\frac{N}{S} = \sigma_{pc}^2 k^2 - \frac{1}{2} k^2 (\pi B)^4 [A_1^4 \sigma^4 + 48A_1^2 \sigma^4 + A_2^2 A_2^2 \sigma^4] \quad (15)$$

where $A_1 = -\frac{d\tau}{d\lambda} L$, $A_2 = \left(\frac{d^2\tau}{d\lambda^2} + \frac{2}{\lambda} \frac{d\tau}{d\lambda}\right) L$

where B is the data rate, σ is the source spectral width. The variance of this noise is given by the following equation:

$$\sigma_{mpj}^2 = \left(\frac{\eta e}{h\nu}\right)^2 \langle M \rangle^2 P_j^2(t) \sigma_{pc}^2 k^2 \quad (16)$$

where k is a statistical factor that can vary from 0 to 1. $k=0.5$ to 0.6 can be used for system design prediction using the present MPN theory.

D. Bit-Error-Rate Curves

The various noise contribution can be added to get the total variance of the noise current as:

$$\sigma_j^2 = \sigma_{c,j}^2 + \sigma_{s,j}^2 + \sigma_{mpj}^2 \quad (17)$$

Equation (9), (11) and (17) can be used to generate the bit-error-rate curves by plotting bit-error-rate P(E) as a function of the average receiver power P_{av} , so that we can estimate the receiver sensitivity which is affected by changing the system parameters. As an illustration of the above theoretical analysis, it is used to simulate the bit-error-rate curves of 6 Mbit/s, 80 Mbit/s and 150 Mbit/s at $\lambda=1.3 \mu\text{m}$ and $\lambda=1.55 \mu\text{m}$, which are shown in Figure 3 and Figure 4 respectively.

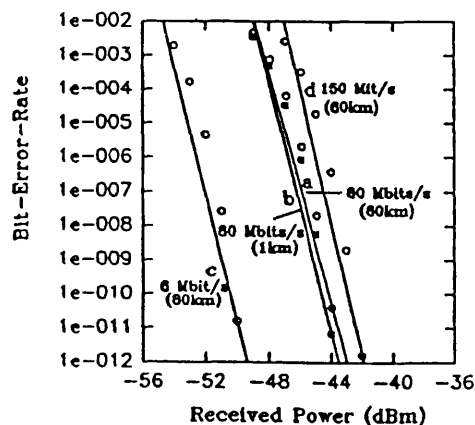


Fig 3 Bit-Error-Rate Curves for different bit rate and distance. ($\lambda=1.3 \mu\text{m}$)

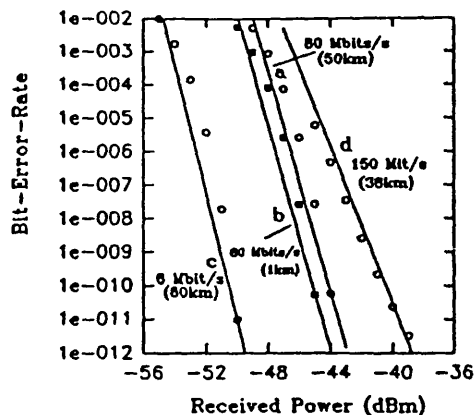


Fig 4 Bit-Error-Rate Curves for different bit rate and distance. ($\lambda=1.55\mu\text{m}$)

The circuit noise, shot noise, and mode-partition noise are simulated with the following system parameters [7][8][9]; $(\eta/h\nu)=0.9$, $\langle M \rangle = 10$, $F(M)=5.01$, $I_2=0.403$, $I_3=0.0361$, $I_4=0.0984$, and the laser spectral width $\sigma=4$ nm.

3 RESULTS and DISCUSSION

The performance of an optical fibre transmission system is best characterized by generating the bit-error-rate curve as a function of the received power. One important feature of the bit-error-rate curves in a logarithmic plot is the change in slope that can result in the appearance of a noise floor. This feature is due to different functional dependence of the noise on the signal power for different noise sources. The circuit noise σ_c is independent of the signal power, the shot noise σ_s is proportional to the square-root of the signal power $\sqrt{P_s}$, and mode-partition noise σ_{mp} is proportional to the power P_s . In addition to these noise contributions, the power penalty P_{1st} is also taken into account. Both mode-partition noise σ_{mp} and P_{1st} are proportional to the square of fibre dispersion. In the case of a transmission system at $\lambda=1.3 \mu\text{m}$, it can be seen by comparing (a) and (b) in Figure 2, there has less fibre dispersion than that at $\lambda=1.55 \mu\text{m}$. By comparing Fig.3 with Fig.4, at bit rate $B=80$ Mbit/s, it has less change (approximately 0.1 dB in slope) when the fibre length changes from 80 km to 1 km than that at $\lambda=1.55 \mu\text{m}$ in which there is a change in slope of 1 dB when the fibre length changes from 50 km to 1 km. Because of large dispersion at $\lambda=1.55 \mu\text{m}$, its maximum one span length is approximately 70 km at bit rate 80 Mbit/s, and 42 km at bit rate 150 Mbit/s. However it can reach one span length of 80 km at lower bit rate 6 Mbit/s. In contrast there is near zero dispersion at $\lambda=1.3 \mu\text{m}$, however its major limitation of one span length is due to fibre attenuation or loss. Since the circuit noise and shot noise increase with an increase in the bit rate B , so the receiver power sensitivity is decreased with an increase in the bit rate

The results of the computer simulation of the bit-error-rate curves have been given in Figure 3 and Figure 4. Simulation result of transmitter output and fibre output lowpass equivalent waveform at $\lambda=1.3 \mu\text{m}$ and $\lambda=1.55 \mu\text{m}$ respectively are also presented. The laser sources are chosen with their spectral width $\sigma=4$ nm, transmitter launch power $P_t = 1 \text{ mw} = 0 \text{ dBm}$, and a typical signal-mode fibre loss is 0.625 dB/km at $\lambda=1.3 \mu\text{m}$ and 0.37 dB/km at $\lambda=1.55 \mu\text{m}$. The transmitter rise and fall times are 2 ns, and its transform function H_{LD} is modelled by a forth-order network consideration [2]. The results of transmitter output waveform and receiver input waveform are shown in Fig.5, Fig.6 and Fig.7 respectively. Comparing the results in Fig.5, 6 and 7, it is clearly seen that there dispersion effect differences between $\lambda=1.3 \mu\text{m}$ and $\lambda=1.55 \mu\text{m}$. At $\lambda=1.3 \mu\text{m}$, the rise and fall time change from 2 ns to 4 ns, however at $\lambda=1.55 \mu\text{m}$ they increase from 2 ns to 16 ns after signal transmission over 80 km.

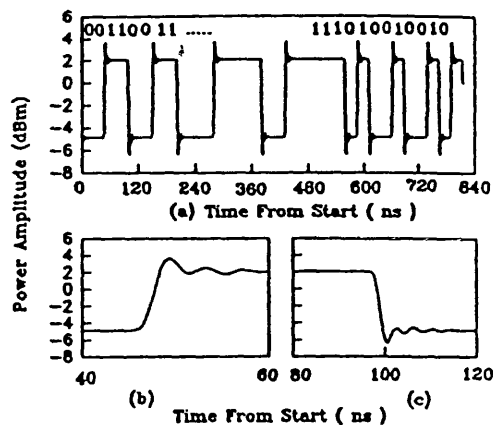


Fig 5 Transmitter output waveform simulation (a) NRZ format Waveform (b) and (c) are the zoom waveform of (a)

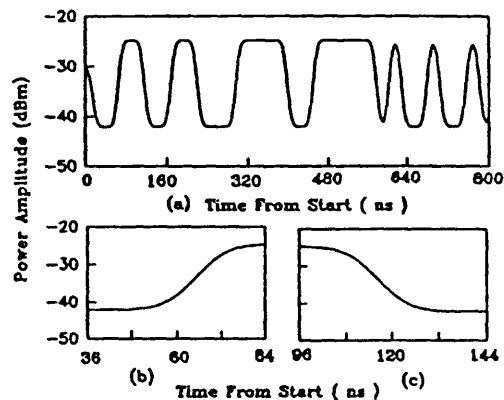


Fig 6 Receiver input waveform simulation (a) Output dispersion waveform of optical fibre ($\lambda=1.55\mu\text{m}$, fibre length=80 km) (b) and (c) are the zoom waveform of (a)

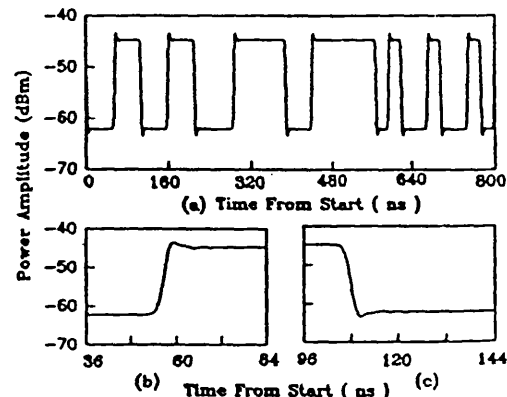


Fig 7 Receiver input waveform simulation (a) Output dispersion waveform of optical fibre ($\lambda=1.3\mu\text{m}$, fibre length=80 km) (b) and (c) are the zoom waveform of (a)

Finally, a decision circuit model has been simulated. The bit-err of equal or less than 10^{-9} is always expected to be in any optic transmission system design. The calculation using practical value

AN IMPROVED MODELLING TECHNIQUE OF A FIBRE OPTICAL DIGITAL SYSTEM FOR POWER SYSTEM PROTECTION RELAY

H. Y. Li and R. K. Aggarwal

School of Electronic and Electrical Engineering
University of Bath, Bath BA2 7AY, UK

Abstract

Fibre optical systems for power system communication are finding widespread use in the Electricity Supply Industry. In this respect, it is important to ascertain the effect on signals transmitted due to the limitation imposed by the various components within the fibre optical system. This paper is thus concerned with describing a complete computer-aided design of a fibre optical system. Results are presented with respect to an EHV transmission line differential protection scheme employing a fibre optical system as a means of communicating between the two ends.

List of symbols

APD	avalanche photodetector
B	bandwidth of low-pass noise filter at receiver
BER	bit error rate
C	diffusion capacitance in laser equivalent circuit
CAD	computer aided design
DBR	data bit rate
FOS	fibre optical system
FFT	fast fourier transform
FWHM	full width half maximum of laser source spectrum
E_a	average photo gain
$I_i(\omega)$	spectrum of laser inject current
i_n	current noise source
L	inductance in laser equivalent circuit
LD	laser diode
LED	light emitter diode
PIN	positive intrinsic negative diode
PCM	pulse coding modulation
q	electron charge
RIN	relative intensity noise
R	resistance in laser equivalent circuit
R_s	resistor in series with L
SNR	signal to noise ratio
$s(t)$	photo density
$S_s(\omega)$	spectrum of photo density $s(t)$
v_n	voltage noise source
z	fibre length
α	average fibre loss
β	fibre propagation constant
ρ	fraction of spontaneous emission in laser rate equations

1. Introduction

A current differential relay can provide unit protection scheme for simple two-ended feeders or more complex multi-ended circuits without the restrictions associated with other forms of protection, but it needs reliable communication media. Conventional relay systems have made use of metallic circuits. These circuits have at times affected the system reliability due to extraneous voltage interference. As pilot circuits are often rented from telecommunication authorities, with the extensive use of electronic signal repeaters and complex switch equipment, direct transmitting of power frequency signals over rented pilots is becoming less feasible. Therefore, a new

generation of unit protection schemes, with very reliable communication circuits suitable for long line power system protection relaying, is required.

Most novel protection schemes have considered FOS's for data transfer [1] because of their advantages, such as, small size, light weight, flexibility, very low signal attenuation, immunity to sparking and electrical influence, over metallic cables. All these attributes make them ideally suited for power system protection relaying.

A few practical short distance FOS's with components: LD or LED as transmitters, multi-mode fibres, PIN or APD as receivers, have been developed [2, 3]. But without electrical signal repeaters, none of them are suitable for long distance signal transmission. While repeaters introduce additional problems for long distance power system protection relaying, supply voltage must be provided to repeaters at remote locations, the repeaters may also be influenced by power environment. So a maximum span of optical fibre along power transmission lines without repeaters is an ideal design of a FOS for power system protection relaying.

In this paper, a noise equivalent circuit of a semiconductor laser circuit model is presented. This model allows a straight forward calculation of RIN and provides measurement of the PCM characteristics of a LD. By combining the laser model and an improved fibre model with the previously developed photodetector model and noise mechanisms at the receiving end [4], a CAD of a FOS for computing the system reception performance is developed. The development of this system introduces CAD techniques systematically to fibre optical digital communication media for power system protection relaying and related areas. Furthermore, the system design parameters which vary from the application domains, and the simulation results are discussed.

2. Laser Model

The transmitter of the system is modelled as a semiconductor LD intrinsic equivalent electrical circuit

operating with multi-longitudinal mode spectrum output at 1.3um or 1.55um light wavelength range. A common practical multi-longitudinal-mode InAsGa laser is considered due to economical requirements in the system design, but many advanced lasers which are more expensive would produce even better results since these lasers, e.g. distributed feed-back type LDs, operate in single or near single longitudinal mode. Firstly, the dynamic behaviour of single mode semiconductor injection laser is described by the well-known laser rate equations [5]. The solution for both small-signal and large-signal response can be obtained by directly solving the laser rate equations using numerical method. An alternative method is to analysis the laser rate equations by using equivalent electrical circuit techniques. The latter method is used to simulate the LD dynamic operation where LD is modeled by a parallel RLC circuit whose elements are presented in [6]. The photon modulation transfer function $H_{laser}(\omega)$ and RIN spectrum of the LD in frequency domain are calculated as following:

$$H_{laser}(\omega) = \frac{S_1(\omega)}{I_1(\omega)} = \frac{1}{LCqg_0D} \quad (1)$$

$$RIN(\omega) = \frac{i_n^2 + v_n^2 [(1/R)^2 + (\omega C)^2] - 2v_n i_n (1/R)}{(LC)^2 DD^* (qg_0)^2} \quad (2)$$

Where $D = -\omega^2 + j\omega[R_w/L + 1/RC] + 1/LC[1 + R_w/R]$, $S_1(\omega)$ spectrum of photo density, $I_1(\omega)$ spectrum of laser injection current and parameters of the laser equivalent electrical circuit model R , C , R_w , L , q , g_0 are represented in [6]. By using the same intrinsic laser parameters as in [5], the comparison results of LDs dynamic operation between numerical solution and the circuit model solution under small signal modulation conditions are shown in Fig.1(a) and Fig.1(b).

3. Optical Fibre Transmission Characteristics

An optical fibre can be considered as a bandpass system. A convolution form of the linear optical fibre transmission characteristics is obtained [7] as:

$$\langle p(z, t) \rangle = h_0 + \int_{-\infty}^{\infty} h(\tau) m(t-\tau) d\tau \quad (3)$$

The ensemble average of the optical power $\langle p(z,t) \rangle$ after distance z in the dispersive optical fibre is a function of h_0 , $h(t)$ and $m(t)$, where:

(i) h_0 is a constant optical power representing the circuit driver bias above the laser threshold.

(ii) Fibre transfer function in time domain $h(t) = \Gamma^{-1} \{1/(2\pi)G_1(\omega) \bullet [G_1(-\omega) S_{xx}(\omega)]\}$, where $G_1(\omega)$ is the fibre baseband characteristic, $S_{xx}(\omega)$ the laser source spectrum, Γ^{-1} a notation of inverse fourier transform and \bullet convolution calculation.

(iii) $m(t) = |\Gamma^{-1} F(\omega)|^2$ where $F(\omega)$ is a spectrum of the square root of a modulated signal at the output of a laser model.

(iv) The equivalent fibre baseband characteristic $G_1(\omega) = A(z)\exp(-j\beta_0 z - j\beta_0' \omega z - j\beta_0''/2 \omega^2 z)$, where the fibre propagation constant β with its expansion form, $\beta - \beta_0 =$

$\beta_0' (\omega - \omega_0) + 1/2 \beta_0'' (\omega - \omega_0)^2$, has the first and secondary propagation constant coefficients, and fibre attenuation $A(z)$ is assumed as $\exp(-\alpha z)$ with average fibre loss α (dB/km).

(v) The laser source spectrum $S_{xx}(\omega)$ without modulated signal is written as:

$$S_{xx}(\omega) = \sum_{i=-N}^N a_i S(\omega - i\Delta\omega) \quad (4)$$

The amplitude a_i of i th multi-longitudinal mode can be regarded as Gaussian decay $a_i = \exp(-i^2 P)$, $\Delta\omega$ is the distance between adjacent spectral lines; $S(\omega)$ Gaussian distribution. An example of laser multi-longitudinal-mode laser spectrum in our simulation system is illustrated in Fig. 2, with the parameters; $N=5$, $P = 1/8$, $\Delta\omega = 2\pi C\Delta\lambda/\lambda_0^2$, $\Delta\lambda = 1\text{nm}$, so that FWHM of this laser source spectrum is 2nm. This spectrum is a measurable parameter for a practical system.

4. Receiver Model and Noise Analysis

A receiver model, composed of PIN diode or an APD, a receiver front-end amplifier, filter and various receiver noise mechanisms, has been developed [4], where the noises consist of mode partition noise arising from the dispersive fibre, shot noise in photodetector, thermal noise at the receiver amplifier. In laser modelling for direct detection optical fibre digital system, intensity noise arising from the spontaneous emission process and the carrier-generation-recombination process is incorporated by adding a Langevin noise source to the laser rate equations. The RIN/ Δf is calculated from equation (2). $SNR = P_t \Delta f / (RIN * B)$, where P_t is transmitter power, Δf is unity frequency. The RIN appearing as signal current at the receiver end is given by:

$$\sigma_{sig}^2 = \left(\frac{\eta q}{h\nu}\right)^2 \langle M \rangle^2 \left(\frac{P_{rj}}{SNR}\right)^2 \quad (5)$$

where h is Planck's constant, η is the quantum efficiency, ν is the optical frequency, M is the mean avalanche gain, P_{rj} is the receiver signal power with $j=0$ or 1 binary status. In equation (5), SNR is in reverse ratio to B . Small SNR increases receiver noise current σ_{sig}^2 , therefore RIN can not be neglected in very large B . By adding RIN to the previously considered noises [4], the receiver noise analyses in direct detection optical fibre digital system, which is suitable for either long distance transmission or high DER, are complete.

5. Simulation Process

The laser, fibre and receiver models together with noise mechanisms have been presented in section 2, 3 and 4. By combining them, a CAD of optical fibre digital system for computing the system reception performance is developed. Multi-longitudinal-mode laser source spectrum is simulated using equation (4). Equation (3) simulates the system in time domain. The FFT and convolution methods are applied to develop the fibre transfer function $h(t)$. The modulated optical envelope power signal $m(t)$ of the laser is obtained from the laser equivalent circuit model. The various noise contributions are added to get the total variance of the noise current under a linear assumption. In order to take into account the pattern effect of the

Apparatus and System, vol. PAS-103, pp.152-159, January 1984.

- [3] Suzuki, M., Matsuda, T., Ohashi, N., Samo, Y., Tsukui, R. and Yoshida, T., "Development of a Substation Protection and Control System Using Fibre-Optic Local Area Network", *IEEE Transactions on Power Delivery*, Vol. 4, pp.1668-1675 July, 1989.
- [4] Aggarwal, R. K. and Li, H. Y., "Computer Modelling of a Fibre Optical Communication System for Power Protection Relaying", presented at the 27th UPEC, UK, pp.679-683, September 1992.
- [5] Boers, P. M. and Vlaardingerbroek, M. T., "Dynamic Behaviour of Semiconductor Lasers", *Electronics Letter*, vol. 11, pp.206-208, 15th May 1975.
- [6] Harder, C. Katz, J., Margalit, S., Shacham, J. and Yariv, A., "Noise Equivalent Circuit of a Semiconductor Laser Diode", *IEEE Journal of Quantum Electronics*, vol. QZ-18, pp.333-337, March 1982.
- [7] Etten, W. V. and Plaats, J.V.D., "Fundamentals of Optical Fibre Communications", *Prentice Hall International UK Ltd.*, 1991, ch.10, pp.185-195.
- [8] Jeruchim, M. C., "Techniques for Estimating the Bit Error Rate in the Simulation of Digital Communication System", *IEEE Journal on Selected Areas in Communications*, vol. SAC-2, pp.153-170, January 1984.
- [9] Blank, L. C., Bickers, L. and Walker, S. D., "Long Span Optical Transmission Experiments at 34 and 140 Mbit/s", *Journal of Light Technology*, vol. LT-3, pp.1017-1026, October 1985.

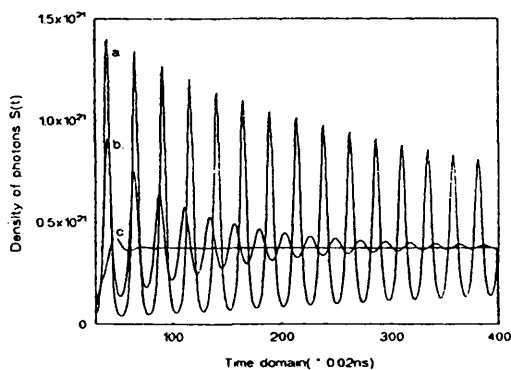


Fig.1(a) Numerical solution to the laser, where curve a, b and c correspond to $\rho = 10^4$, $\rho = 10^3$ and $\rho = 1$

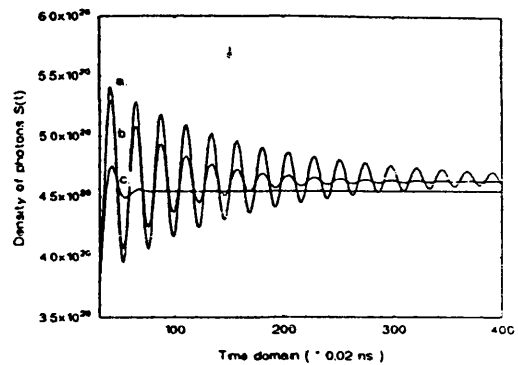


Fig.1(b) Circuit model solution to the laser, where curve a, b and c correspond to $\rho = 10^4$, $\rho = 10^3$ and $\rho = 1$

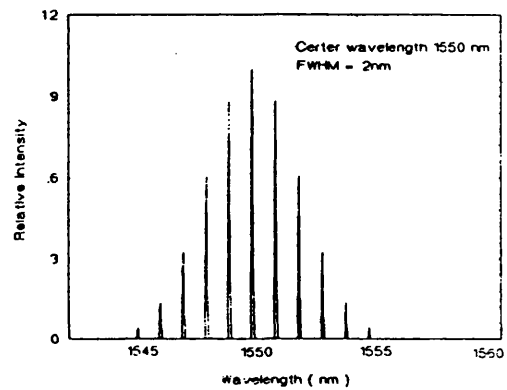


Fig.2 Unmodulated spectrum of the laser at light center wavelength $\lambda = 1.55\mu\text{m}$, FWHM=2nm

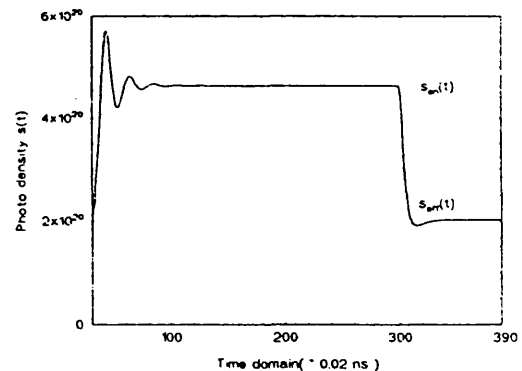


Fig.3 A pulse modulated output signal of the laser

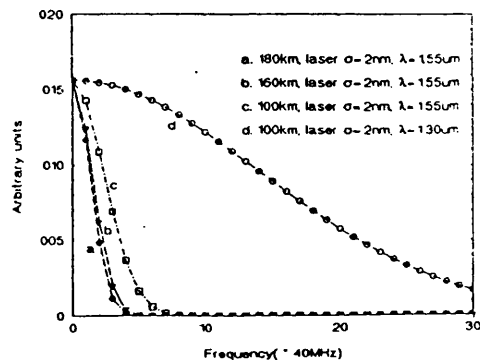


Fig.4 Laser plus dispersive fibre transfer function $H(\omega)$

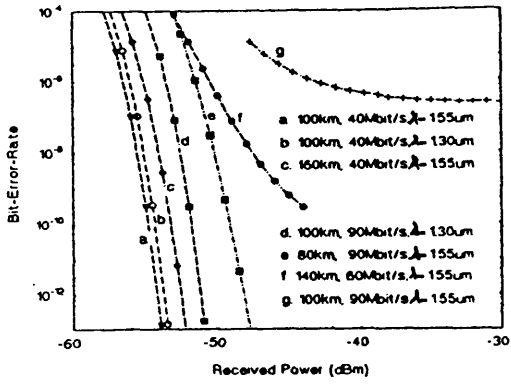


Fig. 5 Bit-error-rate (BER) as a function of mean received optical power

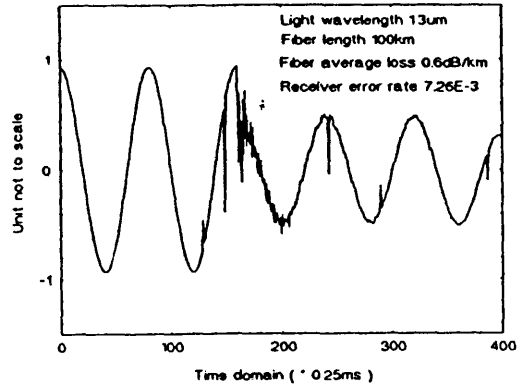


Fig. 6(d) Reception analogue waveform after decision circuit and D/A converter

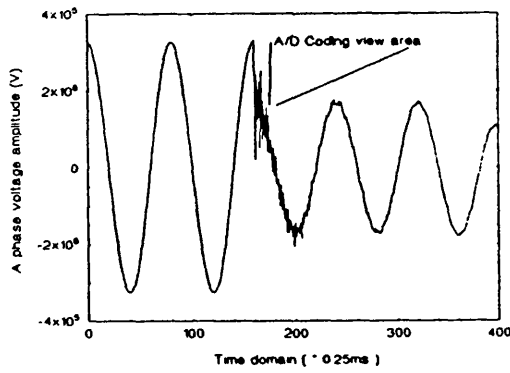


Fig. 6(a) A fault waveform of A phase voltage at one relaying terminal (P)

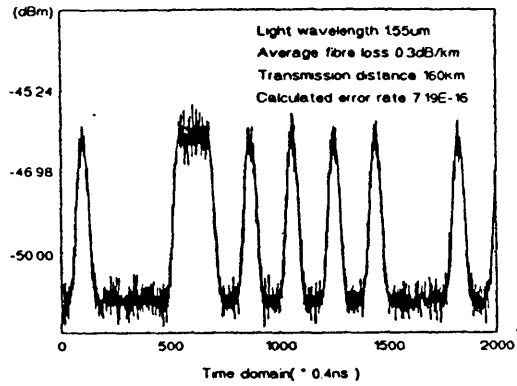


Fig. 7(a) PIN receiver side with added noise, fibre length=160km, $\lambda=1.55\mu\text{m}$, BER=7.26*10⁻¹⁶

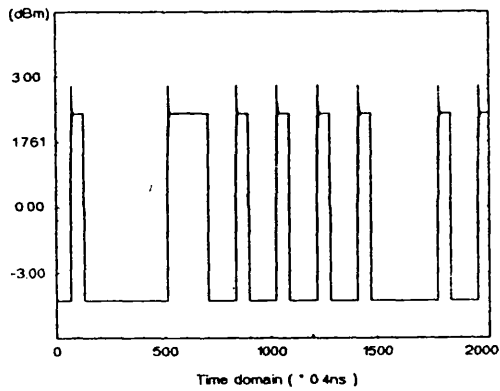


Fig. 6(b) 40Mbit/s modulated signal output of the laser at the transmitter side

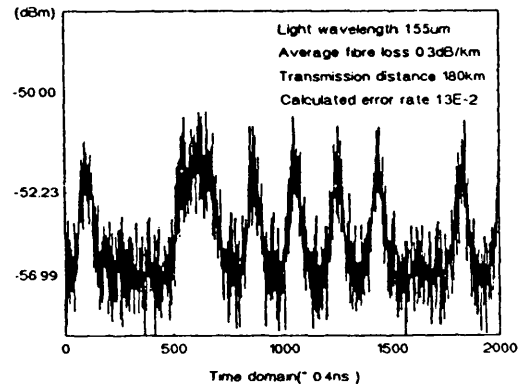


Fig. 7(b) PIN receiver side with added noise, fibre length=180km, $\lambda=1.55\mu\text{m}$, BER=1.3*10⁻²

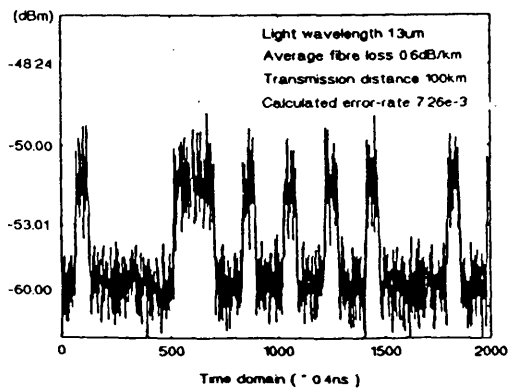


Fig. 6(c) APD receiver side with added noise, fiber length=100km, $\lambda=1.30\mu\text{m}$, BER=7.26*10⁻³

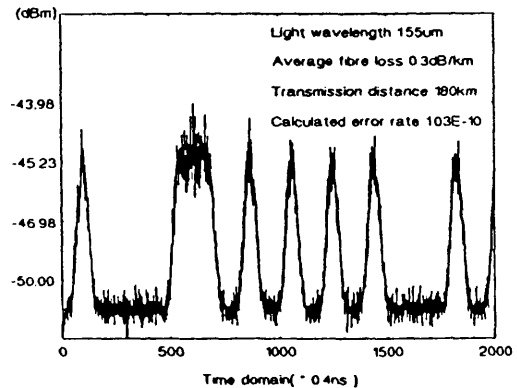


Fig. 7(c) APD receiver side with added noise, fibre length=180km, $\lambda=1.55\mu\text{m}$, BER=1.03*10⁻¹⁰